THE THERMAL CONDUCTIVITY OF LIQUID HYDROCARBONS

A thesis submitted to the University of London

for the degree of Doctor of Philosophy

by

Sam Fong Yau Li
B.Sc. (Eng), ACGI

Department of Chemical Engineering and Chemical Technology
Imperial College of Science and Technology
London SW7

July 1984

ABSTRACT

The work described in this thesis has accomplished five objectives. First, the problem of the contribution of radiation to the measurement of the thermal conductivity in a transient hot-wire instrument has been solved completely. Secondly, experimental results for the thermal conductivity of liquid hydrocarbons including n-hexane, n-octane, 2,3-dimethylbutane, 2,2,4-trimethylpentane, benzene, cyclohexane and toluene have been obtained in a temperature range from 34 to 90^{0}C and a pressure range from 0.1 to 700 MPa. The accuracy of the experimental data is estimated to be ±0.3%. Thirdly, the most developed theories for the transport coefficients of dense polyatomic fluids have been examined and tested against experimental data. In particular, it has been shown that the results calculated using a theory based on the rough hard sphere model agreed to within ±10% of the experimental data within the range of validity of the model. Fourthly, a prediction/correlation scheme has been established on the basis of the rough hard sphere theory. The scheme represents the thermal conductivity data of all the liquids studied in this work to within their experimental uncertainties. It has been shown that generalizations of this scheme allow reliable estimates of the thermal conductivity outside the range of direct measurements for normal alkanes, branched alkanes, cyclohexane and benzene to be obtained with an accuracy of ±4% given accurate density data. Finally, the possibility of measuring the thermal diffusivity and heat capacities of liquids together with the thermal conductivity using the present instrument has been investigated and recommendations have been made to improve the accuracy of these measurements.

ACKNOWLEDGEMENT

I wish to express my sincere thanks to my supervisors, Dr. W. A. Wakeham and Dr. G. C. Maitland for their invaluable advice and encouragement throughout the course of this work. Thanks are especially due to my colleagues, Merih, Marvin, Doris, Rob, Bob, Wendy, Carlos and João for the memorable time that we shared. I am greatly indebted to Ian, Dick and Malcolm for their constant help, and everyone in the workshop and glass-workshop for their excellent work. I would like to extend my thanks to Lesley and Miranda for typing my thesis and Naomi for helping with the drawings.

Finally, I wish to record my deep gratitude to my family and Han for their love and understanding, without whom this work might never have been completed.

C O N T E N T S

CHAPTER 1

Introduction

In a paper presented to the American Society of Mechanical Engineers in 1982[1], we have shown that accurate thermophysical data are essential in order to produce the most cost-effective design of any chemical processing plant or power plant. These facilities tend to be large, and expensive to build and operate. The economic viability of these plants relies on the ability to avoid the overdesign which is necessary when inaccurate property data are used [1,2]. Indeed, errors in the design of a single item of a plant which are attributable directly to errors in thermophysical property data are substantial [1,2]. Moreover, the deficiencies in the design of individual items of a plant may combine to produce an even larger effect upon the design of the entire system [1]. The increased capital costs and decreased efficiency which result from such design errors could be mitigated by a well-organised program of measurement for a fraction of the wasted resources [1].

This thesis is concerned with the study of the thermal conductivity of hydrocarbon liquids over a wide range of temperatures and pressures. A survey of the literature demonstrates the need for this study [3]. The scarcity of liquid phase thermal conductivity data is, principally, a result of the difficulty of its measurement, rather than a lack of need. The present work is a step in the process of overcoming this difficulty.

An absolute transient hot wire instrument has been employed for the measurements of the thermal conductivity of liquids. The theory of

the transient hot-wire method is given in Chapter two. In particular, we have developed a new analytic solution of the contribution of radiation in an absorbing and emitting fluid to the measurement process [4]. As a result of this analysis, it has been possible to establish that a well-designed transient hot-wire instrument is capable of not only high precision [5], but also of high accuracy [4].

In Chapter three the apparatus itself and the experimental procedures are described. The entire body of experimental data obtained in this work is given in Chapter four. Data have been obtained for seven pure liquid hydrocarbons over the temperature range 30^0C to 90^0C, and pressure range from atmospheric up to 700 MPa [4,6-8]. The liquids studied are: n-hexane, n-octane, 2,3-dimethylbutane, 2,2,4-trimethylpentane, benzene, cyclohexane and toluene.

It is envisaged that the data obtained in this work will be used both to examine liquid phase thermal conductivity theories, which have been developed and will be developed in the future, and also for direct application in predicting thermal conductivities of pure liquids at thermodynamic states for which measurements are unavailable. In Chapter five, the existing theories for the thermal conductivity of liquids are discussed. A correlation scheme is developed in Chapter six which allows the prediction of the thermal conductivity of the liquids studied over a wider range of conditions than have been examined experimentally. The relationship between this correlation scheme, the experimental data and the theories of liquids are also discussed in this chapter.

Finally, in Chapter seven the conclusions of this work and

suggestions for future work involving both experimental and theoretical developments will be discussed.

CHAPTER 2

THEORY OF THE TRANSIENT HOT-WIRE TECHNIQUE

2.1 Introduction

The thermal conductivity of an isotropic fluid is formally defined by the Fourier equation of conductive heat transfer:-

$$\vec{Q} = - \lambda \nabla T \qquad (2.1)$$

where λ is the thermal conductivity, $\vec{Q}$ is the three-dimensional heat flux, and T the local fluid temperature. By convention λ is a positive quantity and as heat transfer through a medium occurs in the direction of decreasing temperature, this necessitates the -ve sign in equation (2.1).

Generally the transfer of heat through a fluid occurs by simultaneous conduction, convection and radiation. Conduction is the transmission of heat through a medium by intermolecular forces, or by direct molecular transport of rotational, vibrational or translational energy. Radiative heat transfer is the transfer of heat energy by the emission, absorption and scattering of electromagnetic radiation. Finally, convective heat transfer occurs by the bulk transfer of elements of a fluid due to velocity fields within the fluid medium.

If the thermal conductivity of a fluid is to be obtained experimentally, because the three mechanisms of heat transfer within a fluid are inseparable, the measurements must be performed on apparatus which either compensates for, or renders negligible the effects due to radiative and convective heat transfer.

There are two basic approaches employed in the measurement of fluid phase thermal conductivity. The first is to remove the time dependence from the conduction equation which leads to steady state methods. The second approach is to make a transient measurement of the fluid thermal conductivity. There are advantages to each method which will be discussed in detail. The transient methods have only become reliable during the last few years owing to the development of high speed electronic components.

2.1.1 Steady State Methods

The steady state approach consists of designing a well defined heat transfer configuration consisting of a constant temperature source and a sink, which are operated until a steady state is obtained. Once steady state is achieved, the quantity of energy per unit time input to the source is measured. The rate of energy addition along with the spatial dimensions of the apparatus are sufficient to determine the effective thermal conductivity of the fluid. Care is taken to minimise convection and radiation. Corrections for convection and radiation contributions are often made. There are four common configurations for steady state thermal conductivity instruments. These consist of: hot wire [9], concentric cylinder [10,11], concentric sphere [12,13] and parallel plate instruments [14,15,16]. The alignment of all steady state instruments is crucial to the accuracy of the results because the dimensions of the cell as well as the imperfections in the arrangement of the real cell compared to the ideal model enter the working equation directly in first order [17]. The effect of convection cannot be eliminated entirely from a steady state instrument, although the magnitude of the remaining effect can be made small and its negligible contribution to the measurement is confirmed by the use of different

temperature gradients, since the true thermal conductivity must be independent of the gradient.

The major problem which is present in all steady-state instruments is the required prolonged stabilization times. This fact alone is probably responsible for the scarcity of fluid thermal conductivity data. Experimentalists are now able to achieve reasonably high accuracies with steady state instruments. The parallel plate apparatus is operated so that the top plate is hotter than the bottom plate. This ensures that in the bulk of the fluid warmer, less dense fluid is above cooler, more dense fluid. Near the edges this situation can no longer be maintained unless the plates are infinitely large. An experimental arrangement in the form of a guard-ring surrounding the top plate has been used by Sengers et. al. [18] which approximate most closely to the situation of infinite plates. A steady state instrument operated in this manner will have negligible convective contribution provided that the heating surface is perfectly uniform and homogenous.

The problem of thermal radiation contributions to conduction has been analysed and will be discussed in a later section (see 2.4). Experimentally, this contribution can be reduced through a procedure of decreasing the plate spacing. By changing the plate spacing, the mean radiation path length is varied. The radiation free thermal conductivity is then obtained by back extrapolation to zero plate spacing on a curve of effective thermal conductivity versus plate spacing. Thus it can be seen that a single, high quality steady state data point is the result of measurements at several power levels and plate spacing.

2.1.2 Non-Steady State Methods

A non-steady thermal conductivity measurement is one in which a time-dependent perturbation, in the form of a heat flux, is applied to a fluid initially in equilibrium. The thermal conductivity of the fluid is obtained from an appropriate working equation relating the observed response of the temperature of the fluid to the perturbation. In principle, one can devise a wide variety of techniques of this kind differing in the geometry of the fluid sample employed and the nature of the time-dependent perturbation applied to it. However, the only geometrical arrangement which has gained general acceptance is one in which the perturbing heat flux is applied by means of electrical dissipation in a thin, cylindrical wire. The perturbing heat flux itself has been applied in a number of forms, including a near δ-function, a ramp pulse or a continuously modulated voltage, as well as a sinusoidal function. However, most often the perturbation has been applied in the form of a step-function, and the technique is then known as the transient hot-wire method. The method has quite a long history and was first employed by Stalhane and Pyk in 1931 [19] to determine the thermal conductivity of powders. From that period until about 1970 the development of the theory and application of the method was slow though continuous; a comprehensive bibliography of this work is given in the review by Shpil'rain, Urmanski, and Gorshkov [20]. In the last decade the increasing availability of electronic devices has made it possible to take full advantage of the potential benefits of the technique. The foundation of the modern experimental method was laid by Haarman [21], as well as Kestin, Wakeham and their collaborators [22-26]. Improvement in the practical design of the measuring instrument and the refinement of the theory of the method

have established the method as one of the most accurate ways of determining fluid thermal conductivity. The principal advantage of the method lies in its almost complete elimination of the effects of natural convection from the measurements, which is difficult to analyse mathematically, by virtue of its time scale (see section 2.3). For the same reason, much shorter experimental times are required compared with steady-state methods.

2.2 Principle of the Transient Hot-wire Method

The starting point for the theory of the transient hot-wire method is the ideal experimental arrangement shown in Figure 2.1

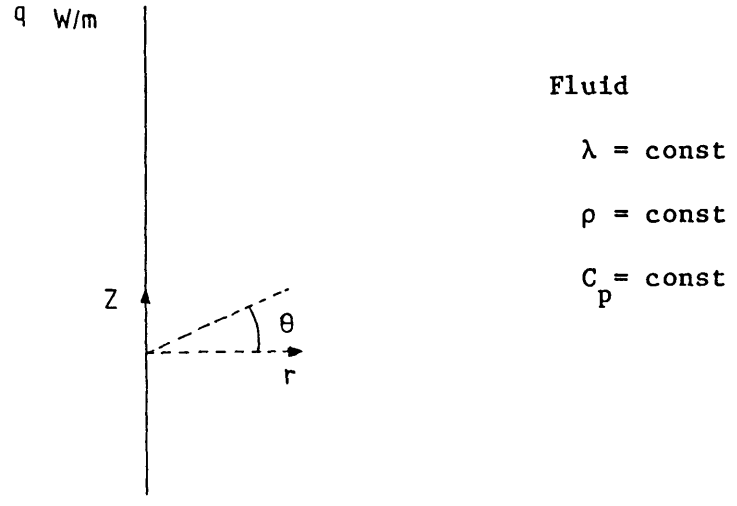

Figure 2.1

The idealized experimental arrangement

The ideal instrument consists of an infinitely long, vertical line source of a radial heat flux, q, per unit length which is applied stepwise at time t=0. The heat source, which is supposed to lose heat only by conduction, is immersed in an infinite fluid which is initially in an equilibrium state and which has temperature-independent

physical properties. The line heat source is coincident with the axis of a cylindrical coordinate system (r, z, θ). Thus the temperature rise of the fluid ΔT, above its equilibrium value, at the radial position, r, is given by the solution of the non-steady conduction equation

$$\frac{\partial T}{\partial t} = \kappa \nabla^2 T \qquad (2.2)$$

together with the definition

$$\Delta T(r,t) = T(r,t) - T_o \qquad (2.3)$$

Here, T_o represents the equilibrium temperature of the fluid, and κ its (constant) thermal diffusivity $\kappa = \lambda/\rho\, C_p$. The solution of equation (2.1) is subjected to the initial and boundary conditions:

initial condition

at $t \leqslant 0$ and any r , $\Delta T(r,t) = 0$ (2.4)

boundary conditions

(i) at $r = 0$ and any $t \geqslant 0$, $\lim_{r \to 0} \left(r \frac{\partial T}{\partial r} \right) = - \frac{q}{2\pi\lambda}$ (2.5)

(ii) and $r = \infty$ and any $t \geqslant 0$, $\lim_{r \to \infty} \Delta T(r,t) = 0$ (2.6)

with the additional constraint, λ = constant. The solution for ΔT may be written [23]

$$\Delta T = \frac{q}{4\pi\lambda} E_1 \left(\frac{r^2}{4\kappa t}\right) \qquad (2.7)$$

where $$E_1(x) = \int_x^{\infty} \frac{e^{-x}}{x} dx = -\gamma - \text{Ln } x + x + 0\{x^2\}$$

and γ is Euler's constant (0.5772156649 ....).

For small values of $\left(r^2/_{4\kappa t}\right)$ the exponential integral E_1 may be expanded to yield, at $r = a$,

$$\Delta T\ (a,t) = \frac{q}{4\pi\lambda} \left\{\text{Ln } \frac{4\kappa t}{a^2 C} + \frac{a^2}{4\kappa t} + \ldots\right\} \qquad (2.8)$$

where $C = \exp \gamma$.

The final step in the ideal model is to identify the temperature rise with that of the surface of the heat source were it of radius a, which is such that, for sufficiently long times, the second term in equation (2.8) is rendered negligible by comparison with the first. The resulting, ideal temperature rise is

$$\Delta T_{id}\ (a,t) = \frac{q}{4\pi\lambda} \text{Ln } \left(\frac{4\kappa t}{a^2 C}\right) \qquad (2.9)$$

This linear relationship between ΔT and Ln t indicates at once the principle of the experimental determination of the thermal conductivity, λ, since it may be obtained directly from the slope of the wire formed by plotting measured values of these two coordinates, without a knowledge of either the radius of the heat source, or the thermal diffusivity of the fluid.

Any practical realization of the principle of the transient hot-wire technique must, inevitably, depart from the idealized model described above. However, the success of the experimental method rests upon the fact that, by proper design, it is possible to construct an instrument that operates very closely in accord with equation (2.9) and for which the effects of the residual departures from the ideal may be readily calculated. It is also worthwhile noting here a further significant feature of the experimental method which is attributable to its transient nature. Strictly speaking, natural convection starts at $t = 0^+$ as the layers of the fluid adjacent to the heat source expand and develop buoyancy forces. However, it is possible to complete a transient conduction measurement in a time short compared with the characteristic time required for these forces to accelerate the fluid and to influence appreciably the heat loss from the source. Moreover, the experimental method provides a means whereby any debilitating effects from natural convection may be detected, since the linearity between ΔT and $\mathrm{Ln}\ t$ of equation (2.9) is only preserved so long as the pure conductive regime prevails. Any systematic departures from this linearity indicates the presence of significant convective flows.

All potential sources of systematic errors except the effects of radiative heat transfer are well understood [23] and hence have been accounted for in the apparatus design and the analysis of the experimental data. The radiation effect has often been considered as a residual systematic error in the thermal conductivity measurement [27]. In the present work, we have been able to resolve this remaining difficulty in the theory of the transient hot-wire technique (see 2.4).

The various departures of any practical instrument from the ideal for fluids which are transparent to radiation will be discussed first. A fuller analysis of the radiation correction will be discussed separately in a later section (2.4).

2.3 Corrections for Transparent Fluids

The departure of a practical instrument from the ideal, which are potential sources of systematic error, may be classified under five main headings according to the assumptions of the ideal model which are deemed inadequate. Since each of these departures has only a small effect upon the measurement it may be treated independently of all the others, and this fact has been utilized to derive a complete set of corrections [23]. Each correction is discussed briefly below and those effects which are eliminated entirely, those which are rendered negligible and those for which a correction must be applied are identified. It has been ascertained that the required corrections to ideality are small [27]. The combined effect can be taken to be additive.

Hence:-

$$\Delta T_{id} = \Delta T + \sum_i \delta T_i$$

where δT_i is a temperature correction due to the physical system in one respect being non-ideal.

(1) Conditions at the inner boundary

The practical version of a transient hot-wire instrument employs a thin metallic wire ($a \simeq 3.5\mu m$) as both the heat source and the monitor of the temperature rise. The non-zero radius of such a wire, and the

differences between its physical properties and those of the fluid require modification of the ideal model at the inner boundary of the fluid. The effect of the non-zero radius alone is readily found by solving equation (2.2). Subject to the new boundary condition, which replaces (2.5), that

$$\lambda \frac{\partial T}{\partial r} = - \frac{q}{2\pi a} \quad \text{at } r = a \quad \text{for any} \quad t > 0 \qquad (2.10)$$

At large values of $\left(4\kappa t/_{r^2}\right)$ the solution for the temperature rise of the fluid is

$$\Delta T(r,t) = \frac{q}{4\pi\lambda} \text{Ln} \left(\frac{4\kappa t}{r^2 C}\right) + O\left(\frac{r^2}{\kappa t}\right) \qquad (2.11)$$

This equation is identical with (2.8) at $r = a$ and reveals that the temperature history of the fluid is independent of the radius of the hot-wire. It is, therefore, unnecessary in the construction of an instrument to secure accurate cylindricity of the hot-wire.

Owing to the non-zero heat capacity of the wire, $(\rho C_p)_w$ per unit volume, some of the heat flux generated within it is required to raise the temperature of the wire itself; it is therefore not conducted to the fluid. Moreover, because of the finite thermal conductivity of the wire material, λ_w, a radial temperature gradient exists in the wire. By solving the two coupled, heat conduction equations for the wire, $0 < r < a$, and the fluid, $a < r < \infty$, it is possible to deduce the temperature profile in both materials as a function of time [28]. Because the metallic heat source itself is also employed as a

resistance thermometer in the measurements, the quantity required from the analysis is the average temperature rise of a cross-section of the infinitely long wire, ΔT_w. For sufficiently large values of $(\kappa t/a^2)$, this temperature rise is related to that of the ideal model by the equation [28]

$$\Delta T_{id}\ (a,t) = \Delta T_w(t) + \delta T_1 \qquad (2.12)$$

where the correction δT_1 is

$$\delta T_1 = \frac{q}{4\pi\lambda} \text{Ln}\ \left(\frac{4\kappa t}{a^2 C}\right)\left[\ \frac{a^2}{2\lambda t}\left[(\rho C_p)_w - (\rho C_p)\right]\right]$$

$$- \frac{q}{4\pi\lambda}\left[\frac{a^2}{2\kappa t} - \frac{a^2}{4\kappa t} + \frac{\lambda}{2\lambda_w}\right] \qquad (2.13)$$

and

$$\kappa_w = \lambda_w / (\rho C_p)_w \qquad (2.14)$$

The last term in this correction is time-independent and therefore has no influence on the determination of the thermal conductivity from the slope of the line ΔT_{id} vs Ln t. Of the remaining, time-dependent terms only the first is significant in most applications. Hence:-

$$\delta T_1 = \frac{q}{4\pi\lambda} \text{Ln}\ \left(\frac{4\kappa t}{a^2 C}\right)\ \left[\frac{a^2}{2\lambda t}\ \left[(\rho C_p)_w - (\rho C_p)\right]\right] \qquad (2.15)$$

or

$$\delta T_1 = \Delta T_{id} \left[\frac{a^2}{2\lambda t}\left[(\rho C_p)_w - (\rho C_p)\right]\right] \qquad (2.16)$$

This term arises solely from the finite heat capacity of the wire, and causes the measured temperature rise to fall below the ideal value at short times as shown in Fig. 2.2. By the choice of a suitable small radius a, (typically 3.5μm) and long measurement times, t, (greater than 50ms) the magnitude of the correction may readily be limited to at most 0.5% of the temperature rise, and it falls rapidly with increasing time so that equation (2.16) is entirely adequate for its calculation.

When the diameter of the wire becomes of the same order of magnitude as the mean free path of a molecule of the fluid under observation, the temperature of the fluid at $r = a$ becomes less than the temperature of the wire surface. This is known as the Knudsen effect and is due to a temperature jump existing at the surface of the wire [29,30]. Because the mean free path of a molecule of a liquid is never of the same order of magnitude as that of the platinum wire diameter (7μm) this effect does not present itself and is only applicable to gases at low densities, and hence the details of this effect is excluded from this discussion.

(2) Conditions at the outer boundary

A practical instrument of the transient hot-wire type must incorporate an outer boundary for the fluid. Simplicity dictates that this boundary should be cylindrical and it is located at $r = b$. During the initial phase of the transient temperature rise the thermal wave spreading out from the wire will be unaffected by the presence of

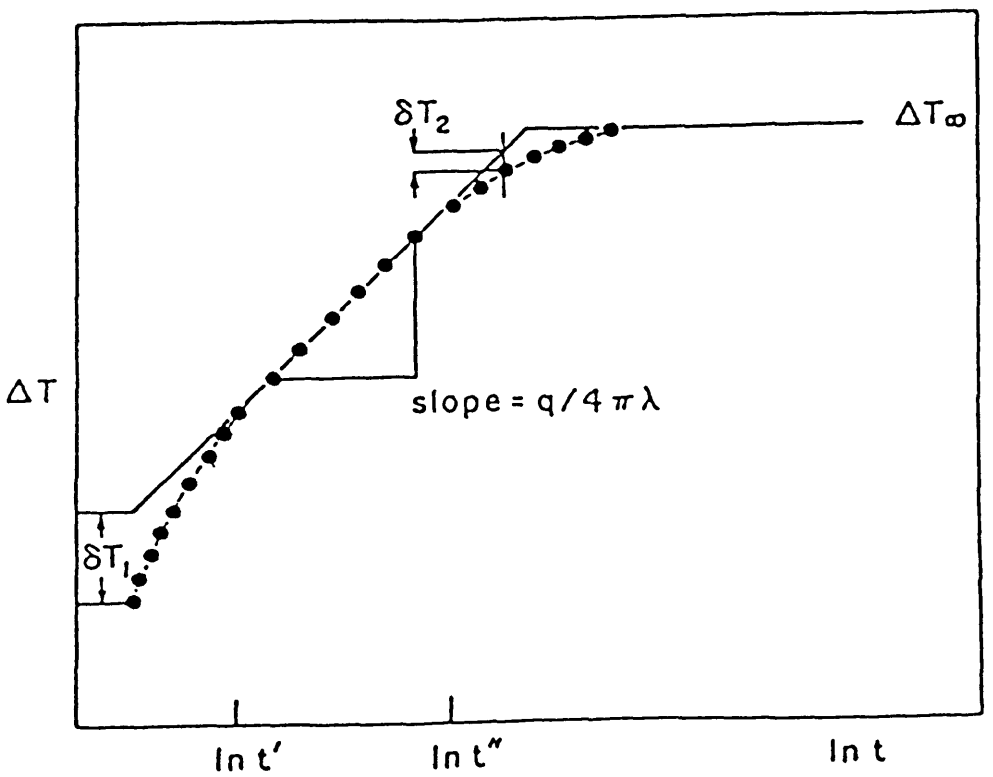

Fig. (2.2) Temperature rise in the wire as a function of time
(Scale in T exaggerated to illustrate the conditions at very long and very short times)

the boundary. However, as time goes on the heat flux at $r = b$ will rise to a non-negligible value and this causes the temperature rise of the wire to fall below that of the ideal model as shown in Figure 2.2.

The introduction of the outer boundary requires the modification of condition (2.6) of the basic problem to read

$$\Delta T(r,t) = 0 \quad \text{for } r = b \quad \text{and} \quad t > 0 \qquad (2.17)$$

A solution of the modified problem for the practical situation when $b/a \gg 1$ and $(4\kappa t/_{a^2}) \gg 1$ has been given by Fisher [31]. The temperature rise of the wire in the finite enclosure is related to that of the ideal model by the equation,

$$\Delta T_{id}\,(a,t) = \Delta T_{w}\,(a,t) + \delta T_2 \qquad (2.18)$$

Here the 'outer-boundary correction', δT_2 is given by the expression

$$\delta T_2 = -\frac{q}{4\pi\lambda}\left\{\text{Ln}\left(\frac{4\kappa t}{b^2 C}\right) + \sum_{\upsilon=0}^{\infty} \exp\left(-\frac{q_\upsilon^2 \kappa t}{b^2}\right)\left[\prod_{\upsilon} Y_o(g_\upsilon)\right]^2\right\} \qquad (2.19)$$

in which q_υ are the consecutive roots of the Bessel function $J_o(q_\upsilon) = 0$. As would be expected intuitively the correction increases with time and thermal diffusivity of the fluid, and decreases as the radius of the outer boundary increases. By a suitable selection of the radius of the outer boundary and the measurement time the correction δT_2 can be limited to 0.5% of the fluid temperature rise even in gases at low

density, and it is then adequately represented by equation (2.19). In the case of gases at elevated densities or liquids the correction is never significant in practice, owing to their low thermal diffusivity.

(3) The variable physical properties of the fluid

In the ideal model it is supposed that the physical properties of the fluid, ρ, λ, C_p and its viscosity, η, are temperature independent. In reality these quantities are usually mild functions of temperature for both gases and liquids. We consider first the effect of introducing a variable fluid density for the case of an infinitely long wire in an infinite fluid. The transient heating of the fluid now induces density variations in it which provide the buoyancy forces necessary to generate a velocity field. The convective motions has, in general, radial and longitudinal components; however, in the case of an infintely long wire only the radial component contributes to the heat transfer. Associated with the relative motion of the fluid there must of course be an irreversible generation of heat through viscous dissipation. In addition, some energy is expended reversibly in the expansion of the fluid, and finally the density variation enters the problem directly through the thermal diffusivity of the fluid (see appendix 1). In both gases and liquids an iterative solution of the fluid-dynamic processes [23] shows that all of these effects contribute only a small amount to the temperature rise of the wire. Even the largest of them, the density-induced variation in the thermal diffusivity and the viscous dissipation, contribute at most 10^{-4}% to the observed temperature rise [22,25] and so are negligible.

In a practical thermal conductivity cell, where the heat source must be of finite length and must be attached at both ends to

relatively massive supports and where the fluid is bounded by a finite wall, the foregoing analysis does not describe all of the effects. First, owing to the finite length of the wire, the one-dimensional regime of velocity and heat transfer characteristic of the infinite wire will not prevail over the entire length of the wire. In particular, as soon as the transient heating is begun, a three-dimensional temperature field develops in the fluid near the ends of the wire. The buoyancy forces which are generated cause upward acceleration of the fluid near the wire and cooler fluid from the bottom is brought upwards, cooling the wire faster than if there were conduction alone. It takes some time for this effect to become important by extending over a significant fraction of the wire length. However, eventually the flow pattern will extend over enough of the wire that its average temperature rise becomes significantly different from that characteristic of the pure conduction regime. At this instant the observed temperature rise of the wire, suitably corrected for other effects, will depart from that of the ideal model. Under these circumstances the linearity between ΔT vs Ln t is not preserved.

The problem of transient, natural convection in a finite cyclindrical geometry is not amenable to rigorous analysis, although there have been a number of approximate studies [9,10,15,32,33]. In the most recent of these Goldstein and Briggs [34] obtained an estimate for the height of penetration, Z_c, of the cool fluid up the heated wire. From this it is possible to deduce an approximate upper bound to the time, t_c, in which useful thermal conductivity measurements can be performed. Allowing ℓ' to be the length of wire over which the

three-dimensional flow pattern may extend before significant effects from convection are observed, we obtain [34]

$$t_c \simeq \left(\frac{\ell'\lambda}{0.32G\beta q}\right)^{\frac{1}{2}} \qquad (2.20)$$

where G is the gravitational constant, β the coefficient of thermal expansion of the fluid and q the radial heat flux.

The transient flow pattern of natural convection in a hot-wire cell has been visually observed in liquids by Pantaloni et al.[35]. Their observations confirm the unicellular flow pattern of the Goldstein and Brigg analysis. They suggest an alternative, heuristic correlation for the characterstic time at which convective motion exerts a significant effect on the observed temperature rise of the wire,

$$t_c^{3/2}\,\mathrm{Ln}\left(\frac{4\kappa t}{a^2 C}\right) = 380\ \mathrm{Pr}\ \kappa^{\frac{1}{2}}\left(\frac{\lambda}{\beta G q}\right) \qquad (2.21)$$

which, it should be noted, is independent of the geometry of the cell in accord with their observations. In equation (2.21) Pr is the Prandtl Number.

Neither of the criteria for t_c, (2.20) and (2.21), should be regarded as definitive; rather they can be used as rough guides for design of the time scale within which transient hot-wire thermal conductivity measurements may be performed. Typically, these limiting times are of the order of several seconds for gases and liquids. In practice, as has already been noted, the occurence of a significant

effect from natural convection in a measurement is easily discerned by a departure from linearity of the ΔT_{id} vs Ln t plot. Measurements in which such a curvature exists must be discarded.

A further dynamic effect arises as a result of the temperature dependence of the fluid density. As the heated layer of fluid near the wire expands it performs compression work on the remainder of the fluid in a container of fixed volume V, and so modifies the temperature history of the wire. An approximate analysis of this effect in gases has shown that the modification to the ideal temperature rise takes the form [23]

$$\Delta T_{id} = \Delta T_w + \delta T_c \tag{2.22}$$

where

$$\delta T_c = \frac{q \ell R t}{\rho C_p C_v V} \tag{2.23}$$

with R being the universal gas constant, V the volume of the containing vessel and ℓ the length of the wire. C_p and C_v are the heat capacities of the fluid at constant pressure and constant volume respectively. The correction may be rendered negligible by employing a sufficiently large container for the gas [23]. In the case of liquids, this effect can be neglected completely because of the much lower compressibility.

Aside from the effects brought about by the variable density of the fluid, it is necessary to account separately for the variation of

the thermal conductivity λ and the product ρC_p. Since the temperature rises employed in the measurements are only a few degrees Kelvin, an analysis based upon a linear expansion of these properties about their values at the equilibrium state of the fluid may be employed [23]. The principal result of the analysis is that the basic form of equation (2.9) is unchanged

$$\Delta T_{id} = \frac{q}{4\pi\lambda(T_r,\rho_r)} \text{Ln} \left(\frac{4\kappa t}{a^2 C}\right) \qquad (2.24)$$

However, the thermal conductivity, $\lambda(T_r)$, obtained from the slope of the line relating ΔT_{id} to Ln t refers to a temperature T_r and a density ρ_r which differ from those of the equilibrium state. In fact, for measurements carried out in the time interval t_1 to t_2

$$T_r = T_o + \left[\frac{\Delta T_{id}(t_1) + \Delta T_{id}(t_2)}{2}\right] \qquad (2.25)$$

and

$$\rho_r = \rho(T_r,P) \qquad (2.26)$$

since the pressure, P, is essentially unaltered during the measurement.

(4) The finite length of the wire

The wire in a practical thermal conductivity cell must be supported in the test fluid by relatively massive connections at either end. Because the heat flux is generated by electrical dissipation in

the wire itself, there will exist a longitudinal, conductive heat flux in both the wire and the fluid. As a result, the longitudinal temperature profile in the wire at any instant will not be uniform along its length. The resistance of the entire wire is not then an accurate measure of the temperature in a central section far removed from its ends. It is not possible to analyse this problem rigorously, although approximate calculations have been performed [21,23]. These calculations yield the minimum length of wire necessary to ensure that at least a central section of the wire behaves as if it were a finite section of an infintely long wire within a specified tolerance. Typically, for wires with a radius of several microns, the minimum length amounts to a few centimetres. It is then necessary to remove from the measurement the effects at the ends of such a wire by experimental means, and to observe the temperature rise of only the central section. The methods whereby this is achieved will be described later (see 3.4.1).

(5) Radiation (Transparent Medium)

In deriving the working equation (2.9), it was assumed that heat transfer occured purely by conduction. In practice, however, simultaneous conductive and radiative heat transfer occurs through the test fluid, but, provided the fluid is transparent and the temperature rise is small (~ 5K) then the error induced due to radiation can be shown to be negligible .

Assuming the fluid to be transparent, the radiative heat flux at the surface can be represented as:-

$$Q_r = A_a E_a F_{ab} - \alpha A_b E_b F_{ba} \qquad (2.27)$$

where A,E refer to the surface area and emissive power of the surface

of the wire (a) and the surface of the cell (b) respectively. α is the absorptivity of the cell.

Using reciprocity the view factor F_{ba} is found as:-

$$F_{ba} = \frac{A_a}{A_b} F_{ab} = \frac{A_a}{A_b} \tag{2.28}$$

with $F_{ab} = 1$. (2.29)

Hence:- $$Q_r = A_a(E_a - \alpha E_b) \tag{2.30}$$

or $$q_r = 2\pi a(\varepsilon \sigma T_a^4 - \alpha\sigma T_b^4) \tag{2.31}$$

where ε is the emissivity of the wire, σ the Stefan-Boltzman constant. If we assume:-

$$\varepsilon \simeq \alpha \tag{2.32}$$

then:-

$$q_r = 2\pi\ a\ \varepsilon\ \sigma\ (\ T_a^4\ -\ T_b^4) \tag{2.33}$$

$$\simeq 8\pi\ a\ \varepsilon\ \sigma\ T_o^3\ \Delta T(a,t) \tag{2.34}$$

and from equation (2.9):-

$$\frac{\delta T_R}{\Delta T} = \frac{q_R}{q} = \frac{8\ \pi a\ \varepsilon\ \sigma\ T_o^3}{q}\ \Delta T(a,t) \tag{2.35}$$

The resulting correction is negligible in the present apparatus which

employs a 7 μm diameter wire; a temperature rise of less than 5 K; a heat input per unit length of wire of approximately $0.7 Wm^{-1}$ and steady state temperature, T_o, of 363K, these conditions corresponding to the worst encountered.

In the case of fluids which absorb and re-emit radiation, there has been until now no exact solution of the full integro-partial-differential equation governing simultaneous conduction and radiation. However, there have been a number of approximate treatments of the problem which indicate that the effects due to radiation are smaller in transient measurement apparati than in those operated at steady state [36,37,38]. Since the purpose of the present work is to perform thermal conductivity measurements with an accuracy of a fraction of 1%, it is clear that these approximate analyses are inadequate for the present purpose. Consequently, the problem of simultaneous conduction and radiation of absorbing fluids in a transient hot-wire apparatus is considered in detail in a separate section where a new, analytic solution will be given (see 2.4.3).

2.4 Radiation Effects in Absorbing Fluids

2.4.1 Historical

The treatment of radiative transfer in absorbing and emitting media is generally formidable. The basic difficulty arises through the effectively instantaneous spatial distribution of radiation which necessitates the use of integral equations for a precise formulation of the problem. In the presence of simultaneous conduction and radiation the integral equations are linked with the Fourier Law through the common temperature boundary conditions, the temperature dependence of the coefficient of emission of radiation and the absorption coefficient.

Solutions have been obtained for simplified one-dimensional versions of the problem, namely steady state transfer between infinite parallel plates at small temperature differences.

On a theoretical basis Leidenfrost using an analysis of Viskanta [39] concludes that in his measurements on toluene radiation can give rise to errors ranging up to 2 per cent, depending on wall emissivities and temperatures.

Poltz [36-38] has made a theoretical and experimental study of the case and concludes that the contribution of radiation to the effective conductivity can be as large as a few per cent at room temperature depending on the plate separation. He also suggested that errors of the same order of magnitude might be expected in measurements by the hot-wire technique.

The steady state pure radiation problem has been treated by Rhyming [40] who used the integral equation formulation and obtained numerical solutions and limiting solutions in closed form for the case of concentric black spheres. Concentric cylinders have been treated by Diessler [41] and Grief and Clapper [42] using the Rosseland diffusion approximation [43] extended by temperature jump boundary conditions.

According to the diffusion approximation the radiant heat flux at large optical depths is given by:

$$Q_r = - \frac{4\sigma}{3K_i} \, n^2 \frac{dT^4}{dr} \qquad (2.36)$$

with n being the refractive index, K_i the mean extinction coefficient and σ the Stefan-Boltzmann constant.

Where temperature changes are small we may linearise T^4 and write

$$Q_r = -\lambda_r \frac{dT}{dr} \tag{2.37}$$

where

$$\lambda_r = \frac{16}{3} n^2 \frac{\sigma T^3}{K_i} \tag{2.38}$$

and forms the radiative contribution to the effective thermal conductivity.

However, in the present work the optical depths of fluid in the cell are not sufficiently large for the diffusion approximation to apply. And although its range of validity may be extended by the use of temperature jump boundary conditions the method does not seem suitable in the present application, where the choice of boundary conditions has a dominant effect because of the small wire diameter.

The concentric cylinder problem has also been studied by Perlmutter and Howell [44], who used the Monte Carlo method. The technique is however, restricted to steady state pure radiative transfer.

Van der Held considered the problem arising from the radiation contribution to the conduction of heat in thermal conductivity measurements for solid materials [45, 46]. His analysis covered both the steady state case and the non-stationary case. However, his solutions applied only to specific, unrealistic cases. In particular, boundary conditions were left out of consideration in his solution for non-stationary problems.

Mani, Saito and Venart [47-49] analysed the problem for the line source method using a modified integral method. These authors divided

the absorbing fluid into three regions according to their optical density. The region next to the wire was treated as optically thin. The next region allowed simultaneous radiative and conductive heat transfer. The third region was considered as optically thick. The boundary between these regions were allowed to expand as the thermal wave spread from the line source outwards. The problem was solved with a combined finite-difference-integral technique. In short, this method is based on artificial assumption about the optical thickness of the medium at different radial positions. Furthermore, the necessary optical properties required for the solution need to be determined by independent methods which do not necessarily reproduce the conditions of measurement in a transient hot-wire instrument.

2.4.2 Numerical Solution

The most recent and most rigorous analysis of simultaneous radiation and conduction in a transient hot-wire instrument is provided by Menashe and Wakeham [50]. Their analysis is based on a numerical solution of the full energy equation describing the process. For a transient hot-wire instrument in which an isotropic grey fluid is bounded internally by a wire radius, r_1, area A_1 and externally by a surface radius r_2, area A_2, the equation governing the temperature rise of the wire is [50],

$$\rho C_p \frac{\partial T}{\partial t} = \lambda \nabla^2 T + Q'_{V \to dV_i} + Q'_{A_1 \to dV_i} + Q'_{A_2 \to dV_i} - 4K_i E_R \qquad (2.39)$$

Here, the second, third and fourth terms on the right represent

gradients of one-way radiant heat fluxes from, respectively, the entire volume of the fluid to a volume element dV_i, from the wire surface to the volume element and from the outer boundary to the volume element. The final term represents the gradient of the radiative heat flux emitted by the volume element dV_i in which K_i is the appropriate mean extinction coefficient of the fluid and

$$E_R = n^2 \sigma T^4 \qquad (2.40)$$

where n is the refractive index of the fluid and σ the Stefan-Boltzmann constant.

The appropriate boundary conditions for the solution of equation (2.39) are :

$$\frac{q}{2\pi r_1} = -\lambda\left(\frac{\partial T}{\partial r}\right)_{r=r_1} - \alpha_1 Q_{A_2 \to A_1} - \alpha_1 Q_{V \to dA_1} + \varepsilon_1 n^2 \sigma T^4_{(r_1)} \qquad r = r_1,\ t > 0 \qquad (2.41)$$

$$T(r_2,t) = T_o \qquad 0 \leq t \leq \infty \qquad (2.42)$$

together with the initial condition:

$$T(r,t) = T_o \qquad t \leq 0 \qquad (2.43)$$

Here dA_1 is an elemental area in A_1 and the second and third terms represent one-way radiant heat transfer flux gradients to this element

from the outer boundary surface and the bulk of the fluid. In addition, α_1 represents the absorptivity of the wire surface and ε_1 its emissivity.

Explicit expressions for the heat fluxes and gradients $Q'_{V\to dV_i}$, $Q'_{A_1\to dV_i}$ $Q'_{A_2\to dV_i}$, $Q_{A_2\to dA_1}$ and $Q_{V\to dA_1}$ are given by Menashe and Wakeham [50]. Each of these terms involve integration over the entire volume of the fluid or the entire surface of the inner or outer boundaries. The full form of the integro-partial differential equation (2.39) cannot be solved analytically. However, Menashe and Wakeham have developed a technique for its numerical solution subject only to the additional assumptions that the extinction coefficient is temperature independent over the small temperature range involved, that the outer bounding cylinder is black and that $\alpha_1 = \varepsilon_1 \neq f(T)$. The method of solution is detailed elsewhere [27]. The essential feature of the method involves converting the multidimensional integrals in the expressions for the radiant heat fluxes and gradients into algebraic series by means of a suitable quadrature procedure [51]. The application of the quadrature formulae reduces the energy equation (2.39) to a single partial differential equation which has been solved by the Method of Lines [52]. The method involves the coversion of the partial differential equation to a set of coupled ordinary differential equations. The coupled ordinary differential equations are integrated using an algorithm developed by Gear [53] and Hindmarsh [54], which allows both variable order of integration and variable step size. Because the evaluation of each of the radiant heat fluxes and

their gradients requires the computation of a two or three dimensional integral at each time step the numerical solution is both time consuming and expensive. Thus, although it has been possible to implement the numerical procedure in a number of specific cases and to compare its results with those in which there is no radiation effect, it has not been possible to apply it universally [50]. Furthermore, in order to apply the technique to measurements in fluids over a wide range of conditions, both the emissivity of the wire ε_1, and the extinction coefficient of the fluid must be known over the same range of conditions. In practice, this information has never been available and values characteristic of just one set of conditions have had to be employed [50].

2.4.3 Analytic Solution

An alternative and new use of the numerical solution, which is investigated in this work, is as a guide to the relative magnitudes of the various terms within the governing equation (2.39). The aim of such a study is the simplification of equation (2.39) to a level where it may be solved analytically. To this end we have employed the numerical procedures of Menashe and Wakeham [50] to simulate a transient hot-wire measurement on toluene using apparatus parameters characteristic of our equipment and representative properties of the pure liquid. All of the quantities employed in the simulation are set out in Table (2.1), including the extinction coefficient K, which was determined experimentally in the manner described elsewhere [50].

Figure 2.3 contains plots of the relative magnitudes of the terms on the right-hand side of equation (2.39) as a function of time at two different radial locations in the fluid, omitting the term $Q_{A_2 \to dV_i}$

which is rendered zero by condition (2.41) [50]. Figure 2.3(a) refers to a radius $r=1.02r_1$ and figure 2.3(b) to a radius $r=115r_1$. In each case it is apparent that the dominant additional contribution to the conduction heat-flux gradient arises from the emission of radiation by the fluid and that both of these terms exceed those arising from absorption by several orders of magnitude. The only exception to this situation arises in figure 2.3(b) at short times, when each of the terms is so small as to be insignificant and the numerical solution is inaccurate. The implication of these results, which are typical of other simulations we have carried out, is that we may neglect the term $Q'_{V\to dV_i}$ and $Q'_{A_1\to dV_i}$ in equation (2.39). Physically, this means that in the transient hot-wire experiment, the principal radiative contribution of the fluid to the heat transfer process arises from emission and not absorption as has frequently been assumed. This result may be understood by noting that the gradient of the radiant heat flux in an emitting volume element is determined by the local temperature gradient, and that in the transient hot-wire instrument the wire is so thin ($r_1 \simeq 3.5\mu m$) that although the temperature rise of the fluid is only a few degrees Kelvin its radial temperature gradient is very large near the edge of the expanding temperature front arising from conduction. On the other hand, because the absorption terms are determined by the value of the extinction coefficient, which is temperature independent, their gradients are considerably smaller.

These observations enable equation (2.39) to be considerably simplified, so that writing

TABLE 2.1

Parameters employed for the simulation of a measurement on toluene

Temperature, T	360K
Hot-wire radius, r_1	3.89 μm
Cell radius, r_2	4.95 mm
Heat Flux, q	0.538 Wm^{-1}
Thermal Conductivity, λ	113.7 $mWm^{-1}K^{-1}$
Density, ρ	802.9 kg m^{-3}
Heat Capacity, C_p	1904.0 J $kg^{-1}K^{-1}$
Mean extinction coefficient, K	4630 m^{-1}
Refractive index, n	1.4961

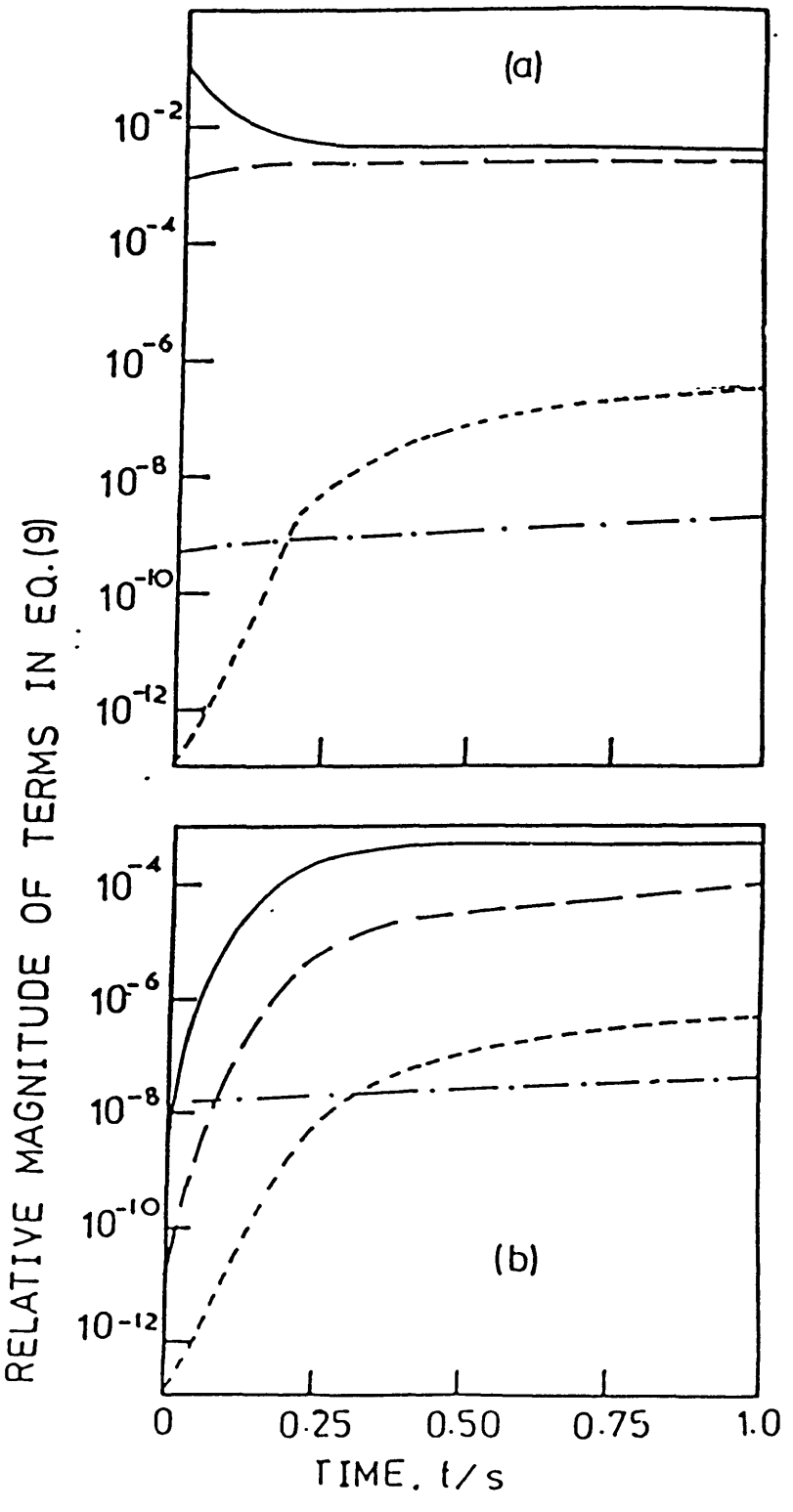

Fig. (2.3) Relative magnitude of the terms on the right hand side of Equation 2.39 as a function of time at two different radial coordinates: 2.3(a) r= 1.02 r_1 and 2.3(b) r= 115 r_1.

——— Conduction , — — — Emission

------- $Q_{V \rightarrow dV_i}$, —·—·— $Q_{A_1 \rightarrow dV_i}$

$$\theta = \frac{(T - T_o)}{T_o} = \frac{\Delta T}{T_o}$$

and $$R = \frac{r}{r_1}$$

we obtain

$$\frac{\partial \theta}{\partial t} = \frac{\lambda}{\rho C_p r_1^2} \left[\frac{\partial^2 \Theta}{\partial R^2} + \frac{1}{R} \frac{\delta \Theta}{\delta R}\right] - \frac{16 Kn^2 \sigma T_o^3 \Theta}{\rho C_p} \qquad (2.44)$$

in which we have made use of the definition of E_R, equation (2.40) and employed the linearisation

$$T^4 - T_o^4 = 4T_o^4 \Theta$$

which is justified for the small temperature rises employed in practice.

An analytic solution of equation (2.44) may now be attempted, but this is most easily accomplished by returning to the simplest model of the apparatus in which the heat source is vanishingly small and the outer boundary is situated at infinity. This is consistent with the approach adopted for other corrections to the ideal model in which all the departures of the real system from the ideal are treated as small, additive effects [23]. Using the fact that the radiation heat flux from the wire is negligibly small [23] the boundary conditions for equation (2.44) then become, following the same substitutions as before,

$$\frac{q}{2\pi T_o} = -\lambda \lim_{R\to 0} R\left(\frac{\partial\theta}{\partial R}\right) \qquad \text{at} \quad R = 0,\ t>0 \qquad (2.45)$$

$$\theta = 0 \qquad \text{at } R = \infty,\ t \geq 0 \qquad (2.46)$$

and

$$\theta = 0 \qquad \text{for} \quad t \leq 0 \qquad (2.47)$$

Equation (2.44) is most easily solved by the use of Laplace transform, denoted by a tilde, whose application leads to the equation

$$Z^2 \frac{d^2\tilde{\theta}}{dZ^2} + Z \frac{d\tilde{\theta}}{dZ} - Z^2\tilde{\theta} = 0 \qquad (2.48)$$

with the boundary conditions

$$\lim_{Z\to 0} Z\left(\frac{d\tilde{\theta}}{dZ}\right) = -\frac{q}{2\pi\lambda s T_o} \qquad (2.49)$$

and $Z = \infty$, $\tilde{\theta} = 0$ (2.50)

Here, $$Z = \left(\frac{s + B}{A}\right)^{\frac{1}{2}} R, \qquad (2.51)$$

where s is the Laplace transform viable

$$A = \frac{\lambda}{\rho C_p r_1^2} \qquad (2.52)$$

and

$$B = \frac{16Kn^2\sigma T_o^3}{\rho C_p} \tag{2.53}$$

The solution of equation (2.48) is [55]

$$\tilde{\theta} = C_1 I_o(z) + C_2 K_o(z) \tag{2.54}$$

where I_o and K_o are modified Bessel functions. By virtue of the boundary condition (2.50) and the properties of I_o [55] this becomes

$$\tilde{\theta} = C_2 K_o(z) \tag{2.55}$$

and from condition (2.49) we obtain

$$\tilde{\theta} = \frac{q}{2\pi\lambda s T_o} K_o(z) \tag{2.56}$$

The inverse of the Laplace transform may be found by application of the convolution theorem and standard inverse transforms [55] so that

$$\tilde{\theta} = -\frac{q}{4\pi\lambda T_o} \int_{\infty}^{R^2/4At} e^{-BR^2/4Au} \left(\frac{e^{-u}}{u}\right) du \tag{2.57}$$

We now recognize that B is a measure of the contribution of radiant emission by the fluid to the heat transfer process, and that $BR^2/4Au \lesssim 0.1$, even in the simulated case of toluene. Consequently, to obtain a first order estimate of the effect of radiation we may expand the first exponential in the integral of equation (2.57) and carry out the integrations to yield the temperature rise in the form

$$\Delta T = \frac{q}{4\pi\lambda} \sum_{n=1}^{\infty} \frac{(-1)^{n-1}}{(n-1)} (Bt)^{n-1} \; E_n\left(\frac{r^2}{4\kappa t}\right) \qquad (2.58)$$

where [55]

$$E_n(\zeta) = \int_1^{\infty} \left(\frac{e^{-\zeta u}}{u^n}\right) du \qquad (2.59)$$

By means of expansion of the exponential integrals E_n [55] we finally obtain for the temperature rise at $r = r_1$

$$\Delta T = \frac{q}{4\pi\lambda} \left[1 + \frac{Br_1^2}{4\kappa}\right] \text{Ln} \left(\frac{4\kappa t}{r_1^2 C}\right)$$

$$+ \frac{Bqr_1^2}{16\pi\kappa\lambda} - \frac{Bq}{4\pi\lambda} t + O\{(Bt)^2 \, , \; r_1^2/4\kappa t\} \qquad (2.60)$$

By comparison of this result with that of equation (2.9), it is possible to discern a radiation correction, δT_{rad}, which, if added to the temperature rise which is observed in the presence of radiation

recovers $\Delta T_{id}\ (r_1,t)$ of the ideal model.

Therefore,

$$\Delta T_{id} = \Delta T + \delta T_{rad} \tag{2.61}$$

$$\delta T_{rad} = -\frac{qB}{4\pi\lambda}\left\{\frac{r_1^2}{4\kappa}\ \mathrm{Ln}\ \left(\frac{4\kappa t}{r_1^2 C}\right) + \frac{r_1^2}{4\kappa} - t\right\} \tag{2.62}$$

In the absence of any radiation effect the thermal conductivity is derived from the slope of the experimentally observed linear relationship between the temperature ΔT and Ln t. Equation (2.60) makes it clear that radiant emission from the fluid yields a relationship which is no longer linear, but is curved, concave to the Ln t axis. Furthermore, the slope of the linear portion of the relationship is altered and a shift of ΔT vs Ln t line along the ΔT axis is produced. So far as the derivation of the thermal conductivity is concerned the shift is of no significance, however, the remaining two effects are potentially important.

In order to confirm that the analytic solution of the conduction - radiation problem is consistent with the numerical solution we have compared the temperature rises calculated in the two ways using the data given in Table (2.1). For this purpose we have added the small correction owing to the finite outer boundary (see 2.3 and 2.5) to the analytic solution in order that the two solutions refer to the same model of the instrument. The comparison is presented in the form of a plot of the deviations between the two solutions in Figure 2.4. It can

Figure 2.4 The deviations between the numerical and analytic solutions of the radiation-conduction problem

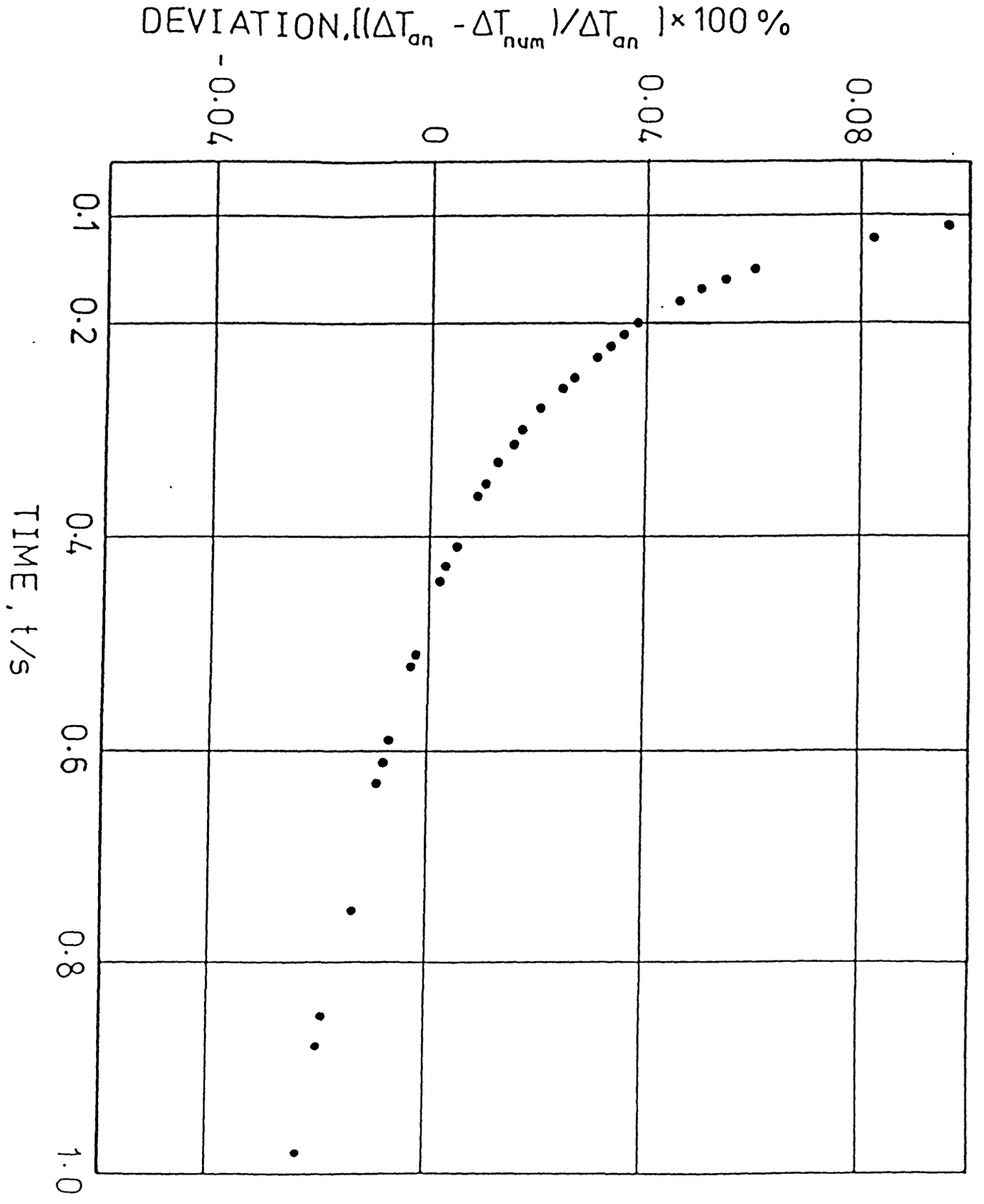

be seen that the deviation does not exceed ±0.1%, its systematic nature being merely a combined result of the small terms neglected in the analytic solution and the limited accuracy of the numerical solution.

The advantages to be gained from an analytic solution of the conduction-radiation problem are twofold. First, the experimental measurements of the temperature rise of the wire may themselves be used to ascertain whether radiation contributes significantly to the measurement process. Thus, if the measured temperature rise of the wire, ΔT_w, corrected for all other effects according to equation (2.9) does not conform to a linear equation in Ln t, it is likely that there is a significant radiation contribution. In such cases, if it can be established that there is no convective contribution to the measurement process, a value for the radiation parameter, B, may be estimated by fitting ΔT to the full form of equation (2.60). The derived value of B may then be employed to evaluate the correction δT_{rad} for each data point, and the radiation-free thermal conductivity evaluated from the slope of the linear relationship between ΔT_{id} and Ln t.

The radiation parameter, B, evaluated in this manner is, of course, considerably more reliable than one deduced from independent, spectrophotometric measurements because it is the directly relevant parameter rather than one deduced from a series of assumptions about the optical characteristics of the fluid [50]. Moreover, the parameter may be determined for each set of experimental conditions.

The second advantage of the analytic solution of the problem is that it is also possible to discern when the radiation contributions

to the measurement are negligible. If the experimentally observed temperature rise, ΔT, defined by equation (2.9) is a linear function of Ln t, it is possible to assert that the term $(Bqt/4\pi\lambda)$ in equation (2.60) is negligibly small by comparison with the term proportional to Ln t. Equation (2.60) may be written in the form:-

$$\Delta T = C_1 + C_2 \cdot \text{Ln } t + C_3 . t \qquad (2.63)$$

in which the coefficients providing the best representation of a set of ΔT versus t points obtained experimentally may be determined by a non-linear least squares procedure. As an example of the results produced we have fitted the results of a measurement on toluene at 360K and 3.2 MPa to an equation of the form of (2.63). The coefficients deduced, together with their standard deviations are listed in Table (2.2). The coefficients C_1 and C_2 have a statistical uncertainty small by comparison with their actual value. On the other hand the coefficient C_3 has a statistical uncertainty almost as large as the value itself. On the basis of this and other similar calculations we may conclude that the coefficient C_3 (and hence the term with which it is associated) is not statistically significant. This illustrates that there is no significant contribution from radiation to the measurement of thermal conductivity in the liquid. For each measurement reported here a similar examination of the data was performed to confirm the absence of a significant radiative component in the measured heat flux.

Table 2.2

Coefficients of the statistical fit to equation (2.63)

	Coefficients	Standard deviation
C_1	3.5341	$\pm$ 0.29 x 10^{-2}
C_2	0.3779	$\pm$ 0.14 x 10^{-2}
C_3	-0.353×10^{-2}	$\pm$ 0.33 x 10^{-2}

Also, it has been confirmed that for our instrument

$$\frac{Br_1^2}{4\kappa} < 10^{-5} \qquad (2.64)$$

So that the thermal conductivity deduced from the slope of the line ΔT vs Ln t is the radiation-free value. As we show in figure (2.5) for toluene, and as we have found for all other liquids we have studied there is no evidence of any curvature in the line ΔT vs Ln t. We therefore conclude that the contribution of radiation to the measurement of thermal conductivity in a transient hot-wire apparatus of the type we employ is entirely negligible for these liquids.

Finally it should be emphasised that the arguments presented here are restricted to the transient hot-wire appartus. In other experimental methods, usually of a steady state type, the temperature

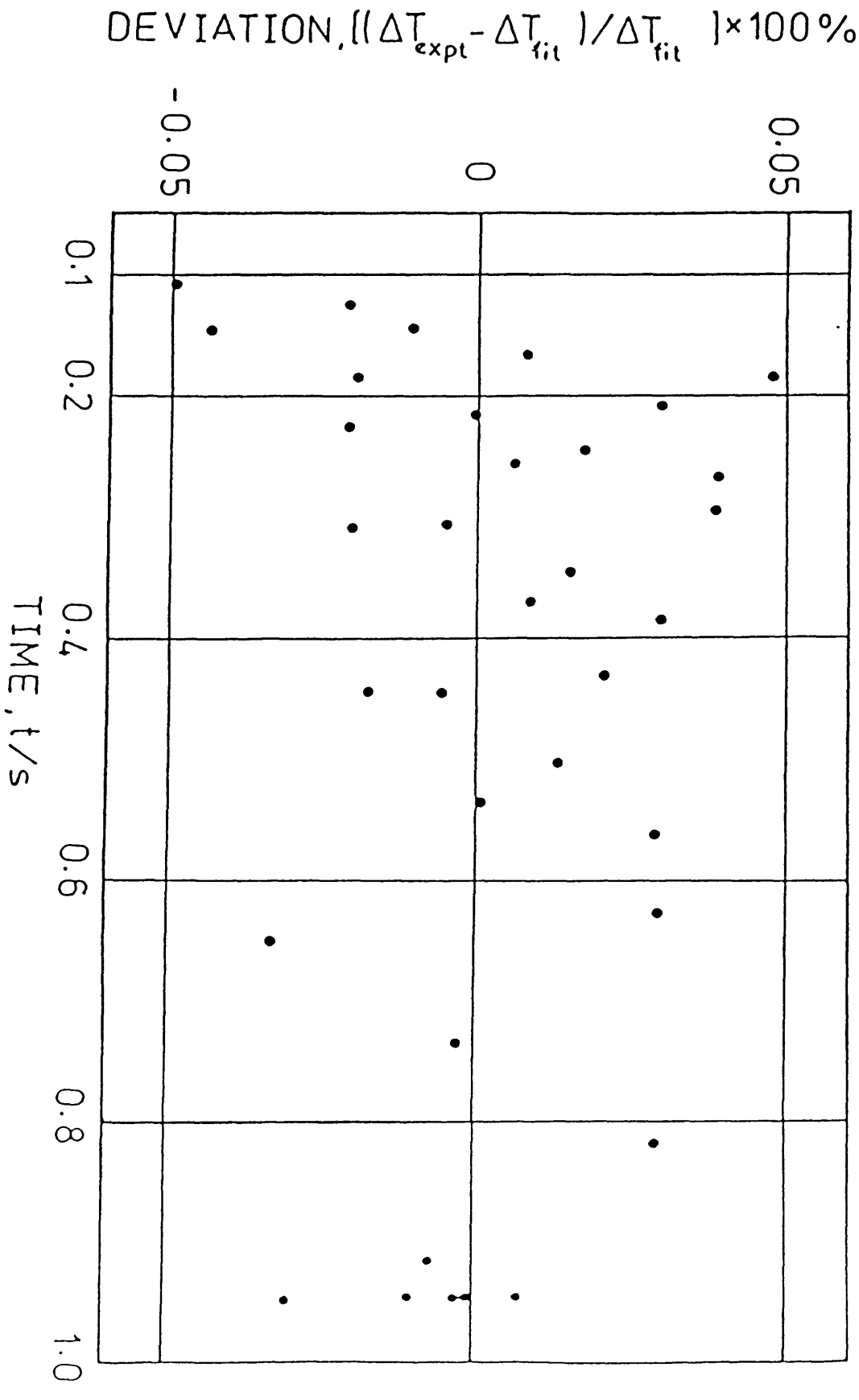

Fig. (2.5) Deviations of experimental values of ΔT from a linear fit to them

gradients involved are much smaller, so that it is not clear that a similar simplification of the problem of the influences of radiation in the fluid is possible.

2.5 Summary of Corrections

In summary, in a transient hot-wire experiment the thermal conductivity of a fluid is obtained from measurements of the temperature history, $\Delta T_w(t)$, of a central section of a wire of radius a, which acts as a source of heat flux, q, per unit length. The thermal conductivity at a thermodynamic state $(T_r, \rho_r, \underline{x})$ is derived from such measurements by application of the working equation

$$\Delta T_{id} = \Delta T_w + \sum_i \delta T_i = \left[\frac{q}{4\pi\lambda_{(T_r,\rho_r,\underline{x})}}\right] \; Ln\left(\frac{4\kappa_o t}{a^2 C}\right) \qquad (2.65)$$

where T_r is given by equation (2.25) and ρ_r the corresponding density at the equilibrium pressure P. In a properly designed instrument, operating under well chosen conditions, the corrections to be applied to the measured temperature rise can be reduced to just two, δT_1 for the heat capcity of the wire and δT_2 for the finite outer boundary of the cell. These two corrections may themselves be rendered small by design.

The combined effect can be taken as additive. Hence

$$\Delta T_{id} = \Delta T_{(t)} + \delta T_1 + \delta T_2 \qquad (2.66)$$

where from (2.16):-

$$\delta T_1 = \frac{a^2}{2\lambda T} \left[(\rho C_p)_w - (\rho C_p) \right] \Delta T_{id} \qquad (2.67)$$

and from (2.19):-

$$\delta T_2 = - \frac{q}{4\pi\lambda} \left\{ \mathrm{Ln} \left(\frac{4\kappa t}{b^2 C} \right) + \sum_{\nu=o}^{\infty} e^{-g_\nu^2 \kappa t / b^2} \left[\prod_{\nu} Y_{o(g_\nu)} \right]^2 \right\} \qquad (2.68)$$

The range of thermodynamic states and the operational zone for which the working equation (2.65) is appropriate is illustrated schematically in Figure 2.6, which shows the exclusion of low densities by temperature jump effects, long times by the influence of natural convection and short times by virtue of the excessive magnitude of the heat-capacity correction.

In principle, according to equation (2.65), the thermal conductivity could be deduced from just one measurement of a pair of temperature versus time coordinates. However, an evaluation in this manner would require an accurate knowledge of the wire radius, and the thermal diffusivity of the fluid as well as all of the time dependent and time-independent corrections mentioned earlier, since they contribute to the absolute value of the temperature rise. Moreover, because equation (2.65) represents only an assymptotic form of the full solution for the temperature rise, the complete solution in the form of the exponential integral solution would have to be employed. On the other hand, if the thermal conductivity is determined from the slope of the line constructed from many pairs of temperature rise-time points the only additional information required to evaluate the thermal

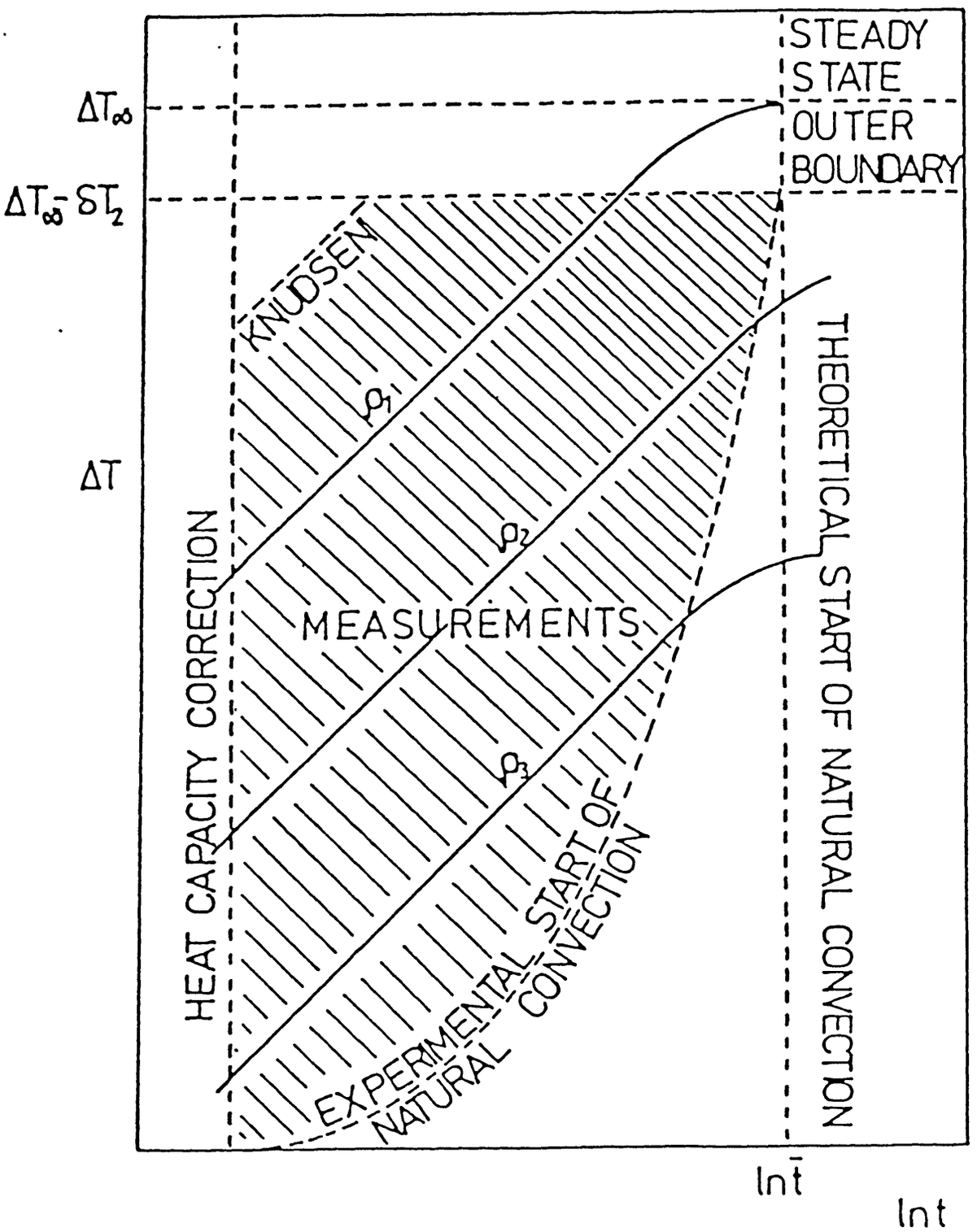

Fig. (2.6) The operating range of the transient hot-wire instrument.

conductivity is the heat flux from the wire. Moreover, the observation of the evolution of the temperature rise of the wire provides the opportunity to establish that the instrument operates in accord with the mathematical model for it, since only in this case will the time dependence of the temperature rise in (2.65) be preserved. For similar reasons, the method is not suitable for the determination of the thermal diffusivity of fluids which may only be evaluated from the absolute value of the temperature rise. Furthermore, the thermal diffusivity is exponentially dependent on the measured temperature rise so that the precision of its determination is naturally worse than that of the thermal conductivity for the same precision in the temperature measurement. A discussion of the experimental determination of the thermal diffusivity and the associated difficulties are given in more detail in appendix 1.

CHAPTER 3

APPARATUS DESIGN AND USE

3.1 Introduction

This chapter describes the application of the transient hot-wire method to the accurate measurement of the thermal conductivity of electrically insulating liquids within the temperature range 300-360K and the pressure range 0.1-700 MPa. The design of the equipment both mechanical and electrical has been such as to produce an apparatus which conforms as closely as possible to the mathematical model analysed in Chapter 2. The resulting instrument has a precision of ±0.2% in the thermal conductivity measurements. The merit of the present work is that the accuracy of the experimental results obtainable is greatly improved over any other previous measurements due to an improved treatment of the radiation contribution to the measurement process as discussed in 2.4. An estimated accuracy of ±0.3% in the thermal conductivity can be obtained using the present instrument.

A detailed description of the design and construction of the apparatus is given elsewhere [27]. Therefore only the essential components are discussed here. In the following sections, the description of the cell, the pressure system, the temperature control system and the electronic apparatus will be given, together with the working equations used in analysing the data. The experimental procedure will also be described, and finally the method of handling and processing the data will be discussed.

3.2 The Hot-Wire Cells

A schematic diagram of the hot-wire cells is given in Figure 3.1. The cell employs two wire heat sources, differing only in length, mounted within two cylindrical compartments contained within a stainless steel cylinder (type EN 85-M), 23.5cm long and 25mm in diameter. The cell was made up from two hemicylindrical sections. The fixed half of the steel cylinder (1) carries the cell top (2) which connects the cell to the pressure vessel plug; and the terminal posts (3) and (4), which provide mechanical support for and electrical connections to the two platinum wires (5) of the cell. The removable half of the cell (6) forms a cover and provides a cylindrical outer surface for both cells when fixed in position. A plan view of the complete cylinder assembly in figure 3.1 shows the channels (7) and (8) used to carry platinum wire connectors (0.5mm diameter), insulated with glass tubing, from each of the terminal posts to the upper end of the cells.

The lower terminal post is fixed to the cell body through the stainless bushing (9). The terminal connection is provided by the stainless steel pin (4) which is insulated from the bushing (9) by glass washers (10) held in place by the threaded collar (11). At its upper end the terminal carries a threaded stainless steel cone (12) and a lock nut (13) which secure a platinum connection lead. The upper terminal post is constructed in a similar fashion, but is not fixed to the cell body. Instead the bushing (14) is screwed to the stainless steel cylinder (15) which holds the insulating washers in position. The steel cylinder (15) has a central thread which carries an adjustment screw (16) passing through a central hole in the top plate of the cell. The adjusting screw head is held against the top plate of the cell with the locating plate (17). The cylinder (15) also has two guide holes drilled in it

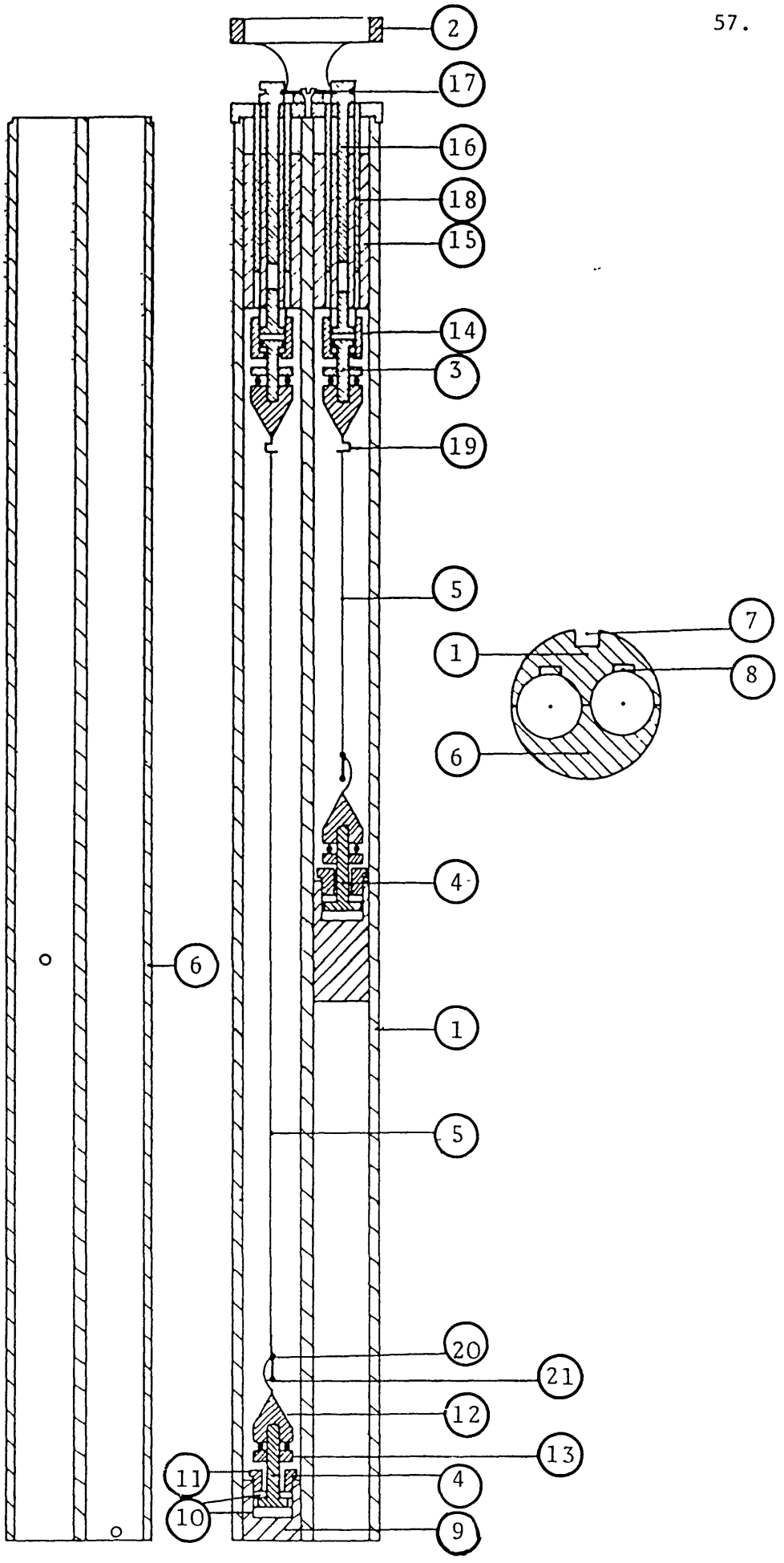

Fig. (3.1) The measurement cell

which accomodate two cylindrical pins (18) fixed in the top plate. As a result of this construction, rotation of the adjustment screw (16) causes a vertical movement of the terminal without its rotation and allows a total of 15mm vertical adjustment.

The hot wires of the cells are made from 7 μm nominal diameter platinum wire (purity >99.9%) supplied by the Sigmund Cohn Corp. At the upper terminal a platinum hook (19) (0.75mm diameter wire) is soldered to the gold tipped cone and the 7 μm platinum wire attached to it using gold as a solder. At its lower end the 7 μm platinum wire is attached to a gold sphere at one end of a cylindrical platinum weight of 50mg, (20). The upper end of the weight is electrically connected to the lower fixing cone by a loop of gold (21) attached at either end with a gold-tin solder. The loop (21) is manufactured by flatting a 2cm piece of 0.06mm diameter gold wire into a thin strip of 1mm width followed by annealling at 1270K. In this way, a lower electrical connection of small electrical resistance (0.15 - 0.20 Ω) is obtained which exerts no horizontal or vertical force on the lower end of the 7 μm platinum wire. The wire, therefore, hangs vertically and is subjected to a constant tension due to the weight, this tension being virtually independent of the thermal expansion of the elements of the cell at the various experimental temperatures used. In the present measurement, this tension in the wire amounts to approximately 10% of the yield stress of platinum. Furthermore, the electrical resistance of the various components providing electrical connection to the 7 μm platinum wires amounts to only 0.2 Ohm, which is small by comparison with the resistance of the long and short wires (≈ 450 Ohms and ≈ 160 Ohms respectively) so that a correction for this resistance may easily be applied.

After assembly of the platinum wires in the fixed half of the cell 1, the wires are annealed by passing an electric current through the wires, providing a power generation of approximately 85 watts/m of wire, for 1 hour, followed by a slow reduction of the current. Subsequently the length of the two 7 μm platinum wires are measured at room temperature with a cathetometer. The characteristics of the two thermal conductivity cells employed for the present measurements are listed in Table 1. The wire radius was determined by electron microscopy.

Table 3.1

Characteristics of the thermal conductivity cells

Internal diameter of the cell	9.90±0.01mm
Platinum wire radius	3.89±0.01μm
Long wire length at 310.8K	150.46±0.05mm
Short wire length at 310.8K	55.98±0.05mm
Long wire resistance at 310.8K,0.1 MPa	416.05±0.05ohm
Short wire resistance at 310.8K,0.1 MPa	155.84±0.05ohm
Platinum wire emissivity	0.037

The resistance-temperature characteristics of the wires have been determined by calibration as described elsewhere by Assael et al [56], at atmospheric pressure under conditions of constant, zero stress. These characteristics determined were found to be insignificantly different from those of pure platinum recommended for the

International Temperature Scale, of 1968 [57]. Owing to the weight suspended from the lower end of the platinum wires the thermal conductivity measurements are carried out with a constant, but non-zero, stress in the wire. The effect of imposed stress on the wire resistance amount to only 0.02% and the effect on the temperature coefficient is even smaller [27]. Consequently, no significant error is incurred by neglecting the effect of this imposed stress.

The resistance-temperature characteristic of the wires are also affected by the hydrostatic pressure to which they are subjected in the cells. This effect has been analysed [27] and the effect is represented by equation (3.7) in 3.4.

3.3 The High Pressure Equipment and Electronic Apparatus

A schematic diagram of the pressure vessel used is given in figure 3.2. The vessel itself (1) was manufactured by Pressure Products Inc. (U.K.) Limited from EN 25 Stainless Steel and has an internal diameter of 38.1 mm and internal length of 0.305 m. The vessel is sealed at its upper end by plug (2). At its lower end this plug carries a phosphor-bronze sealing ring (8) with a "V" groove machined into its circumference, as well as a teflon primary sealing ring (7). The sealing rings are held in place by the backing washer (9) and the retaining ring (10) screwed onto the plug. The plug is also fitted with four electrical feeds-through shown in the details of figure 3.1. They consist of Invar cones (4) lapped into ceramic cones (5) which themselves are lapped into the plug body. Electrial leads from the Invar cones pass through holes in the plug to the exterior of the vessel. At its lower end the pressure vessel is connected through high-pressure piping to a hydraulic pressurizing system. The thermal conductivity cell assembly of figure 3.1 is mounted on the pressure vessel sealing plug with the

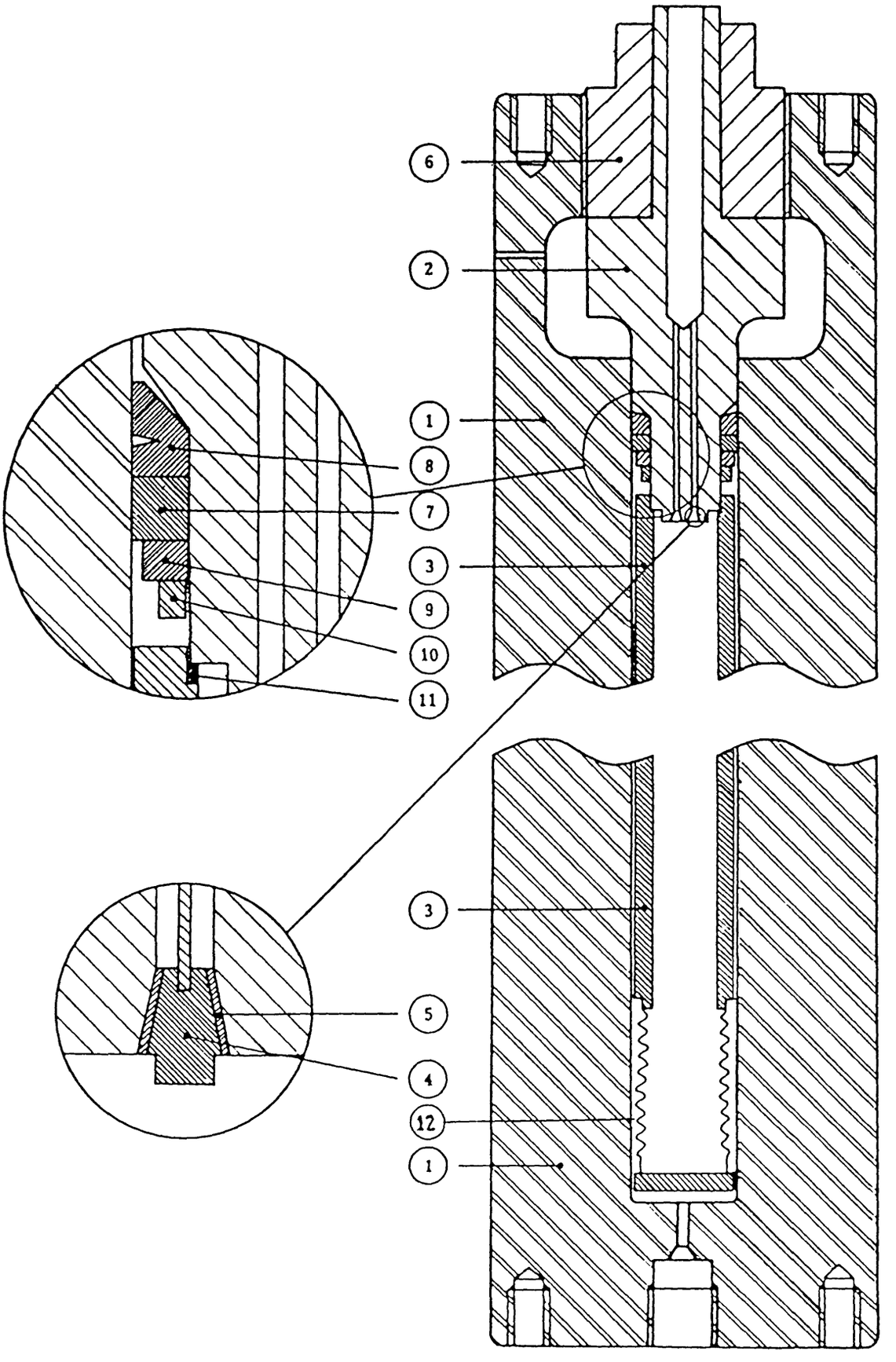

Fig. (3.2) The autoclave (including details of the plug)

aid of the threaded ring (2) shown at the top of the cells. The thermal conductivity cells are mounted within the cylindrical housing (3) of figure 3.2 which contains the liquid under test. The housing (3) is sealed to the pressure vessel cap by means of a lead gasket (11) At its lower end the housing carries a stainless bellows (12) The housing (3), containing the thermal conductivity cells, is filled with the test liquid under vacuum before insertion into the pressure vessel.

The autoclave is pressurised by the pressurising system, a schematic representation of which is shown in figure 3.3. The system consists essentially of a high and a low pressure side. The low pressure side is for pressurisation of the autoclave and high pressure side up to 200 MPa. After this initial pressurisation, the high pressure side, when isolated from the low pressure side by valve (9), pressurises the autoclave via an intensifier (6) from 200 MPa up to 700 MPa.

The specifications of the individual components of the pressurising system are listed below:-

(1) Pressure vessel (autoclave) made by Pressure Products Inc. (UK) limited and rated to 700 MPa working pressure

(2) Pressure Gauge made by Coleraine Instruments, Gallway, Ireland and calibrated up to 700 MPa with an accuracy of ±1 MPa at 700 MPa. (For calibration, see appendix 2 and reference 27)

(3) Vent valve, non rotating spindle, model no V1-110-100, made by Pressure Products Inc. and rated to 100,000 psi (700 MPa approx.)

(4) Pressure vessel isolation valve, model no 530.0432 Nova-Werke AG, and rated to 700 MPa

(5) 10,000 atm pressure gauge, made by Budenburg Gauge Company, accurate to ±1% of full scale deflection (for calibration, see

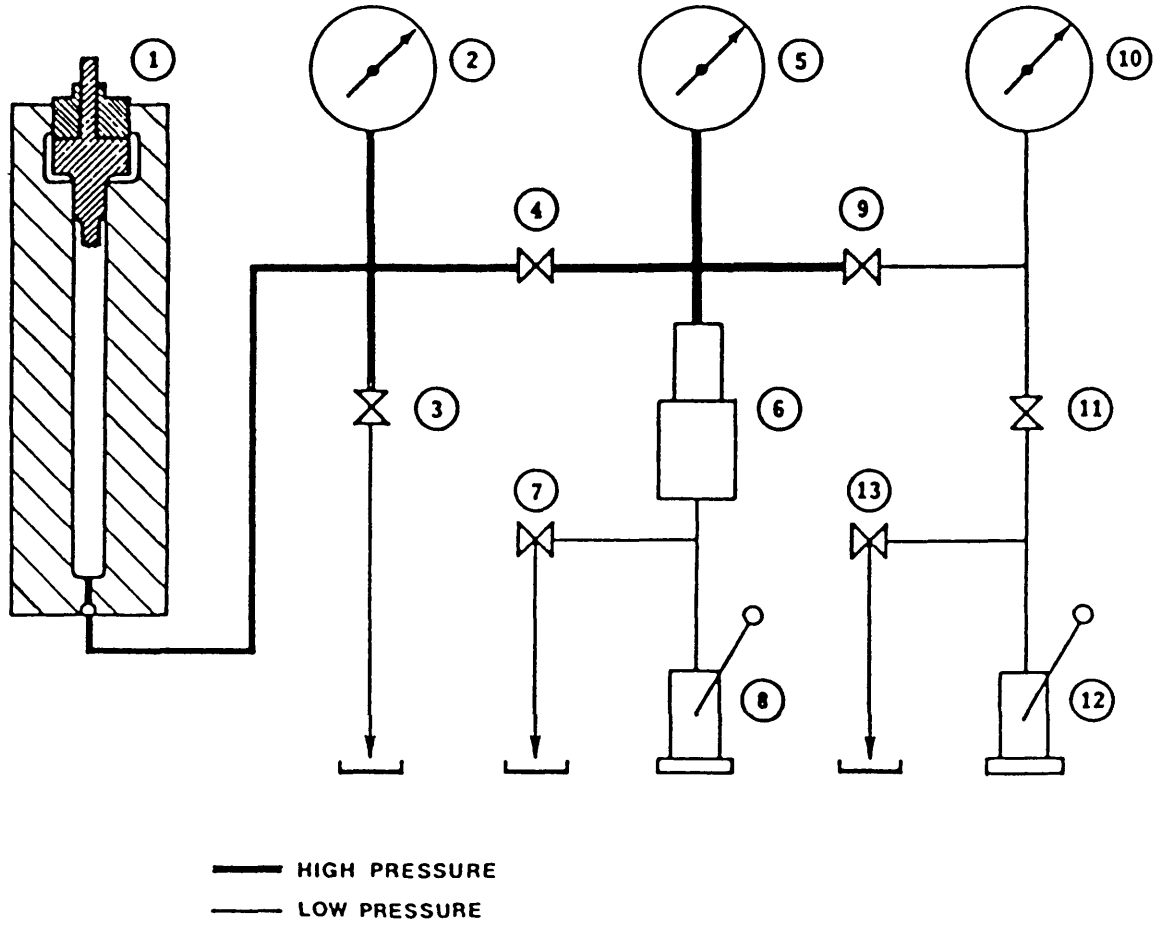

Fig. (3.3) The pressurising system

reference 27)

(6) Intensifier, model no A2.SJ, made by Harwood Engineering Co., USA, with intensification factor of 15 and rated to 200,000 psi (1400 MPa approx.)

(7) Let down valve, non-rotating, spindle type, model no. V-110-20, made by Pressure Products Inc. Ltd. and rated to 20,000 psi (150 MPa approx).

(8) Pressurising pump, hand-operated, stainless steel bodied, model no. HP-218, made by McCartney Manufacturing Co. USA, and rated at 60,000 psi(400 MPa approx.)

(9) High pressure isolation valve, specification as for (4)

(10) 40,000 psi Gauge, made by Budenberg Gauge Company, accurate to ±1% of full scale deflection (for calibration see reference 27)

(11) Low pressure isolation valve, non-rotating, spindle type, model no V-110-60, made by Pressure Products Inc. Ltd. and rated to 60,000 psi (400 MPa approx.)

(12) Pressurising pump, specifications as for (8)

(13) Let down valve, specifications as for (11)

The tubing used in the pressure line were ¼" and 5/16" O.D., 1/32" I.D. type 304 stainless steel seamless tubing supplied by Tube Sales Ltd.

The entire pressurising system, apart from the hand-operated pumps (8) and (12), is enclosed within, but electrically insulated from, a steel cabinet with ¼" thick mild steel plate sides. The reason for the system being insulated from the enclosing cabinet is that the electrical apparatus (described later, see 3.4) is sensitive to electrical noise induced by earth loops which would have otherwise

occurred.

The apparatus is pressurised by initially pumping on the low pressure side pressurising pump (12) until about 200 MPa pressure is attained within the system and autoclave. The low pressure side is then isolated using the isolation valve (9) and the further pressurisation is performed using pump (8).

The entire pressure vessel is suspended from a vibration-free mount within a well-stirred, thermostatically controlled oil bath. In order to maintain a slightly increasing temperature with height in the pressure vessel and thereby inhibit natural convective currents in the test fluid, a temperature differential of about 0.25^0C was maintained across the whole length of the pressure vessel by means of a small auxiliary heater. The temperature differential across the thermal conductivity cells was then only $\pm 0.05^0$C. Observation of the resistance fluctuations of the platinum wire immersed in the test fluid indicated that the variations in the temperature there amounted to no more than $\pm 0.02^0$C in a twelve-hour period. Because an entire measurement cycle extends over no more than 10 minutes this stability is more than adequate. It was confirmed in independent measurements that at equilibrium the temperature of the fluid in the pressure vessel differed by less than $\pm 0.1^0$C from that of the outer wall of the pressure vessel. Consequently the temperature of the test fluid in equilibrium was taken to be that measured with a calibrated platinum resistance thermometer element supplied by Degussa (for calibration see reference 27), which was in good thermal contact with the pressure vessel.

3.3.1 Electronic Apparatus

The purpose of the electronic components in the apparatus is

ultimately to determine the temperature rise of the platinum wires in the thermal conductivity cells as a function of time during their transient heating.

The two wires of the thermal conductivity cells are connected into two arms of a high precision automatic Wheatstone bridge. Figure 3.4 shows a schematic diagram of the bridge, shown in the configuration prior to measurement which is such that the total resistance of the upper right-hand arm exceeds that necessary for balance. Upon initiation of a measurement cycle the mercury wetted relay S_1 is connected to point Y and a current flows through the platinum wires. This current is used to provide a signal through S_2 and the capacitor C to start six timers operating on a 10 MHz clock. Subsequently relay S_2 is opened. Due to the current flow in the wires their resistances, R_ℓ and R_s, increase with R_ℓ, the resistance of the long wire, increasing more. This drives the bridge towards a balance, monitored by a high input impedance ($10^{11}\Omega$), high gain (4×10^6) comparator. At balance the polarity reversal at the comparator is used to stop the first of the timers and 3 ms later to open relay S_5 and so increase the resistance in the right-hand arm of the bridge. This operation throws the bridge out of balance again, from which state it approaches a new balance point owing to the continued heating of the platinum wire.

At this second balance point a further timer is stopped and relay S_6 opened. This process continues until six times of balance have

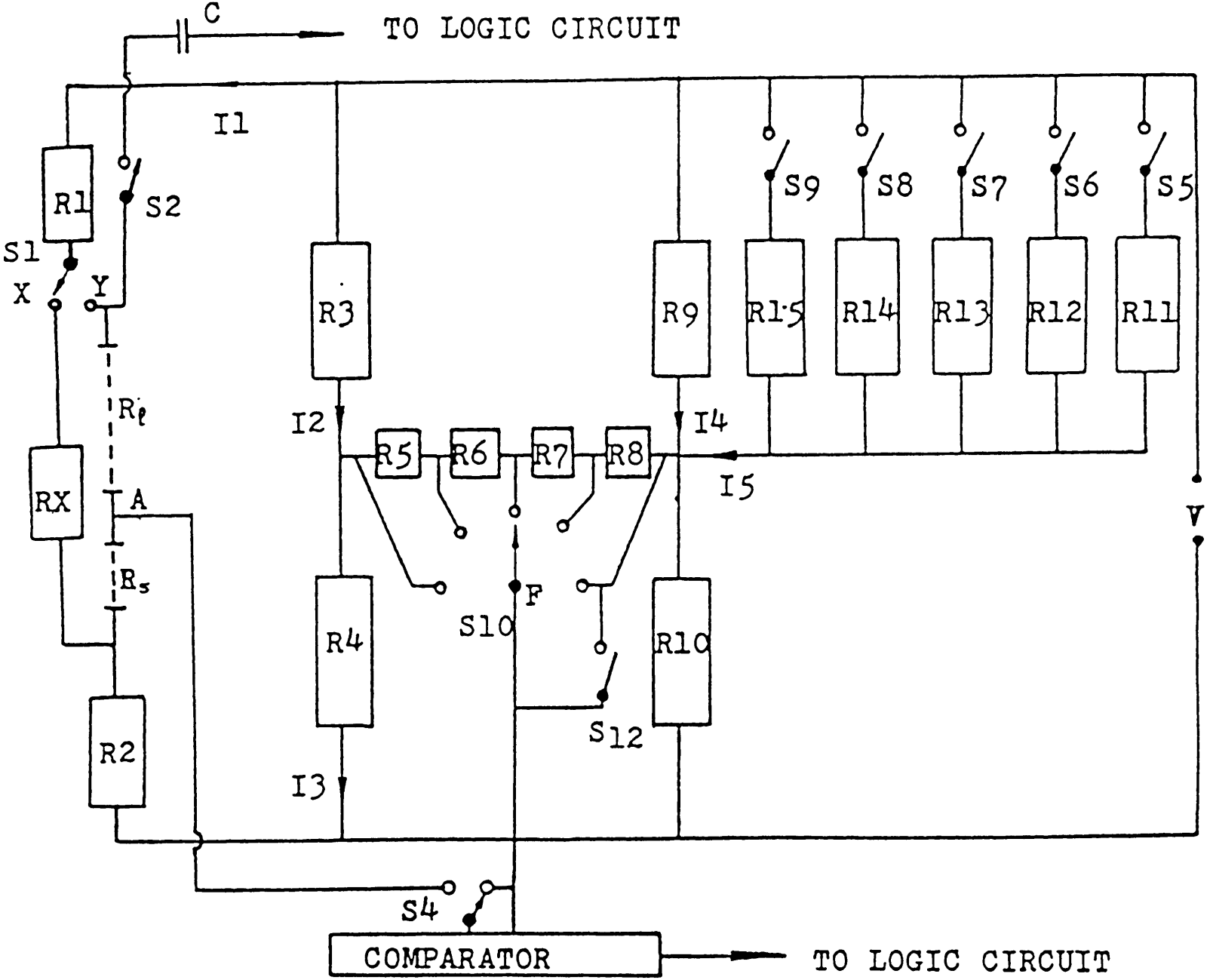

Fig. (3.4) The bridge circuit

been recorded when the bridge is automatically returned to its rest position. Figure 3.5 is a plot of the voltage across points A and B versus Ln (time) during a run. The regular distribution in Ln (time) is accomplished by suitable choice of the resistors in the bridge [58] and is desirable due to the form of the working equation 2.9, from which the known resistances of the bridge are sufficient to determine the resistance difference of the long and short wires at each recorded balance time (see 3.4.1). This cycle is repeated six to ten times for different bridge configuration to yield up to a hundred pairs of values of the resistance difference as a function of time for a particular thermodynamic state of a liquid sample. The total time for one single measurement cycle is usually maintained at one second so that, owing to the inertia of the fluid, convection effects have no influence on the heat transfer from the platinum wires (see 2.3).

The fixed resistors of the bridge are Vishay type HA412 metal-film resistors with a tolerance of ±0.001%. The variable resistors R_1 and R_2 are Vishay resistance boxes (type 1304) with a tolerance of 0.005%, whereas the resistors of the parallel arm $R_{11} - R_{15}$, are Muirhead type D805 wire-wound decade resistors with a tolerance of 0.001%. The power supply to the bridge consists of two Hewlett-Packard type 6112A d.c. power supplies connected in series with a stability and accuracy of ±0.01%. The centre point of the power supply is connected to a noiseless earth post embedded in the ground which provides the only earth for the entire system so as to eliminate electrical interference. The voltage resolution of the capacitor is ±20μV, which corresponds to a resistance resolution of ±0.002Ω. The resolution of the time

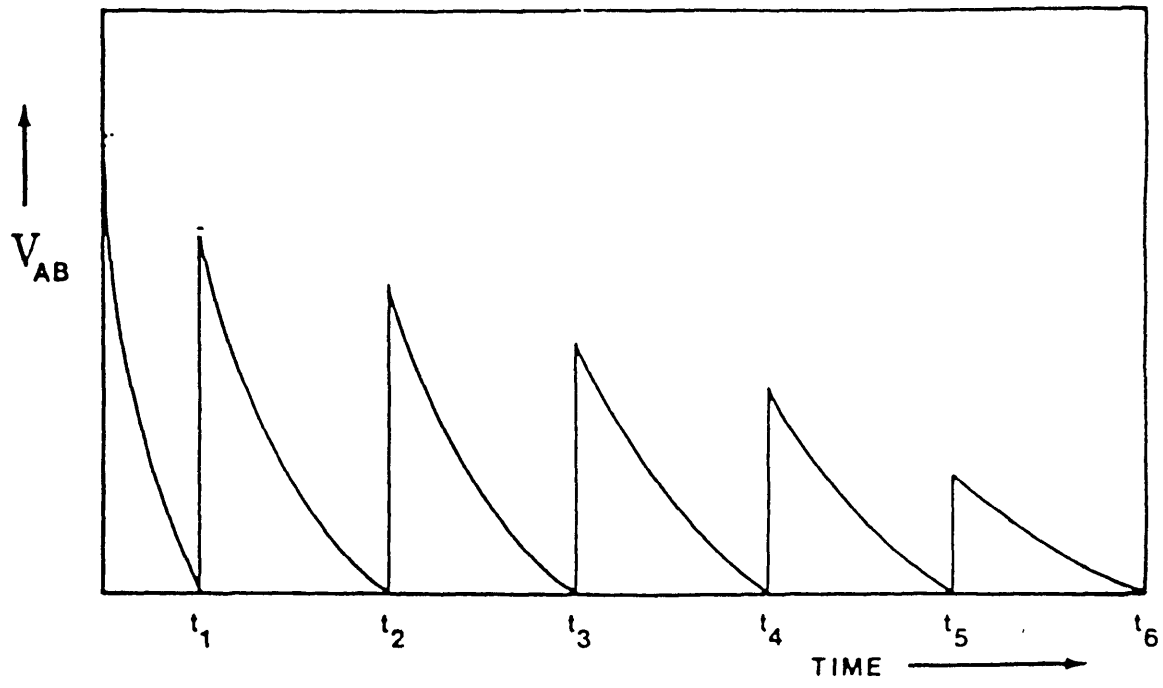

Fig. (3.5) The distribution of the balance points in time

measurements is ±0.1μs. In order to establish the absolute accuracy of the bridge for resistance measurements the resistance of a 50Ω resistor was determined by operating the bridge in a manual mode. The measured value departed by less than 0.01% from the calibrated value.

3.4 The Working Equations

3.4.1 The temperature rise of a finite segment of an infinite wire

The transient hot wire instrument used in this work employs two wire heat sources used in opposite arms of the automatic bridge to eliminate end effects caused by axial heat transfer through the wires to the terminals at their ends (see 2.3). Compensation to eliminate this effect is achieved by measuring the difference in resistance between the two wires. This would yield the temperature rise of the middle position of the long wire, provided the wires were identical apart from their lengths. If the wires were long enough, this temperature rise would differ from that occuring in a finite segment of a hypothetical infinitely long wire by a negligible amount. Unfortunately, in practice the wires are never identical due to, among other things, the non-uniformities in their radii. However, if the resistance per unit length of the two wires differ from each other by less than a few percent, their dissimilarities can be accounted for using an analysis by Kestin and Wakeham [24].

Ignoring all the temperature corrections arising from the non-ideal behaviour of the wire, which after all are small (see 2.3) then the temperature rises of the long and short wire are adequately described by:-

$$(\Delta T)_{\ell} = \frac{q}{4\pi\lambda} \text{Ln} \frac{4\kappa t}{a_{\ell}^2 C}$$

and

$$(\Delta T)s = \frac{q}{4\pi\lambda} \text{Ln} \frac{4\kappa t}{a_{s}^2 C}$$

The subscripts ℓ and s refer to the long and short wires respectively and the radius a_{ℓ} and a_{s} are suitable mean values for each wire.

With the automatic Wheatstone bridge of the type described in the previous section, the temperature rise of the long wire acting as a segment of an infinitely long wire, $(\Delta T)_{\ell}$, may be obtained from the equation [59]:

$$(\Delta T)_{\ell} = \frac{\Delta T'}{1+\varepsilon_3} \qquad (3.1)$$

where $\Delta T'$ is the experimentally measured quantity given as

$$\Delta T' = \frac{(R_{\ell} - R_s) - (R_{\ell}(T_o) - R_s(T_o))}{\alpha(T_o,S,P)\ (R_{\ell}(T_o) - R_s(T_o))} \quad , \qquad (3.2)$$

$$\varepsilon_3 = \frac{R_s(T_o)}{R_{\ell}(T_o) - R_s(T_o)}\ \varepsilon_2 \quad , \qquad (3.3)$$

$$\varepsilon_2 = \frac{\varepsilon\left[\ 1 + \mathrm{Ln}\left(\frac{4\kappa t}{a_s^2 C}\right)\right]}{\mathrm{Ln}\left(\frac{4\kappa t}{a_s^2 C}\right)} \quad , \tag{3.4}$$

$$\simeq \frac{(\Delta T)_\ell - (\Delta T)_s}{(\Delta T)_\ell} \tag{3.5}$$

and $$\varepsilon = 1 - \frac{\sigma_s}{\sigma_\ell} \tag{3.6}$$

Here σ represents the resistance per unit length under equilibrium condition between temperatures T_o and T. $R_s(T_o)$ and $R_\ell(T_o)$ are the resistances of the wires at temperature T_o and R_s and R_ℓ the resistances at temperature T. $\alpha(T_o,S,P)$ is the temperature coefficient of resistance of pure platinum under an axial stress, S, and a hydrostatic pressure, P, between temperatures T_o and T. It can be shown that the effect of the constant axial stress is negligible with the present cell design [27], and the effect of hydrostatic pressure can be expressed as [27]:

$$\alpha\ (T,\ P) = \alpha\ (T,0)\ (1 + \varepsilon_p\ P) \tag{3.7}$$

with $$\varepsilon_p \approx 1.6 \times 10^{-6}\ (\mathrm{MPa})^{-1} \tag{3.8}$$

Hence equation (3.2) can be written in the form:

$$\Delta T' = \frac{(R_\ell - R_s) - (R_\ell(T_o) - R_s(T_o))}{\alpha\,(T_o,0,0)\,(R_\ell(T_o) - R_s(T_o))\,(1+\varepsilon_p P)} \qquad (3.9)$$

The difference $(R_\ell - R_s)$ in equation (3.2) is obtained from the bridge balance equation (59):

$$R_\ell - R_s = \frac{C_1 \cdot R_2 - R_1}{(R_\ell/R_s) - C_1} \cdot \left(\frac{R_\ell}{R_s} - 1\right) \quad , \qquad (3.10)$$

$$\text{where} \quad C_1 = \frac{1 - (B+1)/D}{(1+B/D)} \quad , \qquad (3.11)$$

$$B = \beta\, R'/R \quad , \qquad (3.12)$$

$$D = \left\{ 2\left(\frac{RS}{R}\right) + 1 \right\} \left(1 + \frac{R'}{R}\right) \quad , \qquad (3.13)$$

$$R' = R_5 + R_6 + R_7 + R_8 \qquad (3.14)$$

$$R = R_3 = R_4 = R_q = R_{10}$$

and β is the fraction of R' in the circuit. RS is the total value of the parallel resistors in the circuit in the upper right hand arm of the bridge (see figure 3.4) at the time of polarity change.

We note that in order to calculate the required resistance difference of the wires $(R_\ell - R_s)$ the ratio R_ℓ/R_s should be known. Writing the ratio of the resistance of the wires during a measurement

in the form of a perturbation to that at the equilibrium temperature as:-

$$\frac{R_\ell}{R_s} = \frac{R_\ell(T_o)}{R_s(T_o)} (1 + f) \qquad (3.15)$$

where f represents a small quantity which is only very weakly temperature dependent. To a good approximation, it may be taken to be zero and better approximations are obtained subsequently using an iterative procedure with the aid of the following relationship:

$$\frac{R_\ell}{R_s} = \frac{R_\ell(T_o)}{R_s(T_o)} \{ 1 + \alpha(T_o) [(\Delta T)_\ell - (\Delta T)_s] \} \qquad (3.16)$$

$$= \frac{R_\ell(T_o)}{R_s(T_o)} \{ 1 + \alpha(T_o).(\Delta T)_\ell \varepsilon_2 \} \qquad (3.17)$$

with ε_2 given by equations (3.4) and (3.5), and $\alpha(T_o)$ is the effective temperature coefficient of resistance of the platinum wire given by equation (3.7). The approximate value for $(\Delta T)_\ell$ obtained from the zeroth order approximation can be used in equation (3.17) to generate a better estimate of R_ℓ/R_s which can be returned to the bridge balance equation (3.10) for a better estimate of $(\Delta T)_\ell$. Normally one iteration of this type is sufficient.

3.4.2 The heat flux equation

The bridge arrangement of Figure (3.4) ensures that equal current flows in both wires. However, this alone does not imply an equal rate of heat dissipation per unit length in the wires because the wires are

extremely thin and hence it is difficult to ensure that their radii are exactly the same. The difficulty is overcome by treating the heat flux per unit length of the middle portion of the long wire, q, written in terms of experimental quantities as:

$$q = \frac{q^*}{(1-\varepsilon_4)^2(1+\varepsilon_5)} \tag{3.18}$$

where

$$q^* = \frac{V^2\ (R_\ell - R_s)/(\ell_\ell - \ell_s)}{\{R_1+R_2+(R_\ell-R_s)(\ell_\ell+\ell_s)/(\ell_\ell-\ell_s)\}^2} \tag{3.19}$$

$$\varepsilon_4 = \frac{2\ \sigma_\ell \cdot \varepsilon \cdot \ell_\ell\ \ell_s}{(\ell_\ell-\ell_s)(R_\ell+R_s)+(R_\ell-R_s)(\ell_\ell+\ell_s)} \tag{3.20}$$

$$\varepsilon_5 = \frac{\ell_s \varepsilon}{(\ell_\ell - \ell_s)} \tag{3.21}$$

where V is the applied voltage to the bridge, while R_1 and R_2 are bridge resistances defined previously (see fig. 3.4).

As the temperature at which measurements are performed is often significantly different from that at which the wires' lengths were measured ($\simeq$295K), it is necessary to correct for this temperature difference. The correction used is:

$$\ell_{(T_o)} = \ell_{(T_m)} \left(1 + \gamma(T_o - T_m)\right) \qquad (3.22)$$

where γ is the temperature coefficient of expansion of platinum ($\simeq 8.9 \times 10^{-6}\ K^{-1}$), T_m is the temperature at which the wires measurement were performed, and ℓ is the length of the wire.

Because the temperature rise during a measurement is only 5K, a further correction is not required as this causes an error of less than 0.01% in ΔT_{id}. The correction to $\ell(T_o)$ in practice accounts for at most (when $(T_m - T_o) \approx 70K$) 0.06% change in the calculated thermal conductivity.

The leads whose resistances are of importance are those connecting the long and short platinum wires to the bridge. In the present design, these leads include the golden loops (21) in figure (3.1) which have a resistance of 0.2Ω each. The design of the bridge is such that the effect is manifested in the calculation of the heat flux emitted from the wire but not in the measurement of its resistance. The resistance of these leads are hence included in the resistances of the resistance boxes R_1 and R_2 of figure (3.4).

3.5 Experimental Procedure

In this section the procedure by which the experiments are performed and the required measurements are obtained is briefly discussed.

The measurement cell is mounted in the bellows assembly and the latter is filled with the test liquid whose thermal conductivity is to be determined. The cell and bellows, which are attached to the

pressure vessel plug, are placed inside the autoclave which is then pumped up to the required pressure. The autoclave, containing the cell, is left to attain thermal equilibrium. The time taken to reach equilibrium is of the order of 72 hours when the liquid in the cell has been changed; and 2-3 hours when only the pressure within the autoclave has been altered.

Once the system has reached a steady temperature the equilibrium bath temperature, T_o, is measured using the platinum reistance thermometer which is strapped to the side of the pressure vessel. The pressure is then read. The variable resistors used in the automatic bridge are adjusted to give an approximately linear distribution in Ln t while ensuring that the final balance point during a run will not greatly exceed 1 second. The relevant bridge resistances as well as the mode and selector switch positions are recorded together with the voltage to be supplied across the bridge during a run.

A run is then performed by firing the automatic bridge and the six resulting balance times are recorded. The bridge configuration is altered by changing the mode or selection switch or by changing the values of the variable resistors in the upper right hand arm of the bridge (see 3.3). The new bridge configuration is noted, a second run is initiated and the six new balance times are recorded. Subsequent runs (normally six runs being performed in total) are performed using the same routine and allowing a time lapse of 60 seconds between runs (the optimum time lapse being obtained from previous experience).

Finally the difference of the resistance of the wires and the resistance of each wire is recorded with the bridge operating at a steady state mode. These measurements are performed for several different bridge voltages and the resistance at zero voltage (i.e. at

bath temperature) is obtained by extrapolating the measured resistances against input power to zero voltage. These plots were always found to be linear so that the extrapolation introduces negligible additional uncertainty.

These experimental data are all that is required from an experiment on the test liquid at a particular thermodynamic state. These data used in conjunction with the physical properties of the liquid, cell and platinum wires (these physical properties are given in appendix 2) enable the calculation of the thermal conductivity of the liquid.

3.6 Calculation of Liquid Thermal Conductivity

The experimental measurements yield directly the times of bridge balances; the bridge configuration corresponding to each time; the bridge voltage; the equilibrium resistance of the wires; the equilibrium bath temperature and the hydrostatic pressure within the measurement cell during the experiment. From these data we compute the idealised temperature rise, $(\Delta T)_{\ell}$, of a segment of the platinum wire as a function of time during an experiment according to equation 3.1. An iterative procedure as discussed in 3.4.1 is carried out until the value of $(\Delta T)_{\ell}$ has converged to the required accuracy (±0.01%). The heat flux, q, is calculated from equation (3.18). The corrections for departure from the ideal wire case as discussed in 2.5 are applied. As a consequence of the working equation (2.9), a linear regression analysis of the set of data (ΔT_{id}, Ln t) yields the thermal conductivity directly from the gradient of the line and the value of the heat flux.

In practice, measurements are performed on test liquids over the

pressure range 0-700 MPa at an approximately constant equilibrium bath temperature, T_o. These measurements produced liquid thermal conductivity $\lambda(T_r,\rho_r)$ at different reference density ρ_r and slightly different reference temperature T_r. The difference in reference temperature over the pressure range being of the order of 1-5K which is due to the pressure dependence of the physical properties of the fluid measurement cell. In order to examine the density dependence of a liquid, the thermal conductivity measurements were corrected to a nominal temperautre T_n using the linear equation:-

$$\lambda(T_n, \rho_r) = \lambda (T_r, \rho_r) + \left(\frac{\partial\lambda}{\partial T}\right)_{\rho_r} (T_n - T_r) \qquad (3.23)$$

The derivative $\left(\frac{\partial\lambda}{\partial T}\right)_{\rho_r}$ in equation (3.23) is obtained by first assuming the thermal conductivity to be independent of temperature. This is done for a number of sets of measurements of thermal conductivity versus density at different equilibrium bath temperatures. From these measurements one can then obtain an estimate of $\left(\frac{\partial\lambda}{\partial T}\right)_{\rho_r}$ which is then used in equation (3.23). The process is repeated and as convergence is rapid, usually two iterations are all that is required.

In order to examine the pressure dependence of the thermal conductivity one corrects the value of $\lambda(T_r, P)$ obtained from the measurements to a nominal temperature T_n using:-

$$\lambda(T_n, P) = \lambda(T_r, P) + \left(\frac{\partial\lambda}{\partial T}\right)_p (T_n - T_r) \qquad (3.24)$$

The value of $\left(\frac{\partial\lambda}{\partial T}\right)_p$ is obtained using:-

$$\left(\frac{\partial\lambda}{\partial T}\right)_p = \left(\frac{\partial\lambda}{\partial\rho}\right)_{T_r} \left(\frac{\partial\rho}{\partial T}\right)_p + \left(\frac{\partial\lambda}{\partial T}\right)_{\rho_r}$$

From data on the pressure and temperature dependence of test liquid density we can find $\left(\frac{\partial\rho}{\partial T}\right)_p$ and from the density and temperature dependence of the liquid thermal conductivity, which we have measured, we obatined $\left(\frac{\partial\lambda}{\partial T}\right)_{T_r}$ and $\left(\frac{\partial\lambda}{\partial T}\right)_{\rho_r}$.

3.7 Equipment Performance

From the theory of the transient hot wire apparatus given in Chapter 2, it is seen that, if the apparatus behaves in the manner assumed by the ideal mathematical model, then the experimentally determined values of ΔT_{id} versus Ln t will lie on a perfectly straight line. Since the mathematical description of the apparatus neglects entirely any convective heat transfer from the wire, the observation of the predicted linearity serves to establish that the experimental measurements are free from such effects. The analysis of the radiation contribution to the measurement given in Chapter 2 also indicated that provided the linearity of the ΔT_{id} vs Ln t curve is preserved, the effects of the radiation phenomenon contribute negligibly towards the measurement of the thermal conductivity. The validity of this conclusion has been confirmed by examination of each individual set of experimental ΔT_{id} vs Ln t data.

It is estimated that the small corrections discussed in Chapter 2 introduces errors of no more than ±0.1% in the temperature rise ΔT_{id}.

Figure (3.6) shows a plot of the corrected temperature rise ΔT_{id} versus Ln t for an experimental run on n-hexane at 307.15K and 631.6 MPa in order to illustrate the straightness of the line. In this figure, the deviations of the points from the least-squares fitted straight line have been multiplied by a factor of twenty to make them visible. Figure (3.7) shows a deviation plot for the same results and it is seen that the deviations are indeed randomly distributed with a maximum deviation of only ±0.04%. This is taken as conclusive evidence for the correct operation of our equipment.

It is estimated that the random error in the measurement of the temperature rises and the balance times of the automatic bridge amounts to ±0.2% error in the experimental thermal conductivity data. The precision of the instrument is hence estimated as ±0.2%. Repeated measurements under identical thermodynamic conditions but using different samples of test liquid agree to within ±0.2%. Taking into account a possible error in the temperature coefficient of resistance of the platinum wires to which the reported thermal conductivities are proportional, the overall accuracy of the thermal conductivity is estimated as ±0.3%.

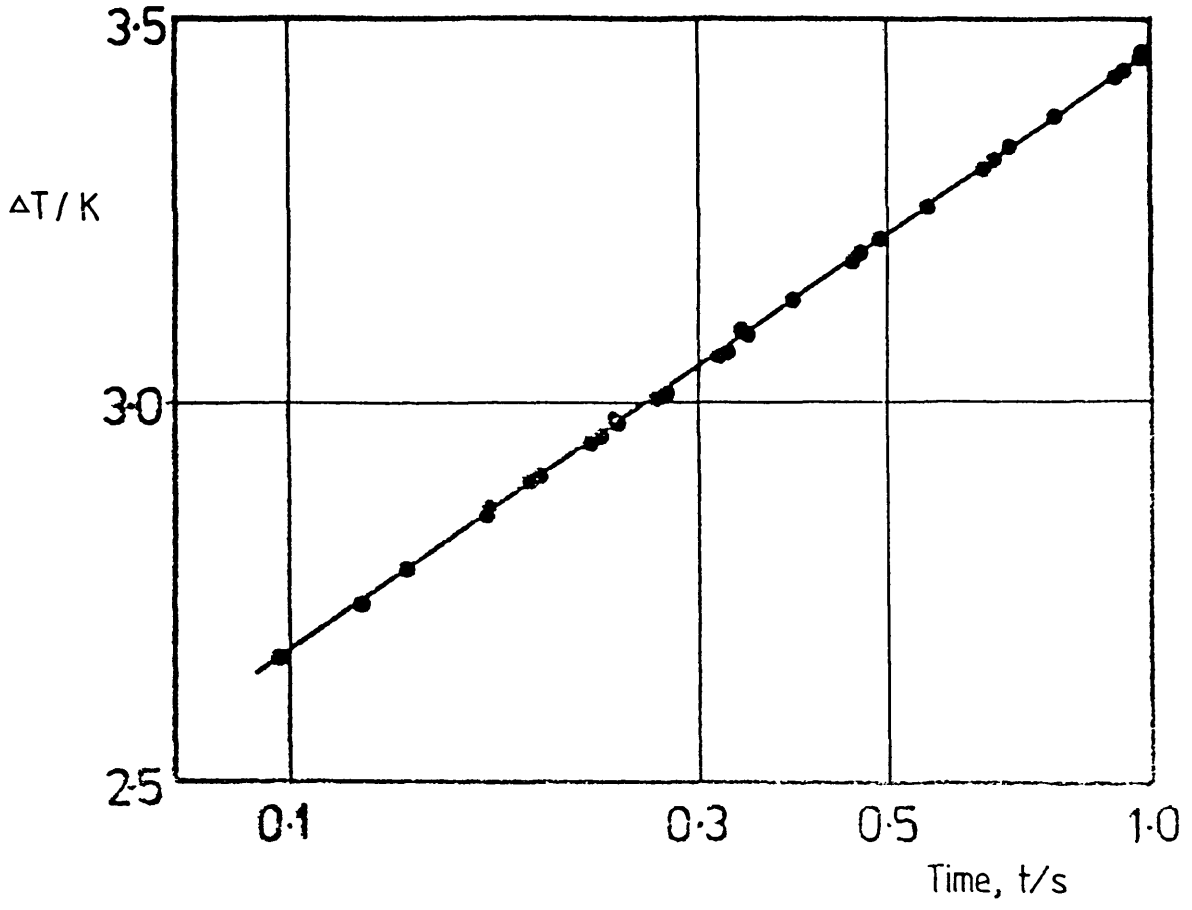

Fig. (3.6) Temperature rise of the platinum wire as a function of time (N-hexane at 307.15k and 631.6 MPa)

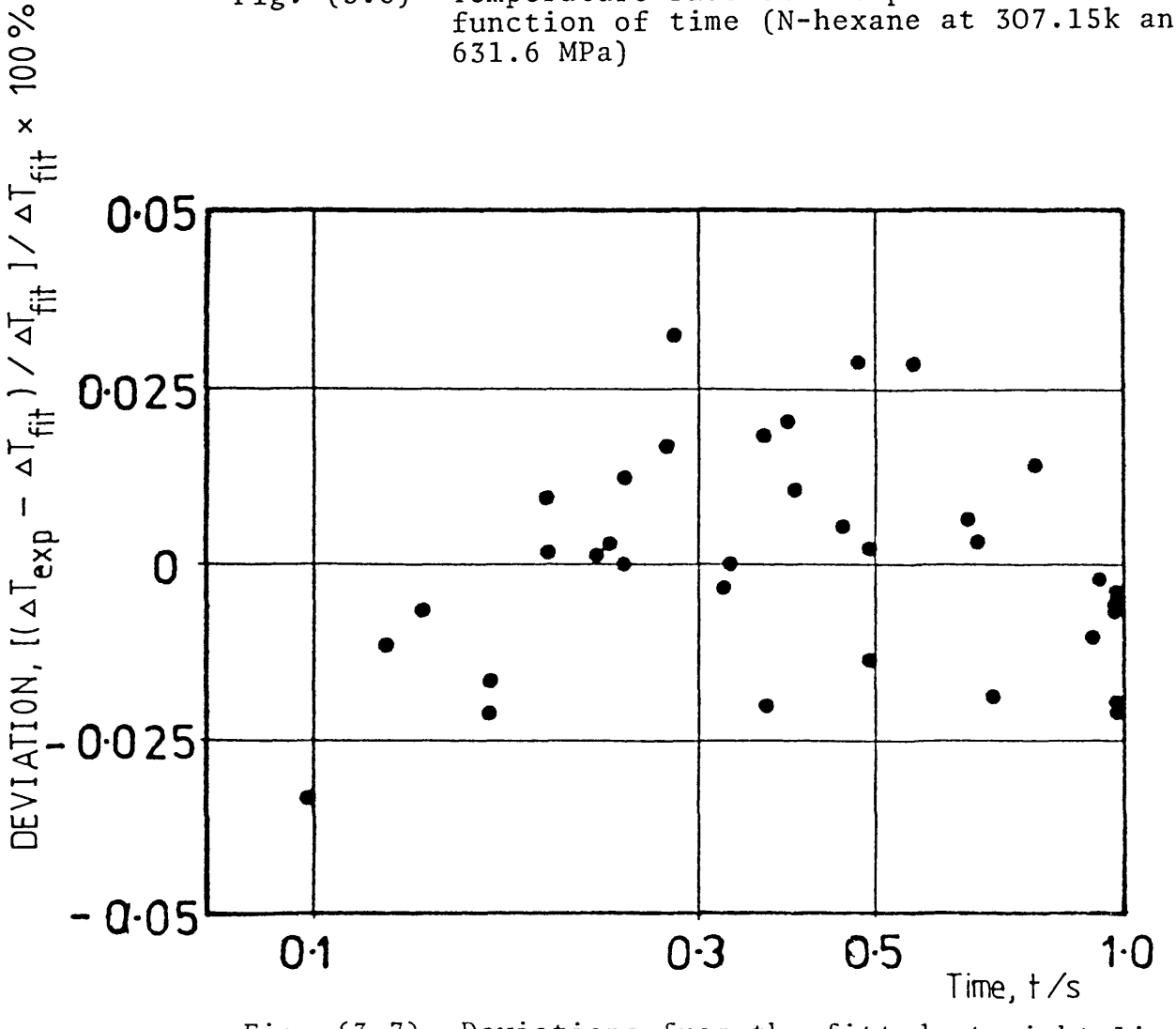

Fig. (3.7) Deviations from the fitted straight line (N-hexane at 307.15k and 631.6MPa)

CHAPTER 4

RESULTS

4 . 1 Pressure Dependence of the Thermal Conductivity of Liquid Hydrocarbons

The previous chapters have presented the theory of the transient hot-wire method and described an apparatus which was used to perform precise, accurate measurements of liquid thermal conductivities. In this chapter results for the thermal conductivity of seven liquid hydrocarbons at temperautre from 30 to 90^0C and pressures from atmospheric up to 700 MPa will be presented.

The seven liquids studied in this work and their purity are listed in Table (4.1). By means of independent tests of gas chromatograph, the stated purities of the liquids were supported. In the case of 2,3-dimethylbutane, the liquid was distilled repeatedly until a subsequent analysis indicated a purity in excess of 99.9%. All the liquids were degassed before use.

Table 4.1

Purity of the Studied Liquid Hydrocarbons

Hydrocarbon	Purity	Supplier
n-hexane	99.0%	BDH
n-octane	99.5%	BDH
2,3-dimethylbutane	97% (99.9% after distillation)	Aldrich
2,2,4-trimethlypentane	99.9%	BDH
Benzene	99.8%	BDH
Cyclohexane	99.5%	BDH
Toluene	99.95%	BDH

The characteristics of the measurement cell and a typical set of wires have been given in Table 3.1. A number of sets of wires were used during the measurement because during the changing of the test liquid, the wires often broke. The lengths of the wires used are included in Table 4.2. Repetition of the experiments with a new set of wires gives results which differed by less than ±0.2%, thus supporting the estimate of the apparatus design (±0.2%).

Table 4.2

Lengths of Individual Sets of Wires Employed for the Measurements

	Length of Long Wire mm ±0.05mm	Length of Short Wire mm ±0.05mm
n-hexane	152.46	49.92
n-octane	150.37	49.49
2,3-dimethylbutane	149.78	48.18
2,2,4-trimethylpentane	150.70	49.69
benzene	154.91	49.50
cyclohexane	151.48	50.33
toluene	153.58	49.22

Modest extension of the pressure range for the measurements over previous work have been achieved by means of small modifications to the pressure vessel and the seals. The lower limit on the pressure range at approximately 50 MPa as found in reference [27] was removed. The

upper pessure limit is also increased from 500 MPa to 650 MPa. However, for n-octane at the lowest isotherm and for benzene and cyclohexane, the upper limit on the pressure during measurements was determined by the freezing pressure at each temperature.

Each set of experimental results are presented in tabular form as in Tables 4.3 to 4.31. Each table contains measurements at one nominal isotherm (as defined in 3.6) for one liquid. In the tables, the reference temperature (see 3.6) and the experimental pressures are given. Also listed are the values of $(\partial\lambda/\partial T)_{\rho_r}$ and $(\partial\lambda/\partial T)_P$, employed to correct the raw data of the thermal conductivity at the reference temperature $\lambda(T_r, \rho_r)$ to that at the nominal temperature and reference density, $\lambda(T_{nom}, \rho_r)$ (see 3.6), and the value at the nominal temperature and the experimental pressure $\lambda(T_{nom}, P)$. Finally, the density data obtained from interpolation of available experimental data are listed. The experimental density data are included in appendix 2. However, a detailed discussion of the density dependence of the thermal conductivity is postponed to chapter six until we have developed a reliable method of correlation in the next chapter. Included in appendix 2 are also the heat capacity data required for the application of small corrections to the experimental data (see 2.5).

For the purpose of correlating the experimental results with pressure, the results $\lambda(T_n, P)$ were fitted to polynomials. It was found that the commonly used least square fit to thermal conductivity, along an isotherm in ascending powers of pressure was inadequate for the representation of the pressure dependence of thermal conductivity, especially in cases where measurements are performed at or near the

saturation conditions of the liquids. Instead, it was found through experimentation, that a polynomial in ascending powers of the square root of the pressure is more suitable. The correlation is expressed in the form:-

$$\lambda = b_o \left(1 + \sum_{i=1}^{3} b_i x^i \right) \qquad (4.1)$$

where

$$x = \left(P/P' \right)^{\frac{1}{2}} \qquad (4.2)$$

In equation (4.2), P' is a scaling parameter and is approximately equal to the mean pressure over the isotherm along which measurements were performed. The coefficients of equation (4.1) are determined by regression analysis. These coefficients as well as the values of P' used for each liquid at each isotherm are contained in Table 4.32.

A literature survey on the thermal conductivity of the liquids studied in this work revealed two major difficulties. Firstly, there are very few data available on the thermal conductivity of these hydrocarbons at elevated pressures and those data that are available are subject to large errors, more than ±5% in most cases.

Figures (4.1) and (4.2) contain plots of the deviations of the present results for n-hexane and n-octane from the correlation of equation (4.1). The same figures include the results of earlier measurements at elevated pressures [60, 61]. The maximum deviation of the present results from the correlation is one of ±1.0%, whereas the standard deviation is one of ±0.24% for n-hexane and ±0.30% for

n-octane. The results of Golubev and Naziev [61] lie as much as 8% above the present data for both n-hexane and n-octane. On the other hand, the results of Mukhamedzyanov et al [60] for n-hexane are in much better agreement with the present correlations over quite a wide range of pressures.

Figures 4.3 and 4.4 contain similar deviation plots for the present experimental results for 2,3-dimethylbutane and 2,2,4-trimethylpentane. For 2,3-dimethylbutane the deviations do not exceed ±0.5% and the standard deviation is one of ±0.11%. For 2,2,4-trimethylpentane the maximum deviation amounts to ±0.6% whereas the standard deviation is one of ±0.13%. These figures are commensurate with the estimated precision of the measurements. The only previous measurements of the thermal conductivity of these two liquids have been carried out at the saturation vapour pressure. Because the correlation of equation 4.1 is suitable only for interpolation, we postpone a comparison with these earlier measurements until the subsequent chapters where a more secure method of extrapolation is established (see Chapter 6).

Figure (4.5) displays the deviations of the experimental data from the correlation of equation (4.1) for benzene and cyclohexane. For benzene the maximum deviation is ±0.4%, and the standard deviation is one of ±0.1% whereas the corresponding values for cyclohexane are ±0.6% and ±0.1%. The only previous measurements of the thermal conductivity of benzene over a range of pressures were carried out by Rastorguev [62]. These earlier results are included in the deviation plot in figure (4.5) and are seen to depart from the present correlation by as much as 7%. For cyclohexane there have been no previous measurements at elevated pressures and again we postpone a comparison with the

results at the saturation vapour pressure for both liquids to a later chapter.

Figure 4.6 contains a plot of the deviations of the present experimental data for toluene from the correlation of equation 4.1. In no case does the deviation exceed ±0.7%. The standard deviation of the entire set of data being one of ±0.30%. The same figure includes the deviation of earlier results [62] at elevated pressures from the present correlation. Here, the deviations rise to as much as 5%. The present results are to be preferred owing to their higher accuracy.

A large number of measurements of the thermal conductivity of toluene along the saturation line have been reported and they have recently been reviewed by Nagasaka and Nagashima [63]. These authors have proposed a correlation for the thermal conductivity of toluene along the saturation line, in the form

$$\lambda = 0.1377_2 - 2.91_3 \times 10^{-4} (T - 273.15) \qquad (4.3)$$

for 248 K $\leq$ T $\leq$ 413K.

We have extrapolated the correlation of our experimental data to the saturation vapour pressure in order to provide a comparison with this correlation, (due to a lack of density data for toluene at elevated pressures, the pressure correlation, equation 4.1, is considered more suitable for the purpose of these extrapolation of the present experimental data). The comparison is inlcuded in figure (4.7) which also includes the deviations of the experimental results of Nagasaka and Nagashima [64] and Castro et al. [65] from the same correlation (equation 4.3). These two sets of measurements were also

performed with modern versions of the transient hot-wire instrument. The extrapolation of the present experimental results obviously degrades their accuracy somewhat, nevertheless, the three sets of measurements are seen to be consistent within their mutual uncertainty.

Table 4.3

Thermal Conductivity of n-hexane at T_n = 307.15K

T_r (K)	P (MPa)	$(\frac{\partial\lambda}{\partial T})_{\rho_r}$ (mW m^{-1} K^{-2})	$(\frac{\partial\lambda}{\partial T})_p$ (mW m^{-1} K^{-2})	$\lambda(T_r, \rho_r)$ (mW m^{-1} K^{-1})	$\lambda(T_n,\rho_r)$ (mW m K^{-1})	$\lambda(T_n,P)$ (mW m K^{-1})	ρ_r (Kg m^{-3})
306.780	1.880	0.132E+00	-0.268E+00	115.582	115.631	115.483	649.06
307.390	7.900	0.135E+00	-0.267E+00	119.268	119.236	119.332	654.61
307.250	17.800	0.140E+00	-0.264E+00	124.046	124.032	124.072	664.00
307.190	23.610	0.143E+00	-0.260E+00	126.830	126.824	126.840	669.10
307.045	24.925	0.144E+00	-0.259E+00	128.782	128.797	128.755	670.32
307.130	26.780	0.145E+00	-0.258E+00	128.622	128.625	128.617	671.79
306.740	29.960	0.146E+00	-0.255E+00	130.880	130.940	130.775	674.66
306.860	67.420	0.158E+00	-0.226E+00	145.690	145.736	145.624	700.47
306.750	99.200	0.163E+00	-0.209E+00	156.680	156.745	156.597	717.76
306.950	141.560	0.165E+00	-0.198E+00	168.973	169.006	168.933	736.28
307.010	177.690	0.165E+00	-0.196E+00	178.209	178.232	178.182	749.48
306.760	212.710	0.163E+00	-0.198E+00	187.077	187.140	187.000	760.79
307.200	240.110	0.160E+00	-0.202E+00	192.926	192.918	192.936	769.50
306.830	309.910	0.150E+00	-0.218E+00	207.374	207.437	207.282	786.63
307.400	357.260	0.142E+00	-0.229E+00	215.855	215.820	215.912	797.19
307.120	367.280	0.140E+00	-0.232E+00	217.636	217.640	217.629	799.54
306.640	397.380	0.133E+00	-0.243E+00	223.314	223.382	223.190	806.27
306.780	449.210	0.120E+00	-0.257E+00	231.410	231.454	231.315	817.00
306.340	496.610	0.107E+00	-0.273E+00	239.018	239.103	238.796	826.84
307.350	533.110	0.957E-01	-0.230E+00	244.155	244.136	244.211	833.65
307.007	574.790	0.806E-01	-0.294E+00	249.396	249.408	249.354	842.18
307.100	599.750	0.719E-01	-0.302E+00	253.040	253.044	253.025	847.15
306.890	601.430	0.701E-01	-0.303E+00	252.846	252.864	252.767	847.60
307.050	631.580	0.575E-01	-0.312E+00	256.810	256.816	256.779	853.64
307.170	643.690	0.552E-01	-0.316E+00	258.326	258.325	258.332	865.05

Table 4.4

Thermal Conductivity of n-hexane at T_n = 321.15K

T_r (K)	P (MPa)	$(\frac{\partial\lambda}{\partial T})_{\rho_r}$ (mW m^{-1} K^{-2})	$(\frac{\partial\lambda}{\partial T})_p$ (mW m^{-1} K^{-2})	$\lambda(T_r, \rho_r)$ (mW m^{-1} K^{-1})	$\lambda(T_n, \rho_r)$ (mW m K^{-1})	$\lambda(T_n, P)$ (mW m K^{-1})	ρ_r (Kg m^{-3})
321.350	5.630	0.127E+00	-0.232E+00	112.958	112.923	112.994	639.75
321.260	16.090	0.133E+00	-0.251E+00	119.065	119.050	119.093	650.77
321.160	24.210	0.137E+00	-0.259E+00	123.539	123.538	123.542	658.58
320.750	50.700	0.149E+00	-0.263E+00	135.611	135.671	135.506	680.38
321.200	109.940	0.162E+00	-0.239E+00	156.399	156.391	156.411	714.88
321,190	144.290	0.165E+00	-0.225E+00	166.409	166.402	166.418	729.98
320.670	157.140	0.165E+00	-0.220E+00	169.276	169.355	169.170	735.27
320.650	209.890	0.164E+00	-0.207E+00	183.652	183.734	183.549	753.25
320.870	258.960	0.160E+00	-0.200E+00	194.936	194.981	194.880	767.21
320.950	311.400	0.154E+00	-0.197E+00	205.456	205.487	205.417	780.40
320.630	359.940	0.146E+00	-0.198E+00	214.620	214.696	214.517	791.68
321.380	408.590	0.138E+00	-0.198E+00	222.895	222.863	222.941	801.83
321.230	450.790	0.128E+00	-0.203E+00	229.773	229.763	229.789	810.61
321.160	501.580	0.115E+00	-0.210E+00	237.706	237.705	237.708	820.88
321.100	543.830	0.103E+00	-0.218E+00	243.315	243.320	243.304	829.31
321.160	550.800	0.101E+00	-0.219E+00	244.714	244.713	244.716	830.67
320.880	595.910	0.851E-01	-0.230E+00	250.833	250.856	250.771	839.77
321.080	631.380	0.717E-01	-0.238E+00	255.280	255.285	255.263	846.81

Table 4.5

Thermal Conductivity of n-hexane at T_n = 345.15K

T_r (K)	P (MPa)	$(\frac{\partial\lambda}{\partial T})_{\rho_r}$ (mW m^{-1} K^{-2})	$(\frac{\partial\lambda}{\partial T})_p$ (mW m^{-1} K^{-2})	$\lambda(T_r, \rho_r)$ (mW m^{-1} K^{-1})	$\lambda(T_n,\rho_r)$ (mW m K^{-1})	$\lambda(T_n,P)$ (mW m K^{-1})	ρ_r (Kg m^{-3})
344.790	25.590	0.127E+00	-0.228E+00	117.864	117.910	117.782	639.23
344.790	25.600	0.127E+00	-0.228E+00	117.864	117.910	117.782	639.24
344.950	51.700	0.139E+00	-0.233E+00	130.231	130.259	130.184	662.31
345.330	85.400	0.151E+00	-0.226E+00	142.529	142.502	142.570	685.62
345.170	104.670	0.156E+00	-0.222E+00	149.600	149.597	149.604	696.91
345.080	156.930	0.164E+00	-0.211E+00	165.369	165.380	165.354	721.71
345.720	207.580	0.165E+00	-0.201E+00	178.149	178.055	178.264	740.20
345.140	238.800	0.165E+00	-0.194E+00	184.854	184.856	184.852	750.44
344.960	255.760	0.164E+00	-0.190E+00	189.836	189.867	189.800	755.53
345.080	307.820	0.160E+00	-0.177E+00	200.798	200.809	200.786	769.53
344.690	357.950	0.153E+00	-0.162E+00	210.231	210.302	210.157	781.83
344.770	369.550	0.152E+00	-0.158E+00	211.638	211.696	211.578	784.46
345.520	296.590	0.148E+00	-0.149E+00	216.822	216.767	216.877	790.21
345.160	452.270	0.137E+00	-0.126E+00	226.380	226.379	226.381	802.24
345.260	503.250	0.126E+00	-0.101E+00	234.510	234.496	234.521	812.63
345.580	550.580	0.114E+00	-0.724E-01	241.436	241.387	241.467	822.00
345.190	581.900	0.104E+00	-0.564E-01	245.957	245.953	245.959	828.29
345.580	598.570	0.993E-01	-0.411E-01	248.113	248.071	248.131	831.50
345.150	628.030	0.893E-01	-0.264E-01	252.397	252.397	252.397	837.39

Table 4.6

Thermal Conductivity of n-hexane at T_n = 360.15K

T_r (K)	P (MPa)	$(\frac{\partial\lambda}{\partial T})_{\rho_r}$ (mW m^{-1} K^{-2})	$(\frac{\partial\lambda}{\partial T})_p$ (mW m^{-1} K^{-2})	$\lambda(T_r, \rho_r)$ (mW m^{-1} K^{-1})	$\lambda(T_n, \rho_r)$ (mW m K^{-1})	$\lambda(T_n, P)$ (mW m K^{-1})	ρ_r (Kg m^{-3})
359.870	24.800	0.119E+00	-0.150E+00	113.958	113.991	113.916	626.37
359.410	53.500	0.135E+00	-0.173E+00	127.577	127.677	127.449	654.06
359.970	95.650	0.150E+00	-0.181E+00	143.389	143.416	143.356	683.25
359.440	153.600	0.161E+00	-0.210E+00	161.086	161.201	160.944	712.61
359.810	206.270	0.165E+00	-0.211E+00	175.477	175.533	175.405	732.51
359.850	241.520	0.165E+00	-0.212E+00	182.513	182.563	182.449	743.92
359.370	257.360	0.165E+00	-0.209E+00	187.204	187.333	187.041	748.92
360.140	307.320	0.162E+00	-0.197E+00	197.657	197.659	197.655	762.42
359.580	357.950	0.157E+00	-0.168E+00	207.722	207.811	207.626	775.51
359.930	406.610	0.150E+00	-0.130E+00	216.334	216.367	216.305	786.94
359.700	455.730	0.141E+00	-0.792E+00	224.605	224.668	224.569	798.28
359.430	505.110	0.129E+00	-0.195E-01	232.236	232.329	232.222	809.44
359.430	526.930	0.124E+00	0.989E-02	235.159	235.248	235.166	814.30
359.540	552.280	0.116E+00	0.467E-01	239.256	239.327	239.285	819.96
359.610	583.180	0.106E+00	0.939E-01	243.620	243.677	243.671	826.91
359.460	607.640	0.977E+00	0.131E+00	247.122	247.289	247.212	832.46
359.530	628.630	0.895E+00	0.165E+00	249.779	249.835	249.881	837.29

Table 4.7

Thermal Conductivity of n-octane at T_n = 307.15K

T_r (K)	P (MPa)	$(\frac{\partial\lambda}{\partial T})_{\rho_r}$ (mW m^{-1} K^{-2})	$(\frac{\partial\lambda}{\partial T})_p$ (mW m^{-1} K^{-2})	$\lambda(T_r, \rho_r)$ (mW m^{-1} K^{-1})	$\lambda(T_n, \rho_r)$ (mW m K^{-1})	$\lambda(T_n, P)$ (mW m K^{-1})	ρ_r (Kg m^{-3})
307.530	7.271	0.728E-01	-0.299E+00	126.175	126.147	126.288	697.70
306.946	9.531	0.784E-01	-0.297E+00	127.770	127.785	127.709	700.10
306.313	24.202	0.844E-01	-0.284E+00	133.900	133.916	133.662	712.24
307.300	53.115	0.103E+00	-0.255E+00	144.274	144.258	144.312	730.75
307.264	68.131	0.113E+00	-0.242E+00	149.499	149.486	149.527	739.20
306.933	106.400	0.131E+00	-0.217E+00	160.842	160.871	160.795	757.58
307.520	129.600	0.139E+00	-0.206E+00	165.517	165.466	165.593	766.59
306.923	135.990	0.141E+00	-0.204E+00	168.135	168.167	168.089	769.30
306.209	167.520	0.148E+00	-0.195E+00	175.002	175.141	174.818	780.60
306.190	186.240	0.150E+00	-0.191E+00	179.395	179.539	179.211	786.53
306.809	212.410	0.150E+00	-0.187E+00	184.434	184.485	184.370	793.95
306.908	254.860	0.148E+00	-0.183E+00	192.417	192.453	192.373	805.42
307.323	283.780	0.143E+00	-0.181E+00	197.137	197.112	197.168	812.54
306.784	305.830	0.138E+00	-0.182E+00	201.550	201.600	201.483	818.16
306.563	356.260	0.121E+00	-0.183E+00	212.050	212.121	211.942	830.08
306.601	362.820	0.118E+00	-0.184E+00	212.090	212.155	211.989	831.57
306.865	425.110	0.845E-01	-0.188E+00	221.860	221.884	221.806	845.58
307.374	452.670	0.673E-01	-0.191E+00	225.373	225.358	225.416	851.63
306.457	452.760	0.661E-01	-0.192E+00	225.881	225.927	225.748	851.98

Table 4.8

Thermal Conductivity of n-octane at T_n = 321.15K

T_r (K)	P (MPa)	$(\frac{\partial\lambda}{\partial T})_{\rho_r}$ (mW m^{-1} K^{-2})	$(\frac{\partial\lambda}{\partial T})_p$ (mW m^{-1} K^{-2})	$\lambda(T_r, \rho_r)$ (mW m^{-1} K^{-1})	$\lambda(T_n,\rho_r)$ (mW m K^{-1})	$\lambda(T_n,P)$ (mW m K^{-1})	ρ_r (Kg m^{-3})
321.152	47.115	0.904E-01	-0.240E+00	138.445	138.445	138.445	718.39
320.791	70.260	0.105E+00	-0.232E+00	146.504	146.542	146.421	732.44
321.039	93.014	0.118E+00	-0.221E+00	153.555	153.568	153.530	743.88
321.102	103.250	0.122E+00	-0.217E+00	156.263	156.269	156.253	748.55
320.487	133.250	0.135E+00	-0.205E+00	164.584	164.673	164.448	761.26
321.362	154.510	0.141E+00	-0.197E+00	169.667	169.637	169.709	768.61
320.976	204.660	0.149E+00	-0.184E+00	180.669	180.695	180.637	784.91
321.261	228.530	0.150E+00	-0.178E+00	185.455	185.438	185.475	791.65
321.384	249.150	0.150E+00	-0.173E+00	189.773	189.738	189.814	797.23
321.306	281.880	0.147E+00	-0.167E+00	195.606	195.583	195.632	805.80
321.094	299.930	0.145E+00	-0.164E+00	198.636	198.644	198.627	810.42
320.912	353.370	0.131E+00	-0.157E+00	207.907	207.938	207.870	823.45
320.764	402.440	0.111E+00	-0.152E+00	216.439	216.482	216.380	835.08
321.309	450.000	0.839E-01	-0.149E+00	223.211	223.198	223.235	846.12
321.087	501.100	0.435E-01	-0.153E+00	233.665	233.668	233.655	858.45
321.018	545.930	-0.320E-02	-0.163E+00	237.015	237.015	236.993	869.60
320.985	571.830	-0.361E-01	-0.173E+00	242.458	242.452	242.429	876.26
321.160	572.130	-0.363E-01	-0.173E+00	243.067	243.067	243.069	876.30

Table 4.9

Thermal Conductivity of n-octane at T_n = 345.15

T_r (K)	P (MPa)	$(\frac{\partial\lambda}{\partial T})_{\rho_r}$ (mW m^{-1} K^{-2})	$(\frac{\partial\lambda}{\partial T})_p$ (mW m^{-1} K^{-2})	$\lambda(T_r, \rho_r)$ (mW m^{-1} K^{-1})	$\lambda(T_n,\rho_r)$ (mW m K^{-1})	$\lambda(T_n,P)$ (mW m K^{-1})	ρ_r (Kg m^{-3})
345.258	19.765	0.657E-01	-0.235E+00	121.412	121.405	121.437	680.88
345.028	45.319	0.760E-01	-0.245E+00	132.233	132.222	132.203	702.33
345.322	70.666	0.908E-01	-0.234E+00	141.668	141.652	141.708	718.78
345.260	100.620	0.108E+00	-0.216E+00	151.089	151.077	151.113	734.71
345.230	130.310	0.122E+00	-0.199E+00	159.198	159.188	159.214	747.80
344.784	154.210	0.131E+00	-0.188E+00	165.259	165.307	165.190	757.19
345.080	205.160	0.144E+00	-0.167E+00	177.232	177.242	177.220	773.98
345.531	209.490	0.145E+00	-0.165E+00	176.638	176.583	176.701	775.10
344.859	252.460	0.150E+00	-0.150E+00	186.797	186.841	186.753	787.75
344.868	305.630	0.149E+00	-0.135E+00	196.913	196.955	196.875	801.82
344.804	334.940	0.146E+00	-0.127E+00	200.808	200.858	200.764	809.28
344.929	349.660	0.143E+00	-0.124E+00	204.737	204.769	204.710	812.91
345.671	409.980	0.125E+00	-0.112E+00	213.668	213.603	213.727	827.63
345.198	451.780	0.104E+00	-0.109E+00	222.109	222.104	222.114	838.31
345.340	499.540	0.705E-01	-0.110E+00	229.433	229.420	229.454	850.59
345.052	520.590	0.514E-01	-0.114E+00	230.881	230.886	230.870	856.28
344.785	543.720	0.271E-01	-0.120E+00	234.250	234.260	234.206	862.65
344.906	574.200	-0.107E-01	-0.134E+00	241.262	241.259	241.229	871.19
345.140	576.070	-0.130E-01	-0.135E+00	238.826	238.826	238.825	871.67

Table 4.10

Thermal Conductivity of n-octane at T_n = 362.15K

T_r (K)	P (MPa)	$(\frac{\partial\lambda}{\partial T})_{\rho_r}$ (mW m^{-1} K^{-2})	$(\frac{\partial\lambda}{\partial T})_p$ (mW m^{-1} K^{-2})	$\lambda(T_r, \rho_r)$ (mW m^{-1} K^{-1})	$\lambda(T_n, \rho_r)$ (mW m K^{-1})	$\lambda(T_n, P)$ (mW m K^{-1})	ρ_r (Kg m^{-3})
361.356	19.469	0.663E-01	-0.201E+00	116.835	116.888	116.675	668.95
362.504	26.571	0.653E-01	-0.213E+00	120.100	120.077	120.175	675.30
362.205	45.818	0.696E-01	-0.230E+00	128.261	128.257	128.274	692.22
361.257	49.912	0.717E-01	-0.231E+00	129.823	129.887	129.616	695.92
361.990	75.133	0.845E-01	-0.223E+00	139.228	139.242	139.192	712.38
362.834	83.160	0.886E-01	-0.219E+00	140.906	140.845	141.056	716.61
362.076	119.980	0.108E+00	-0.199E+00	152.717	152.725	152.702	735.34
362.277	136.900	0.116E+00	-0.190E+00	156.430	156.415	156.454	742.41
361.451	151.380	0.122E+00	-0.183E+00	161.017	161.103	160.889	748.45
362.049	176.990	0.131E+00	-0.171E+00	167.351	167.364	167.334	757.37
362.984	204.360	0.139E+00	-0.158E+00	173.386	173.270	173.518	765.91
362.800	253.260	0.148E+00	-0.140E+00	183.555	183.459	183.646	780.44
362.634	303.430	0.150E+00	-0.123E+00	193.406	193.333	193.465	794.11
362.945	365.590	0.145E+00	-0.104E+00	203.284	203.169	203.367	810.07
362.978	390.740	0.139E+00	-0.981E-01	209.012	208.897	209.093	816.51
362.938	450.500	0.117E+00	-0.882E-01	218.219	218.127	218.289	832.04
363.429	500.900	0.857E-01	-0.873E-01	227.346	227.237	227.458	845.49
363.276	546.460	0.323E-01	-0.967E-01	232.832	232.783	232.941	858.47
363.275	591.860	-0.154E-01	-0.120E+00	239.967	239.984	240.103	872.16

Table 4.11

Thermal Conductivity of 2,3-dimethylbutane at T_n = 309.15K

T_r (K)	P (MPa)	$(\frac{\partial\lambda}{\partial T})_{\rho_r}$ (mW m^{-1} K^{-2})	$(\frac{\partial\lambda}{\partial T})_p$ (mW m^{-1} K^{-2})	$\lambda(T_r, \rho_r)$ (mW m^{-1} K^{-1})	$\lambda(T_n,\rho_r)$ (mW m K^{-1})	$\lambda(T_n,P)$ (mW m K^{-1})	ρ_r (Kg m^{-3})
310.010	0.300	0.344E+00	-0.606E-01	97.360	97.065	97.413	647.52
309.050	0.300	0.341E+00	-0.645E-01	97.631	97.665	97.624	648.40
310.220	0.300	0.345E+00	-0.597E-01	97.980	97.611	98.044	647.32
309.130	56.620	0.217E+00	-0.121E+00	122.093	122.097	122.090	699.95
309.040	69.250	0.207E+00	-0.119E+00	126.213	126.236	126.200	707.87
309.280	82.040	0.200E+00	-0.116E+00	130.135	130.109	130.150	715.03
309.210	189.360	0.173E+00	-0.105E+00	156.891	156.881	156.897	762.38
309.240	240.410	0.167E+00	-0.122E+00	166.514	166.499	166.525	778.77
308.950	305.630	0.159E+00	-0.130E+00	178.540	178.572	178.514	796.09
309.440	355.360	0.152E+00	-0.133E+00	186.618	186.574	186.657	807.74
309.340	403.430	0.143E+00	-0.136E+00	193.515	193.488	193.541	818.25
309.350	453.360	0.133E+00	-0.143E+00	200.408	200.382	200.437	828.15

Table 4.12

Thermal Conductivity of 2,3-dimethylbutane at T_n = 321.15K

T_r (K)	P (MPa)	$(\frac{\partial\lambda}{\partial T})_{\rho_r}$ (mW m^{-1} K^{-2})	$(\frac{\partial\lambda}{\partial T})_p$ (mW m^{-1} K^{-2})	$\lambda(T_r, \rho_r)$ (mW m^{-1} K^{-1})	$\lambda(T_n,\rho_r)$ (mW m K^{-1})	$\lambda(T_n,P)$ (mW m K^{-1})	ρ_r (Kg m^{-3})
321.250	19.360	0.305E+00	-0.595E-01	105.616	105.586	105.622	658.97
321.500	21.530	0.299E+00	-0.658E-01	106.224	106.120	106.247	661.08
321.160	49.890	0.238E+00	-0.112E+00	117.775	117.773	117.777	686.99
320.850	84.380	0.205E+00	-0.102E+00	129.078	129.139	129.047	709.44
320.580	97.380	0.198E+00	-0.973E-01	133.577	133.690	133.521	716.54
320.610	97.480	0.198E+00	-0.972E-01	133.032	133.139	132.980	716.57
320.690	110.150	0.193E+00	-0.943E-01	136.081	136.170	136.038	722.68
321.140	151.680	0.181E+00	-0.946E-01	146.283	146.285	146.282	741.53
320.910	205.560	0.173E+00	-0.102E+00	158.605	158.647	158.581	762.68
320.610	255.260	0.167E+00	-0.112E+00	168.391	168.481	168.330	777.91
320.550	274.960	0.165E+00	-0.114E+00	172.015	172.115	171.947	783.29
321.260	305.530	0.162E+00	-0.116E+00	177.319	177.301	177.332	790.78
321.110	355.660	0.155E+00	-0.120E+00	185.375	185.381	185.370	803.01
320.930	404.820	0.147E+00	-0.123E+00	192.732	192.764	192.705	813.99
320.760	439.990	0.140E+00	-0.126E+00	197.580	197.634	197.530	821.22
320.810	452.170	0.138E+00	-0.128E+00	199.322	199.369	199.279	823.60
320.730	471.650	0.134E+00	-0.130E+00	202.000	202.056	201.945	827.36
320.690	499.630	0.127E+00	-0.135E+00	205.527	205.586	205.465	832.48

Table 4.13

Thermal Conductivity of 2,3-dimethylbutane at T_n = 345.15K

T_r (K)	P (MPa)	$(\frac{\partial\lambda}{\partial T})_{\rho_r}$ (mW m^{-1} K^{-2})	$(\frac{\partial\lambda}{\partial T})_p$ (mW m^{-1} K^{-2})	$\lambda(T_r, \rho_r)$ (mW m^{-1} K^{-1})	$\lambda(T_n,\rho_r)$ (mW m K^{-1})	$\lambda(T_n,P)$ (mW m K^{-1})	ρ_r (Kg m^{-3})
345.220	42.300	0.298E+00	-0.601E-01	112.248	112.228	112.253	661.49
344.760	84.180	0.225E+00	-0.648E-01	127.070	127.157	127.044	694.88
345.450	89.560	0.220E+00	-0.604E-01	128.630	128.564	128.648	697.98
345.050	120.580	0.199E+00	-0.577E-01	137.548	137.568	137.542	715.24
345.090	130.310	0.195E+00	-0.607E-01	139.736	139.748	139.733	720.07
344.890	171.450	0.182E+00	-0.701E-01	149.848	149.895	149.830	738.92
344.750	183.630	0.180E+00	-0.704E-01	151.614	151.686	151.586	744.10
344.860	185.540	0.179E+00	-0.704E-01	152.586	152.638	152.566	744.82
345.310	252.660	0.171E+00	-0.772E-01	165.402	165.375	165.414	766.58
344.970	304.730	0.166E+00	-0.830E-01	174.360	174.390	174.345	780.78
344.840	357.560	0.160E+00	-0.895E-01	182.590	182.640	182.562	794.01
344.880	397.970	0.155E+00	-0.931E-01	188.698	188.739	188.672	803.34
344.700	454.150	0.146E+00	-0.961E-01	196.407	196.473	196.364	815.24
345.200	501.190	0.137E+00	-0.976E-01	202.494	202.488	202.499	824.16
345.220	506.780	0.136E+00	-0.979E-01	202.964	202.954	202.970	825.18
345.070	535.080	0.130E+00	-0.100E+00	206.745	206.756	206.737	830.28

Table 4.14

Thermal Conductivity of 2,3-dimethylbutane at T_n = 361.15K

T_r (K)	P (MPa)	$(\frac{\partial\lambda}{\partial T})_{\rho_r}$ (mW m^{-1} K^{-2})	$(\frac{\partial\lambda}{\partial T})_p$ (mW m^{-1} K^{-2})	$\lambda(T_r, \rho_r)$ (mW m^{-1} K^{-1})	$\lambda(T_n,\rho_r)$ (mW m K^{-1})	$\lambda(T_n,P)$ (mW m K^{-1})	ρ_r (Kg m^{-3})
360.990	78.590	0.251E+00	0.704E-02	125.100	125.150	125.111	680.46
361.010	88.240	0.236E+00	0.522E-03	129.081	129.114	129.081	687.88
361.460	104.570	0.220E+00	-0.696E-02	132.642	132.574	132.644	698.12
361.400	128.390	0.204E+00	-0.257E-01	138.861	138.810	138.868	711.09
361.140	156.430	0.191E+00	-0.463E-01	145.459	145.461	145.458	724.59
361.060	202.240	0.180E+00	-0.556E-01	154.711	154.727	154.706	743.96
361.050	204.060	0.180E+00	-0.558E-01	155.331	155.349	155.325	744.60
361.070	234.170	0.175E+00	-0.591E-01	161.151	161.165	161.146	754.50
361.540	269.450	0.172E+00	-0.620E-01	167.516	167.449	167.541	764.80
361.320	296.720	0.169E+00	-0.657E-01	171.652	171.623	171.663	772.26
361.330	311.400	0.168E+00	-0.680E-01	174.426	174.396	174.439	776.04
361.080	357.750	0.163E+00	-0.744E-01	181.530	181.542	181.525	787.82
361.130	397.380	0.159E+00	-0.772E-01	187.043	187.046	187.041	797.13
361.110	410.080	0.157E+00	-0.774E-01	189.109	189.116	189.106	799.96
361.050	446.460	0.152E+00	-0.766E-01	194.105	194.120	194.097	807.83
361.530	496.320	0.144E+00	-0.730E-01	200.882	200.827	200.910	817.76
361.560	528.880	0.138E+00	-0.711E-01	204.367	204.311	204.397	823.86

Table 4.15

Thermal Conductivity of 2,2,4-trimethylpentane at T_n = 313.15K

T_r (K)	P (MPa)	$(\frac{\partial\lambda}{\partial T})_{\rho_r}$ (mW m^{-1} K^{-2})	$(\frac{\partial\lambda}{\partial T})_p$ (mW m^{-1} K^{-2})	$\lambda(T_r, \rho_r)$ (mW m^{-1} K^{-1})	$\lambda(T_n,\rho_r)$ (mW m K^{-1})	$\lambda(T_n,P)$ (mW m K^{-1})	ρ_r (Kg m^{-3})
313.090	46.230	0.157E+00	-0.153E+00	109.682	109.691	109.673	716.11
312.820	66.610	0.180E+00	-0.139E+00	116.185	116.244	116.139	729.67
312.550	97.580	0.207E+00	-0.117E+00	124.438	124.562	124.367	746.80
313.290	140.450	0.231E+00	-0.913E-01	135.103	135.071	135.116	765.29
311.470	140.450	0.233E+00	-0.951E-01	135.329	135.720	135.170	766.33
314.160	140.450	0.231E+00	-0.894E-01	134.766	134.533	134.756	764.79
312.190	149.350	0.236E+00	-0.894E-01	136.583	136.810	136.498	769.35
313.260	164.400	0.241E+00	-0.806E-01	140.370	140.344	140.379	774.27
312.100	202.550	0.252E+00	-0.694E-01	147.431	147.695	147.358	787.49
312.830	223.960	0.256E+00	-0.596E-01	152.775	152.857	152.756	796.04
312.630	250.450	0.257E+00	-0.559E-01	155.897	156.030	155.868	800.94
312.690	282.280	0.258E+00	-0.497E-01	161.081	161.200	161.058	809.13
312.450	303.430	0.257E+00	-0.468E-01	164.129	164.309	164.096	814.42
312.460	344.550	0.253E+00	-0.418E-01	170.362	170.537	170.333	823.94
312.000	350.460	0.252E+00	-0.419E-01	171.194	171.484	171.146	825.48
312.460	380.140	0.247E+00	-0.388E-01	175.454	175.625	175.428	831.77
312.900	400.060	0.243E+00	-0.369E-01	177.634	177.695	177.625	835.84
313.520	428.450	0.236E+00	-0.350E-01	180.977	180.890	180.990	841.54
312.910	448.720	0.229E+00	-0.358E-01	184.419	184.474	184.410	846.00

Table 4.16

Thermal Conductivity of 2,2,4-trimethylpentane at T_n = 321.15K

T_r (K)	P (MPa)	$(\frac{\partial\lambda}{\partial T})_{\rho_r}$ (mW m^{-1} K^{-2})	$(\frac{\partial\lambda}{\partial T})_p$ (mW m^{-1} K^{-2})	$\lambda(T_r, \rho_r)$ (mW m^{-1} K^{-1})	$\lambda(T_n,\rho_r)$ (mW m K^{-1})	$\lambda(T_n,P)$ (mW m K^{-1})	ρ_r (Kg m^{-3})
322.030	15.180	0.101E+00	-0.154E+00	97.759	97.669	97.894	683.70
321.770	47.570	0.148E+00	-0.147E+00	109.351	109.260	109.443	711.12
321.090	96.460	0.198E+00	-0.113E+00	123.833	123.845	123.826	741.14
320.810	150.770	0.231E+00	-0.807E-01	136.577	136.656	136.550	765.15
321.370	176.180	0.241E+00	-0.677E-01	141.498	141.445	141.513	774.06
321.110	202.750	0.248E+00	-0.577E-01	147.105	147.115	147.103	782.88
321.240	241.120	0.255E+00	-0.451E-01	154.087	154.064	154.091	794.10
321.070	275.060	0.258E+00	-0.364E-01	159.524	159.544	159.521	803.23
320.940	304.730	0.258E+00	-0.299E-01	164.415	164.469	164.409	810.68
320.750	353.970	0.254E+00	-0.211E-01	171.813	171.915	171.805	822.25
320.730	368.860	0.252E+00	-0.188E-01	174.156	174.262	174.149	825.59
320.630	402.140	0.246E+00	-0.144E-01	178.189	178.317	178.181	832.89
320.560	450.300	0.234E+00	-0.971E-02	184.518	184.656	184.512	843.13
320.880	487.270	0.221E+00	-0.721E-02	188.189	188.248	188.187	850.71
320.440	498.560	0.216E+00	-0.740E-02	190.545	190.698	190.540	853.23
321.220	548.990	0.194E+00	-0.700E-02	195.605	195.591	195.605	863.42
320.930	571.530	0.181E+00	-0.882E-02	198.365	198.405	198.364	868.23
321.070	591.860	0.169E+00	-0.108E-01	200.459	200.473	200.458	872.47

Table 4.17

Thermal Conductivity of 2,2,4-trimethylpentane at T_n = 337.15K

T_r (K)	P (MPa)	$(\frac{\partial\lambda}{\partial T})_{\rho_r}$ (mW m^{-1} K^{-2})	$(\frac{\partial\lambda}{\partial T})_p$ (mW m^{-1} K^{-2})	$\lambda(T_r, \rho_r)$ (mW m^{-1} K^{-1})	$\lambda(T_n,\rho_r)$ (mW m K^{-1})	$\lambda(T_n,P)$ (mW m K^{-1})	ρ_r (Kg m^{-3})
337.450	16.850	0.851E-01	-0.148E+00	96.092	96.067	96.137	673.43
337.160	31.260	0.108E+00	-0.148E+00	101.338	101.337	101.340	687.73
336.930	51.580	0.137E+00	-0.133E+00	108.321	108.351	108.291	704.58
336.550	101.020	0.189E+00	-0.895E-01	123.341	123.454	123.287	735.34
336.620	101.530	0.189E+00	-0.891E-01	123.427	123.527	123.380	735.56
337.220	136.390	0.213E+00	-0.659E-01	131.924	131.909	131.929	751.43
336.200	151.280	0.222E+00	-0.573E-01	135.419	135.630	135.364	757.95
336.270	151.580	0.222E+00	-0.572E-01	135.452	135.648	135.402	758.03
336.880	196.610	0.240E+00	-0.388E-01	144.454	144.519	144.444	773.69
336.840	221.970	0.247E+00	-0.308E-01	149.827	149.904	149.817	781.58
336.010	250.150	0.253E+00	-0.232E-01	154.799	155.088	154.773	790.00
335.840	300.330	0.258E+00	-0.132E-01	163.480	163.818	163.463	803.10
336.220	333.940	0.258E+00	-0.784E-02	168.105	168.345	168.098	811.00
336.260	345.450	0.258E+00	-0.617E-02	170.227	170.456	170.221	813.66
336.100	399.960	0.252E+00	0.205E-03	177.691	177.956	177.691	825.93
336.120	429.130	0.247E+00	0.298E-02	181.513	181.767	181.516	832.25
336.090	439.500	0.244E+00	0.375E-02	183.071	183.330	183.075	834.48
336.130	441.260	0.244E+00	0.397E-02	183.322	183.571	183.326	834.84
336.070	496.030	0.288E+00	0.679E-02	190.347	190.594	190.355	846.50
336.310	512.430	0.223E+00	0.795E-02	192.227	192.414	192.233	849.88
335.950	541.520	0.210E+00	0.662E-02	195.673	195.925	195.681	856.18
336.460	572.520	0.196E+00	0.760E-02	199.236	199.371	199.242	862.64

Table 4.18

Thermal Conductivity of 2,2,4-trimethylpentane at T_n = 351.15K

T_r (K)	P (MPa)	$(\frac{\partial\lambda}{\partial T})_{\rho_r}$ (mW m^{-1} K^{-2})	$(\frac{\partial\lambda}{\partial T})_p$ (mW m^{-1} K^{-2})	$\lambda(T_r, \rho_r)$ (mW m^{-1} K^{-1})	$\lambda(T_n,\rho_r)$ (mW m K^{-1})	$\lambda(T_n,P)$ (mW m K^{-1})	ρ_r (Kg m^{-3})
351.910	19.030	0.722E-01	-0.162E+00	94.163	94.108	94.286	664.64
351.960	19.340	0.727E-01	-0.162E+00	94.659	94.601	94.790	664.95
351.300	66.000	0.140E+00	-0.138E+00	112.100	112.079	112.120	706.39
350.960	106.290	0.181E+00	-0.103E+00	123.733	123.767	123.713	730.57
351.430	146.010	0.209E+00	-0.771E-01	133.298	133.239	133.320	748.49
350.450	150.370	0.212E+00	-0.740E-01	134.634	134.783	134.583	750.73
351.120	200.740	0.235E+00	-0.497E-01	144.982	144.989	144.980	768.46
350.910	245.240	0.248E+00	-0.315E-01	153.332	153.392	153.325	781.99
351.000	247.150	0.248E+00	-0.308E-01	153.785	153.822	153.780	782.48
351.000	304.630	0.257E+00	-0.944E-02	164.188	164.227	164.187	797.66
351.260	356.060	0.258E+00	0.927E-02	171.834	171.805	171.833	809.93
351.230	373.100	0.257E+00	0.156E-01	173.966	173.945	173.965	813.98
351.150	379.950	0.257E+00	0.179E-01	175.003	175.003	175.003	815.49
351.050	422.850	0.252E+00	0.332E-01	180.904	180.930	180.908	825.20
350.920	459.480	0.246E+00	0.459E-01	185.429	185.486	185.440	833.37
350.800	498.760	0.235E+00	0.588E-01	190.806	190.888	190.827	842.09
350.850	517.050	0.229E+00	0.648E-01	193.104	193.173	193.124	846.13
350.750	533.110	0.223E+00	0.692E-01	194.999	195.088	195.026	849.73
350.710	563.980	0.209E+00	0.774E-01	198.129	198.221	198.163	856.67
350.720	570.740	0.206E+00	0.791E-01	199.272	199.360	199.306	858.20

Table 4.19

Thermal Conductivity of benzene at T_n = 310.15K

T_r (K)	P (MPa)	$(\frac{\partial\lambda}{\partial T})_{\rho_r}$ (mW m^{-1} K^{-2})	$(\frac{\partial\lambda}{\partial T})_p$ (mW m^{-1} K^{-2})	$\lambda(T_r, \rho_r)$ (mW m^{-1} K^{-1})	$\lambda(T_n,\rho_r)$ (mW m K^{-1})	$\lambda(T_n,P)$ (mW m K^{-1})	ρ_r (Kg m^{-3})
310.230	1.628	0.127E+00	-0.366E+00	137.657	137.647	137.687	862.10
309.865	7.936	0.128E+00	-0.346E+00	140.279	140.316	140.181	867.84
309.828	10.277	0.128E+00	-0.340E+00	141.342	141.383	141.233	869.80
310.189	19.737	0.133E+00	-0.316E+00	144.298	144.293	144.310	876.88
310.110	30.722	0.140E+00	-0.293E+00	148.030	148.036	138.019	885.01
309.968	41.703	0.148E+00	-0.279E+00	151.587	151.614	151.537	892.60
310.034	51.361	0.153E+00	-0.272E+00	154.851	154.869	154.820	898.69
309.876	61.322	0.157E+00	-0.271E+00	157.513	157.556	157.439	904.80
309.761	74.533	0.158E+00	-0.284E+00	161.594	161.655	161.484	912.36
309.745	81.846	0.156E+00	-0.297E+00	163.346	163.409	163.225	916.33
310.798	91.389	0.153E+00	-0.317E+00	166.500	166.401	166.706	920.50

Table 4.20

Thermal Conductivity of benzene at T_n = 320.65K

T_r (K)	P (MPa)	$(\frac{\partial\lambda}{\partial T})_{\rho_r}$ (mW m^{-1} K^{-2})	$(\frac{\partial\lambda}{\partial T})_p$ (mW m^{-1} K^{-2})	$\lambda(T_r, \rho_r)$ (mW m^{-1} K^{-1})	$\lambda(T_n, \rho_r)$ (mW m K^{-1})	$\lambda(T_n, P)$ (mW m K^{-1})	ρ_r (Kg m^{-3})
320.965	4.579	0.132E+00	-0.321E+00	135.544	135.502	135.645	853.35
321.055	10.887	0.128E+00	-0.325E+00	137.449	137.398	137.581	858.77
320.840	13.430	0.127E+00	-0.325E+00	139.117	139.092	139.178	861.14
320.759	20.144	0.127E+00	-0.322E+00	141.552	141.538	141.587	866.74
320.577	40.992	0.138E+00	-0.294E+00	148.879	148.889	148.858	882.52
320.411	60.713	0.151E+00	-0.260E+00	154.911	154.947	154.849	895.61
320.411	79.409	0.157E+00	-0.235E+00	160.289	160.326	160.232	906.52
320.311	81.542	0.158E+00	-0.234E+00	160.958	161.011	160.879	907.77
320.339	100.215	0.156E+00	-0.230E+00	165.913	165.962	165.842	917.50
320.609	122.409	0.142E+00	-0.257E+00	171.312	171.318	171.301	927.93
320.549	122.612	0.141E+00	-0.258E+00	171.273	171.287	171.247	928.07
320.566	138.926	0.122E+00	-0.307E+00	175.314	175.324	175.288	935.45
320.534	147.130	0.109E+00	-0.342E+00	176.866	176.879	176.826	939.11
320.430	161.172	0.800E-01	-0.422E+00	179.825	179.842	179.732	945.42

Table 4.21

Thermal Conductivity of benzene at T_n = 344.15K

T_r (K)	P (MPa)	$(\frac{\partial\lambda}{\partial T})_{\rho_r}$ (mW m^{-1} K^{-2})	$(\frac{\partial\lambda}{\partial T})_p$ (mW m^{-1} K^{-2})	$\lambda(T_r, \rho_r)$ (mW m^{-1} K^{-1})	$\lambda(T_n,\rho_r)$ (mW m K^{-1})	$\lambda(T_n,P)$ (mW m K^{-1})	ρ_r (Kg m^{-3})
344.723	11.090	0.178E+00	-0.255E+00	130.325	130.223	130.471	834.55
345.012	20.144	0.151E+00	-0.267E+00	134.040	133.910	134.271	842.62
344.495	34.484	0.130E+00	-0.270E+00	139.750	139.705	139.843	855.48
344.512	43.228	0.127E+00	-0.263E+00	142.958	142.912	143.053	862.51
344.304	62.136	0.133E+00	-0.239E+00	149.431	149.411	149.468	876.73
344.172	81.846	0.145E+00	-0.211E+00	154.764	154.761	154.769	889.88
344.421	102.445	0.155E+00	-0.191E+00	161.169	161.127	161.220	901.82
344.263	120.280	0.158E+00	-0.183E+00	165.611	165.593	165.632	911.32
344.205	137.912	0.154E+00	-0.188E+00	170.311	170.302	170.321	919.78
344.105	158.347	0.140E+00	-0.208E+00	174.645	174.652	174.636	928.73
344.005	178.999	0.117E+00	-0.248E+00	179.489	179.506	179.453	937.01
344.012	185.037	0.108E+00	-0.263E+00	180.946	180.961	180.910	939.30
344.203	200.936	0.820E-01	-0.311E+00	184.114	184.109	184.130	945.03
344.152	225.402	0.288E-01	-0.415E+00	189.352	189.352	189.352	953.78
344.132	242.929	-0.202E-01	-0.514E+00	192.272	192.272	192.263	960.01
344.088	261.155	-0.839E-01	-0.647E+00	195.947	195.942	195.907	966.66

Table 4.22

Thermal Conductivity of benzene at T_n = 360.65K

T_r (K)	P (MPa)	$(\frac{\partial\lambda}{\partial T})_{\rho_r}$ (mW m^{-1} K^{-2})	$(\frac{\partial\lambda}{\partial T})_p$ (mW m^{-1} K^{-2})	$\lambda(T_r, \rho_r)$ (mW m^{-1} K^{-1})	$\lambda(T_n, \rho_r)$ (mW m K^{-1})	$\lambda(T_n, P)$ (mW m K^{-1})	ρ_r (Kg m^{-3})
361.139	9.463	0.288E+00	-0.753E-01	124.588	124.447	124.625	816.08
360.920	26.145	0.183E+00	-0.178E+00	132.152	132.103	132.200	833.23
360.758	39.161	0.145E+00	-0.213E+00	136.748	136.733	136.771	845.29
360.593	59.493	0.127E+00	-0.228E+00	144.536	144.543	144.523	862.04
360.558	81.339	0.133E+00	-0.225E+00	151.159	151.171	151.138	877.52
360.701	101.837	0.145E+00	-0.222E+00	157.376	157.368	157.387	889.99
360.943	122.612	0.155E+00	-0.224E+00	163.169	163.124	163.235	900.96
360.838	142.775	0.158E+00	-0.232E+00	168.059	168.029	168.102	910.58
360.706	162.382	0.154E+00	-0.245E+00	172.952	172.943	172.966	918.98
360.545	183.930	0.143E+00	-0.263E+00	177.355	177.370	177.328	927.36
360.568	205.160	0.124E+00	-0.285E+00	182.448	182.459	182.425	934.85
360.456	222.882	0.101E+00	-0.307E+00	185.434	185.454	185.375	940.87
360.417	232.962	0.862E-01	-0.321E+00	188.002	188.022	187.927	944.19
360.351	254.657	0.462E-01	-0.360E+00	192.236	192.250	192.129	951.22
360.666	274.758	0.891E-03	-0.403E+00	195.803	195.803	195.810	957.48
360.925	290.507	-0.423E-01	-0.446E+00	198.645	198.657	198.767	962.47
360.824	312.291	-0.120E+00	-0.541E+00	202.444	202.465	202.538	969.92
360.765	332.140	-0.209E+00	-0.664E+00	205.858	205.882	205.934	977.02

Table 4.23

Thermal Conductivity of Cyclohexane at T_n = 309.15K

T_r (K)	P (MPa)	$(\frac{\partial\lambda}{\partial T})_{\rho_r}$ (mW m^{-1} K^{-2})	$(\frac{\partial\lambda}{\partial T})_p$ (mW m^{-1} K^{-2})	$\lambda(T_r, \rho_r)$ (mW m^{-1} K^{-1})	$\lambda(T_n,\rho_r)$ (mW m K^{-1})	$\lambda(T_n,P)$ (mW m K^{-1})	ρ_r (Kg m^{-3})
309.644	5.258	0.125E+00	-0.303E+00	117.348	117.286	117.498	767.79
309.627	11.341	0.129E+00	-0.274E+00	119.897	119.835	120.027	772.81
309.519	14.844	0.134E+00	-0.258E+00	120.887	120.838	120.983	775.69
309.521	15.772	0.135E+00	-0.254E+00	121.321	121.271	121.415	776.41
309.447	21.435	0.145E+00	-0.231E+00	123.301	123.259	123.370	780.79
309.378	25.243	0.152E+00	-0.216E+00	124.675	124.641	124.725	783.64
309.351	30.385	0.162E+00	-0.198E+00	126.270	126.238	126.310	787.30
309.297	38.087	0.179E+00	-0.172E+00	128.720	128.694	128.745	792.51
309.247	40.344	0.184E+00	-0.165E+00	129.257	129.239	129.273	794.00
309.260	44.445	0.193E+00	-0.152E+00	130.559	130.538	130.576	796.55
309.298	45.469	0.198E+00	-0.148E+00	130.948	130.897	130.948	797.15

Table 4.24

Thermal Conductivity of Cyclohexane at T_n = 324.15K

T_r (K)	P (MPa)	$(\frac{\partial\lambda}{\partial T})_{\rho_r}$ (mW m^{-1} K^{-2})	$(\frac{\partial\lambda}{\partial T})_p$ (mW m^{-1} K^{-2})	$\lambda(T_r, \rho_r)$ (mW m^{-1} K^{-1})	$\lambda(T_n,\rho_r)$ (mW m K^{-1})	$\lambda(T_n,P)$ (mW m K^{-1})	ρ_r (Kg m^{-3})
324.482	12.990	0.125E+00	-0.267E+00	116.358	116.316	116.446	761.16
324.388	23.391	0.126E+00	-0.252E+00	120.173	120.143	120.233	769.94
324.268	29.048	0.132E+00	-0.236E+00	122.226	122.211	122.254	774.51
324.262	31.618	0.135E+00	-0.227E+00	123.159	123.144	123.185	776.49
324.238	33.673	0.138E+00	-0.220E+00	123.713	123.701	123.732	778.06
324.199	40.139	0.150E+00	-0.194E+00	126.966	126.959	126.976	782.82
324.120	47.517	0.164E+00	-0.161E+00	128.733	128.738	128.728	788.01
324.091	52.224	0.174E+00	-0.138E+00	129.751	129.761	129.743	791.15
324.033	57.536	0.186E+00	-0.112E+00	131.502	131.523	131.488	794.58
324.041	61.616	0.195E+00	-0.922E-01	132.475	132.496	132.465	797.08
324.909	70.471	0.212E+00	-0.524E-01	134.856	134.696	134.896	801.71
324.856	73.622	0.218E+00	-0.368E-01	135.845	135.691	135.871	803.50
324.774	76.773	0.225E+00	-0.208E-01	136.482	136.342	136.495	805.25

Table 4.25

Thermal Conductivity of Cyclohexane at T_n = 353.15K

T_r (K)	P (MPa)	$(\frac{\partial\lambda}{\partial T})_{\rho_r}$ (mW m^{-1} K^{-2})	$(\frac{\partial\lambda}{\partial T})_p$ (mW m^{-1} K^{-2})	$\lambda(T_r, \rho_r)$ (mW m^{-1} K^{-1})	$\lambda(T_n,\rho_r)$ (mW m K^{-1})	$\lambda(T_n,P)$ (mW m K^{-1})	ρ_r (Kg m^{-3})
353.682	18.553	0.189E+00	-0.156E+00	111.458	111.358	111.541	741.13
353.469	32.029	0.136E+00	-0.183E+00	116.775	116.732	116.833	754.07
353.363	38.908	0.126E+00	-0.190E+00	119.110	119.084	119.151	760.05
353.257	51.303	0.126E+00	-0.196E+00	123.288	123.274	123.309	769.83
353.210	62.533	0.138E+00	-0.202E+00	126.963	126.955	126.975	777.70
353.116	71.691	0.152E+00	-0.209E+00	129.624	129.629	129.617	783.55
353.039	81.141	0.168E+00	-0.219E+00	132.190	132.209	132.166	789.07
353.919	84.999	0.172E+00	-0.228E+00	133.417	133.285	133.593	790.49
353.780	93.421	0.187E+00	-0.243E+00	135.716	135.598	135.869	794.91
353.765	102.848	0.203E+00	-0.264E+00	138.111	137.986	138.273	799.37
353.687	103.153	0.204E+00	-0.264E+00	138.143	138.034	138.285	799.58
353.589	112.376	0.219E+00	-0.287E+00	140.581	140.484	140.707	803.69
353.580	120.281	0.231E+00	-0.309E+00	142.459	142.360	142.592	806.94

Table 4.26

Thermal Conductivity of Cyclohexane at T_n = 361.15K

T_r (K)	P (MPa)	$(\frac{\partial\lambda}{\partial T})_{\rho_r}$ (mW m^{-1} K^{-2})	$(\frac{\partial\lambda}{\partial T})_p$ (mW m^{-1} K^{-2})	$\lambda(T_r, \rho_r)$ (mW m^{-1} K^{-1})	$\lambda(T_n,\rho_r)$ (mW m K^{-1})	$\lambda(T_n,P)$ (mW m K^{-1})	ρ_r (Kg m^{-3})
361.431	24.420	0.192E+00	-0.110E+00	112.185	112.131	112.216	740.60
361.328	35.418	0.144E+00	-0.167E+00	116.298	116.272	116.328	751.02
361.357	44.752	0.128E+00	-0.200E+00	119.678	119.652	119.719	758.83
362.378	50.792	0.124E+00	-0.215E+00	121.530	121.377	121.794	762.72
361.082	63.348	0.129E+00	-0.250E+00	125.690	125.699	125.673	772.37
361.215	75.248	0.141E+00	-0.284E+00	129.382	129.373	129.401	779.44
361.749	81.445	0.149E+00	-0.306E+00	131.296	131.207	131.479	782.36
361.571	103.659	0.180E+00	-0.395E+00	137.428	137.352	137.594	792.84
361.460	120.281	0.203E+00	-0.476E+00	141.734	141.671	141.882	799.37
361.285	133.353	0.221E+00	-0.541E+00	144.356	144.326	144.429	804.12
361.212	144.698	0.235E+00	-0.599E+00	147.290	147.276	147.327	807.98

Table 4.27

Thermal Conductivity of Toluene at T_n = 308.15K

T_r (K)	P (MPa)	$(\frac{\partial\lambda}{\partial T})_{\rho_r}$ (mW m^{-1} K^{-2})	$(\frac{\partial\lambda}{\partial T})_p$ (mW m^{-1} K^{-2})	$\lambda(T_r, \rho_r)$ (mW m^{-1} K^{-1})	$\lambda(T_n, \rho_r)$ (mW m K^{-1})	$\lambda(T_n, P)$ (mW m K^{-1})	ρ_r (Kg m^{-3})
307.850	0.887	0.732E-01	0.735E-01	128.880	128.901	128.902	853.61
307.840	1.476	0.746E-01	0.749E-01	129.110	129.133	129.133	854.09
308.430	3.735	0.781E-01	0.784E-01	129.670	129.648	129.648	855.33
308.230	11.399	0.969E-01	0.972E-01	132.460	132.452	132.452	861.56
307.940	16.810	0.111E+00	0.111E+00	134.620	134.643	134.643	866.04
308.120	33.396	0.153E+00	0.154E+00	139.570	139.575	139.575	878.33
308.120	51.713	0.201E+00	0.201E+00	145.530	145.536	145.536	891.41
308.010	55.924	0.212E+00	0.212E+00	146.280	146.310	146.310	894.42
307.970	64.284	0.233E+00	0.234E+00	148.630	148.672	148.672	900.11
308.000	66.307	0.238E+00	0.239E+00	149.070	149.106	149.106	901.42
307.960	129.810	0.367E+00	0.367E+00	163.760	163.830	163.830	938.92
308.190	153.600	0.397E+00	0.398E+00	168.100	168.084	168.084	950.42
308.010	202.450	0.435E+00	0.435E+00	177.600	177.661	177.661	971.11
307.960	253.660	0.444E+00	0.444E+00	185.940	186.024	186.024	988.18
308.070	303.930	0.433E+00	0.434E+00	193.330	193.365	193.365	1001.48
307.890	353.970	0.410E+00	0.410E+00	200.080	200.187	200.187	1013.24
307.950	401.250	0.376E+00	0.376E+00	206.370	206.445	206.445	1023.86
307.810	450.200	0.318E+00	0.318E+00	211.820	211.928	211.928	1036.45
308.780	463.540	0.302E+00	0.303E+00	213.590	213.400	213.399	1039.17
308.730	463.540	0.302E+00	0.302E+00	213.640	213.465	213.465	1039.23
307.500	463.640	0.293E+00	0.294E+00	213.490	213.681	213.681	1040.69
307.940	495.250	0.228E+00	0.229E+00	217.040	217.088	217.088	1050.47
307.910	502.370	0.208E+00	0.209E+00	217.670	217.720	217.729	1053.09
307.740	531.350	0.105E+00	0.105E+00	220.910	220.953	220.953	1065.04
308.000	531.560	0.107E+00	0.107E+00	220.940	220.956	220.956	1064.83

Table 4.28

Thermal Conductivity of Toluene at T_n = 320.15K

T_r (K)	P (MPa)	$(\frac{\partial\lambda}{\partial T})_{\rho_r}$ (mW m^{-1} K^{-2})	$(\frac{\partial\lambda}{\partial T})_p$ (mW m^{-1} K^{-2})	$\lambda(T_r, \rho_r)$ (mW m^{-1} K^{-1})	$\lambda(T_n,\rho_r)$ (mW m K^{-1})	$\lambda(T_n,P)$ (mW m K^{-1})	ρ_r (Kg m^{-3})
320.493	1.378	0.431E-01	0.433E-01	125.280	125.265	125.265	841.82
320.290	2.360	0.454E-01	0.456E-01	126.640	126.634	126.634	842.79
320.679	24.100	0.892E-01	0.895E-01	133.700	133.653	133.653	859.05
320.508	32.210	0.108E+00	0.109E+00	135.640	135.601	135.601	865.18
320.675	59.140	0.173E+00	0.173E+00	143.710	143.619	143.619	883.79
320.584	84.990	0.234E+00	0.235E+00	150.630	150.528	150.528	900.41
320.465	109.540	0.287E+00	0.288E+00	156.360	156.269	156.269	914.85
320.356	132.540	0.330E+00	0.331E+00	161.800	161.732	161.732	927.17
320.620	164.000	0.375E+00	0.375E+00	168.330	168.154	168.154	941.76
320.456	202.040	0.413E+00	0.413E+00	175.440	175.314	175.314	957.31
320.580	252.760	0.438E+00	0.438E+00	183.790	183.602	183.602	973.85
320.570	303.730	0.444E+00	0.444E+00	192.030	191.844	191.843	987.30
320.386	353.470	0.437E+00	0.437E+00	198.720	198.617	198.617	998.84
320.393	358.050	0.436E+00	0.436E+00	199.490	199.384	199.384	999.84
320.258	402.340	0.418E+00	0.419E+00	205.130	205.085	205.085	1009.89
320.562	439.010	0.395E+00	0.395E+00	209.520	209.357	209.357	1018.52
320.452	460.270	0.373E+00	0.374E+00	212.180	212.067	212.067	1024.50
320.359	501.580	0.309E+00	0.309E+00	216.840	216.775	216.775	1038.00
320.292	542.050	0.195E+00	0.195E+00	221.500	221.472	221.472	1054.79
320.342	556.020	0.137E+00	0.137E+00	223.080	223.054	223.054	1061.57
320.318	571.730	0.547E-01	0.550E-01	224.280	224.271	224.271	1070.06

Table 4.29

Thermal Conductivity of Toluene at T_n = 330.15K

T_r (K)	P (MPa)	$(\frac{\partial\lambda}{\partial T})_{\rho_r}$ (mW m^{-1} K^{-2})	$(\frac{\partial\lambda}{\partial T})_p$ (mW m^{-1} K^{-2})	$\lambda(T_r, \rho_r)$ (mW m^{-1} K^{-1})	$\lambda(T_n,\rho_r)$ (mW m K^{-1})	$\lambda(T_n,P)$ (mW m K^{-1})	ρ_r (Kg m^{-3})
330.860	7.270	0.314E-01	0.316E-01	124.506	124.483	124.483	836.22
330.870	11.500	0.379E-01	0.382E-01	125.350	125.322	125.322	839.45
330.860	19.910	0.525E-01	0.528E-01	128.360	128.323	128.323	845.78
330.140	33.200	0.806E-01	0.810E-01	132.775	132.775	132.775	856.20
330.860	37.260	0.870E-01	0.874E-01	135.167	135.105	135.105	858.36
330.870	51.010	0.117E+00	0.118E+00	138.185	138.101	138.100	867.87
330.300	77.670	0.180E+00	0.180E+00	146.106	146.079	146.079	885.75
330.400	101.730	0.233E+00	0.233E+00	152.147	152.089	152.089	899.91
329.850	126.060	0.283E+00	0.284E+00	158.414	158.499	158.499	913.65
330.260	153.300	0.328E+00	0.328E+00	163.959	163.923	163.923	926.42
330.600	177.590	0.360E+00	0.360E+00	169.049	168.887	168.887	936.56
330.500	201.940	0.387E+00	0.387E+00	173.173	173.038	173.038	946.09
330.350	252.260	0.423E+00	0.423E+00	182.130	182.046	182.046	962.62
330.520	302.430	0.439E+00	0.440E+00	190.070	189.907	189.907	975.56
330.310	352.770	0.444E+00	0.444E+00	197.470	197.399	197.399	987.16
330.580	375.390	0.443E+00	0.443E+00	200.470	200.280	200.280	991.76
330.340	400.550	0.438E+00	0.439E+00	204.123	204.040	204.040	997.64
330.820	451.680	0.418E+00	0.419E+00	210.242	209.962	209.961	1009.74
330.450	546.040	0.271E+00	0.272E+00	220.291	220.210	220.210	1044.20
330.500	583.770	0.111E+00	0.111E+00	223.488	223.449	223.449	1064.41

Table 4.30

Thermal Conductivity of Toluene at T_n = 345.15K

T_r (K)	P (MPa)	$(\frac{\partial\lambda}{\partial T})_{\rho_r}$ (mW m^{-1} K^{-2})	$(\frac{\partial\lambda}{\partial T})_p$ (mW m^{-1} K^{-2})	$\lambda(T_r, \rho_r)$ (mW m^{-1} K^{-1})	$\lambda(T_n,\rho_r)$ (mW m K^{-1})	$\lambda(T_n,P)$ (mW m K^{-1})	ρ_r (Kg m^{-3})
344.400	2.330	0.703E-02	0.727E-02	118.140	118.146	118.146	818.87
344.390	2.390	0.708E-02	0.732E-02	118.502	118.508	118.508	818.93
344.400	13.270	0.161E-01	0.164E-01	121.985	121.997	121.998	827.13
345.090	23.360	0.269E-01	0.272E-01	126.464	126.466	126.466	833.83
344.290	51.310	0.746E-01	0.750E-01	135.932	135.996	135.996	854.09
343.930	101.130	0.177E+00	0.178E+00	149.945	150.162	150.162	884.98
344.580	127.580	0.227E+00	0.227E+00	155.786	155.915	155.915	898.29
344.430	153.200	0.272E+00	0.273E+00	161.283	161.479	161.479	910.64
344.410	175.680	0.307E+00	0.307E+00	165.881	166.108	166.108	920.27
344.180	203.150	0.342E+00	0.343E+00	170.901	171.234	171.234	931.00
344.390	253.060	0.388E+00	0.389E+00	179.949	180.243	180.244	946.65
344.270	306.030	0.419E+00	0.419E+00	188.623	188.991	188.991	960.31
344.040	355.360	0.435E+00	0.436E+00	196.319	196.803	196.803	971.47
343.940	402.840	0.443E+00	0.444E+00	202.209	202.746	202.746	981.89
344.130	451.970	0.441E+00	0.442E+00	208.486	208.937	208.937	993.69
344.390	455.280	0.441E+00	0.441E+00	208.762	209.097	209.097	994.27
344.370	497.590	0.424E+00	0.424E+00	213.957	214.287	214.288	1007.30
344.320	542.990	0.370E+00	0.370E+00	219.449	219.756	219.756	1025.43
344.250	584.760	0.250E+00	0.250E+00	223.602	223.827	223.827	1047.45
344.200	585.250	0.247E+00	0.247E+00	223.806	224.040	224.041	1047.81

Table 4.31

Thermal Conductivity of Toluene at T_n = 360.15K

T_r (K)	P (MPa)	$(\frac{\partial\lambda}{\partial T})_{\rho_r}$ (mW m^{-1} K^{-2})	$(\frac{\partial\lambda}{\partial T})_p$ (mW m^{-1} K^{-2})	$\lambda(T_r, \rho_r)$ (mW m^{-1} K^{-1})	$\lambda(T_n,\rho_r)$ (mW m K^{-1})	$\lambda(T_n,P)$ (mW m K^{-1})	ρ_r (Kg m^{-3})
360.700	3.240	0.439E-02	0.467E-02	113.678	113.675	113.675	802.84
360.900	26.470	0.754E-02	0.787E-02	123.377	123.371	123.371	819.49
360.610	49.210	0.295E-01	0.299E-01	131.202	131.188	131.188	835.26
360.680	50.610	0.311E-01	0.315E-01	130.254	130.237	130.237	836.10
360.430	74.520	0.671E-01	0.676E-01	139.549	139.530	139.530	851.41
360.630	104.170	0.118E+00	0.119E+00	146.673	146.616	146.616	868.15
360.480	126.770	0.159E+00	0.160E+00	152.141	152.088	152.088	880.00
360.990	152.290	0.201E+00	0.201E+00	158.053	157.884	157.884	891.35
360.910	203.650	0.276E+00	0.276E+00	168.248	168.038	168.038	911.67
360.770	255.660	0.333E+00	0.333E+00	177.926	177.719	177.719	927.94
360.840	304.330	0.370E+00	0.370E+00	185.657	185.402	185.402	940.00
359.700	338.640	0.394E+00	0.394E+00	190.318	190.495	190.495	948.92
360.830	353.170	0.398E+00	0.398E+00	193.231	192.961	192.960	950.60
360.940	405.810	0.421E+00	0.422E+00	200.566	200.234	200.233	961.66
360.760	453.060	0.437E+00	0.438E+00	206.340	206.074	206.073	973.29
360.670	497.880	0.444E+00	0.444E+00	212.476	212.245	212.245	986.84
360.620	508.260	0.443E+00	0.444E+00	212.422	212.214	212.214	990.53
360.740	543.830	0.428E+00	0.429E+00	217.376	217.123	217.123	1004.72
360.650	577.640	0.383E+00	0.383E+00	220.544	220.352	220.352	1021.85

Table 4.32

Coefficients of the Correlation of the Pressure Dependence of the Thermal Conductivity of Equation (4.1)

N-hexane

T (^{0}C)	P' (MPa)	b_o ($mWm^{-1}K^{-1}$)	b_1	b_2	b_3
34.0	250	110.54	0.3403	0.6164	-0.1936
48.0	250	104.31	0.4347	0.6002	-0.1901
72.0	250	92.59	0.7182	0.4476	-0.1355
87.0	250	89.31	0.7302	0.4953	-0.1522

N-octane

T (^{0}C)	P' (MPa)	b_o ($mWm^{-1}K^{-1}$)	b_1	b_2	b_3
34.0	250	118.30	0.3185	0.4136	-0.1106
48.0	250	101.39	0.8271	0.0069	0.0359
72.0	250	100.58	0.6659	0.2206	-0.0387
89.0	250	96.22	0.6710	0.2919	-0.0633

2,3-dimethylbutane

T (^{0}C)	P' (MPa)	b_o ($mWm^{-1}K^{-1}$)	b_1	b_2	b_3
36.0	250	96.72	0.2705	0.7148	-0.2414
48.0	250	88.78	0.5453	0.5022	-0.1631
72.0	250	76.88	1.0841	0.0912	-0.0297
88.0	250	81.51	0.8736	0.1900	-0.0526

2,2,4-trimethylpentane

T (^{0}C)	P' (MPa)	b_o ($mWm^{-1}K^{-1}$)	b_1	b_2	b_3
40.0	250	80.03	0.7498	0.2917	-0.0955
48.0	250	85.46	0.4589	0.5284	-0.1687
64.0	250	81.24	0.5557	0.5059	-0.1589
78.0	250	77.30	0.6890	0.4497	-0.1427

Benzene

T (^{0}C)	P' (MPa)	b_o ($mWm^{-1}K^{-1}$)	b_1	b_2	b_3
37.0	50	136.55	0.0260	0.1084	-0.0058
47.5	90	133.58	-0.0010	0.3075	-0.0849
71.0	140	122.86	0.1225	0.3676	-0.1017
87.5	180	116.39	0.2063	0.4467	-0.1343

Cyclohexane

T (^{0}C)	P' (MPa)	b_o ($mWm^{-1}K^{-1}$)	b_1	b_2	b_3
36.0	20	114.77	0.0185	0.0582	-0.0057
51.0	40	114.70	-0.1254	0.3188	-0.0935
80.0	60	101.72	0.0645	0.2243	-0.0489
88.0	70	103.91	-0.0712	0.4195	-0.1171

Toluene

T (^{0}C)	P' (MPa)	b_o ($mWm^{-1}K^{-1}$)	b_1	b_2	b_3
35.0	250	127.28	0.1128	0.5081	-0.1651
47.0	250	123.95	0.1131	0.5330	-0.1685
57.0	250	118.42	0.1727	0.5430	-0.1808
72.0	250	114.99	0.1968	0.5402	-0.1733
87.0	250	109.42	0.2441	0.5447	-0.1759

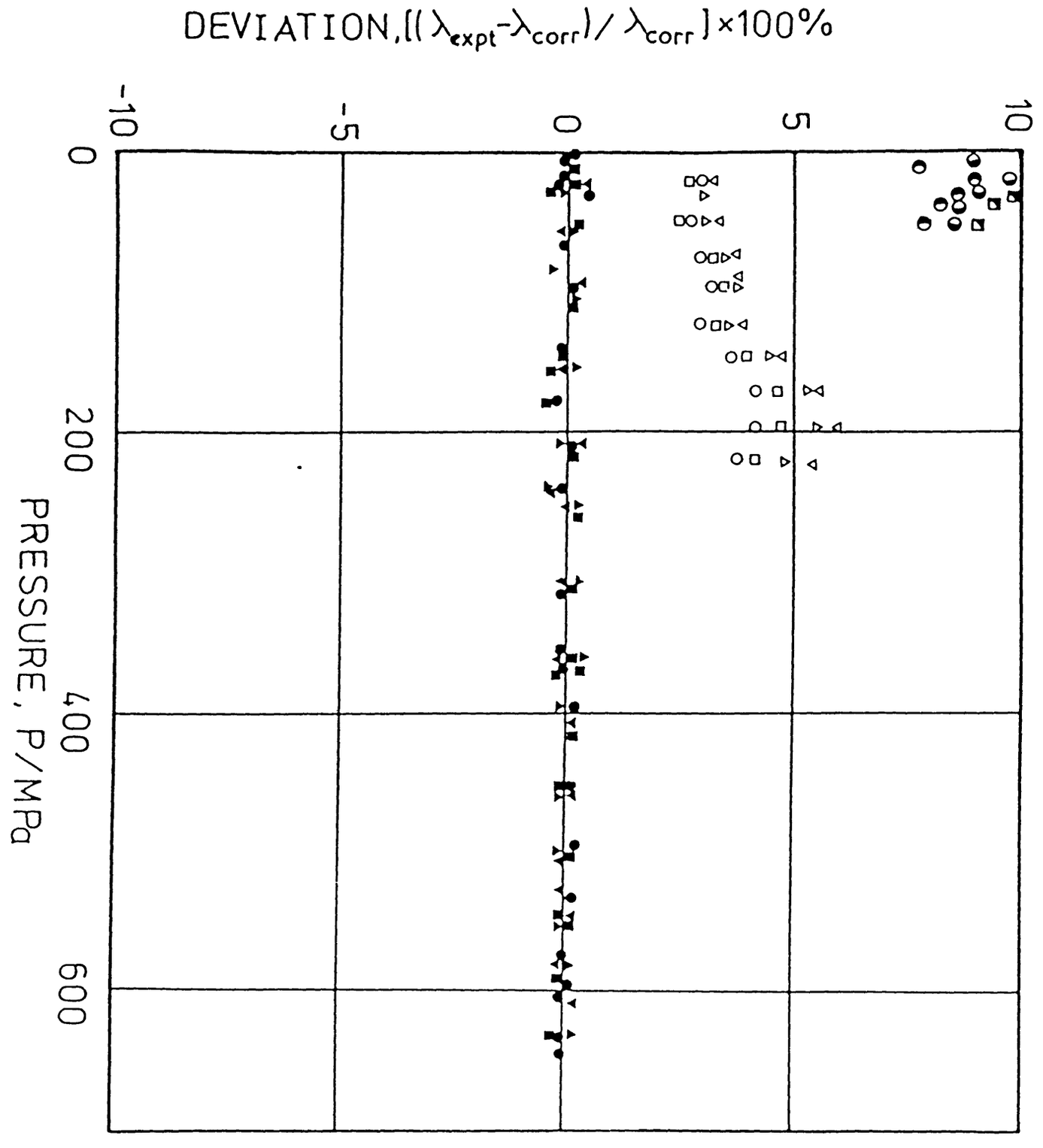

Fig. (4.1) Deviations of experimental thermal conductivity data for n-hexane from the correlation of Eq. (4.1)

Present work : ● - 34°C ; ■ - 48°C ; ▲ - 72°C ; ▼ - 87°C
Mukhamedzyanov et al (60) : ○ - 34°C ; □ - 48°C ; △ - 72°C ; ▽ - 87°C
Golubev and Naziev (61) : ◐ -34°C ; ◑ - 48°C ; ◪ - 72°C

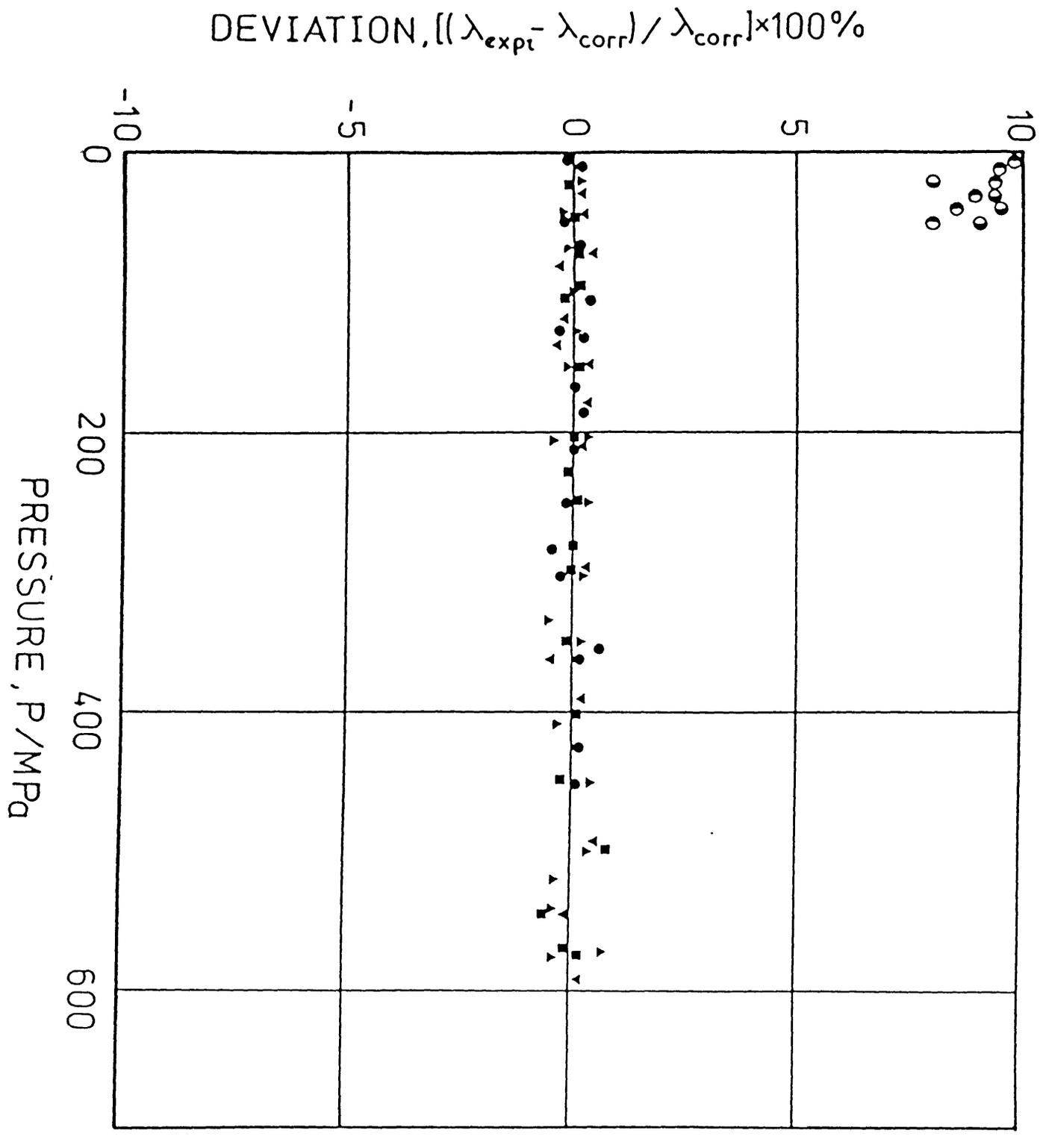

Fig. (4.2) Deviation of experimental thermal conductivity data for n-octane from the correlation of Eq. (4.1)

Present work : ● - 34°C ; ■ - 48°C ; ▲ -72°C ; ▼ -89°C
Golubev and Naziev (61) : ◐ - 34°C ; ◑ -48°C

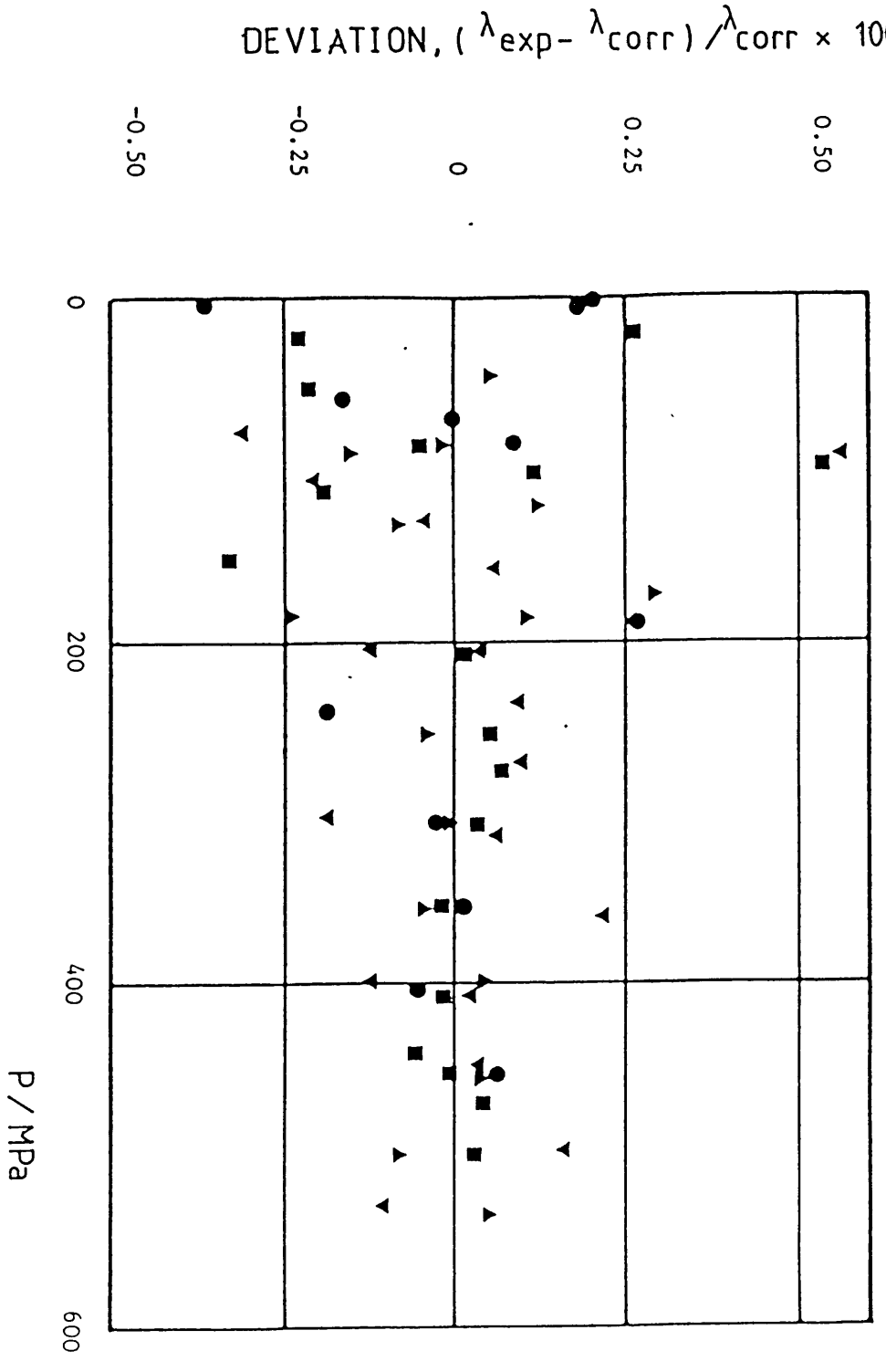

Fig. (4.3) Deviations of experimental thermal conductivity data for 2,3-dimethylbutane from the correlation of Eq. (4.1)

● - 36°C ; ■ - 48°C ; ▲-72°C ; ▼- 88°C

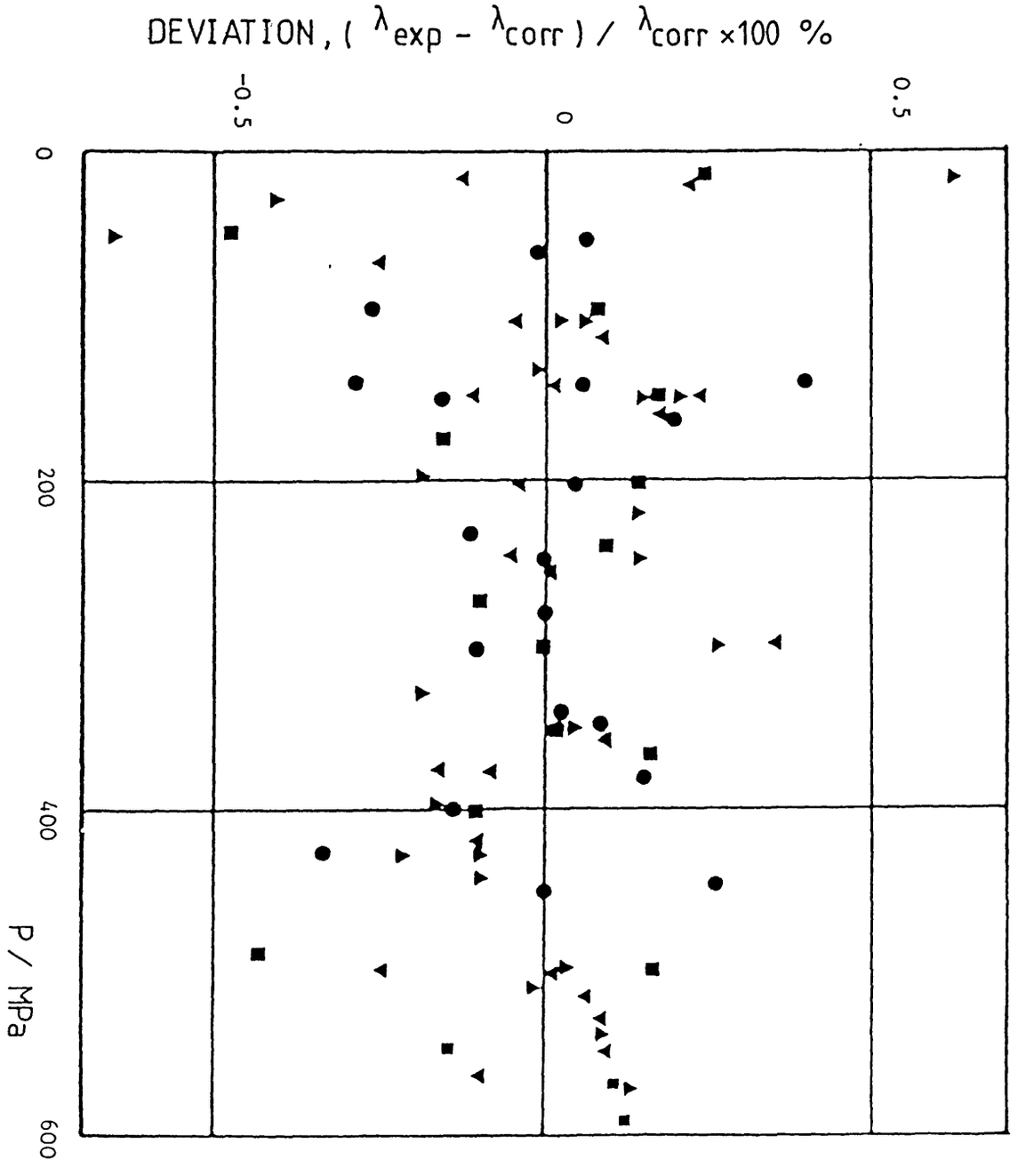

Fig. (4.4) Deviations of experimental thermal conductivity data for 2,2,4-trimethylpentane from the correlation of Eq. (4.1)

● - 40°C ; ■ - 48°C ; ▲-64°C ; ▼ -78°C

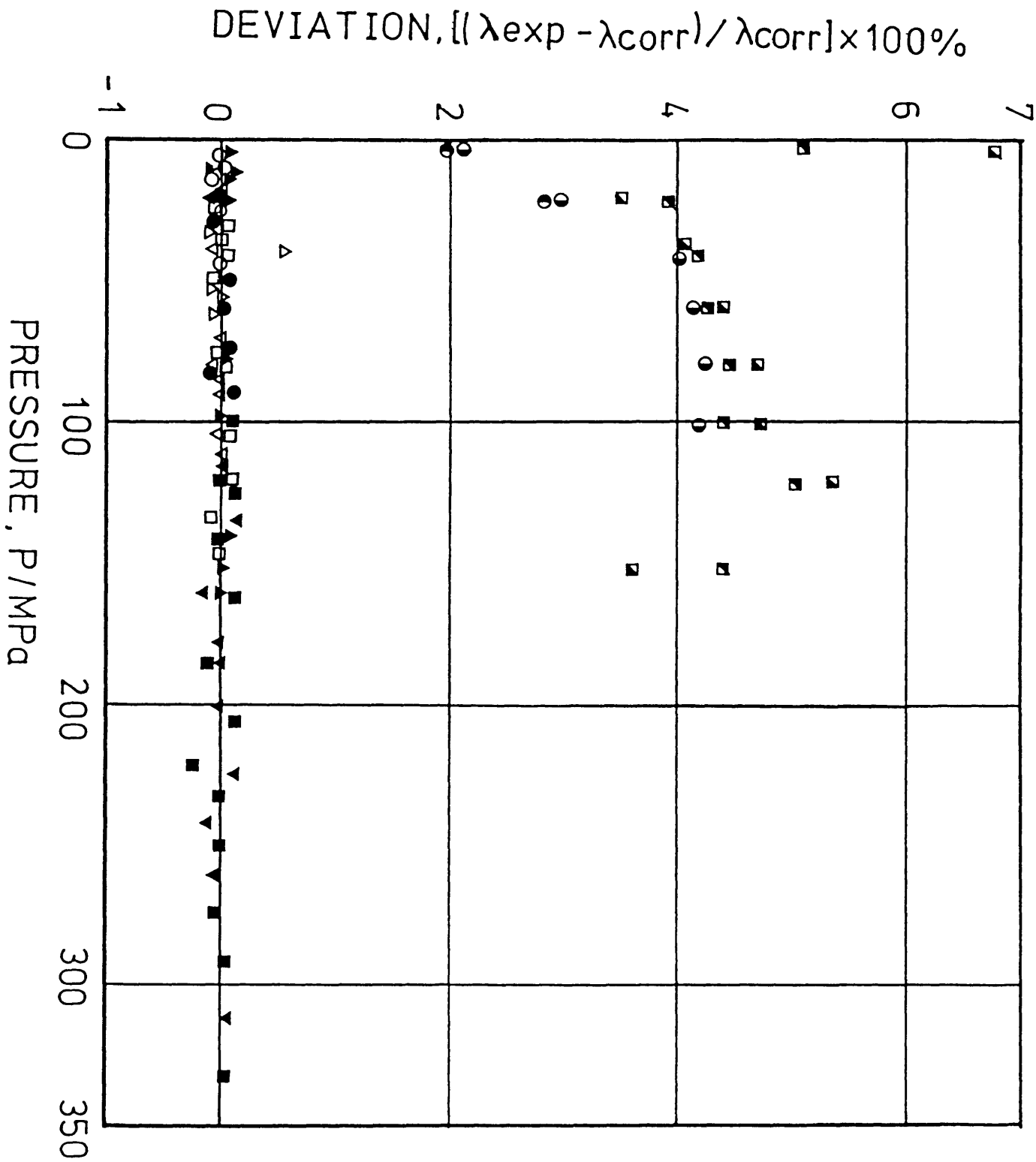

Fig. (4.5) Deviations of experimental data for the thermal conductivity of benzene and cyclohexane from the correlation of Eq. (4.1)

Present work:
Benzene: ● -37°C ; ▲ -47.5°C ; ▼ -71°C ; ■ -87.5°C
Cyclohexane: ○ -36°C ; △ -51°C ; ▽ -80°C ; □ -88°C
Rastorgueu (62);
Benzene: ◐ -37°C ; ◑ -47.5°C ; ◪ -71°C ; ◪ -87.5°C

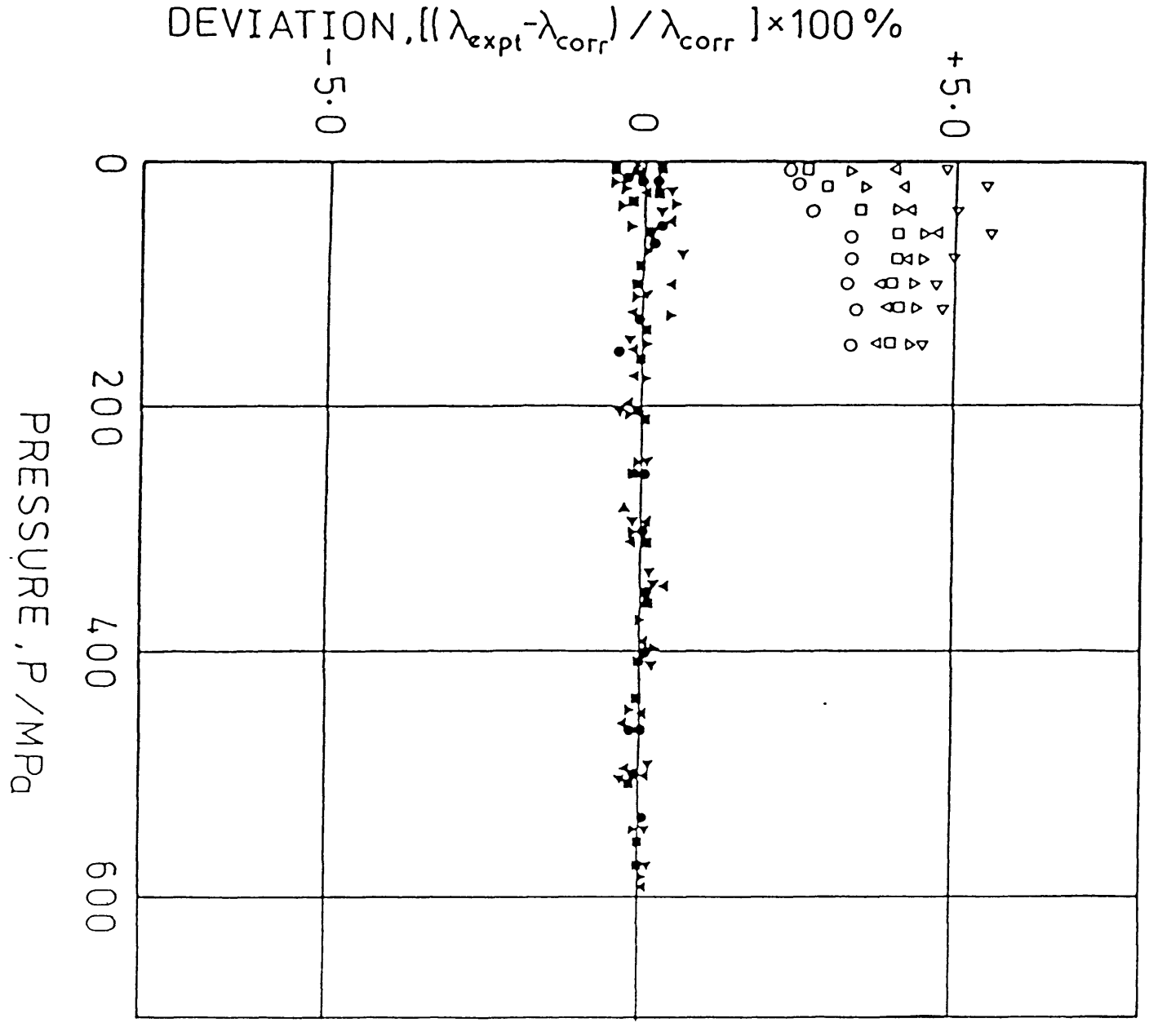

Fig. (4.6) The deviations of experimental thermal conductivity data for toluene from the correlation of Eq. (4.1)

Present work: ● -35°C ; ■ -47°C ; ▲ -57°C ; ▼ -72°C ; ► -87°C

Rastorguev et al (62): ○ -35°C ; □ -47°C ; △ -57°C ; ▽ -72°C ; ▷ -87°C

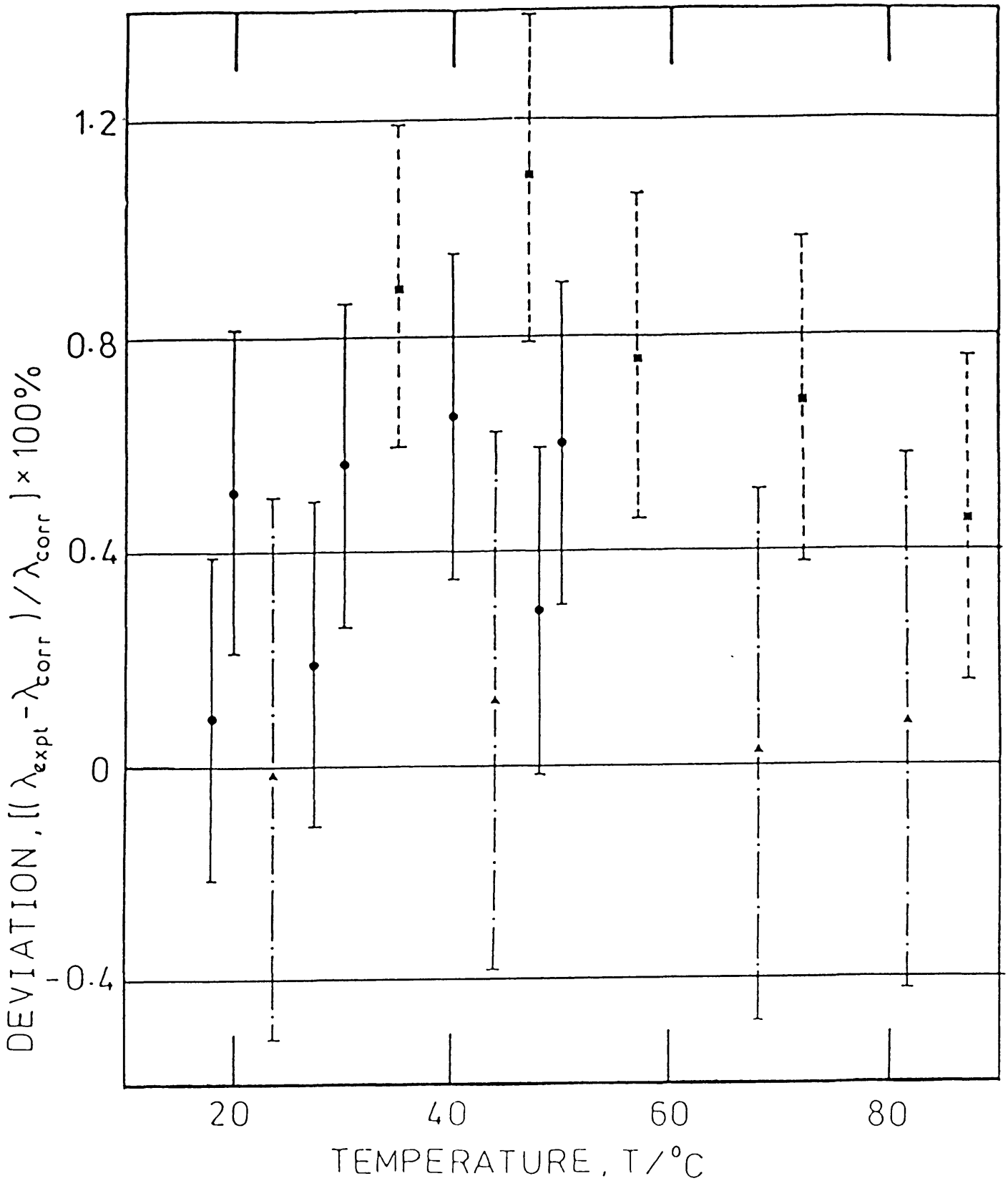

Fig. (4.7) The deviations of measurements of the thermal conductivity of tolulene at its saturation vapour pressure from the recommended correlation of Nagasaka and Nagashima (63)

■-extrapolation of present results
●-Nagasaka et al (64); ▲-Castro et al (65)

CHAPTER 5

THE KINETIC THEORY OF THE TRANSPORT PROPERTIES OF DENSE FLUIDS

5.1 Introduction

The development of the kinetic theory of fluids is intended to relate the macroscopic properties of fluids to the motion and interaction of the molecules they contain. The interpretation of the experimental results obtained in the present work necessitates a kinetic theory of dense polyatomic fluids.

At present, an exact kinetic theory is available only for monatomic gases at low density. This is based on the work of Boltzmann [66,67], Enskog [68,69] and Chapman [70,71]. They were able to relate the transport properties of such gases, i.e. the viscosity, thermal conductivity and diffusion coefficient, to the properties of their molecules. Provided that the intermolecular pair potential for the interaction of the monatomic species is known it is possible to calculate the transport properties of a gas consisting of such molecules to any desired degree of accuracy at any temperature.

The theory of dilute polyatomic gases and dense gases of monatomic or polyatomic species is currently far from complete and is undergoing extensive development. For dilute polyatomic gases a formal kinetic theory exists but exact evaluation of properties from it for an assumed intermolecular pair potential is still far from routine. For dense fluids even the formal kinetic theory is not fully developed. For these reasons, treatment of these more complex systems places a greater reliance on approximate analyses and approximate models than is necessary for the dilute monatomic system. The theories of the dense

fluid state are therefore not of comparable quality to that for the simplest system, and an ab initio evaluation of the transport properties from an assumed pair potential is not practicable. The most that can be expected from a theory of transport in the dense fluid state at the moment is therefore the provision of a suitable framework for the correlation of experimental data. If the theory incorporates the major features of the transport processes in dense fluids it may also be expected to allow a modest extrapolation of experimental data and to lead to the development of a predictive procedure.

The present chapter reviews the kinetic theory results for dilute and dense monatomic fluids as a precusor to the more approximate theory of dense polyatomic fluids. The latter is then applied to the interpretation of the present results for the thermal conductivity of polyatomic liquids in a subsequent chapter in the spirit outlined above.

5.2 Summary of Results for the Transport Properties of a Dilute Gas of hard spheres

A knowledge of the distribution of molecular velocities as a function of time and space allows the macroscopic properties of a gas to be calculated. The microscopic mechanical state of a monatomic particle gas at time t is defined by the specification of the position r_1, ..., r_N and of momenta P_1, ..., P_N of all the N particles. For conciseness, we introduce the notations:

$$x_i = (r_i, P_i) \tag{5.1}$$

a six-dimensional vector defining the state of the particle labelled i ($1 \leq i \leq N$), and

$$x = (x_1, \ldots\ldots, x_N) \qquad (5.2)$$

a 6N-dimensional vector defining the state of the complete system.

The distribution function of the variables x is denoted by $f_N(x,t)$. The expression $f_N(x,t)dx$ represents the probability that, at time t, the coordinates and momenta of the particles have values within a range dx around x. The function f_N is normalised as follows:

$$\int f_N(x,t)dx = 1 \qquad (5.3)$$

Boltzmann derived an integrodifferential equation for the distribution function for a dilute gas in which only binary collisions are important. For a gas whose molecules are not subject to external forces the only means whereby the velocity of a molecule can change is by collision with other molecules. Boltzmann assumed that for these gases during collisions all possible states of motion occur with equal frequency. Thus each molecule is as likely to be found in one position as in another; furthermore, except for the simple fact that the molecules cannot get inside each other, there is on the average no correlation whatever between the positions and velocities of different molecules. This statistical assumption, known as "Stosszahlansatz" or "Molecular Chaos", makes the Boltzmann equation irreversible in time,

i.e. if at some instant of time, the velocities of all the particles in the system were reversed, then the particles would not retrace their trajectories in the phase space so that earlier states of the system in phase space would not be recovered.

The Chapman-Enskog method [72] enables the Boltzmann equation to be solved by a method of successive approximations. The first term is the Maxwellian equilibrium distribution of velocities and the higher order terms represent successive stages away from this equilibrium distribution.

The most significant feature of the Chapman-Enskog solution is that each of the transport coefficient of a gas or gas mixture can be expressed in terms of well defined collision integrals over the intermolecular potential for each of the possible binary encounters in the system [72]. If the atoms of the gas interact according to the rigid sphere potential

$$U(r) = 0 \qquad r > \sigma \tag{5.4}$$

$$U(r) = \infty \qquad r \leqslant \sigma \tag{5.5}$$

where σ is the diameter of the rigid spheres, then the expressions for the self-diffusion coefficient, viscosity and thermal conductivity of the gas are

$$D^0 = \frac{3}{8\,\rho^0\sigma^2\pi}\,(\pi m k T)^{\frac{1}{2}} \tag{5.6}$$

$$\eta^0 = \frac{5}{16\sigma^2\pi}\,(\pi m k T)^{\frac{1}{2}} \tag{5.7}$$

and

$$\lambda^0 = \frac{75}{64\sigma^2\pi}\left(\frac{\pi k^3 T}{m}\right)^{\frac{1}{2}} = \frac{25}{32}\left(\frac{\pi kT}{m}\right)^{\frac{1}{2}}\frac{C_v}{\pi\sigma^2} \qquad (5.8)$$

where the superscript ^{0} denotes the dilute gas limit, ρ is the mass density of the gas, k is Boltzmann's constant, T is the absolute temperature and C_v is the constant volume heat capacity.

For molecules which interact through a general form of intermolecular pair potential U(r), the dynamics of binary collisions are quite different and this has an influence upon the transport properties.

In place of equations (5.6) to (5.8) we find

$$D^0 = \frac{3}{8\rho^0}\left(\frac{(\pi mkT)}{\bar{\Omega}^{(1,1)}(T)}\right)^{\frac{1}{2}} \qquad (5.9)$$

$$\eta^0 = \frac{5}{16\bar{\Omega}^{(2,2)}(T)}\,(\pi mkT)^{\frac{1}{2}} \qquad (5.10)$$

and

$$\lambda^0 = \frac{75}{64\bar{\Omega}^{(2,2)}(T)}\left(\frac{\pi k^3 T}{m}\right)^{\frac{1}{2}} \qquad (5.11)$$

The quantities $\bar{\Omega}^{(\ell,s)}(T)$ which occur in these expressions are known as collision integrals and are functionals of the intermolecular pair

potential U(r) readily evaluated by standard quadrature techniques. For the rigid sphere case $\bar{n}^{(\ell,s)} = \pi\sigma^2$.

5.3 The Theory of the Transport Properties of Simple (monatomic) Dense Fluids

Rigorous theories of transport processes in dense fluids based on a generalised Boltzmann equation [73] have not yet progressed to the stage where they may be employed for reliable predictions. Although a formal statistical mechanical theory for the transport coefficients exists [74,75], its implementation for calculations for real fluids has only been accomplished by means of approximations whose physical basis is uncertain. Furthermore, calculations of transport coefficients in simple liquids based on these approximations are generally in poor agreement with experiments [74,75]. For these reasons, only a brief discussion of the vigorous kinetic theories of dense fluids is given in section 5.3.1. The remaining sections of this chapter deal with simpler theories of transport in fluids which incorporate the major features of the process at a molecular level. Although such theories do not allow the calculation of the transport coefficients of dense fluids from information about their constituent molecules, they can serve as a useful framework for the correlation of thermophysical properties.

5.3.1 Rigorous statistical mechanical theory

The most complete statistical mechanical description of the behaviour of a fluid is given by the Liouville equation [74] which describes the evolution of the N-particle distribution function f_N (see 5.2) in the 6N-dimensional phase space for a fluid of N-particles. The Boltzmann equation described in the above section is a simplified form

of this equation and is valid only in the low density range of thermodynamic states.

According to the usual statistical mechanical hypothesis the value of any macroscopic property, α, for a fluid is given by the average of the corresponding microscopic quantity $\alpha(x)$ over the relevant phase space so that

$$\alpha\ (\underline{r},t) = \int \alpha(x)\ f_N(x;t)\ dx \qquad (5.12)$$

where x represents a point in 6N-dimensional phase space. With the aid of the Liouville equation it is then possible to obtain the equations of change for any quantity $\alpha(\underline{r},t)$, such as mass, momentum and energy in terms of integrals over the N-particle distribution function f_N. Thus if the distribtuion function f_N were known, the equations of motion could be evaluated and the coefficient of the gradients of the macroscopic variables identified with the transport coefficients and expressed in terms of the microscopic properties of the molecules of the fluid.

There remain considerable difficulties in carrying out this program. First, a kinetic equation must be established for the function f_N, which involves, in principle, the solution of a dynamical problem involving N particles. In other words, the solution of the Liouville equation requires the solution of the equations of motion of all the particles in the system. The development of the theory in this direction is far from complete. Secondly, because the Liouville equation is reversible, it is necessary to somehow introduce irreversibility into the theory in order that it agrees with practical experience. In the case of the dilute gases the first difficulty is

overcome by the rarity of many body events, whereas the irreversibility is introduced by the molecular chaos assumption (see 5.2). For dense fluids, neither of these difficulties has been fully resolved so that it has been necessary to develop approximate theories [76-85]. Generally, these theories employ a contracted description of the fluid in terms of the single particle and two-particle distribution functions. The introduction of irreversibility into the theory is then accomplished by a statistical assumption concerning a lack of correlation of molecular motion on some microscopic time scale. In the particular case of the dilute gas, the appropriate time scale is the duration of a single collision, t_{coll}, but in a dense fluid, it may be much longer.

5.3.2 Time correlation functions

An alternative method of formulating the transport coefficient of dense fluids is based on the fluctuation-dissipation theorem [86]. This theorem provides a relationship between a correlation function for spontaneous fluctuation in a system in a stationary state to the dissipation (or entropy production) of the system under time dependent driving forces. If the time-dependent driving forces are concentration, flow velocity or temperature it is possible to express the corresponding transport coefficients in terms of auto-correlation functions of microscopic fluxes. Hence the self-diffusion coefficient of a fluid is written in terms of the velocity autocorrelation function as [87,88]

$$D = \frac{1}{3} \int_0^\infty \langle C_{i(o)} \cdot C_{i(\tau)} \rangle \, d\tau \qquad (5.13)$$

where $C_{i(0)}$ represents the velocity of molecule i at time t=0 and $C_{i(\tau)}$ the velocity of the same molecule some time τ later. The angular brackets denote an ensemble average of the quantity using an N-particle distribution function for the unperturbed system. Similar expressions may be written for the viscosity coefficients in terms of correlation functions of mircroscopic momentum fluxes and for thermal conductivity in terms of energy fluxes, both involving just molecular velocities. spatial coordinates and intermolecular energies [87].

In order to evaluate the correlation functions, it is necessary to find the time-dependence of the microscopic variables involved in the correlation function. In turn this requires, in principle, a solution of the Liouville equation, which, it has already been pointed out, is not yet available. Hence the expression of the transport properties in terms of time correlation functions does not immediately alleviate the problems encountered in the development of a rigorous theory of dense gases mentioned in 5.3.1. However, the formulation does have two advantages which have proved to be of great value in the understanding of dense fluid behaviour. First, it can provide a method for the description of phenomena in liquids, such as asborption and scattering of electromagnetic radiation, which yield information about the details of molecular motion [87]. Secondly, it enables the calculation of the transport coefficient of a hypothetical dense fluid by means of a molecular dynamics simulation on a computer.

Molecular dynamics simulation is a computational method whereby the position and velocities of N-particles contained in a cell of fixed volume are followed over a period of time by the numerical solution of Newton's Law of Motion. Knowing quantities such as the positions,

velocities and intermolecular forces as a function of time, the correlation functions for these microscopic variables can be calculated. Using relationships similar to equation (5.13), it is possible to calculate equilibrium properties such as temperature and pressure as well as transport properties such as coefficients of diffusion, viscosity and thermal conductivity. Evidently, for even a small number of particles ($N \sim 100$) over even quite a short time, the computational effort required to carry out such a calculation is enormous. Consequently, it was not until the advent of fast digital computers that such calculations became feasible [89-91].

Since the molecular dynamics method represents the behaviour of the molecule of a fluid having the microscopic properties specified by the investigator, it is therefore possible to determine the motion of the molecules in the fluid essentially exactly and to calculate the transport coefficients of this fluid. For this reason, the technique is sometimes thought of as a method for carrying out an 'experimental' determination of the properties of a hypothetical fluid. Of course, if the intermolecular potentail selected were exactly that of a real fluid the method should yield the observable properties of the real fluid. Thus, in principle, the simulation method provides a means whereby intermolecular potentials proposed for the fluid may be examined, although the computational effort necessary often inhibits the systematic investigation required [92].

Among the earliest results from molecular dynamics studies of dense fluid was a clear demonstration of the breakdown of the molecular chaos assumption used in the dilute gas (see 5.2). It was found that velocity correlations persisted over several collisions and that this has a significant effect on the transport coefficients of a dense

fluid. Experimental evidence for this effect has been obtained [93-99]. The results of molecular dynamics simulations for hard spheres systems will be of use in a later section (5.3.3) and they are therefore discussed more fully there. For the present it is sufficient to note some general features of the motion of molecules in dense fluids which have cast doubt on some popular theories of the dense fluid state and reinforced the validity of others.

An important application of molecular dynamics results has been the assessment of the applicability of statistical mechanical theories and the models that they employ. The details of the molecular motion obtained from a molecular dynamics calculation enable simple models of it to be examined. For example, the results of this type of study contradict the model upon which the activation energy theory of liquid transport [100] is based. In this theory, a molecule is envisaged to make a large number of oscillations about an equilibrium position in a cell formed by its immediate neighbours, with occasional, but large, jumps to a new equilibrium position. An examination of the mean free path distribution in a molecular dynamics simulation indicates that this is not a significant contribution to molecular motion in liquids [101]. Instead, the computer simulation indicates that the motion of the molecule is close to that of the van der Waals model of a fluid in which the molecules travel essentially unperturbed between a succession of hard-core collisions [102]. Indeed, the similarity of the molecular dynamics results to those of the van der Waals model has encouraged the development of a successful method of correlating the transport properties of fluids based upon it.

5.3.3 Van der Waals theory (Smooth Hard Sphere Theory)

This section begins with a description of the van der Waals model

of a dense fluid. The equivalence of this model to the smooth hard sphere model is then established. Subsequently, the application of the smooth hard sphere (SHS) theory for the interpretation of transport properties of dense monatomic fluids is examined.

The van der Waals model of a dense fluid considers the molecules to have an effective intermolecular pair potential made up of a repulsive spherical hard core surrounded by a weak, long-ranged, uniform attractive potential as sketched in Figure 5.1. The model represents a reasonable approximation to the pair potential for real fluids when the temperature is sufficiently high that the attractive potential is weak by comparison with the molecular kinetic energy, the density sufficiently high that there are only small fluctuations in a uniform attractive potential and when it is recognized that the diameter of the hard core must be made temperature dependent to account for the finite steepness of the repulsive wall of the true intermolecular pair potential.

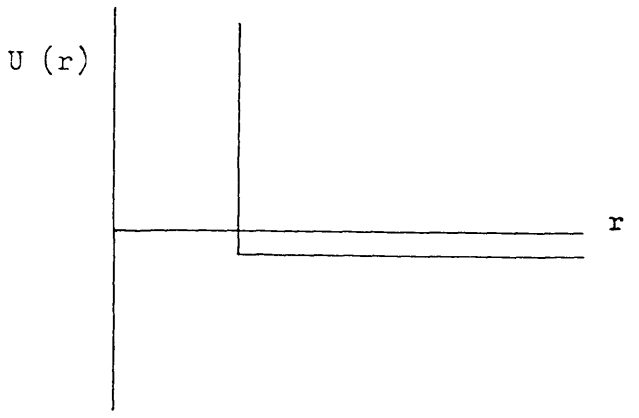

Figure 5.1

The Van der Waals model of dense fluids

From the theoretical point of view the van der Waals model has the considerable advantage that the molecules move in straight line trajectories between hard core collisions. This means that on the one hand the model is consistent with molecular dynamics simulations and on the other hand that one can make use of a kinetic theory of rigid spheres in describing the system. It has been found that real fluids do conform to the van der Waals equation of state at high densities and temperatures when the core size is allowed to be temperature dependent.

The formal restriction of the validity of the van der Waals model to high temperatures and densities is combined with a limit imposed by the fact that a hard sphere fluid exhibits a solid-like transition at densities such that the molar volume is less than 1.5 V_o, where V_o is the volume of close packing of the hard spheres. Thus, formally, the applicability of the van der Waals model should be restricted to the high density gas region up to this limiting density. However, it has been found empirically that correlations based on this model may be reliably extended to higher densities and lower temperatures within the liquid phase. The model has also been extended to lower densities where perturbation theory has been used to account for the increasing influence of attractive forces [103-105].

A kinetic theory for transport in a dense hard sphere fluid has been given by Enskog [106] and as was shown above this is exactly what is needed for an analysis of the van der Waal's model. In the Enskog theory, empirical modifications to the Boltzmann theory are made to provide a first approximation to the behaviour of dense systems. In a dilute gas, the mechanism for the transport of momentum across a plane is the movement of molecules themselves across the plane. As the

density increases, a molecule on one side of the plane can collide with a molecule on the other side of the plane and transfer its momentum even though neither molecule itself crosses the plane. This mechanism of momentum and energy transfer is called the collisional transfer. In addition, the rate of collision is higher in a dense system because the interparticle distance becomes comparable to the diameter of the particles. The Enskog theory [106] assumes that a hard sphere system at high densities behaves exactly as hard sphere system at low densities except that the frequency of collision is increased by a factor g, which may depend on density, and the difference in position between two colliding molecules is no longer neglected.

By making these modifications to the Boltzmann equation, and following essentially the same method of solution as for the dilute gas, expressions for the transport coefficients may be derived for a dense hard-sphere fluid. The results for the first order approximation to the diffusion coefficient, viscosity and thermal conductivity written in terms of the dilute gas values (superscript ^{0}) are:

$$\frac{nD_E}{(nD)^0} = \frac{1}{g} \tag{5.14}$$

where g is the multiplying factor to the collision frequency in the Enskog theory called the radial distribution function.

$$\frac{\eta_E}{\eta^0} = \left[\frac{1}{g} + 0.8\,\frac{b}{V} + 0.761\,g\,\left(\frac{b}{V}\right)^2\right] \tag{5.15}$$

and

$$\frac{\lambda_E}{\lambda^0} = \left[\frac{1}{g} + 1.2\,\frac{b}{V} + 0.755\,g\,\left(\frac{b}{V}\right)^2\right] \qquad (5.16)$$

Here we have introduced the subscript E to denote that the Enskog theory is employed. Furthermore, the molar volme V is used as the independent variable so that b represents the molar co-volume

$$b = \frac{2\pi\,N_A\,\sigma^3}{3} = \frac{2}{3}\,\pi\,\sqrt{2}\,V_o \qquad (5.17)$$

where N_A is the Avogadro's constant and σ is the hard sphere diameter, V_o is the core volume of the rigid spheres and is defined in equation (5.23). The transport coefficients in the zero-density limit for the smooth rigid spheres may be obtained from 5.2.

In order to employ equations (5.14) to (5.16) for the calculation of the dense gas transport coefficients it is necessary only to find the radial distribution function for hard spheres at contact g and a suitable value for the co-volume b. In the original application of the method, b was obtained by fitting the PVT data for the noble gases to the van der Waals equation of state and g was taken from the results of computer simulation for hard spheres [102]. It was found that the calculated high density transport coefficients differed by less than 10% from the experimental values.

However, the Enskog theory neglects all correlations of molecular velocities in the evaluation of the transport coefficients. Molecular

dynamics simulations of the type describd in the previous section (5.3.2) have been employed to deduce the corrections to the Enskog theory which arise from velocity correlations for smooth hard sphere. These corrections may be cast in the form of ratios of the exact hard sphere results (subscript MD) to the Enskog results (subscript E) so that

$$\frac{nD}{(nD)^0} = \left(\frac{D_E}{D^0}\right)\left(\frac{D_{MD}}{D_E}\right) \tag{5.18}$$

$$\frac{\eta}{\eta^0} = \left(\frac{\eta_E}{\eta^0}\right)\left(\frac{\eta_{MD}}{\eta_E}\right) \tag{5.19}$$

and

$$\frac{\lambda}{\lambda^0} = \left(\frac{\lambda_E}{\lambda^0}\right)\left(\frac{\lambda_{MD}}{\lambda_E}\right) \tag{5.20}$$

with the superscript ^{0} indicating the low density results. The corrections to the Enskog theory for each of the transport properties obtained have been given by Alder *et al* [107-108] and correlated as functions of molar volume by Dymond [93].

As we mentioned earlier computer simulations of a hard sphere system in equilibrium have also provided the pair distribution function. A good representation of the results has been given by Carnahan and Starling [109]. It takes the form

$$g = \frac{(1 - \frac{1}{2}\xi)}{(1 - \xi)^3} \qquad (5.21)$$

where

$$\xi = \frac{b}{4V} = \frac{\pi N_A \sigma^3}{6V} = \sqrt{2}\,\frac{\pi V_o}{6\,V} \qquad (5.22)$$

with

$$V_o = \frac{N_A \sigma^3}{\sqrt{2}} \qquad (5.23)$$

for the hard spheres.

Dymond [93,99,103,110-114] has considered a number of ways of applying the corrected Enskog theory to the calculation and correlation of the transport properties of dense gases and liquids. The results of his analysis for each of the transport properties are discussed briefly in the following paragraphs. This discussion is restricted to a consideration of monatomic fluids while modifications to the smooth hard sphere required for polyatomic fluids are discussed in the next section.

(i) Diffusion Coefficient

The result for g given by equation (5.21) to (5.23) may be combined with the molecular dynamics results for (D_{MD}/D_E) by means of the definition

$$D^{+} = \frac{V}{V_o} \frac{1}{g} \frac{D_{MD}}{D_E} \qquad (5.24)$$

where V_o is the core volume of the smooth hard sphere. This yields an equation for the self-diffusion coefficient for the hard sphere:

$$D = D^{+} D^{0} ({}^{V_o}/_{V}) \qquad (5.25)$$

Dymond [93,112] has given equations which represent the volume dependence of D^{+} obtained from the computer simulations of hard spheres

$$D^{+} = 1.27 ({}^{V}/_{V_o} - 1.384) \quad ; \; 1.5 < {}^{V}/_{V_o} < 2.5 \qquad (5.26)$$

and

$$D^{+} = 2.379 \left[({}^{V}/_{V_o})^{2/3} - 1.256 \right] \quad ; \; 1.6 < {}^{V}/_{V_o} < 6.6 \qquad (5.27)$$

The low volume (high density) limit of these correlations is imposed by the metastability of the rigid sphere fluid at higher densities. For a real fluid the high density limit corresponds to approximately 3 times the critical density and the low density limit to 0.8 times the critical denisty. Equations (5.26) and (5.27) may be used to represent the density dependence of the self-diffusion coefficient of real monatomic fluids under the conditions for which the van der Waals model is applicable ($T > 0.7\ T_c$, high density) in both gaseous and liquid phases. Employing just equation (5.26) and the rigid sphere result

for D^0 (see 5.2) we find

$$D = 0.4763 \frac{(kT/\pi m)^{\frac{1}{2}}}{(2N_A)^{1/3} V_o^{2/3}} [V - 1.384\ V_o] \qquad (5.28)$$

for $1.5 < V/V_o < 2.5$

It is therefore predicted that along an isotherm the self-diffusion coefficients of a real dense fluid should be a linear function of the molar volume V over this density range. The core volume itself, V_o, may be derived from the slope of such a plot or from the intercept of an extrapolation on the molar volume axis. Dymond [112] and Van Loef [115-117] have demonstrated that, within the range of its validity, equation (5.28) provides a description of the observed density dependence of the self-diffusion coefficient of liquids with an accuracy comparable with that of the measurements themselves. The core volume, V_o, displays a weak temperature dependence as a result of the softness of the real repulsive wall of the intermolecular pair potential compared with that of a rigid sphere.

Over the larger density range of equation (5.27), representative of the dense gaseous region, a different technique may be employed to confirm the theory and determine V_o. It is convenient to define a reduced diffusion coefficient D* by the equation [99,110]

$$D^* = \frac{n\ D}{(nD)^0} \left(\frac{V}{V_o}\right)^{2/3} \qquad (5.29)$$

which is related to D^+. We may then write for the corrected Enskog theory:

$$D^*_{th} = \frac{1}{g} \left(\frac{D_{MD}}{D_E}\right) \left(\frac{V}{V_o}\right)^{2/3} = f\left(\frac{V}{V_o}\right) \qquad (5.30)$$

so that D* is a function of V/V_o alone. D* may also be calculated from experimental data along an isotherm because, using the rigid sphere result for D^0 in equation (5.29), we find

$$D^*_{exp} = \frac{8D}{3V^{1/3}} (2N_A)^{1/3} \left(\frac{\pi m}{kT}\right)^{\frac{1}{2}} \qquad (5.31)$$

It follows that it should be possible to superimpose a plot of D^*_{exp} against log V upon a plot of D^*_{th} against log (V/V_o) merely by a shift along the log V axis. The amount of shift then determines V_o. It has been shown that the available experimental data for several fluids conform extremely well to equation (5.30).

(ii) Viscosity

A similar type of analysis may be carried out for the viscosity coefficient. In this case, too, Dymond [99] has given correlations of the results of molecular dynamics simulation of hard spheres. The correlations may be written as the ratio of the simulated viscosity to the Enskog result in the form

$$\frac{\eta_{MD}}{\eta_E} = 1.02 \quad \text{for } {}^{V}/_{V_o} > 2.3 \qquad (5.32)$$

$$\frac{\eta_{MD}}{\eta_E} = 1.02 + 15\left[\left(\frac{V_o}{V}\right) - 0.35\right]^3 \text{ for } 1.74 < {}^{V}/_{V_o} < 2.3 \qquad (5.33)$$

and

$$\frac{\eta_{MD}}{\eta_E} = 1.02 + 915\left[\left(\frac{V_o}{V}\right) - 0.35\right]^3 \text{ for } 1.55 < {}^{V}/_{V_o} < 1.74 \qquad (5.34)$$

In addition, correlations of the hard sphere viscosity have been predicted on the basis of similar simulations so that in the liquid phase

$$\frac{\eta^0}{\eta} = 0.2195\left[\left(\frac{V_o}{V}\right) - 1.384\right] \text{ for } 1.5 < {}^{V}/_{V_o} < 2.5 \qquad (5.35)$$

whereas in the dense gaseous region

$$\left(\frac{\eta^0}{\eta}\right)\left(\frac{V}{V_o}\right) = 0.528\left[\left({}^{V}/_{V_o}\right)^{4/3} - 2.32\right] \text{ for } 2 < {}^{V}/_{V_o} < 7 \qquad (5.36)$$

Equation (5.35) shows that along an isotherm, the fluidity ($^{1}/_{\eta}$) of a

rigid sphere liquid should be a linear function of the molar volume and, invoking the van der Waals model, the same should be true for real liquids at sufficiently high temperatures. The core volume V_o may be deduced from experimental data as for the diffusion coefficient. It should also be noted that equation (5.28) and (5.35) taken together mean that if a core volume, V_o, is deduced from measurements of one property at a particular temperature the second property may be calculated.

It is also advantageous to define a quantity, η^*, analgous to D^*, by the equation [114]

$$\eta^* = \left(\frac{\eta}{\eta^0}\right) \left(\frac{V}{V_o}\right)^{2/3} \qquad (5.37)$$

As before, theoretical values of η^*_{th} may be derived from the equations (5.7), (5.15), (5.19) and (5.37), and experimental values from the equation

$$\eta^*_{exp} = \frac{16}{5} \frac{2^{1/3}}{N_A^{2/3}} \left(\frac{\pi}{mkT}\right)^{\frac{1}{2}} \eta \, V^{2/3} \qquad (5.38)$$

Superposition of plots of η^*_{th} against log $\left(V/V_o\right)$ and η^*_{exp} against log V by shifts along the log V axis yield V_o directly. Again, if this

process is carried out for one datum at a particular temperature, it should be possible to use the theory to calculate the density dependence of the viscosity along an isotherm.

(iii) Thermal Conductivity

For the rigid sphere fluid, Dymond [99] has given the following correlations based on computer simulation results

$$\frac{\lambda^0}{\lambda} = 0.1611\left[\left(\frac{V}{V_o}\right) - 1.217\right] \text{ for } 1.5 < \frac{V}{V_o} < 2 \qquad (5.39)$$

and

$$\left(\frac{\lambda^0}{\lambda}\right)\left(\frac{V}{V_o}\right) = 0.470\left[\left(\frac{V}{V_o}\right)^{4/3} - 2.32\right] \text{ for } 2 < \frac{V}{V_o} < 7 \qquad (5.40)$$

Again, using the low density results for λ^0 core volumes may be determined from experimental data with either of these equations.

It is again useful to define a quantity, λ^*, by means of the equation

$$\lambda^* = \left(\frac{\lambda}{\lambda^0}\right)\left(\frac{V}{V_o}\right)^{2/3} \qquad (5.41)$$

which for rigid spheres, is a function of V/V_o only. Theoretical values of λ^*_{th} may be obtained from the molecular dynamics simulation results and experimental values from the equation

$$\lambda^*_{exp} = \frac{64}{75}\left(\frac{m\pi}{k^3T}\right)^{\frac{1}{2}} \frac{2^{1/3}}{N_A^{2/3}} \lambda V^{2/3} \qquad (5.42)$$

so that whenever the van der Waals model is applicable, i.e. for dense monatomic fluids, it should be possible to superimpose plots of λ^*_{th} against $\log(V/V_o)$ and λ^*_{exp} against $\log V$.

Summary of the use of the smooth hard sphere theory

In summary, the quantities D^*, η^* and λ^* are functions of the ratio V/V_o alone according to the smooth hard sphere theory. Consequently it should be possible to superimpose the plots of any property as a function of volume for all isotherms, because the temperature dependence of D^*, η^* and λ^* is completely contained in V_o. Furthermore, each of these curves should conform to the theoretical plot for the same property and superposition then leads to a value of V_o for each temperature. Extensive tests carried out by Dymond et al have confirmed the applicability of the smooth hard-sphere theory to the interpretation of the transport properties of dense monatomic fluids.

This type of interpretation of experimental results has an immediate value in terms of property calculations since it means that once V_o for a particular fluid at one temperature has been evaluated from data for one property, other properties may be deduced immediately. Furthermore, the density dependence of a particular property along an isotherm can in fact be generated from observations at just one density at the same isotherm.

5.4 Rough Hard Sphere Theory for Dense Polyatomic Fluids

5.4.1 Introduction

The smooth hard sphere theory discussed in the previous section has been shown to be remarkably successful for monatomic fluids. It has also been applied in an ad hoc manner to polyatomic liquids [118]. However, as it will be shown in 6.2, it does have some deficiences for such systems. This is not surprising since polyatomic fluids differ from monatomic ones in three major respects, the non-spherical nature of the molecules, the fact that the molecules possess internal energy and the energy transfer by virtue of the coupling which occurs between translational and rotational motions. None of these effects can be accounted for by the smooth hard sphere theory. An attempt has therefore been made to introduce a more appropriate theory, based on the rough hard sphere model [RHS], to describe the transport properties of such fluids.

In the rough hard sphere model the molecules are considered as rigid spheres each of diameter σ and mass m. A moment of inertia I is associated with the spherically symmetric distribution of this mass about the molecular centre of gravity. Hence the molecules possess rotational degrees of freedom. A collision between two rough spheres is instaneous (i.e of zero duration). During this collision, the relative velocity of the points of contact of two spheres is completely reversed, so that one sphere can transfer not only linear momentum but also angular momentum (spin) to the other sphere.

Thus the model incorporates the essential characteristics of a polyatomic fluid in a rather simple manner. From the present point of

view the simplicity of the model renders it attractive because the radial distribution function is the same as that of smooth hard spheres and because many of the integrals occuring in the necessary theory have already been evaluated. From a more fundamental point of view the model has deficiencies because it tends to overemphasise the role of inelastic collisions and lacks any account of molecular shape. However, these deficiencies are a price which must be paid at present to develop a practicable correlation scheme.

The rough hard sphere model was first suggested by Bryan [99] and the dilute gas theory for the transport coefficient was calculated by Pidduck [120], using the nonequilibrium techniques of Enskog. Chapman and Cowling [26] gave a very detailed account of these techniques and the application of such methods to the theory of rough spheres. They neglected those terms in the nonequilibrium distribution function which were anisotropic in the angular velocity, i.e. terms which depend not only upon the magnitude but also upon the orientation of the molecular spin velocity. Afanasev [121] questioned the validity of this approximation for a gas of polyatomic molecules. Also, Waldmann [122] found that anisotropic effects were significant for a Lorentz gas of rough spheres. As a result, Condiff, Lu, and Dahler [123] included these effects in calculations performed on a dilute gas of rough spheres. They derived a kinetic equation which was also applicable to dense gases and used the Chapman-Enskog approach to develop a theory for the transport equations. The work of Condiff et al [123] is used by McCoy, Sandler and Dahler [124], as a basis for the development of a theory for a dense gas of rough spheres. This theory has subsequently been revised by Klein, Hoffman and Dahler [125].

At present, there are two approaches to the calculation of the

transport coefficients of a dense fluid of polyatomic molecules by means of a rough sphere model. The first is due to Chandler [126-128] and is based on the correlation function formalism discussed in 5.3.2. This approach has been tested extensively by Dymond and others (see 5.4.2). The alternative approach employs a kinetic description involving the solution of an appropriate kinetic equation (see appendix 3). This latter approach is essentially a continuation of Dahler's work described above. Theodosopulu and Dahler [129,130] proposed a complete and computationally practical theory for the transport coefficients of polyatomic liquids. The relationship of this theory to the smooth hard-sphere has been investigated [131]. However, few comparisons with experimental results have been made for this kinetic model of dense fluids.

In the following section, these two theories using the rough hard-sphere model applied to dense polyatomic fluids are discussed in more detail and their essential features and numerical predictions are compared.

5.4.2 Chandler's Rough Hard Sphere Model

In this model, the transport coefficients for the SHS theory are modified by a parameter called the "roughness" of the hard-sphere which is the degree of coupling between translatioal and rotational motion. The value of the roughness parameter is determined from experimental data for the transport coefficient under consideration.

Chandler has demonstrated using an approximate theory [128] that for a rough sphere fluid at densities greater than twice the critical density, the self-diffusion coefficient is proportional to the self-diffusion for a smooth hard-sphere so that [128]

$$D_{RHS} = A\, D_{SHS} \qquad (5.43)$$

The symbol A represents a translational-rotational coupling factor, less than unity, which is assumed to be independent of temperature and density. Introducing this parameter into equation (5.24), we find that for the rough hard sphere model [114]

$$D = \frac{0.4763A}{V_o^{2/3}(2N_A)^{1/3}} \left(\frac{kT}{\pi m}\right)^{\frac{1}{2}} [V - 1.284V_o] \qquad (5.44)$$

so that both A and V_o may be determined from experimental data.

A plot of the experimental diffusion coefficient data against the molar volume V at constant temperature should be linear if the model is valid, and both V_o and A could then be obtained from the slope and intercept. Diffusion coefficients for tetramethylsilane at 25^0C obey equation (5.44) for pressures up to 150 MPa [114]. Between this pressure and the highest pressure investigated (450 MPa), Dymond found that equation (5.44) is not applicable. Similar results were found for benzene [114] at 160^0C and 75^0C. However, using a method analogous to that discussed in 5.3.3 for monatomic fluids, Dymond et al [114] found that the rough hard sphere theory can be used as the basis for a useful empirical correlation technique, valid over a wider range of experimental conditions. For the correlation of experimental diffusion coefficient of polyatomic molecules, they suggested a dimensionless diffusion coefficient, defined by the equation

$$D^* = 5.030 \times 10^8 \left(\frac{M}{RT}\right)^{\frac{1}{2}} D/V^{1/3} \qquad (5.45)$$

for the correlation of experimental data.

In the density region where the rough hard-sphere model is applicable, D^*_{RHS} will be proportional to $(D^*_{SHS}/D^0)(V/V_o)^{2/3}$ on the basis of Chandler's theory and thus will depend only on V/V_o and a coupling constant A. Consequently, it is to be expected that the curves of experimental values of D* may only be superimposed upon the theoretical curves for smooth hard spheres by shifts along both axes in a plot of log D* against log V. As before, the shift required along the volume axis yield the 'effective' spherical core volume of the molecules, but in this case, the shift along the log D* axis determines the factor A. Plots of D* versus log V for a given compound at different temperatures should be superimposable on the curve obtained for any reference temperature, T_R. The amount by which log V has to be adjusted leads to a value for $V_o(T)/V_o(T_R)$ and hence gives a measure of the effect of temperature changes on the closed-packed volume. Results are given for tetramethylsilane and benzene [114], methane and ethane [131], carbon disulphide [132] and acetonitrile [133].

Similarly, for viscosity at densities above twice critical, the rough hard-sphere coefficient, η_{RHS} could be given in terms of η_{SHS} by

$$\eta_{RHS} = C\,\eta_{SHS} \qquad (5.46)$$

where C is another coupling coefficient and is assumed to be essentially constant and greater than or equal to unity. A combination of this result with that of equations (5.31) and (5.38) for smooth hard spheres leads to the equation

$$\frac{1}{\eta_{RHS}} = \frac{0.7024\ C\ 2^{1/3}\ (^{mkT}/_{\pi})^{\frac{1}{2}}\ [V-1.384V_o]}{N_A^{2/3}\ V_o^{1/3}} \qquad (5.47)$$

Dymond [114] found that a plot of the fluidity $^{1}/_{\eta}$ against molar volume V for the experimental viscosity data of tetramethylsilane and n-hexane at 25^0C conformed to a linear relationship according to equation (5.47) up to 150 MPa.

An analogous method to that described in 5.3.3 for monatomic fluids should hold for the correlation of experimental viscosity coefficient data for polyatomic fluids. Equation (5.34) for η^*_{exp} may be simplified to

$$\eta^*_{exp} = 9.118\ X\ 10^7\ \eta V^{2/3}/(MRT)^{\frac{1}{2}} \qquad (5.48)$$

with η in units of Nsm^{-2}. Plots of η^* versus log V for a given compound at different temperatures should be superimposable on the curve obtained for any reference temperature, T_R, over the range for which the rough hard sphere theory holds. It has ben shown [114] that plots of η^*_{exp} against log V are superimposable over the whole density

range and not only over that range for which the rough hard sphere theory should hold. The method also works for aspherical molecules such as bicyclic hydrocarbons and perhydrochrysene where the shape is not expected to vary with changes in temperature [113] and for the systems n-hexane + n-hexadecane [134], n-octane + n-dodecane [135], n-hexane + cyclohexane [136] and benzene + hexafluorobenzene [137] at elevated pressures.

The contribution of the internal energy is more significant for the coefficients of thermal conductivity and simple expressions for correlating the thermal conductivities of monatomic fluids (5.3.3) cannot be so readily extended to polyatomic fluids. This is because of not only the coupling between motions which must be included but also because of the direct internal energy transport. For these reasons no comparable treatment to that for the diffusion coefficient and viscosity is provided by Chandler's rough hard-sphere theory. An empirical correlation scheme for the thermal conductivity of dense polyatomic liquids has been developed by Menashe et al [118], which will be discussed in more detail in the next chapter (see 6.3.1).

5.4.3 Dahler's Rough Hard Sphere Theory

Dahler et al [129,130] have developed a kinetic theory of polyatomic liquids for three model systems. These models - rough spheres, rigid ellipsoids and square-well ellipsoids - have been selected not only because they are more tractable than other more complex models from a computational point of view but also because they mimic, with varying degrees of success, several characteristics of

real polyatomic fluids. Formulae are derived for the transport coefficients and for the relaxation times which describe the establishment and maintainence of a steady state of transport of energy and of linear and angular momentum. Using the approximations of Enskog (see 5.3) these phenomenological coefficients can be expressed in terms of integrals of the same type as occured in the dilute gas theory. The integrals of these have been evaluated for the rough sphere case. For the other two cases the evaluation is complicated by the fact that reliable estimates are not available for the equilibrium pair distribution function [131].

In Dahler's Rough Hard Sphere theory, the dynamical state of a rough hard sphere is fully specified by the location of its centre of mass x_i, by its linear momentum, $P_i = mc_i$, and by its internal angular momentum $L_i = I\omega_i$. The internal distribution of mass is characterised by the moment of inertia I, which can be rewritten in dimensionless form as:

$$K = \frac{4I}{m\sigma^2} \qquad (5.49)$$

where m is the mass and σ the diameter of the rough spheres. The dimensionless moment of inertia K, can vary in value from zero, when the mass is localized at the centre of the sphere to $^2/_3$ when the mass is uniformly distributed over the surface of the sphere.

The principal shortcoming of this model is its failure to provide an entirely realistic description of inelastic collisions. There is

no value of K for which the collisions are truly elastic. Even when K→0 and no transfer between rotational and translational degrees of freedom can occur, the mechanism for collisional exchange of spin or angular momentum still remains. Whether this will have major effects on the resulting bulk properties is, however, not clear.

It is possible to proceed to the results which follow by the application of the moment method to the Enskog theory of a dense gas of perfectly rough spheres. The algebra involved is rather complex. Hence only an outline of the procedure used to obtain the relevant transport properties is presented in appendix 3. Full details can be found elsewhere [129,130]. The viscosity coefficient for Dahler's RHS theory, $\eta_{RHS,D}$, where the subscript RHS,D refers to Dahler's rough hard sphere theory is given by

$$\eta_{RHS,D} = \eta^{(K)} \left(1 + \frac{(5\ K+2)}{5\ (K+1)}\ bng\right)^2 + \frac{1}{10}\ \rho\ \sigma\ \left(\frac{kT}{\pi m}\right)^{\frac{1}{2}}\ bng\ \frac{(7K+4)}{(K+1)} \qquad (5.50)$$

where $\eta^{(K)}$ is the Pidduck approximation [120],

$$\eta^{(K)} = \left(\frac{15}{8\sigma^2 g}\right)\ \left(\frac{mkT}{\pi}\right)^{\frac{1}{2}}\ \frac{(K+1)^2}{(13K+6)} \qquad (5.51)$$

which reduces to the result for the dilute gas of rough spheres when g in $\eta^{(K)}$ is set to unity. It is noted that n is the number density and b, the molar co-volume, is given by equation (5.17) so that $bn = {}^{b}/_{V}$.

The thermal conductivity consists of a translational contribution

(λ^t) and a rotational contribution (λ^r), which are given by the following equations:

$$\lambda_{RHS,D} = \lambda^t + \lambda^r \tag{5.52}$$

$$\lambda^t = \lambda^t_k \left(1 + \frac{1}{5}\frac{(5K+3)}{(K+1)}\,bng\right) + \lambda^r_k \frac{1}{3}\frac{(3K+2)}{(K+1)}\,bng$$

$$+ \beta \left(\frac{kT}{\pi I}\right)^{\frac{1}{2}} \frac{K^{\frac{1}{2}}}{(K+1)}\,bng + \left[\left(\frac{kT}{\pi m}\right)^{\frac{1}{2}} \frac{p\sigma}{T}\frac{(2K+1)}{(K+1)}\,bng\right] \tag{5.53}$$

and

$$\lambda^r = \lambda^r_K \left(1 + \frac{2}{3}\frac{1}{(K+1)}\,bng\right) + \beta \left(\frac{kT}{\pi I}\right)^{\frac{1}{2}} \frac{K^{\frac{1}{2}}}{(K+1)}\,bng$$

$$+ \left[\left(\frac{kT}{\pi m}\right)^{\frac{1}{2}} \frac{p\sigma}{T}\frac{1}{(K+1)}bng\right] \tag{5.54}$$

where k is the Boltzmann constant, I (or K in dimensionless form) the moment of inertia, g the radial distribution function, σ the diameter of the sphere, T the absolute temperature and p is given by

$$p = nkT \tag{5.55}$$

and the coefficients λ^t_κ, λ^r_K and β are expressed in terms of ratios of determinants of matrices as follows:

$$\lambda_k^t = - \frac{\det \begin{vmatrix} -\frac{1}{2}\frac{kp}{m}\left(5+\frac{(5k+3)}{(K+1)}\,bng\right) & \frac{-40}{9}\,d\,\frac{K}{(K+1)} & 0 \\ -\frac{3}{2}\frac{kp}{m}\left(1+\frac{2}{3}\frac{bng}{(K+1)}\right) & \frac{8}{3}\,d\,\frac{(2K^2+2K+1)}{(K+1)^2} & \frac{-kT}{I}\,bng\,\frac{K}{(K+1)} \\ \frac{16}{3}\frac{pd}{nR}\frac{I}{(K+1)} & \frac{2}{3}\,bng\,\frac{K}{(K+1)} & \frac{16}{3}\,d \end{vmatrix}}{\det(a)}$$

.... (5.56)

$$\lambda_k^r = - \frac{\det \begin{vmatrix} \frac{4}{15}\,d\,\frac{34K+8}{(K+1)^2} & -\frac{1}{2}\frac{kp}{m}\left(5+\frac{5K+3}{(K+1)}\,bng\right) & 0 \\ \frac{-8}{3}\,d\,\frac{K}{(K+1)^2} & -\frac{3}{2}\frac{kp}{m}\left(1+\frac{2}{3}\frac{bng}{(K+1)}\right) & \frac{-KT}{I}\,bng\,\frac{K}{(K+1)} \\ 0 & \frac{16}{3}\frac{pd}{mT}\frac{I}{(K+1)} & \frac{16}{3}\,d \end{vmatrix}}{\det\,(a)}$$

.....(5.57)

and

$$\beta = - \frac{\det \begin{vmatrix} \frac{4}{15}\,d\,\frac{(34K+8)}{(K+1)^2} & \frac{-40}{9}\,d\,\frac{K}{(K+1)^2} & -\frac{1}{2}\frac{kp}{m}\left(5+\frac{(5K+3)}{(K+1)}\,bng\right) \\ \frac{-8}{3}\,d\,\frac{K}{(K+1)^2} & \frac{8}{3}\,d\,\frac{(2K^2+2K+1)}{(K+1)^2} & -\frac{3}{2}\frac{kp}{m}\left(1+\frac{2}{3}\frac{bng}{(K+1)}\right) \\ 0 & \frac{2}{3}\,bng\,\frac{K}{(K+1)} & \frac{16}{3}\frac{pd}{mT}\,\frac{I}{(K+1)} \end{vmatrix}}{\det\,(a)}$$

.....(5.58)

with

$$a = \begin{vmatrix} \frac{4}{15} d \frac{(34K+8)}{(K+1)^2} & -\frac{40}{9} d \frac{K}{(K+1)^2} & 0 \\ -\frac{8}{3} d \frac{K}{(K+1)^2} & \frac{8}{3} d \frac{(2K^2+2K+1)}{(K+1)^2} & \frac{-kT}{I} bng \frac{K}{(K+1)} \\ 0 & \frac{2}{3} bng \frac{K}{(K+1)} & \frac{16}{3} d \end{vmatrix} \tag{5.59}$$

and

$$d = n\, g\, \sigma^2 \left(\frac{\pi kT}{m}\right)^{\frac{1}{2}} \tag{5.60}$$

It should be noted that equation (5.53) is different from that given in ref (130) owing to a typographical error in the above reference.

It is shown in appendix 3 that the viscosity coefficient and the thermal conductivity can be expressed as a funtion of just two quantities, namely the reduced volume V/V_o and the dimensionless moment of inertia K. Only the final results representing this functional dependence are given here. The result for the viscosity coefficient $\eta_{RHS,D}$ is expressed in units of $H^0 = \frac{5}{16\sigma^2}\left(\frac{mkT}{\pi}\right)^{\frac{1}{2}}$

$$\frac{\eta_{RHS,D}}{H^0} = \frac{6}{g}\frac{(K+1)^2}{(13K+6)} + \frac{12}{5}\,\frac{(K+1)^2}{(13K+6)}\frac{(5K+2)}{(K+1)}\frac{b}{V}$$

$$+\left\{\frac{6(K+1)^2}{(13K+6)}\left[\frac{5K+2}{5(K+1)}\right]^2+\frac{12}{25\pi}\frac{(7K+4)}{(K+1)}\right\}\left(\frac{b}{V}\right)^2 g \qquad (5.61)$$

where g is given by equation (5.21) and b is given by equation (5.17),

$$b=\frac{2}{3}\pi\sqrt{2}\,V_o$$

For K = 0, Equation (5.61) reduces to

$$\frac{\eta_{RHS,D}}{H^0}=\left[\frac{1}{g}+0.8\left(\frac{b}{V}\right)+0.771\,g\left(\frac{b}{V}\right)^2\right] \qquad (5.62)$$

In the case of the smooth hard sphere fluid, H^0 represents the low density result for the viscosity coefficient (see equation 5.7)

The small numerical difference in the last coefficient and the corresponding term in equation (5.15) is due to the fact that in the derivation of equation (5.15), the second Chapman-Enskog approximation to η^0 has been used, which is of the form

$$\eta^{0(2)}=1.016\times\frac{5}{16\,\sigma^2\,\pi}(\pi\,m\,kT)^{\frac{1}{2}} \qquad (5.63)$$

instead of equation (5.7). Using this second approximation as the low density limit for the viscosity coefficient, it is found that equation (5.62) is equivalent to Enskog's result for smooth hard spheres.

Similarly for the thermal conductivity we expressed the results in units of $\Lambda^0=\frac{75}{64}\frac{1}{\sigma^2}\left(\frac{k^3T}{\pi m}\right)^{\frac{1}{2}}$. It can be shown that (see appendix 3)

$$\frac{\lambda_{RHS,D}}{\Lambda^0} = \frac{\left[\frac{80}{\pi}(2K+1) + \frac{20}{3}K\right](K+1)^2 \times \frac{64}{75}}{\frac{128}{15\pi}(34K+8)(2K^2+2K+1) - \frac{1280}{9\pi}K^2 + \frac{32}{45}(34K+8)} \times \frac{1}{g}$$

$$+\left\{\frac{16}{\pi}(5K+3)(2K^2+2K+1) + \frac{160}{3\pi}K - \frac{16K^2}{3\pi(K+1)} + \frac{4}{3}(5K+3)K\right.$$

$$+ \frac{1}{5}(5K+3)\left[\frac{80}{\pi}(2K+1) + \frac{20}{3}K\right]$$

$$+ \left[\frac{3}{4\pi} \times \frac{(3K+2)}{(K+1)}\right] \times \left[\frac{32}{15}\frac{(34K+8)}{(K+1)^2} + \frac{320}{9}\frac{K}{(K+1)^2}\right]$$

$$+ \frac{9}{4\pi}\left[\frac{64}{45}(34K+8) - \frac{64}{45}\frac{(34K+8)}{(K+1)}K + \frac{64}{9}(5K+3)K\right]$$

$$+ \left[\frac{32}{15}(34K+8) + \frac{320}{9}K\right] \times \frac{3}{2\pi}$$

$$+ \frac{2}{(K+1)}\left[\frac{27K}{16\pi^2}\left\{\frac{5120}{81}\frac{K^2}{(K+1)^2} - \frac{512}{135}(34K+8)(2K^2+2K+1)\right\}\right.$$

$$\left.\left. - \frac{4}{5\pi}(34K+8)K - \frac{40}{9}K^2\right]\right\} \times \frac{(K+1) \times \frac{64}{75} \times \left(\frac{b}{V}\right)}{\frac{128}{15\pi}(34K+8)(2K^2+2K+1) - \frac{1280}{9\pi}K^2 + \frac{32}{45}(34K+8)}$$

$$+\left\{\left[\frac{16}{\pi}(5K+3)(2K^2+2K+1) + \frac{160}{3\pi}K - \frac{160}{3\pi}\frac{K^2}{(K+1)} + \frac{4}{3}(5K+3)\right]\right.$$

$$\times \frac{1}{5}\frac{(5K+3)}{(K+1)} + \left\{\left[\frac{3}{4\pi}\left(\frac{3K+2}{K+1}\right) + \frac{3}{2\pi(K+1)}\right] \times \left[\frac{64}{45}(34K+8)\right.\right.$$

$$\left.\left. - \frac{64}{45}\frac{(34K+8)K}{(K+1)} + \frac{64}{9}(5K+3)K\right]\right\}$$

$$\left. - \frac{2}{(K+1)}\left\{\frac{8}{15\pi}\frac{(34K+8)K}{(K+1)} + \frac{8}{3\pi}\frac{(5K+3)}{(K+1)}K^2\right\}\right]$$

$$\times \frac{(K+1)}{\frac{128}{15\pi}(34K+8)(2K^2+2K+1) - \frac{1280}{9\pi}K^2 + \frac{32}{45}(34K+8)} + \frac{3}{\pi}\Big\} \times \frac{64}{75} \times \left(\frac{b}{V}\right)^2 g$$

.....(5.64)

When K is set to 0, i.e. when the mass of the rough sphere is considered to be concentrated at the centre

$$\frac{\lambda_{RHS,D}}{\Lambda^0} = \frac{1.48}{g} + 3.16\left(\frac{b}{V}\right) + 2.20157\ \left(\frac{b}{V}\right)^2 g \qquad (5.65)$$

which is not identical with Enskog's results for smooth spheres because the RHS theory takes into account the internal energy contribution to the thermal conductivity coefficient even when K = 0. In order to recover the result for the thermal conductivity a system of smooth hard spheres it is also necessary to omit the internal energy terms from equation (5.52) before setting K = 0. In this case, $\Lambda^0 = \lambda^0$, and we obtain

$$\lambda = \lambda^t = \lambda_k^t\ (1 + \frac{3}{5}\ bng) + \left(\frac{kT}{\pi m}\right)^{\frac{1}{2}} \frac{p\sigma}{T}\ bng$$

$$\text{where } \lambda_k^t = \Lambda^0\ (1 + \frac{3}{5}\ bng).$$

Because, bn = b/V, this result may be written in the form

$$\lambda = \lambda^t = \Lambda^0\ \left(\frac{1}{g} + 1.2\left(\frac{b}{V}\right) + 0.757\ \left(\frac{b}{V}\right)^2 g\right)$$

which is the Enskog result for smooth hard spheres.

Equations (5.61) and (5.64) for the transport properties can be written in the form

$$\frac{\eta_{RHS,D}}{H^0} = f_1(V/V_o, K) \qquad (5.66)$$

and

$$\frac{\lambda_{RHS,D}}{\Lambda^0} = f_2(V/V_o, K) \qquad (5.67)$$

5.5 Comparison between Chandler's and Dahler's RHS Theory

Dahler's RHS theory provides relatively simple, explicit expressions for the numerical estimates of the transport coefficients of this model of dense polyatomic fluids. Consequently, it should be possible to use these expressions to investigate the features of the model appropriate for the description of the behaviour of real polyatomic fluids.

The first test carried out is to use equation (5.50) to calculate $\eta_{RHS,D}$. Since Chandler's theory suggests that the viscosity coefficient for the rough hard sphere fluid is directly proportional to that for the smooth hard sphere fluid (see equation 5.46), it would be interesting to investigate whether Dahler's theory exhibits this behaviour. Figure 5.2 contains a plot of the ratio $\eta^*_{RHS,D}/\eta^*_{SHS}$ as a function of V/V_o at K = 0.11, 0.33 and 0.66. The superscript * indicates that a definition of η^* consistent with that given by equation (5.37) is used. The range of V/V_o investigated encompasses

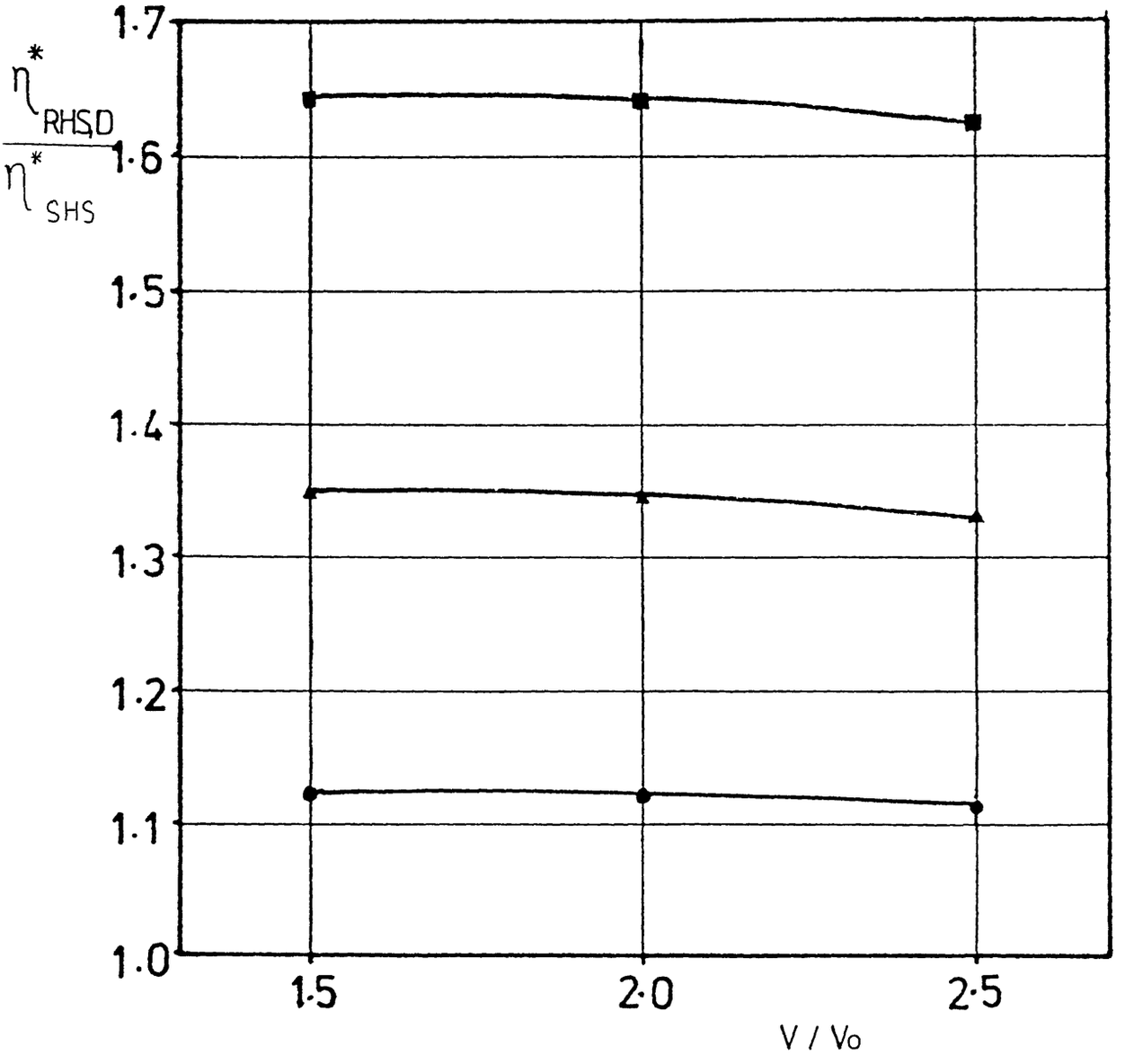

Fig. (5.2) The dimensionless viscosity coefficient calculated using Dahler's rough hard sphere theory, $\eta^*_{RHS,D}/\eta^*_{SHS}$ versus V/V_o at different values of moment of inertia, K: ● -K= 0.11, ▲ -K=0.33, ■ -K=0.66

the density range of the available experimental data. The ratio of $\eta^*_{RHS,D}/\eta^*_{SHS}$ varies by less than 2%. Hence, although it has not been possible to derive analytically the proportionality between η_{RHS} and η_{SHS}, it seems that numerically, at least, the two theories of the rough hard sphere model are consistent.

In view of the remarkable success of the rough hard sphere model for the interpretation of experimental diffusion and viscosity coefficient data by means of Chandler's analysis it is worthwhile to examine the application of the same model to thermal conductivity data. The consistency demonstrated between Chandler's treatment and that of Dahler and his collaborator's allows us to carry out this examination with the most appropriate theory. Since only the work of Dahler et al deals with thermal conductivity we adopt this analysis in future discussions.

The density dependence of the total thermal conductivity of the rough hard sphere fluid, $\lambda_{RHS,D}$, is illustrated in Figures (5.3) for a number of different values of K. By analogy with D* and η^* discussed in 5.4.2, a dimensionless thermal conductivity is defined as

$$\lambda^*_{RHS,D} = \left(\frac{\lambda_{RHS,D}}{\Lambda^0}\right)\left(\frac{V}{V_o}\right)^{2/3} \qquad (5.68)$$

where Λ^0 is a unit of thermal conductivity as defined in the previous section, and V_o is a characteristic volume. The variation of $\lambda^*_{RHS,D}$

with K amounts to less than 10% over the entire density range of the plot whereas $\lambda^*_{RHS,D}$ changes by a factor of 16 in the same range. Figure (5.4) shows the dependence upon K of the translational (λ^t) and rotational (λ^r) contributions to the total thermal conductivity of the rough hard sphere fluid at two different densities. It can be seen that although the variation of the total thermal conductivity with K is small the individual contributions vary more strongly and in opposite directions. In particular, the rotational contribution to the thermal conductivity varies by almost a factor of 2 as K varies from 0 to 2/3.

In the next chapter an attempt is made to apply the results of this rough hard sphere theory to the description of the present experimental results. In view of the relative simplicity of the model it is not expected that the theory will prove successful in an absolute, quantitative sense but rather that it can act as a guide to the formulation of a correlation procedure with some predictive capability.

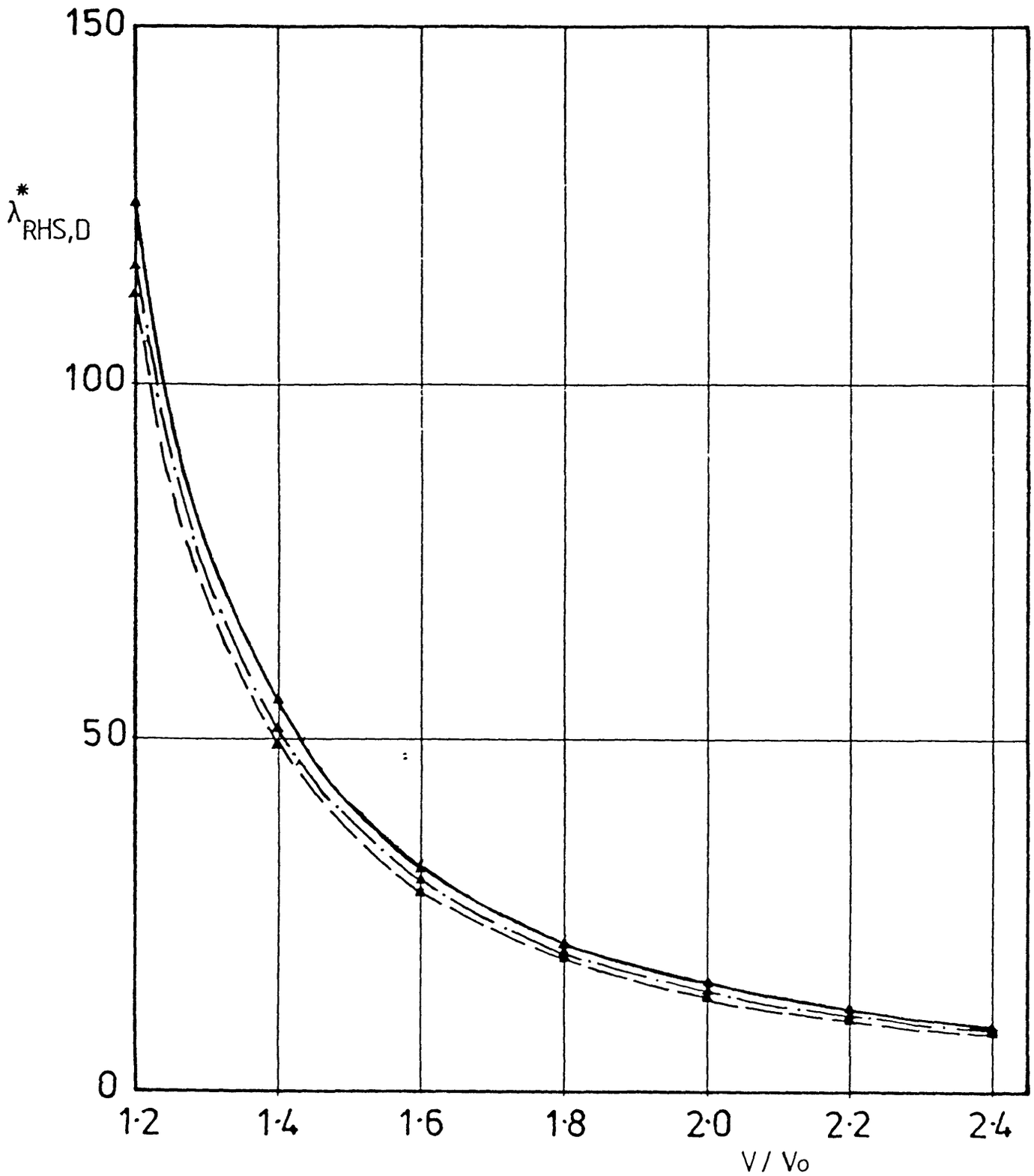

Fig. (5.3) The dimensionless thermal conductivity calculated using Dahler's rough hard sphere theory. $\lambda^*_{RHS,D}$ versus V/V_o at different values of moment of inertia, K: — K= 0 ; – – K= 0.22 ; —·—·— K =0.66

Fig. (5.4a)

$V/V_o = 1.5$

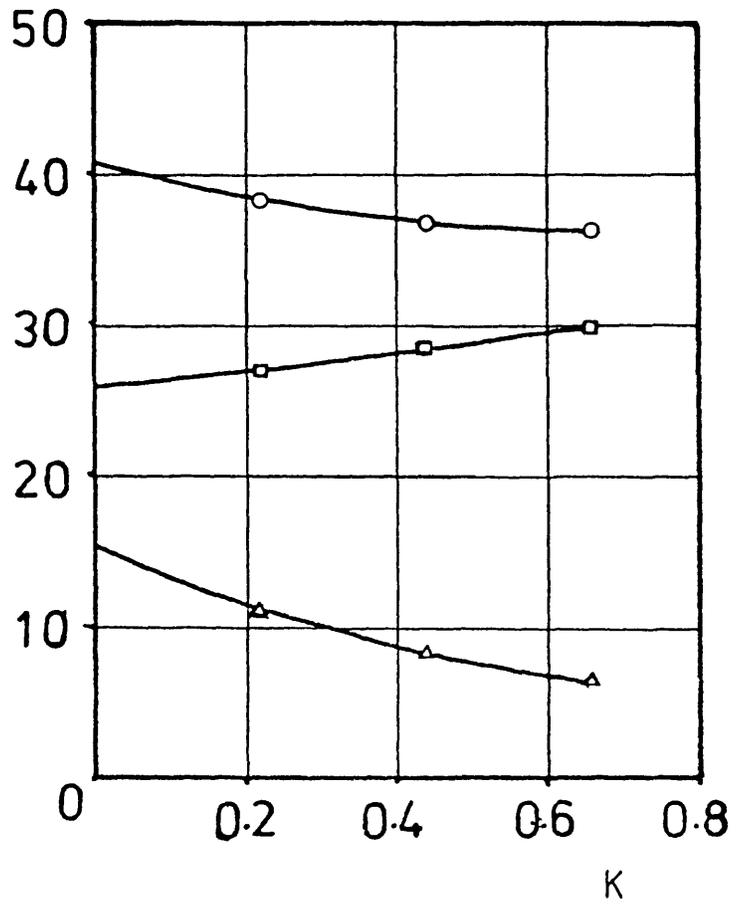

Fig. (5.4b)

$V/V_o = 2.0$

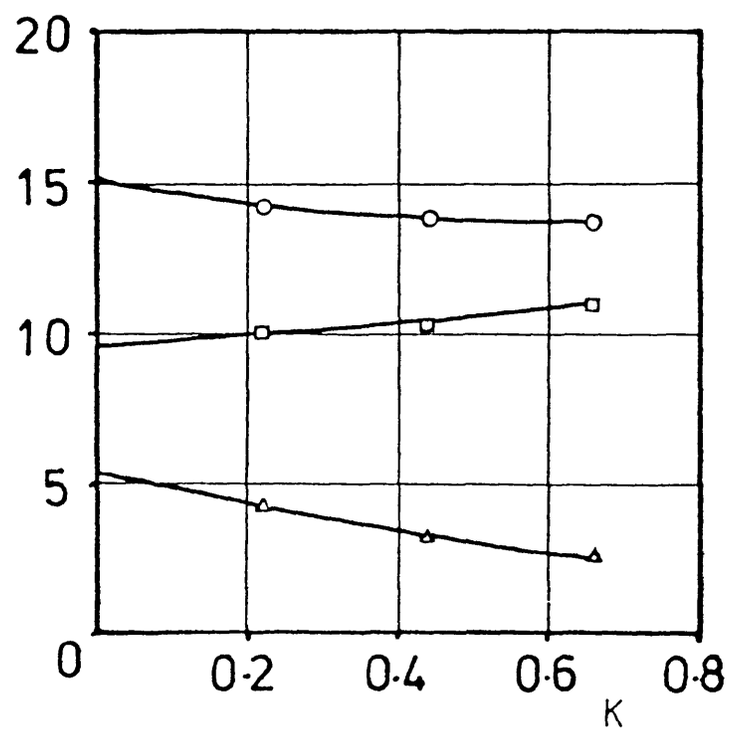

Fig. (5.4) Dependence of the thermal conductivity, $\lambda_{RHS,D}$, the translational contribution (λ^t) and the rotational contribution (λ^r) on the moment of inertia,

○ - $\lambda_{RHS,D}$; □ - λ^t ; △ - λ^r

CHAPTER 6

DISCUSSION

6.1 Introduction

In the previous chapter, it was argued that theories of dense fluids of monatomic or polyatomic species based on relatively simple molecular models lead to a good description of the behaviour of the viscosity and diffusion coefficients for such fluids in a defined region of thermodynamic states. In a wider range of thermodynamic states, the same theories and models suggest the form of a correlation procedure for the properties which has some theoretical foundation and predictive capability, despite the fact that the original model is no longer strictly applicable. It follows that any fundamental interpretation of the experimental data in terms of the models must be confined to the restricted range of thermodynamic states whereas the application of the wider ranging correlative procedure may have a greater range of validity.

It is the latter element of the analysis which is of greatest significance in an engineering context because it frequently happens that process design engineers require the properties of fluids under conditions different from that at which measurements have been performed. The entirely empirical process of representing the data by means of arbitrary functions is usually quite successful for the purpose of interpolation, but for the more frequent need of extrapolation a similar procedure is doomed to failure. On the other hand a

correlation procedure which incorporates at least some of the elements of physical reality is much more likely to succeed.

The purpose of this Chapter is to examine the extent to which a soundly based correlation scheme can be based on the rough hard sphere model. The present experimental data provide the necessary basis for this examination. The analysis begins with an investigation of the applicability of the rough hard sphere theory with respect to experimental data. Unfortunately the range of densities for which the applicability of the rough hard sphere theory and the present experimental data overlap turns out to be very small so that in subsequent sections attention is concentrated upon the development of a wider ranging correlation procedure based on the general form of the theory. In this development experimental data for liquid hydrocarbons from the present work as well as from earlier studies [5, 138-140] with the same type of equipment are examined and incorporated into a single universal correlation scheme. In general the thermal conductivity data considered are only those for which reliable density data exist so that the entire set of data for toluene, as well as data points for other fluids where extrapolation of the density was necessary have had to be omitted.

6.2 Applicability of the RHS Theory

In the case of viscosity and diffusion coefficient Dymond [114, 134] was able to establish the validity of the rough hard sphere theory from the known algebraic form of the relationship between the property and density (see 5.4.2). In particular, one of the parameters of the theory entered as a simple multiplicative factor so that it could easily be determined by curve fitting. In the case of Dahler's theory

for the thermal conductivity of the rough hard sphere model no such simple relationship is available. Consequently it is necessary to use a more indirect method of examining the applicability of this rough hard sphere theory. At the same time, as will become apparent the method of assessment adopted provides a very severe test of the theory indeed.

6.2.1 Test of applicability of the RHS theory

In order to test the extent to which Dahler's theory of the rough hard sphere fluid may be used to describe liquid thermal conductivity, we must proceed in a number of steps. First, for each fluid the experimental viscosity data are analysed in terms of Chandler's theory of the rough hard-sphere model to yield the values of the parameters C and V_o for each isotherm (see 5.4.2). Secondly, we use the fact that Dahler's theory and Chandler's theory are mutually consistent to derive a value of K from the value of C. Finally with the derived values of K and V_o we calculate the thermal conductivity of the same fluid using Dahler's theory for the rough hard sphere model and compare it with experiment. As was mentioned earlier it is a severe test of the theory because no information about the thermal conductivity itself is involved in the calculation.

Dymond *et al* [114] have determined the values of the molecular core volume (V_o) and the coupling constant (C) from viscosity data for n-hexane which are only applicable up to a pressure of 150 MPa because of the limited range of validity of the RHS model. The values they obtained were C = 1.45 and $V_o = 78 \times 10^{-6}$ m^3 mol^{-1} for n-hexane at 25°C. Using the procedures given in [114], we have deduced the corresponding

values for n-octane using the experimental viscosity data of Dymond et al [135] as C = 1.7 and $V_o = 105 \times 10^{-6}$ m^3 mol^{-1}.

From the values of C, it is possible to calculate the appropriate values of K in each case using the ratios of $\eta^*_{RHS,D}/\eta^*_{SHS}$ obtained in 5.5. It is found that K = 0.44 for n-hexane and K = 0.66 for n-octane. Subsequently, values of $(\lambda_{RHS,D}/\Lambda^0)$ are calculated using equation (5.64). The results are plotted in figs (6.1) and (6.2) and are expressed in dimensionless form, $\lambda^*_{RHS,D}$, defined in the same manner as in equation (5.68) as

$$\lambda^* = \left(\frac{\lambda_{RHS,D}}{\Lambda^0}\right)\left(\frac{V}{V_o}\right)^{2/3}$$

The experimental λ^*_{exp} for n-hexane and n-octane are calculated using equation (5.42) and are included in these figures.

The agreement between the experimental thermal conductivity and that predicted using equation (5.64) for n-hexane is within 5% over the thermodynamic range of the experimental data. For the few data points for n-octane that lies in the range of validity of the model the agreement is less satisfactory but the disagreement amounts to no more than 10%. In view of the simplicity of the RHS model, and the severity of the test these estimations are remarkably good. In the absence of any other information this procedure would allow at least a rough

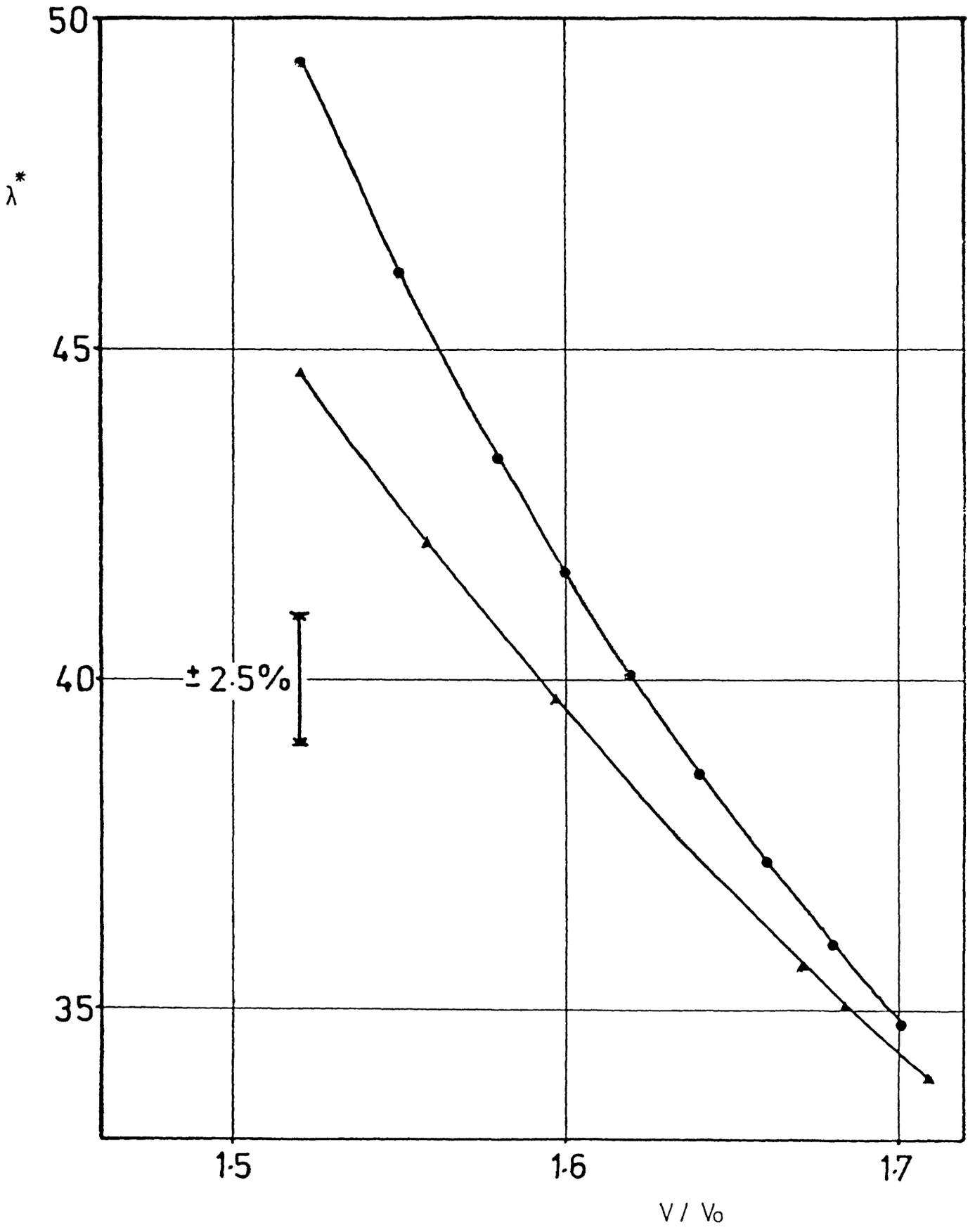

Fig. (6.1) Comparing experimental thermal conductivity data for n-hexane with the values calculated using Dahler's rough hard sphere theory

▲ – λ^{*}_{exp}

● – $\lambda^{*}_{RHS,D}$

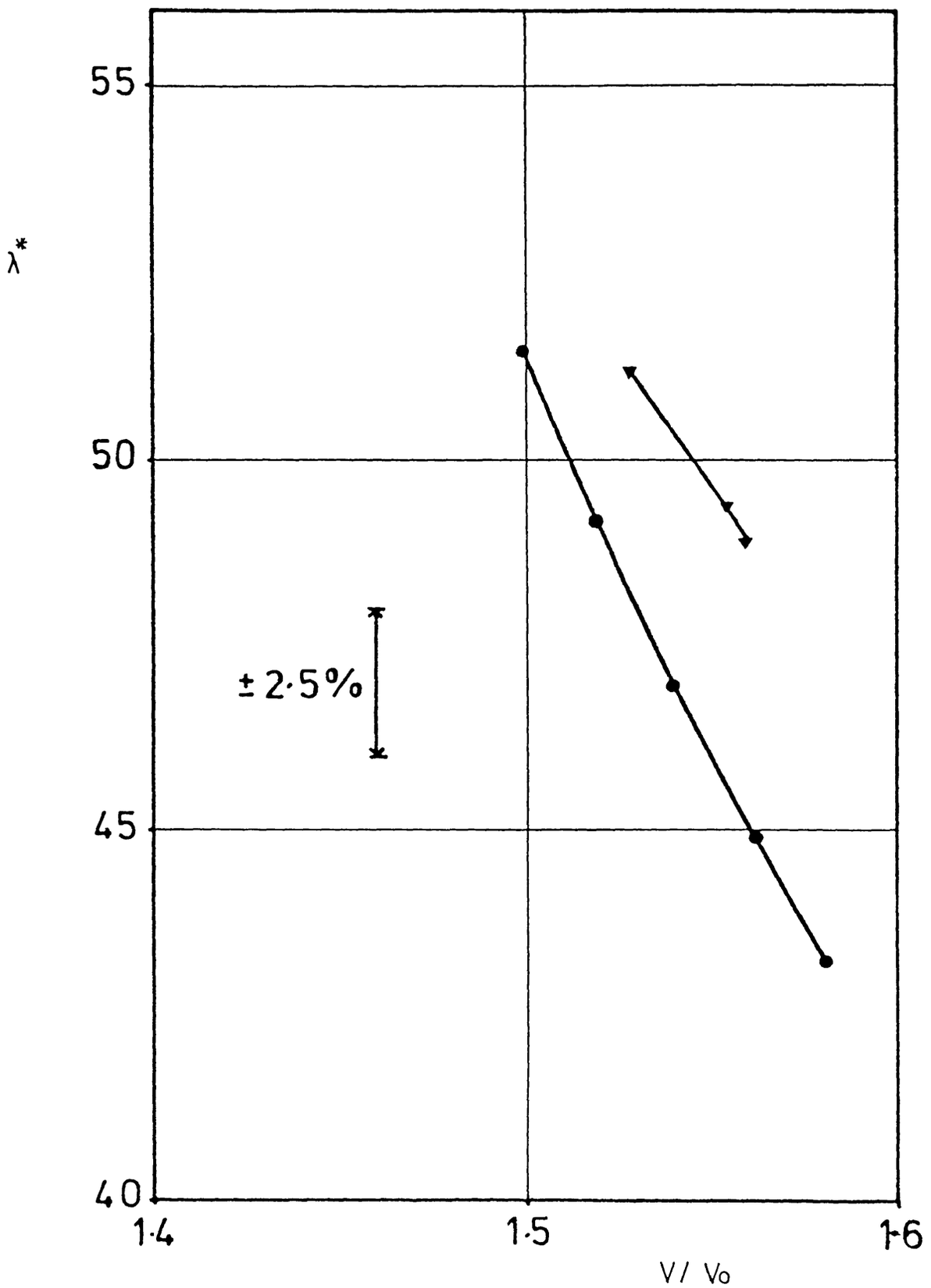

Fig. (6.2) Comparing experimental thermal conductivity data for n-octane with the values calculated using Dahler's rough hard sphere theory

▼ – λ^*_{exp}

● – $\lambda^*_{RHS,D}$

estimate of the thermal conductivity of a liquid from its measured viscosity.

The thermodynamic range for which this estimation procedures is applicable is severely restricted by the range of validity of the RHS model. Moreover, the accuracy of the estimate is very much worse than that of the experimental data obtained using modern measurement techniques. In order to obtain a better representation of the present experimental data and a correlation/prediction scheme of higher accuracy it is clearly advisable to make use of the available thermal conductivity data in its formulation.

6.3 Correlation of Experimental Thermal Conductivity Data

6.3.1 Preamble

In order to provide a useful correlation of their experimental thermal conductivity of dense fluids Menashe *et al* [118] adopted an entirely empirical approach to the problem. They supposed that the density dependence of the internal and translational contributions to the thermal conductivity of the fluids were the same. Using the fact that to a good approximation the zero-density thermal conductivity of a dilute polyatomic gas can be written as [141]

$$\lambda^{o} = \frac{15}{4} \frac{R}{M} \left(1 + 0.352 \frac{C_{v,int}}{R}\right) \eta^{o} \qquad (6.1)$$

where R is the universal gas constant, M the molecular weight, and $C_{v,int}$ the internal part of the molar heat capacity at zero density. They made the hypothesis, by analogy with the monatomic case, that the group,

$$\lambda' = \left(\frac{\lambda}{\lambda^o}\right)\left(\frac{V}{V_o}\right)^{2/3} \qquad (6.2)$$

should be a function of (V/V_o). In terms of experimental quantities

$$\lambda' = \frac{1.936 \times 10^7 \, \lambda V^{2/3} \, (M/RT)^{\frac{1}{2}}}{(1+0.352 \, C_{v,int}/R)} \qquad (6.3)$$

It is important to distinguish between the λ^o used here, which represents the low density limit of the thermal conductivity of a polyatomic gas and Λ^0 used previously for the definition of λ^* in 5.5 and 6.2.1. Thus the functional forms of λ' and λ^* are different.

According to the hypothesis of Menashe et al [118], it should be possible to superimpose plots of λ' against log V for one fluid at several different temperatures upon each other by shifts along the log V axis. This was indeed found to be possible for normal alkanes with an odd number of carbon atoms from C_3 to C_{13}, with an accuracy comparable with the uncertainty in the experimental data. Furthermore, it was found that the curves for all of these liquids could be superimposable on one another. This entirely empirical scheme therefore provided a useful correlation procedure. However, there is no firm foundation for the original hypothesis of their scheme and it is found that the relationship between λ' and (V/V_o) for polyatomic fluids is quite different from that between λ^* and (V/V_o) for monatomic fluids. In view of the fact that the latter was used to provide the analogy for the development of the former the situation is unsatisfactory. This observation is reinforced by the fact that the temperature variation of V_o found by analysis of the thermal conductivity data was markedly different from that obtained by an

analysis of viscosity data. A more soundly based analysis of the problem of thermal conductivity in dense polyatomic fluids is therefore desirable.

6.3.2 Correlation methods based on the RHS theory

According to the analysis of 5.4.3, the thermal conductivity of the RHS fluid can be represented by a simplified form of equation (5.64) as

$$\frac{\lambda_{RHS,D}}{\Lambda^0} = C_1(\frac{1}{g}) + C_2(\frac{b}{V}) + C_3[(\frac{b}{V})^2 g] \qquad (6.4)$$

where both the radial distribution function (g) and the ratio (b/V) are functions of (V/V_o) alone. The coefficients C_1, C_2 and C_3 are algebraic functions of K only.

In view of the fact that K, the dimensionless moment of inertia, is a parameter of the model and the mass distribution of realistic molecules may not be represented in such a simplistic manner, it should be recognised that these coefficients derived for the rough hard sphere theory do not necessarily reflect the exact behaviour of real fluids.

Instead the form of equations (5.64) and (6.4) suggests that even though the use of these equations in the direct calculation of the thermal conductivity may be restricted by the range of validity of the RHS model (see 5.4.2 and 6.2), it should, however, be possible to establish on the basis of this analysis that the thermal conductivity of a rough hard sphere fluid depends predominantly on the ratio (V/V_o), and the dependence on the mass distribution of the molecule enters only

in the coefficients of a correlation equation relating the thermal conducitivity and (V/V_o) (see equation 6.4).

The underlying principle of the correlation method proposed here is to represent the thermal conductivity data primarily by its dependence on (V/V_o), and determine empirically the coefficients which optimize this representation.

The approach can be justified by the following reasoning. It has already been shown that for the rough sphere model the dependence of the thermal conductivity on the parameter K is weak. Furthermore, within the model K is a temperature independent quantity and even for a real molecule is likely to be a weak function of temperature. It is therefore entirely reasonable to expect that the quantity λ^* should be a function only of (V/V_o). Consequently, by analogy with the analysis of the diffusion coefficient, D^*, and the viscosity coefficient, η^*, it should be possible to superimpose plots of λ^* vs log V for a number of different isotherms for a single fluid upon each other. The amount of the relative shift for any two isotherms then determines the ratio of the V_o values at the two temperatures. Of course absolute values of V_o cannot be determined by this procedure. A further extension of this argument which acknowledges the weak dependence of λ^* on K would suggest that even among different fluids λ^* may be a universal function of (V/V_o).

In the sections which follow we consider the application of these ideas to the present thermal conductivity data. We begin with the establishment of a simple and convenient method for the representation

of the thermal conductivity of one fluid along a single isotherm. Subsequently we consider the proposal that the density dependence of λ^* is universal among several isotherms for each liquid. Finally, we consider the hypothesis that the universality of λ^* extends to different fluids. It is to be expected that the increasing generality of the correlation scheme implied by these steps will lead to some loss of accuracy. However, as will be shown the scope which is provided for the extension of the thermodynamic range of given set of data by the most general procedure makes the marginal loss of accuracy acceptable for many purposes.

6.4 The Correlation Schemes

6.4.1 Individual Isotherms

We first consider the representation of the density dependence of the thermal conductivity of a single liquid along an isotherm. The thermal conductivity of n-hexane at 307 K as a function of molar volume is plotted in Fig. 6.2, to illustrate the form of the dependence and the smoothness and scatter of the experimental data, which is typical of all systems studied. A number of forms of empirical relationship between the thermal conductivity and the molar volume have been examined in order to represent the experimental data. The most successful equation takes the form

$$\log \lambda^* = a_o - a_1 \log (V/V_o) \qquad (6.5)$$

where

$$\lambda^* = 1.936 \times 10^7 \lambda V^{2/3} (M/RT)^{\frac{1}{2}} \qquad (6.6)$$

with λ in units of $Wm^{-1} K^{-1}$. V is the molar volume, M the molecular mass, R the universal gas constant and T the absolute temperature.

In equation (6.5), V_o is an arbitrary scaling parameter. For simplicity, and later use it is preferable to assign a value to V_o for each liquid at each temperature which is at least physically realistic. The values employed for each liquid at each temperature are listed in Table 6.1 and the manner of their selection will be described in the next section. The same table includes the optimum values of the coefficients a_o and a_1 as well as the standard deviation of the experimental data from the correlation of equation (6.5). Figure (6.4) to (6.9) contains plots of the deviations from the correlation of equation (6.5) for each liquid. In no case do the deviations exceed ± 1.2%, whereas the standard deviation is less than 0.5% for the whole set of data. These figures are consistent with the combined uncertainties of the experimental density and thermal conductivity data. It is particularly noted that a typical error of ± 0.3% in the density data introduces a projected error of ± 1.5% in the thermal conductivity.

The correlation given by equation (6.5) and Table (6.1) provides a secure means of extrapolation of the present thermal conductivity data to the conditions of saturation at a particular isotherm given accurate

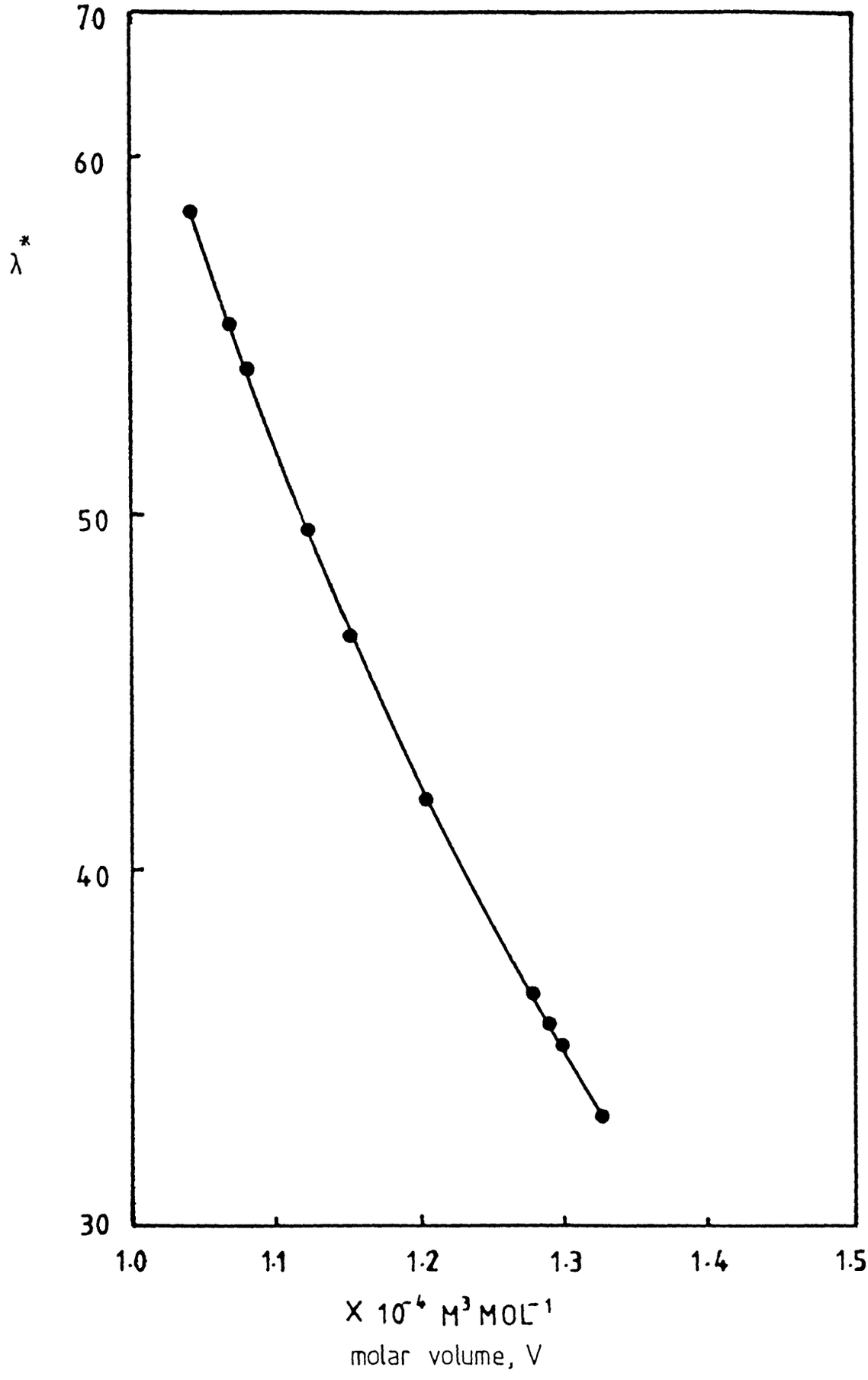

Fig. (6.3) Density dependency of the thermal conductivity of n-hexane for the isotherm T=34°C

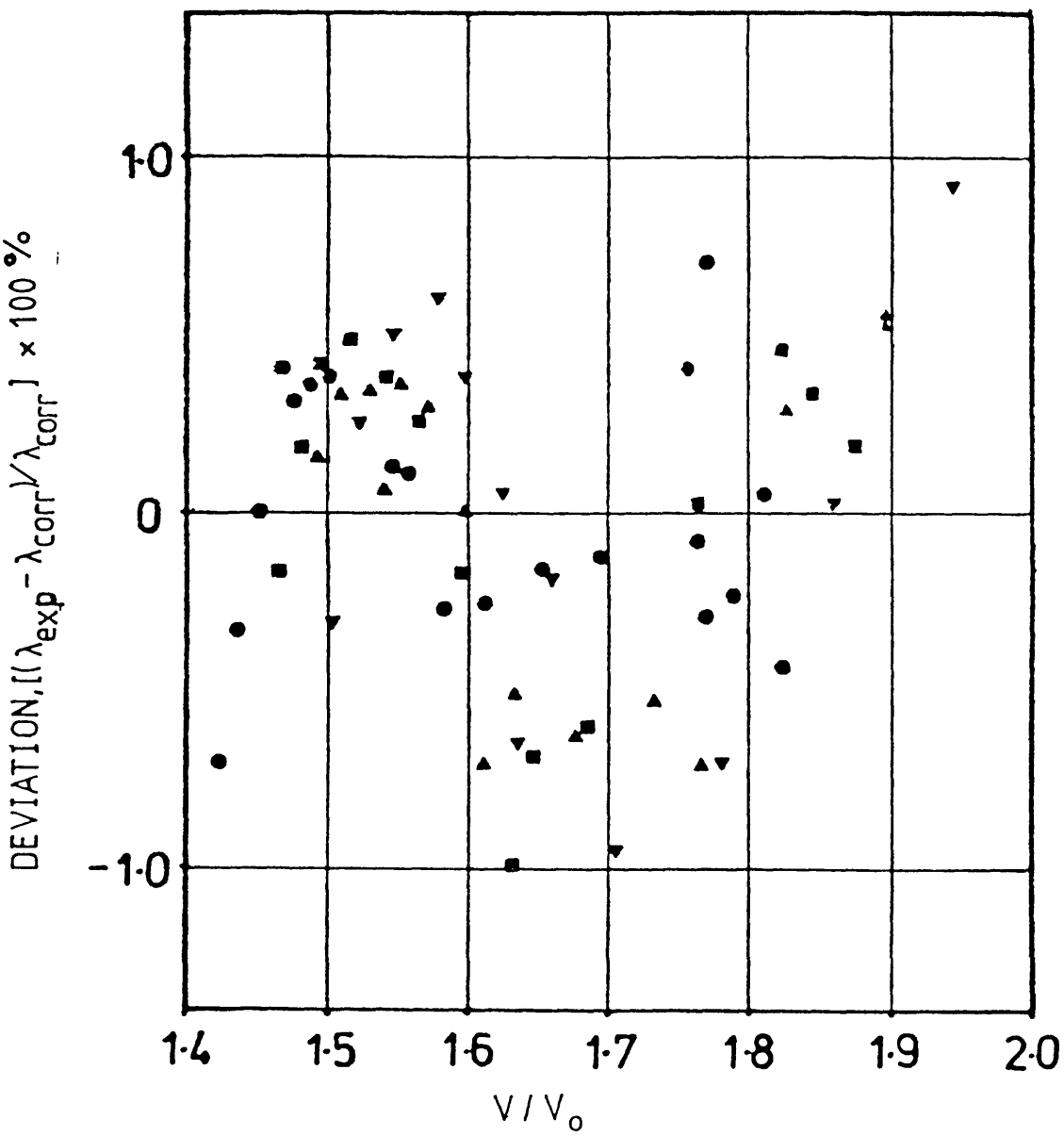

Fig. (6.4) Deviation of the experimental thermal conductivity data for n-hexane from the correlation of Eq. (6.5), with the coefficients given in Table 6.1

● -34°C ; ■ -48°C ; ▲ -72°C ; ▼ -87°C

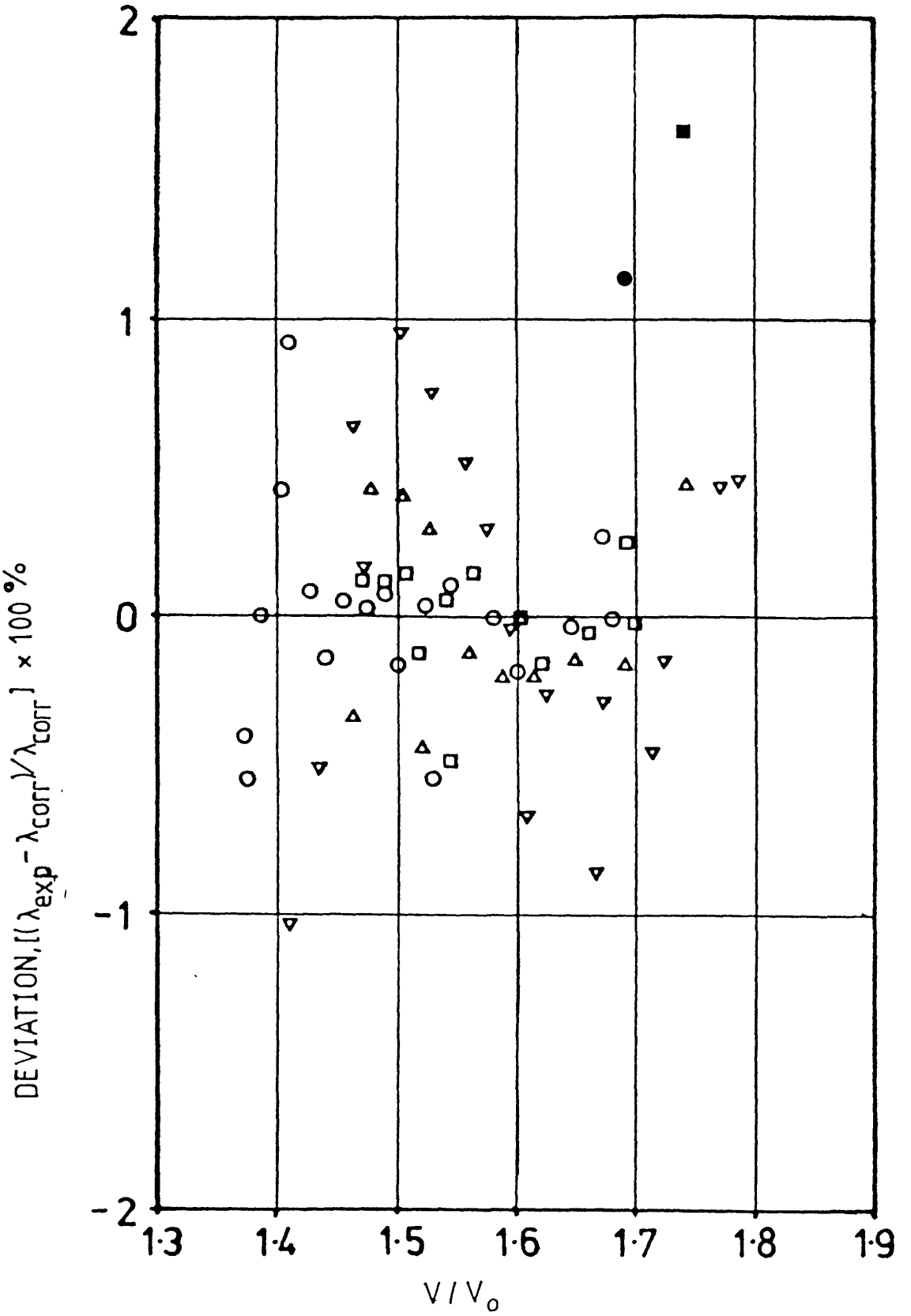

Fig. (6.5) Deviation of the experimental thermal conductivity data for n-octane from the correlation of Eq. (6.5), with the coefficients given in Table 6.1

Present work: ○ -34°C ; □ -48°C ; △ -72°C ; ▽ -89°C
Castro et al (142): ● -34°C ; ■ -48°C

Fig. (6.6) Deviation of the experimental thermal conductivity data for 2,3-dimethylbutane from the correlation of Eq. (6.5), with the coefficients given in Table 6.1

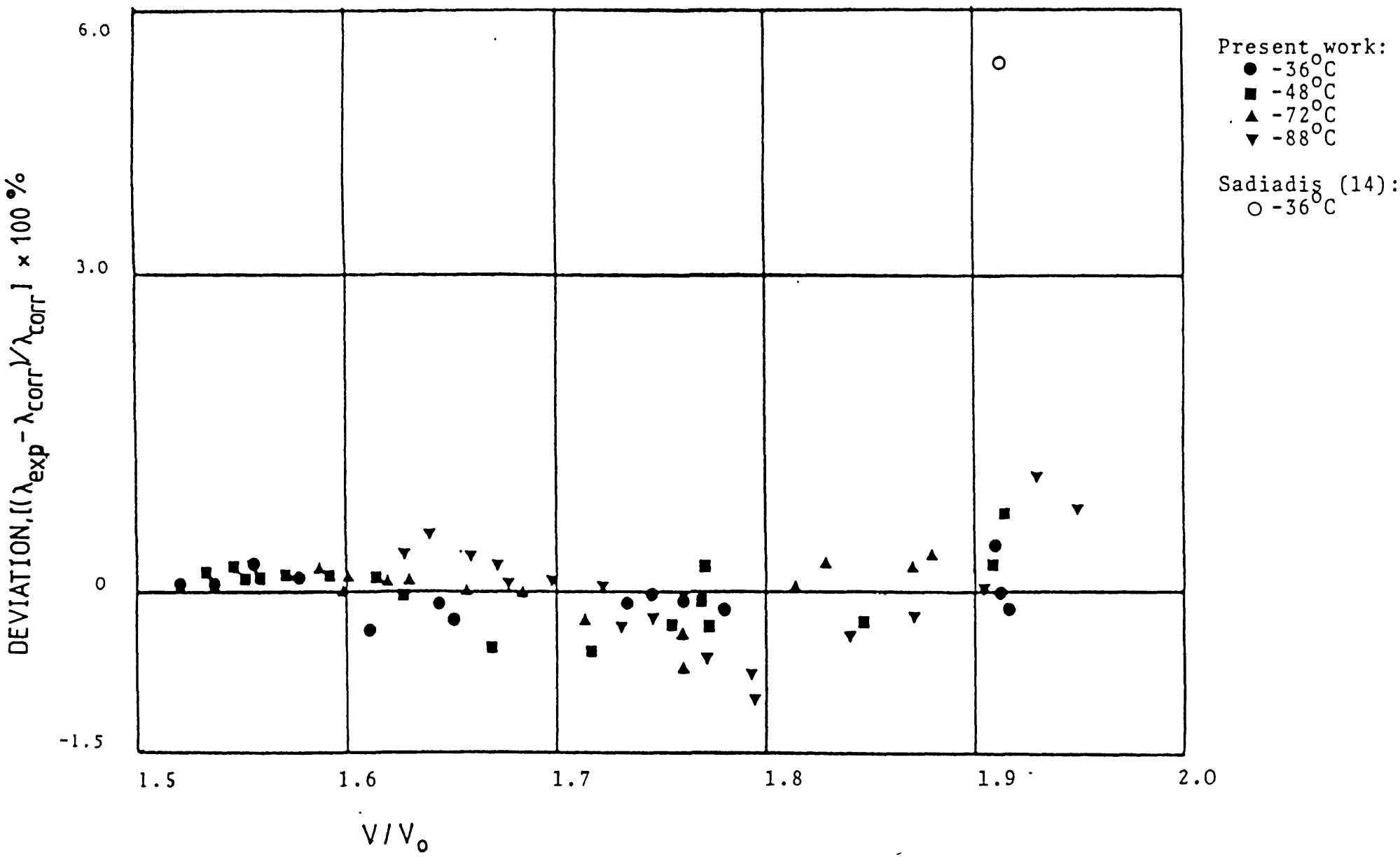

Fig. (6.7) Deviations of the experimental thermal conductivity data for 2,2,4-trimethylpentane from the correlation of Eq. (6.5) with the coefficients given in Table 6.1

Present work: ● -40°C ; ■ -48°C ; ▲ -64°C ; ▼ -78°C
Calado et al (151): ○ -40°C ; □ -48°C ; △ -64°C ; ▽ -78°C

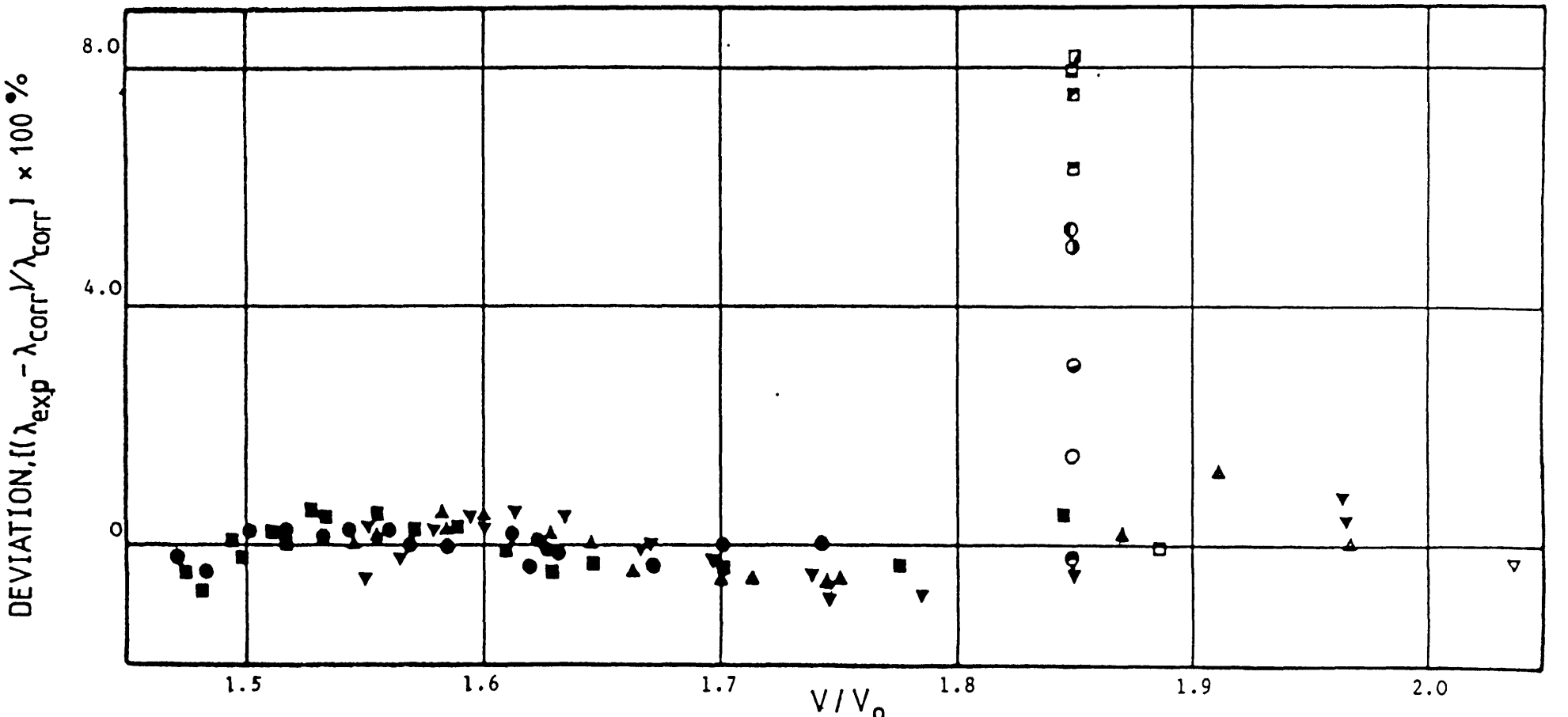

Sadiadis (143): ◐ ; Kerimov (144): ◑ ; Rastorguev (145): ◓
Rastorguev (146): ◒ ; Mukhamedzyanov (147): ◩ ; Frontasev (148): ◪
Filippov (149): ◘ ; Riedel (150) : ◙

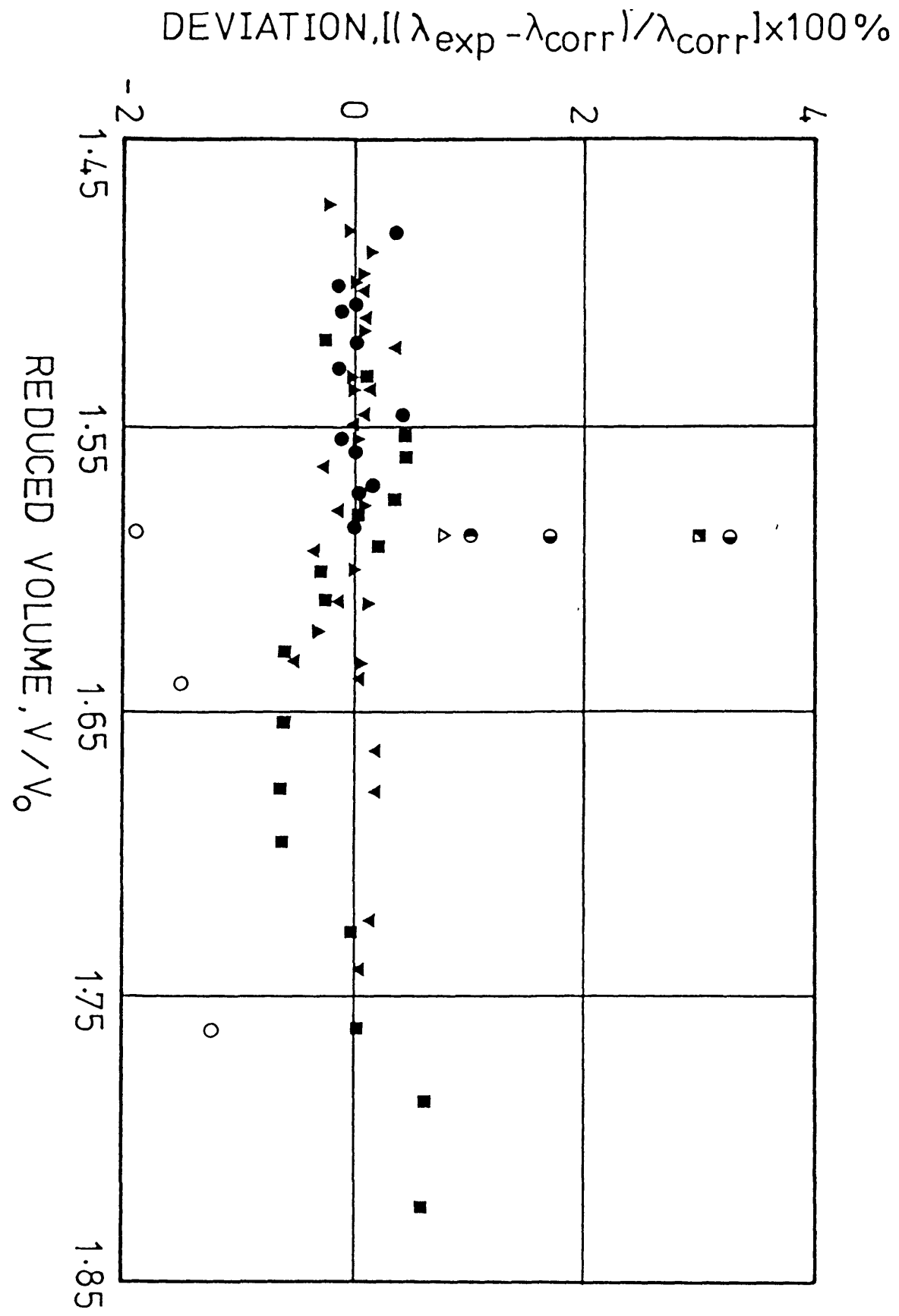

Fig.(6.8) Deviations of the experimental thermal conductivity data for benzenz from the correlation of Eq. (6.5) with the coefficients given in Table 6.1

Present work: ● -37°C ; ▲ -47.5°C ; ▼ -71°C ; ■ -85.5°C
Kashiwagi (152): ○ ; Horrocks (153) : △ ; Poltz (38) : ◐
Riedel (12) : ◑ ; Schmidt (154) : ◪

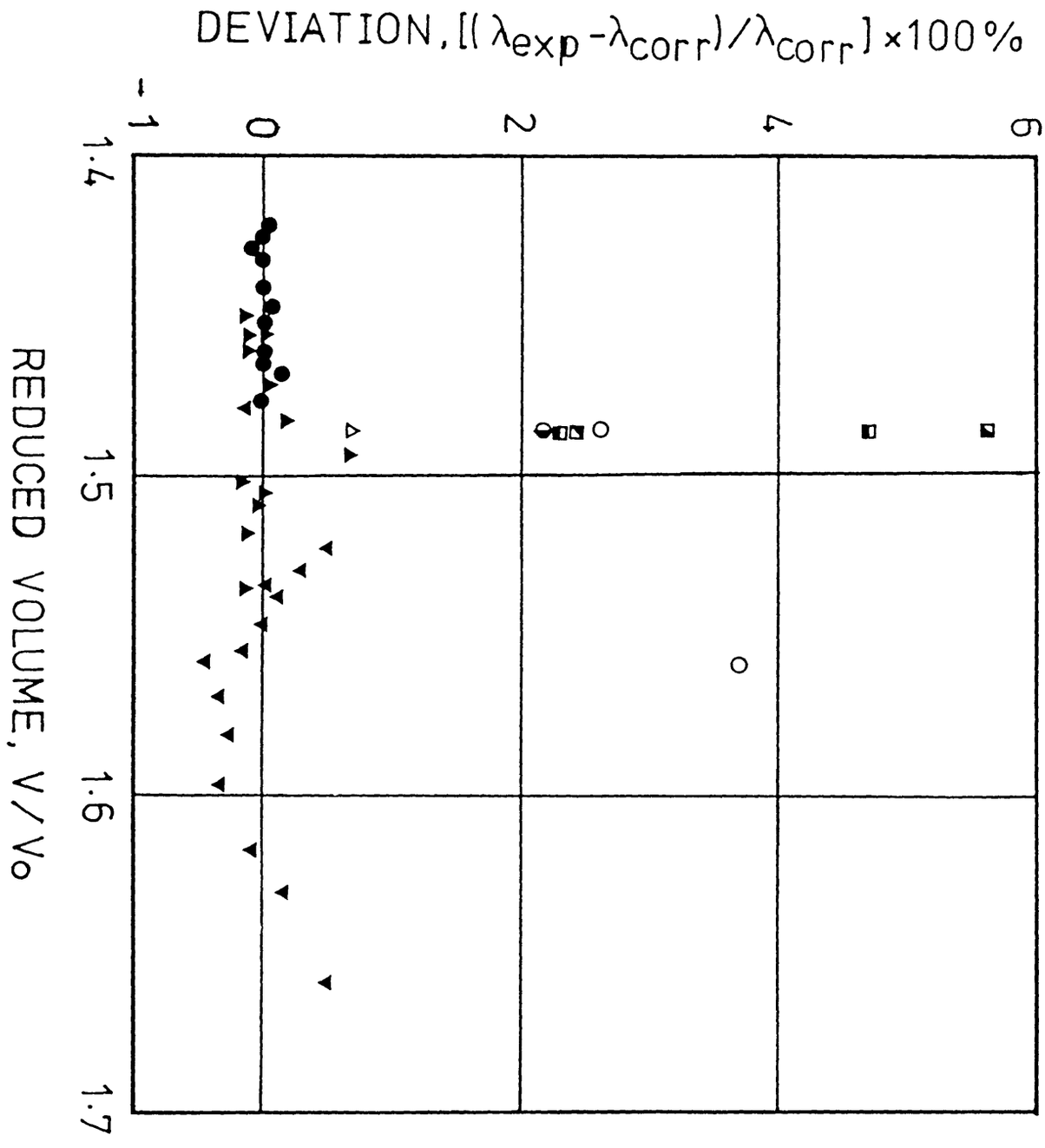

Fig. (6.9) Deviations of the experimental thermal conductivity data for cyclohexane from the correlation of Eq. (6.5) with the coefficients given in Table 6.1

Present work: ● -36°C ; ▲ -51°C ; ▼-80°C
Kashiwagi (152): ○ ; Horrocks (153): △ : Barnette (155): ○ ;
Briggs (156): ◪ ; Mukhamedzyanov (147): ◪ ;
Sakiadis (143): ◨ ; Filippov (149): ◨

density data. The extrapolation has been carried out for each liquid at each isotherm. Accounting for the uncertainty in the density and the thermal conductivity. The extrapolated value has an estimated error of ± 1.8%. Figure (6.4) and (6.9) include the departure of the most reliable of earlier results under these conditions [142-159] from the extrapolation of the present results.

The measurement of Castro et al [142] for n-octane and those of Calado et al [151] for 2,2,4-trimethylpentane are the only data obtained with a high precision transient hot-wire instrument. In the case of these two sets of results we have consistently used for comparison the data 'uncorrected' for radiation. This is because, as we have demonstrated earlier (see 2.4) the correction applied was in fact unnecessary. The agreement between the data of Castro et al and Calado et al and the present extrapolation is within ± 1.7% and is within the mutual uncertainties of these sets of data. The deviations of the remaining measurements by the other workers from the correlation of equation (6.5) amounts to as much as 8% in some cases although a few measurements are in much better agreement with those reported here. In any case, the results obtained using the transient hot-wire method are to be preferred owing to their higher accuracy.

6.4.2 Individual liquids

An immediate generalization of the correlation scheme is to follow the earlier argument (see 3.2) and to consider that the density dependence of the thermal conductivity is the same for all isotherms. As expected on the basis of the RHS theory, we should be able to carry out the superposition of curves of λ^* against log V for different

temperatures by shifts on the log V axis alone. The lowest isotherm for each liquid is chosen to be the reference datum. Thus the curves at high temperatures are superimposed onto the curve at the lowest isotherm.

The shift of the curve corresponding to a temperature T necessary to superimpose it on the curve for the reference temperature, T_R, determines the ratio $V_o(T)/V_o(T_R)$. Thus, if a value for $V_o(T_R)$ is adopted the characteristic volumes, V_o, for high temperatures may be generated. The reference values of V_o for n-hexane, n-octane, benzene and cyclohexane have been taken from the analysis of their viscosities carried out by Dymond [134-137]. For 2,3-dimethylbutane and 2,2,4-trimethylpentane the reference values have been determined by superposition of the λ^* vs log V curve for the lowest isotherm on that for the respective normal isomer. All of the values of V_o for the liquids studied here are collected in Table 6.1.

Since the graphical superposition procedures for λ^* and log V are carried out on a similar basis to that of Dymond's analysis of viscosity data [134-137], it is interesting to examine the ratio $V_o(T)/V_o(T_R)$ determined using the two properties. Figures (6.10) to (6.12) illustrate the temperature dependence of the ratio $V_o(T)/V_o(T_R)$, deduced from these two independent analyses for n-hexane, n-octane and benzene. For n-hexane the two sets of results are remarkably close, and even though the agreement for n-octane and benzene is not as good

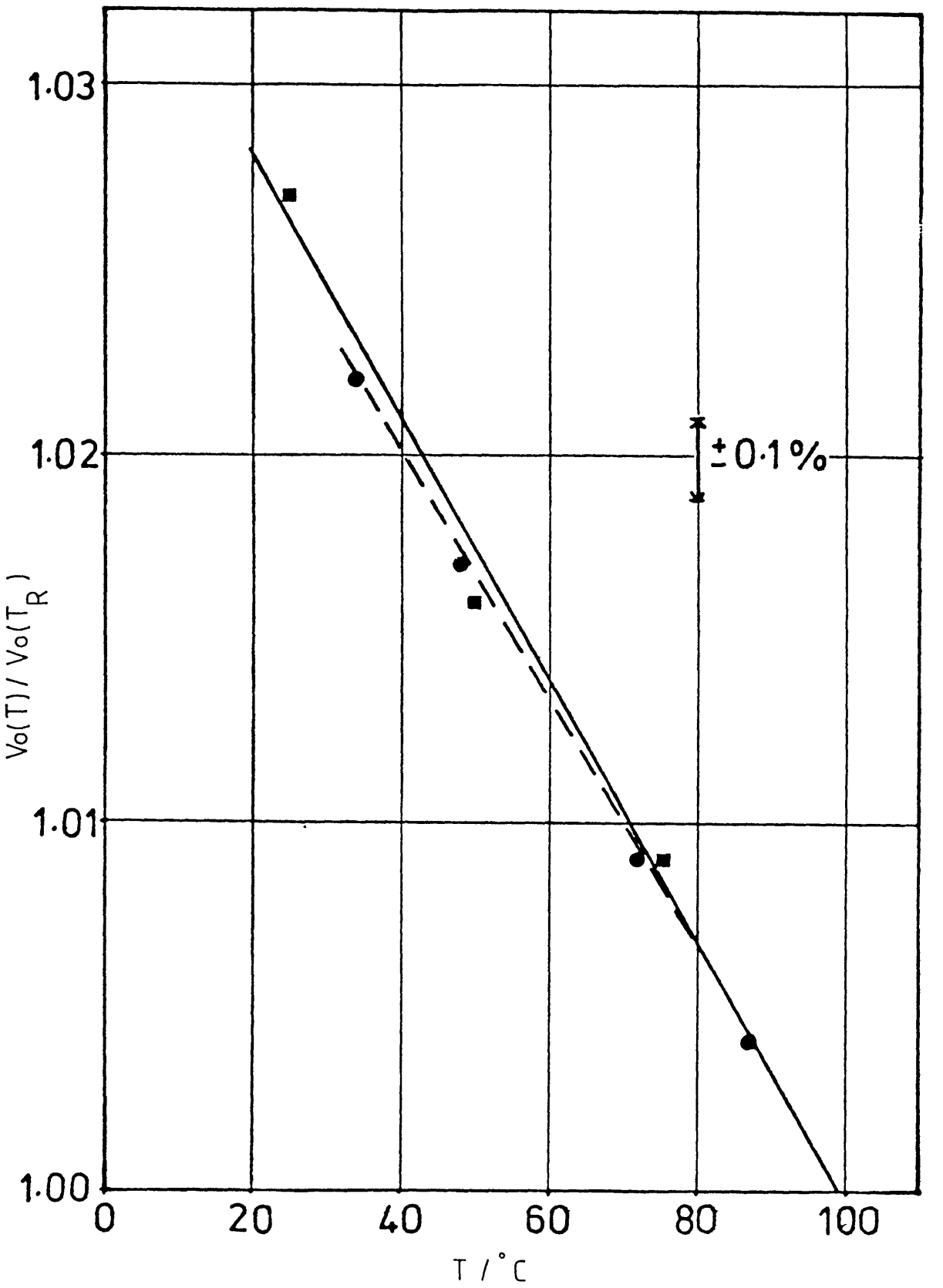

Fig. (6.10) Temperature dependence of the ratio $Vo(T)/Vo(T_R)$ for n-hexane

■-this work ; ● - Dymond et al (134)

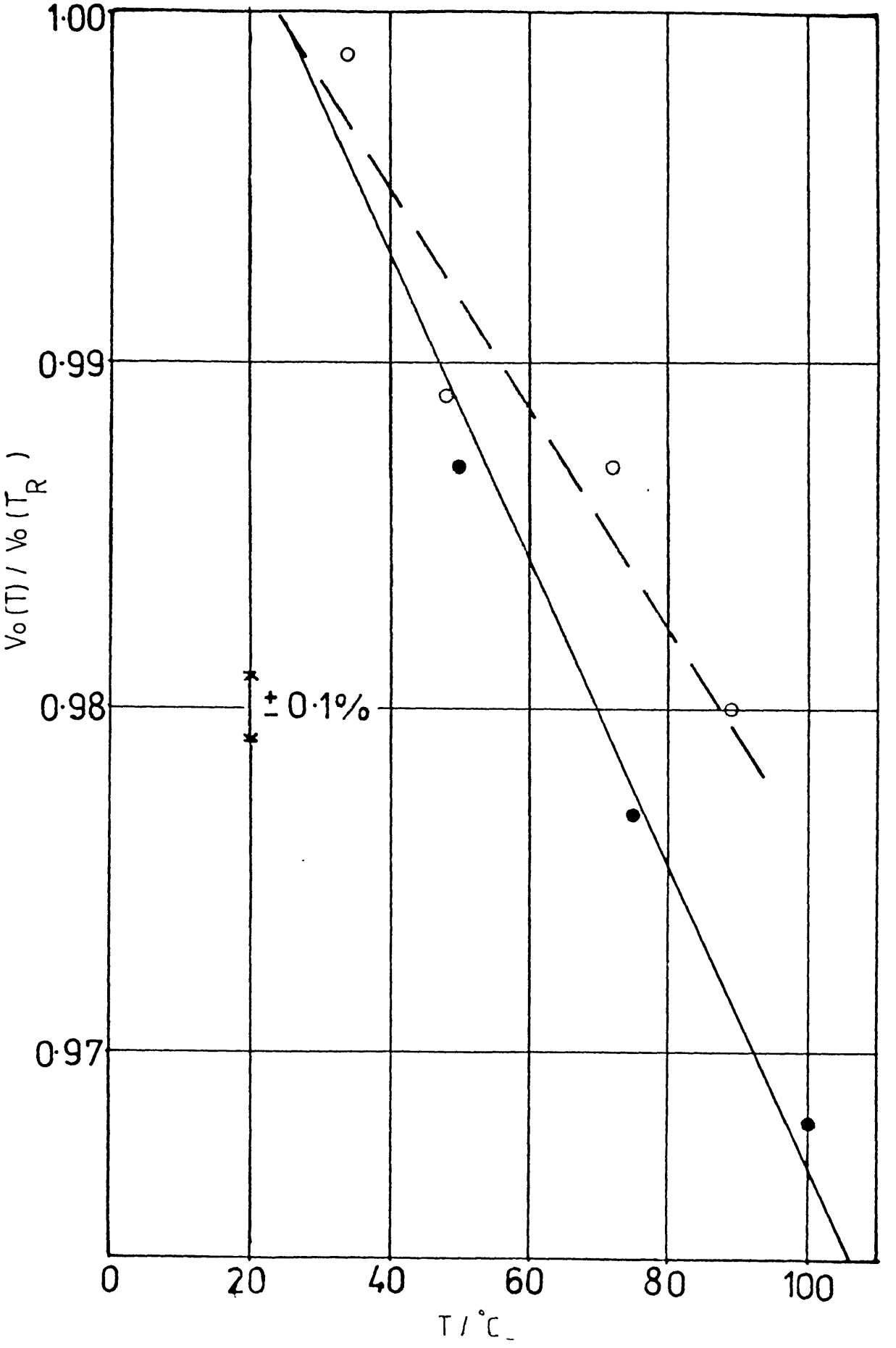

Fig. (6.11) Temperature dependence of the ratio $Vo(T)/Vo(T_R)$ for n-octane

o - this work ; ● - Dymond et al (135)

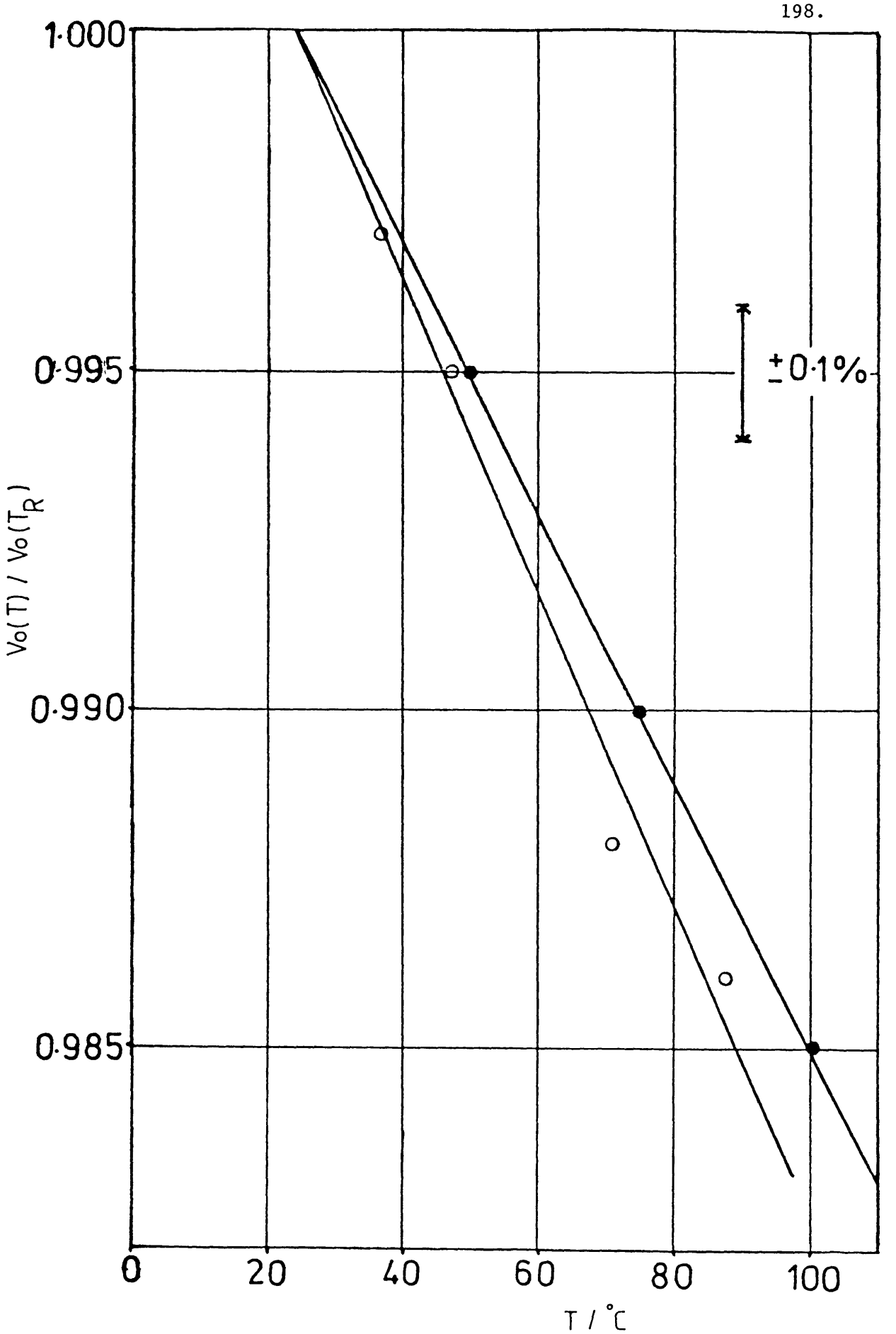

Fig. (6.12) Temperature dependence of the ratio $Vo(T)/Vo(T_R)$ for benzene

○ - this work ; ● - Dymond et al (136)

the discrepancies are still not large. Further analyses of the two properties would be necessary to establish the full extent of the compatibility of these analysis on the basis of the same rough sphere model.

As a result of the superposition procedure, a single curve of λ^* against log V can be obtained for each liquid. Figure (6.13) to (6.18) contain plots of the quantity λ^*_{exp} against V/V_o for each liquid. These graphs demonstrate that satisfactory superposition is indeed possible. The dependence of λ^* on temperature can hence be essentially accounted for by the dependence of V_o on temperature. This observation is consistent with the arguments based upon the RHS theory.

For the representation using the form of equation (6.5), we may assume that the coefficients a_i for the correlating equations are temperature independent. The success of the superposition process means that it should be possible to represent the entire body of data of each liquid studied in this work by a single equation of the form of Equation (6.5), using the values of V_o listed in Table (6.1). The optimum coefficients of the correlation of this type are listed in table 6.2, together with the standard deviations of the fit. Figure (6.19) to (6.24) illustrate the deviations of the experimental λ^* from the correlation of Equation (6.5) and Table (6.2). All the deviations are within ± 1.5% except for 1 data point for n-hexane and 1 data point for 2,3-dimethylbutane where they amount to as much as ± 3%. These deviations are somewhat larger than those which occur when individual isotherms are represented by seperate equations. Furthermore, it is possible to discern from the deviation plots some systematic trends. However, bearing in mind the uncertainties in both the thermal conductivity and density it is not possible to assert with

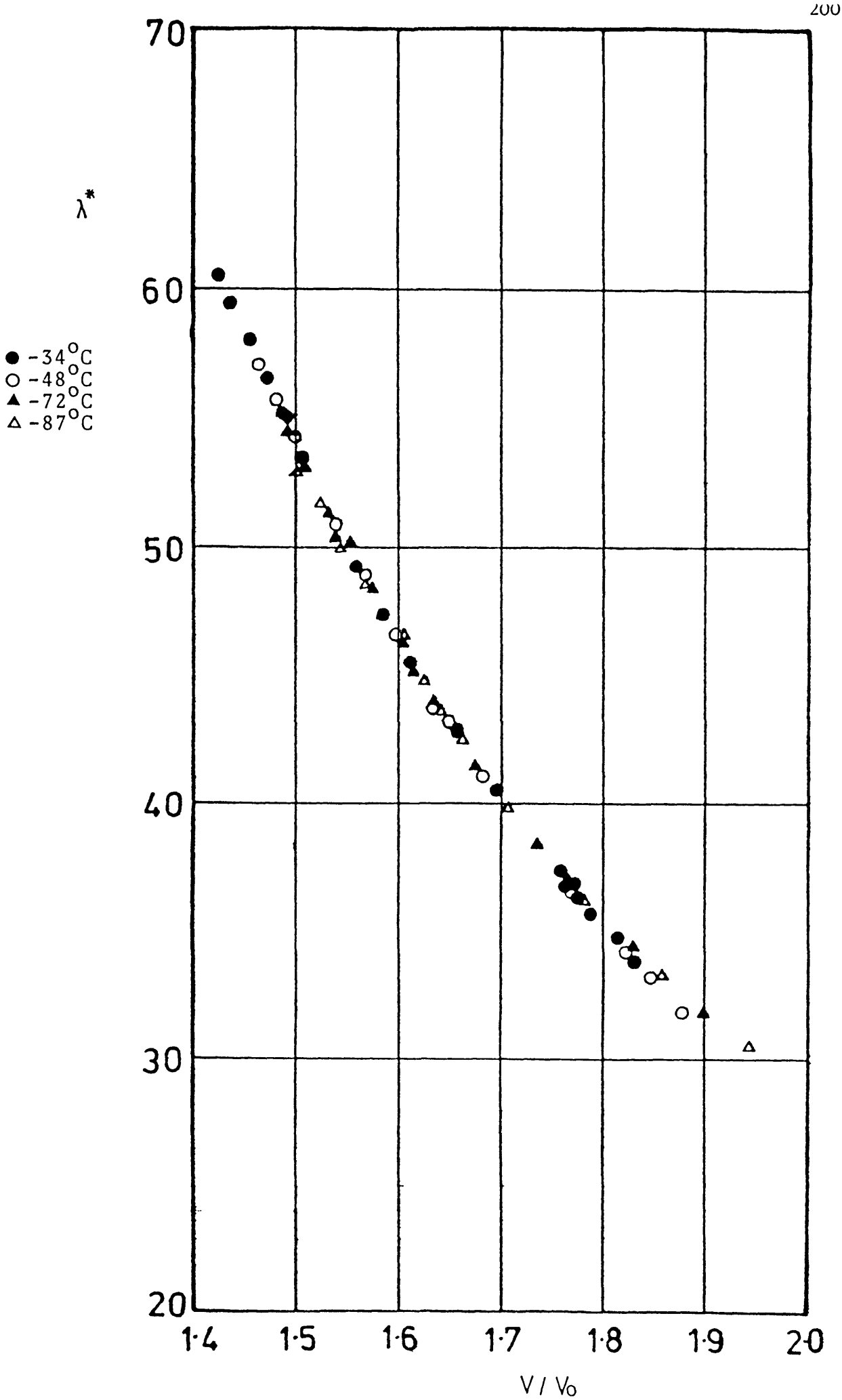

Fig. (6.13) The thermal conductivity ratio λ* for n-hexane as a function of reduced molar volume

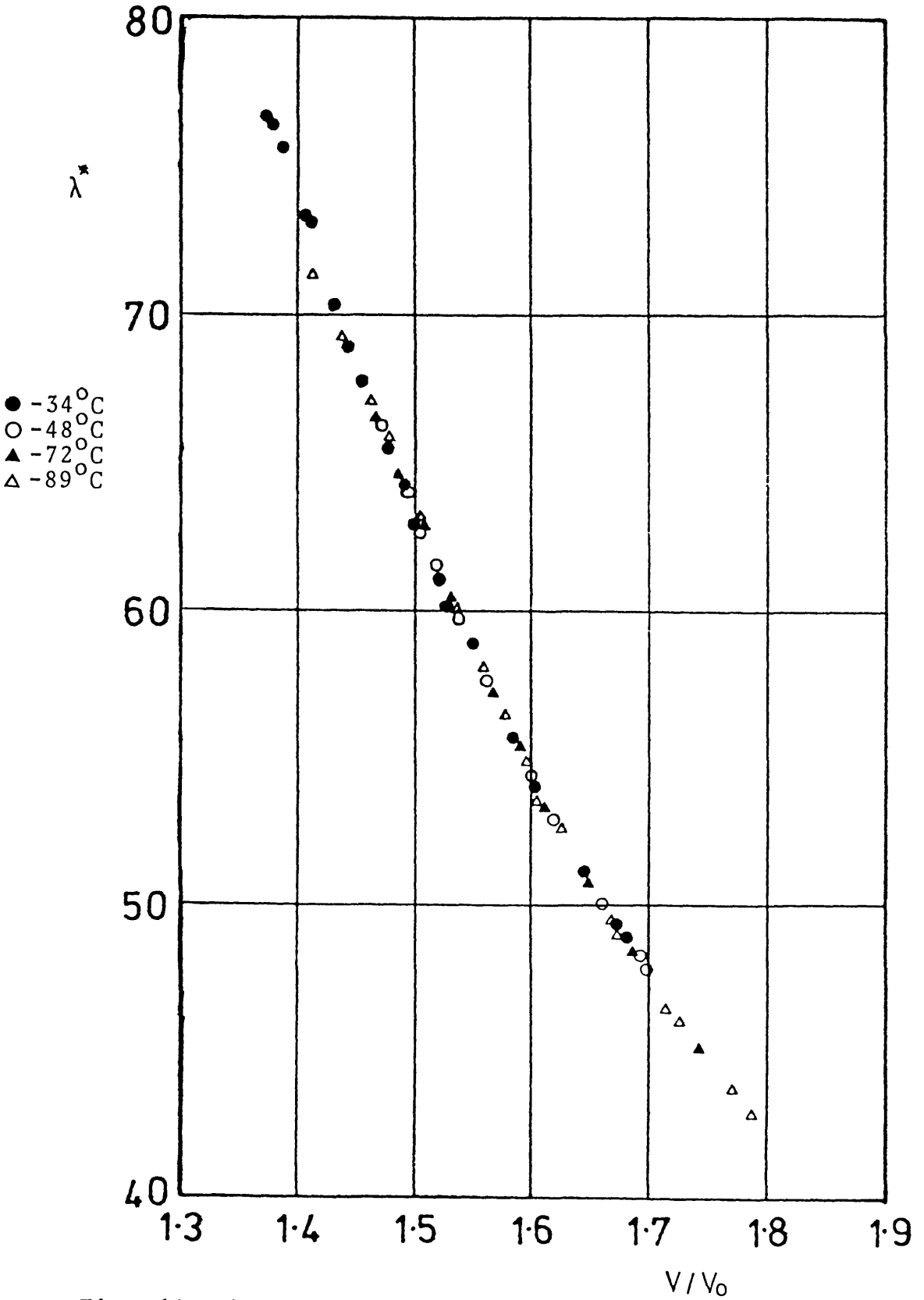

Fig. (6.14) The thermal conductivity ratio λ^* for n-octane as a function of reduced molar volume

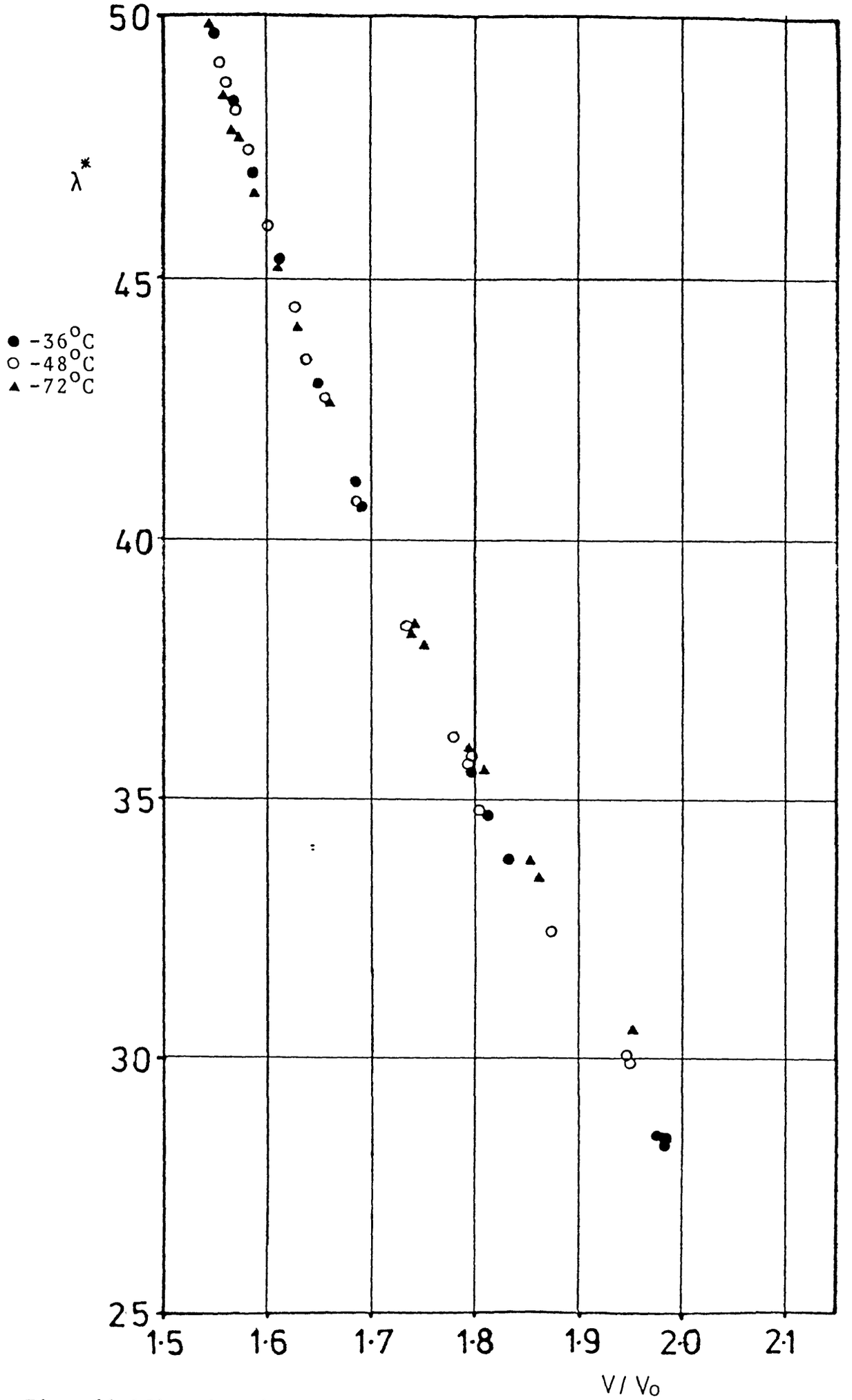

Fig. (6.15) The thermal conductivity ratio λ* for 2,3-dimethyl-butane as a function of reduced molar volume

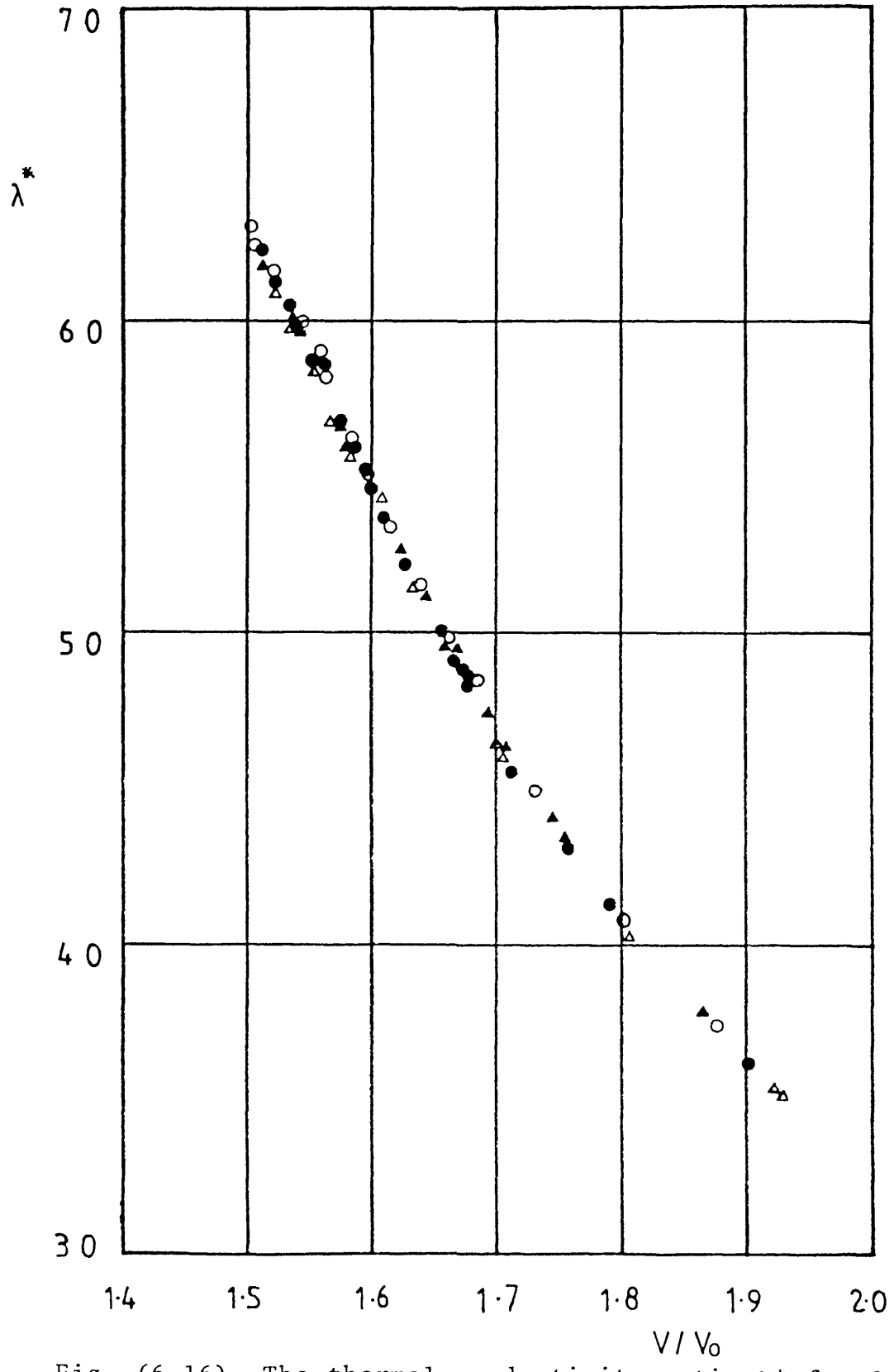

Fig. (6.16) The thermal conductivity ratio λ* for 2,2,4-trimethylpentane as a function of reduced molar volume

●-40 °C ; ○-48 °C ; ▲-64 °C ; △-78 °C

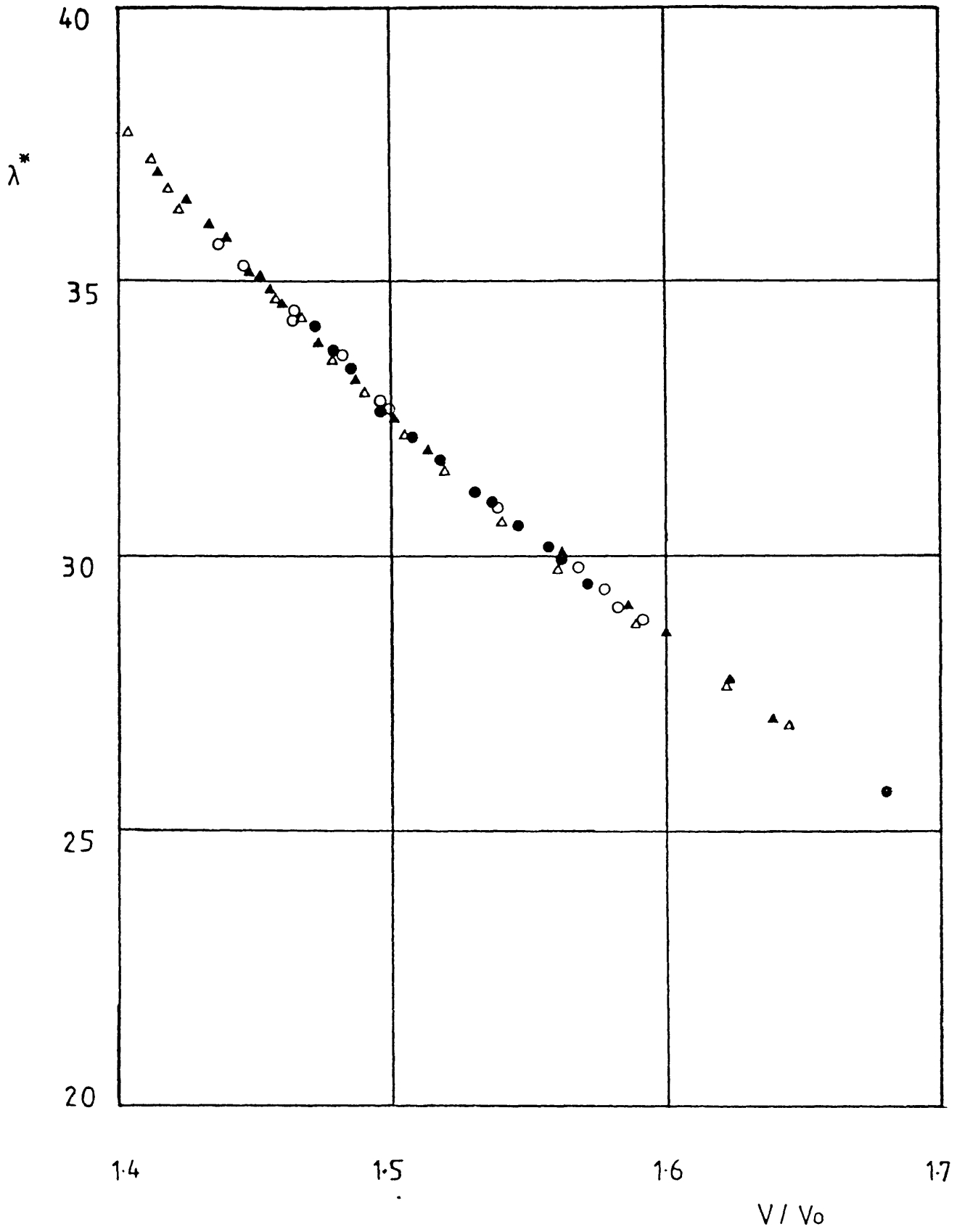

Fig. (6.17) The thermal conductivity ratio λ^* for benzene as a function of reduced molar volume

● $-37^{o}C$; ○ $-47.5^{o}C$; ▲ $-71^{o}C$; △ $-88^{o}C$

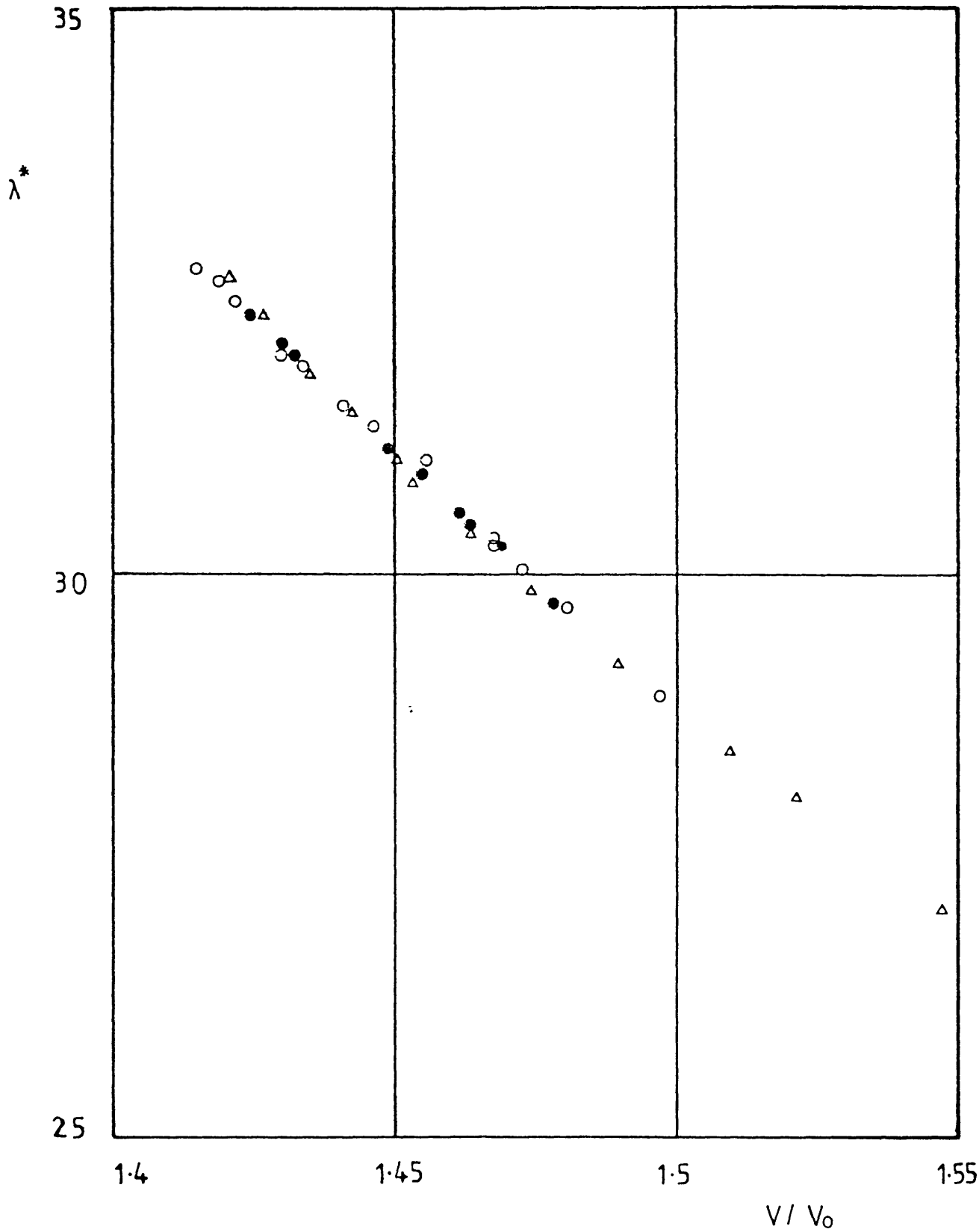

Fig. (6.18) The thermal conductivity ratio λ* for cyclohexane as a function of reduced molar volume

● -36°C ; ○ -51°C ; △ -80°C

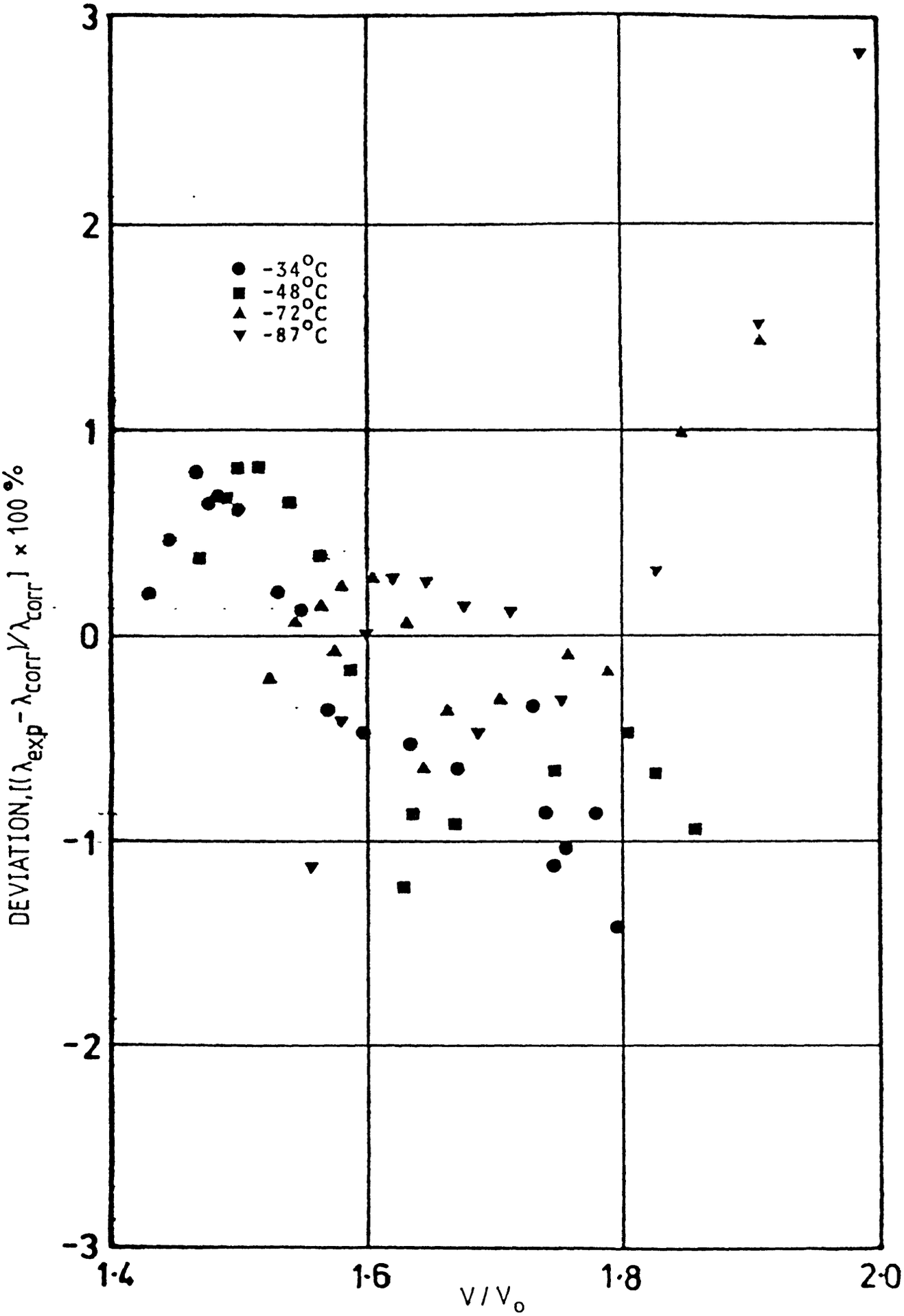

Fig. (6.19) Deviation of the experimental thermal conductivity data for n-hexane from the correlation of eq.(6.5) & Table 6.2

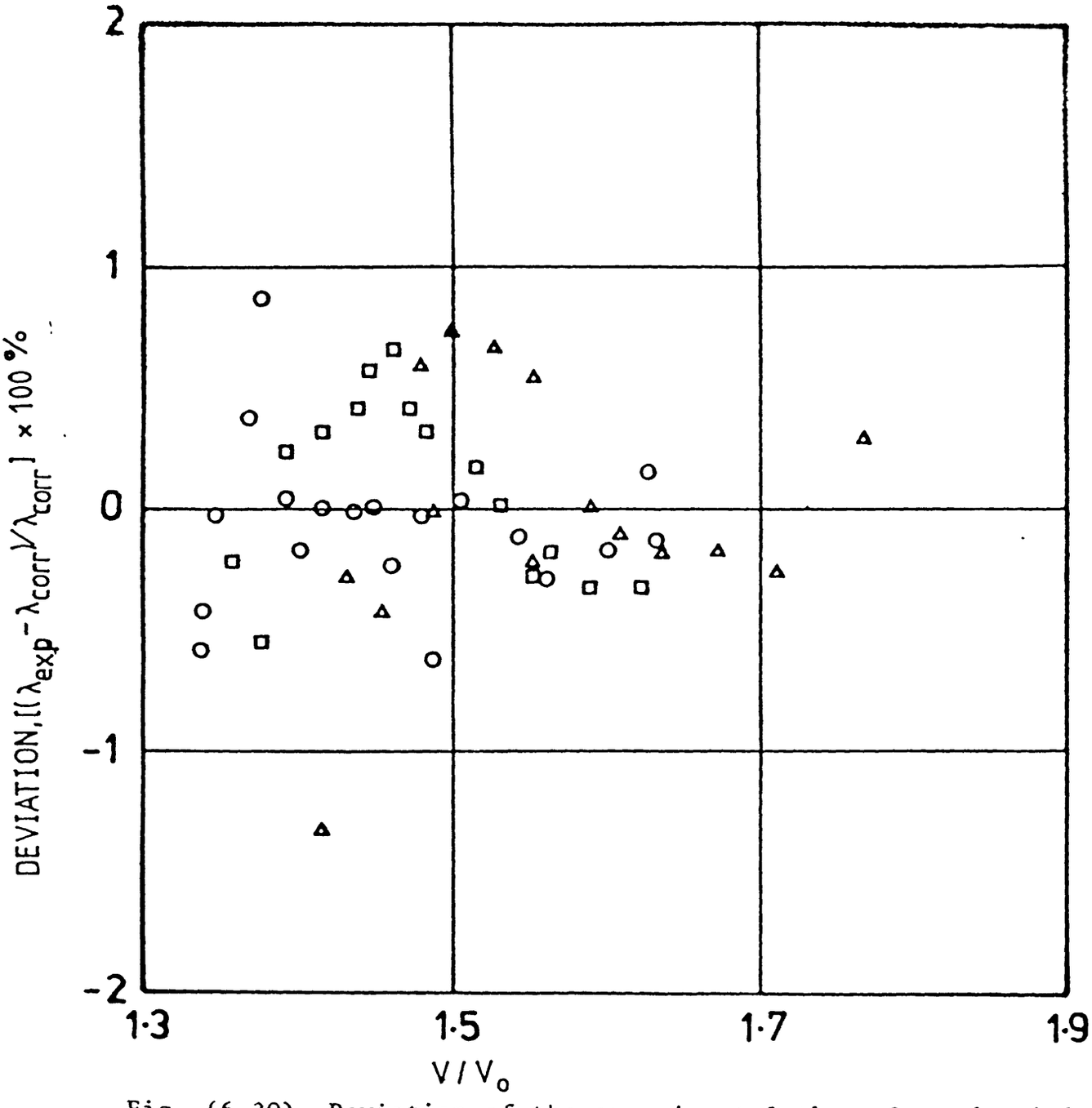

Fig. (6.20) Deviation of the experimental thermal conductivity data for n-octane from the correlation of Eq.(6.5) and Table 6.2

○ -34°C ; □ -48°C ; △ -72°C ; ▽ -89°C

Fig. (6.21) Deviation of the experimental thermal conductivity data for 2,3-dimethylbutane from the correlation of Eq.(6.5) and Table 6.2

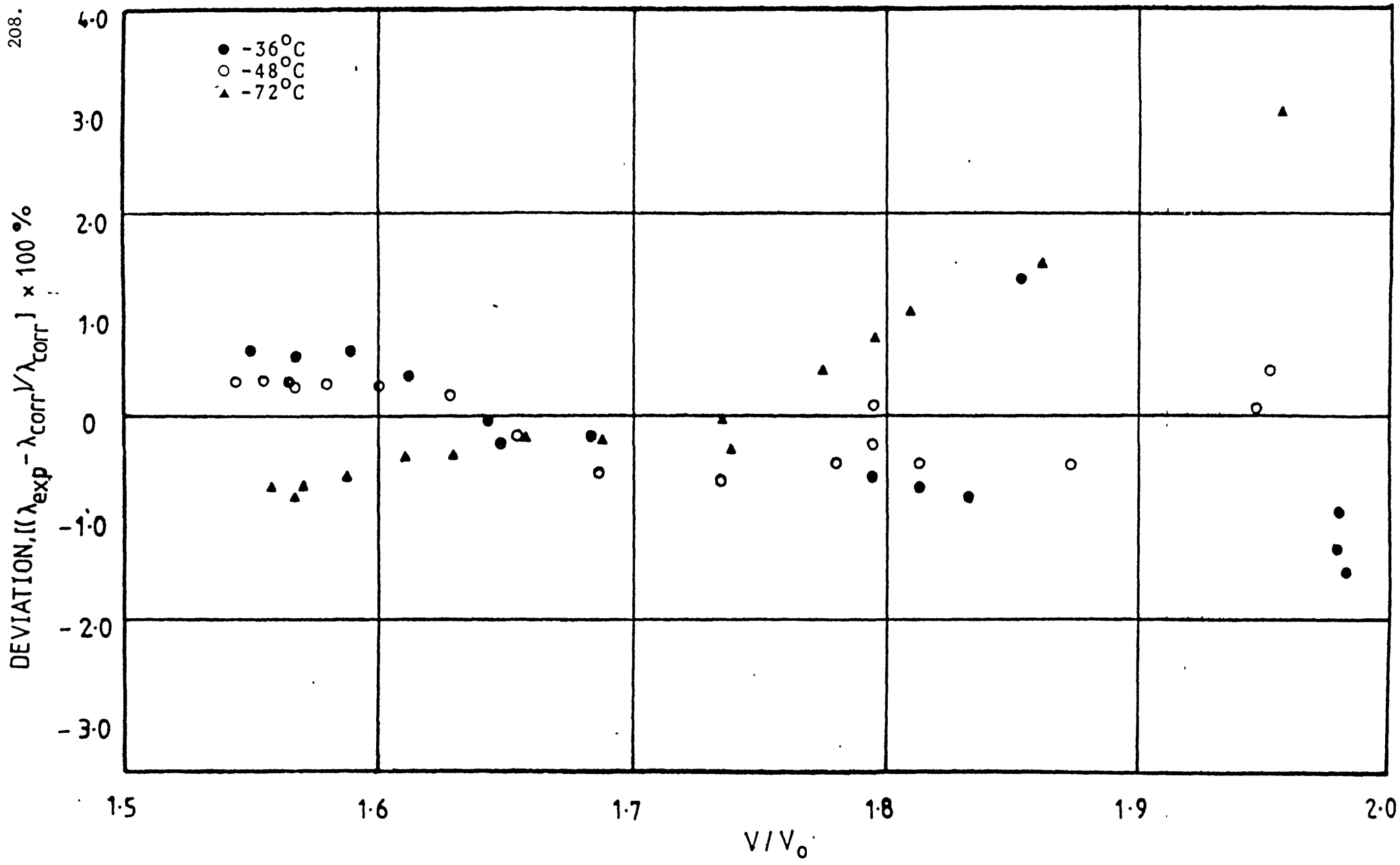

Fig. (6.22) Deviation of the experimental thermal conductivity data for 2,2,4-trimethylbutane from the correlation of Eq.(6.5) and Table 6.2

■ -40°C ; ○ -48°C ; ▲ -64°C ; △ -78°C

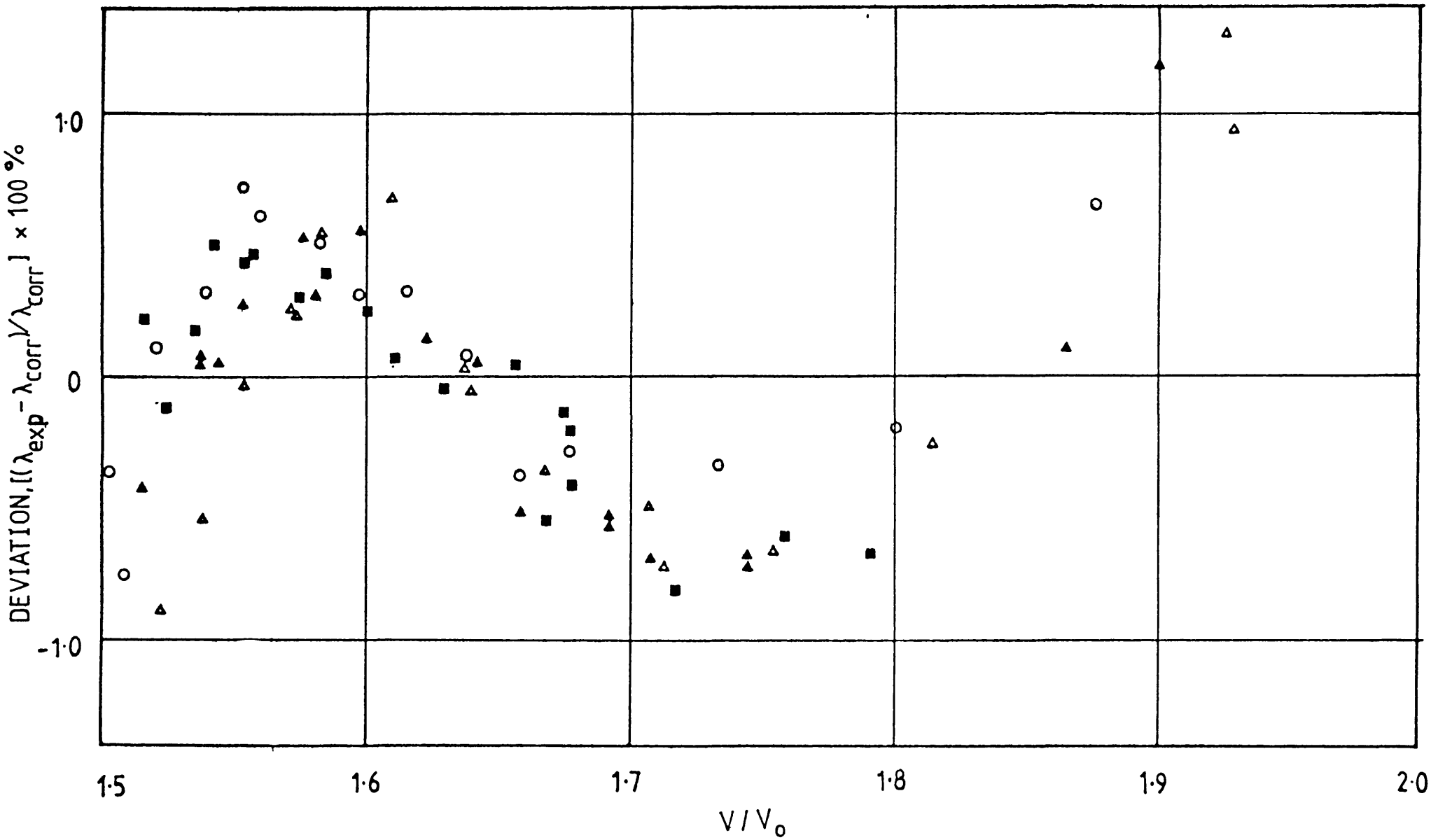

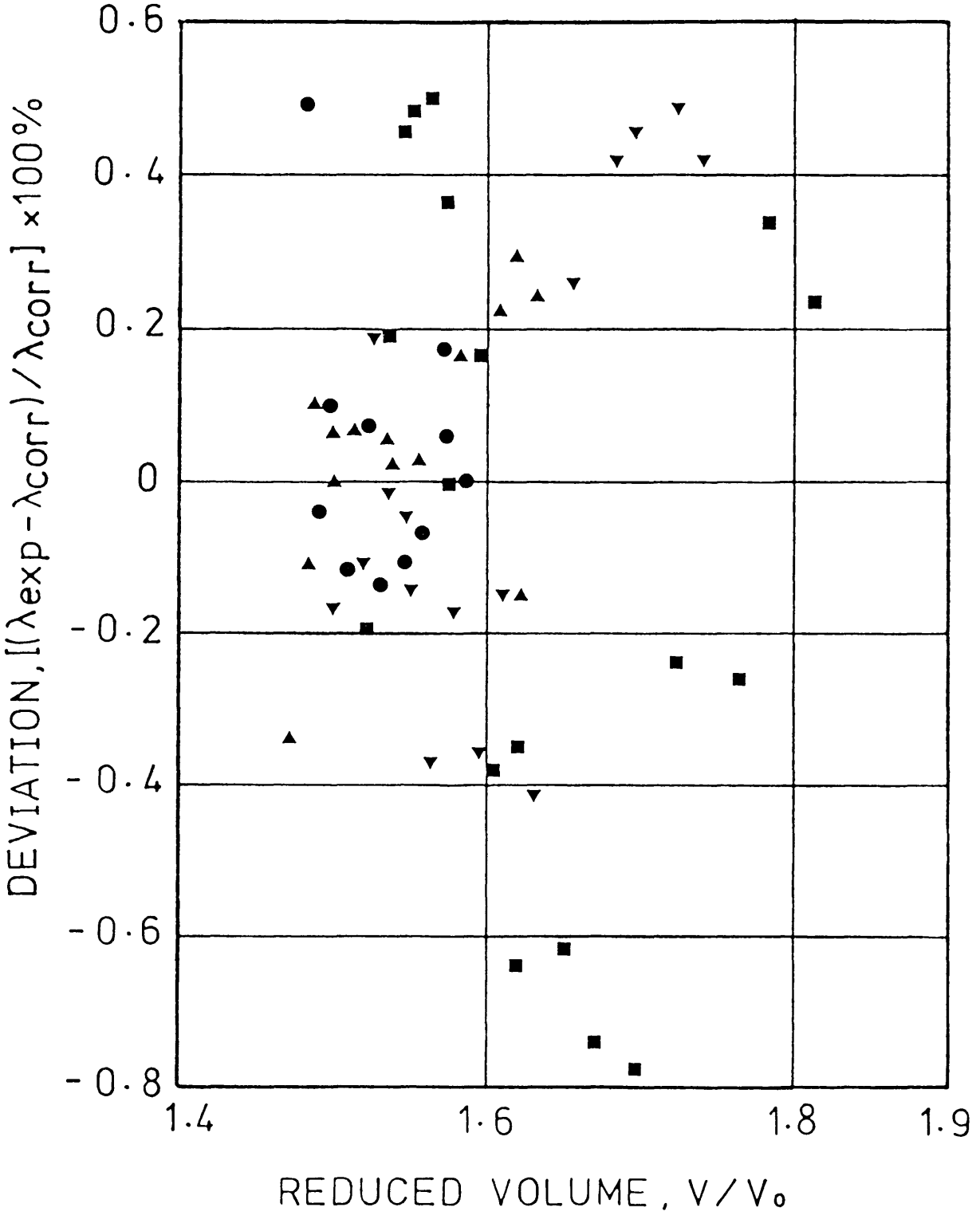

Fig. (6.23) Deviation of the experimental thermal conductivity data for benzene from the correlation of Eq. (6.5) and Table 6.2

● -37°C ; ▲ -47.5°C ; ▼ -71°C ; ■ -88°C

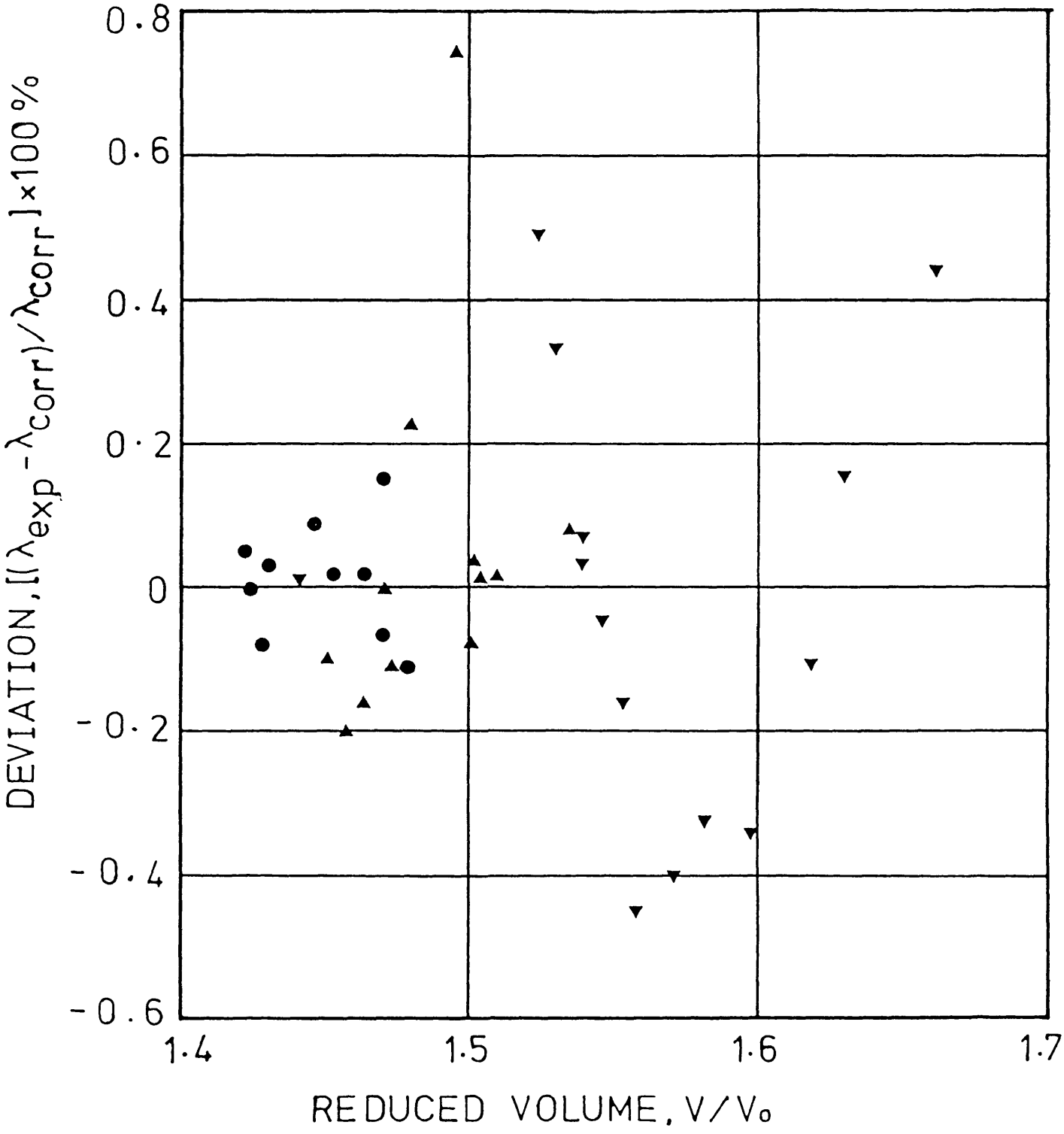

Fig. (6.24) Deviation of the experimental thermal conductivity data for cyclohexane from the correlation of Eq. (6.5) and Table 6.2

● -36 °C ; ▲ -51 °C ; ▼ -80 °C

certainty that these trends are real. More accurate density data are necessary before such an assertion could be made and its consequences investigated.

In any event, from a practical point of view the temperature independent correlation scheme has distinct advantages. This is because it allows the prediction of the density dependence of the thermal conductivity of a liquid along an isotherm merely from measurements of the value at one density. Thus it is possible to generate thermal conductivity data over a wider range of thermodynamic states than covered by direct measurements. Judged on the basis of the preceding comparison the precision of these predictions should be only slightly inferior to that of the direct measurements.

6.4.3 The universal correlation

In view of the fact that all the systems being studied can be correlated satisfactory on the basis of the rough hard sphere model, it is also worthwhile to examine the extent to which the (V/V_o) dependence of λ^* is conformal among all the fluids. Such an examination allows us to include those earlier measurements of the thermal conductivity of liquid alkanes, including propane [138], n-heptane [5], n-nonane and n-undecane [139], as well as n-tridecane [140], which have an accuracy commensurate with that of the present data. For n-heptane, n-nonane, n-undecane and n-tridecane the data lie in a similar range of thermodynamic states to that covered in the present work. However for propane the measurements extend over the wider temperature range from 112 K to 298 K although only for pressures up to 70 MPa. Taking all these hydrocarbons together we have a total of eleven hydrocarbons and an extremely wide range of thermodynamic states.

The curve of λ^* against log V for n-hexane at 307 K has been adopted as a reference, and we have sought to superimpose the corresponding plots for all the other fluids at all temperatures upon it, by shifts along the log V axis alone. Figure (6.25) shows the result of this procedure. The consistency between the curves is striking, particularly in view of the large temperature and density range now represented in the figure.

In order to quantify the agreement the entire body of data in Fig. (6.19) has been represented by the simple equation

$$\log \lambda^* = A - B \log(V/V_o^u) \qquad (6.7)$$

where A = 4.8991, and B = 2.2595, as obtained from a regression analysis. This equation is of the same form as those employed earlier, but the superscript 'u' on V_o is adopted to indicate that the basis for the selection of the characteristic volume is different from that which we employed in the previous two sections. The derived values of V_o^u are included in Table 6.3. The quoted values are, of course, all relative to the assumed value for n-hexane at 307 K and for this reason, they should not be endowed with too much physical significance. Nevertheless, the characteristic volume do show the expected trend with increasing molecular weight of the hydrocarbons. Figure (6.26) illustrates this trend of V_o^u for the normal alkanes with increasing

Fig. (6.25) The thermal conductivity ratio λ^* for liquid hydrocarbons as a function of reduced molar volume:

n-propane(138): ▧ - -161°C ; ▨ - -132°C ; ⊟ - -100°C ; ▥ - -77°C ; ⊞ - -46°C ; ⊠ - -13°C ; ⊡ - +25°C

n-hexane: ○ -34°C ; ● -48°C ; ◐ -72°C ; ◑ -87°C

n-heptane(5): ⊡ -35°C ; ⊠ -50°C ; ▨ -75°C

n-octane: △ -34°C ; ▽ -48°C ; ▲ -72°C ; ▼ -89°C

n-nonane(139): ◆ -35°C ; ◆ -50°C ; ◆ -75°C ; ◆ -90°C

n-undecane(139): ◈ -35°C ; ◆ -50°C ; ◇ -75°C

n-tridecane(140): + -35°C ; × -48°C ; ★ -73°C

2,3-dimethylbutane: ◒ -36°C ; ◓ -48°C ; ⊗ -72°C

2,2,4-trimethylpentane: □ -40°C ; ■ -48°C ; ▪ -64°C ; ▬ -78°C

benzene: ◩ -37°C ; ◪ -47.5°C ; ◧ -71°C ; ◧ -88°C

cyclohexane: ⊕ -36°C ; ⊙ -51°C ; ⊖ -80°C

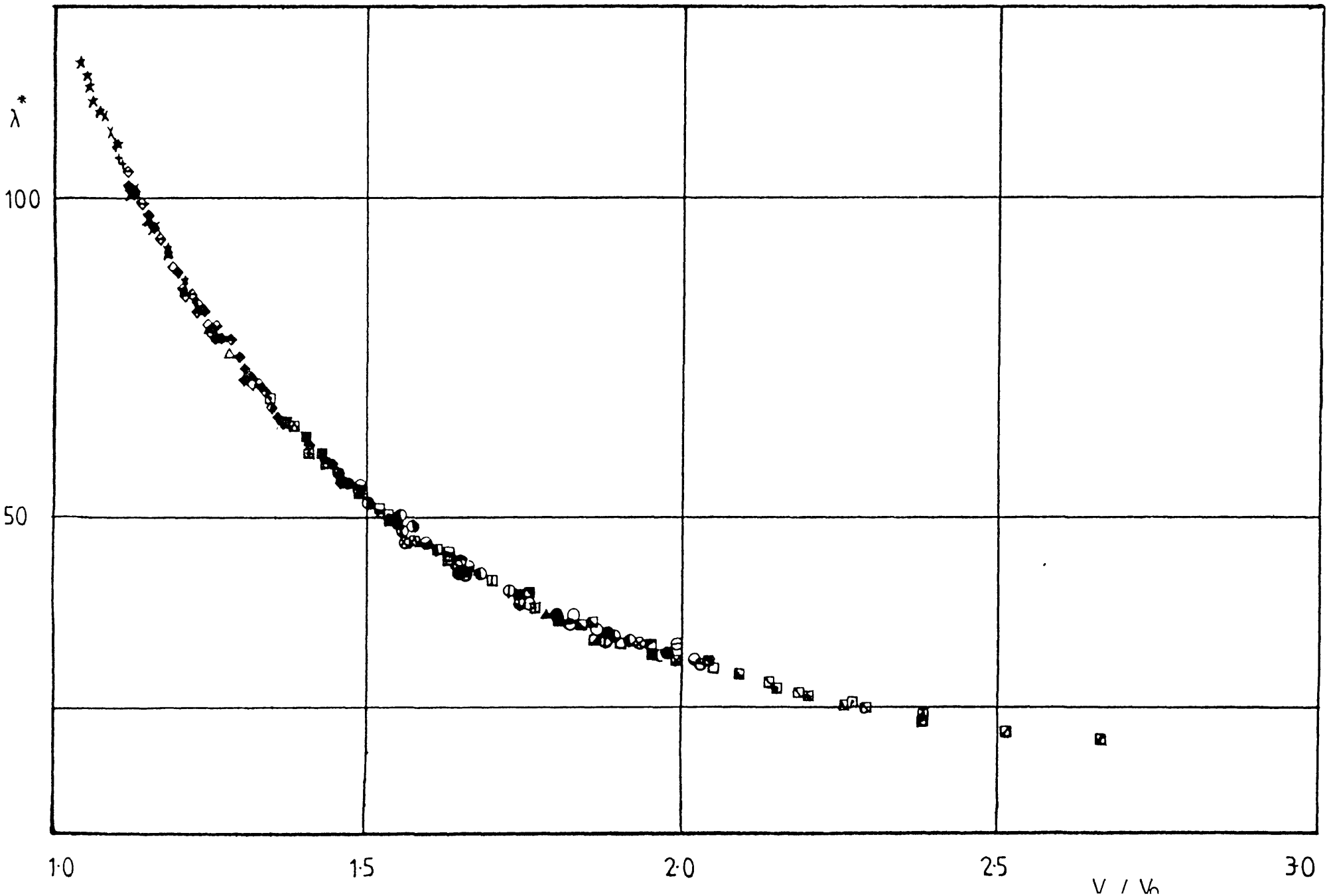
λ*
100
50
1·0
1·5
2·0
2·5
3·0
V / V6

Fig. (6.26) The characteristic volume (V_o^u) as a function of the number of carbon atoms of a series of normal alkanes

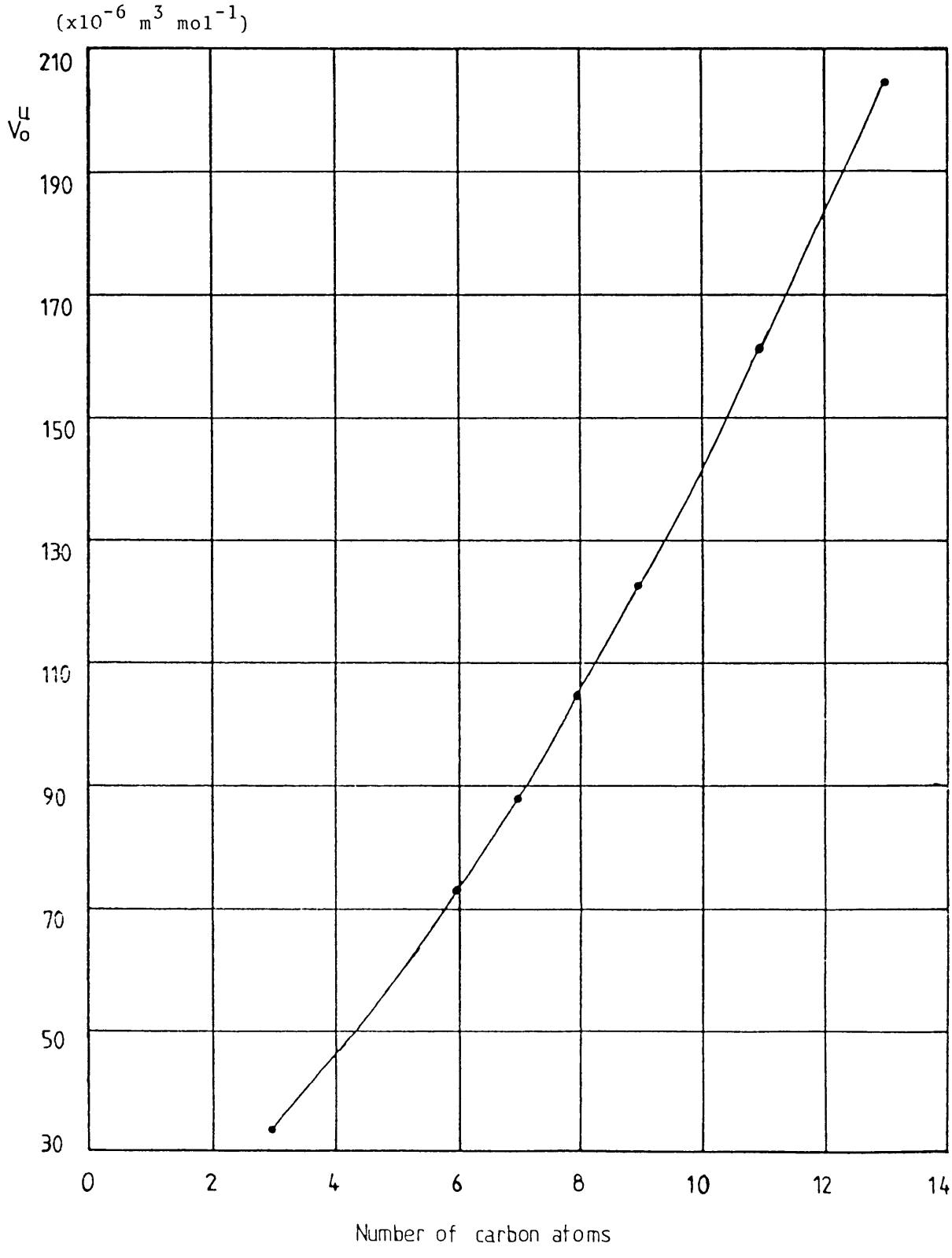

Fig. (6.27) Deviation of the experimental thermal conductivity data from the correlation of eq.(6.7) and Table 6.3:

n-propane(138): ⧅ - -161°C ; ⧄ - -132°C ; ⊟ - -100°C ; ⧈ - -77°C ; ⊞ - -46°C ; ⊠ - -13°C ; ⧇ - +25°C

n-hexane: ○ -34°C ; ● -48°C ; ◐ -72°C ; ◑ -87°C

n-heptane(5): ⧇ -35°C ; ⧆ -50°C ; ⧅ -75°C

n-octane: △ -34°C ; ▽ -48°C ; ▲ -72°C ; ▼ -89°C

n-nonane(139): ◈ -35°C ; ◈ -50°C ; ◈ -75°C ; ◈ -90°C

n-undecane(139): ◈ -35°C ; ◆ -50°C ; ◇ -75°C

n-tridecane(140): + -35°C ; × -48°C ; ★ -73°C

2,3-dimethylbutane: ⊖ -36°C ; ⊖ -48°C ; ⊗ -72°C

2,2,4-trimethylpentane: □ -40°C ; ■ -48°C ; ⧈ -64°C ; ⧈ -78°C

benzene: ⧈ -37°C ; ⧄ -47.5°C ; ⧅ -71°C ; ⧅ -88°C

cyclohexane: ⊕ -36°C ; ⊕ -51°C ; ⊖ -80°C

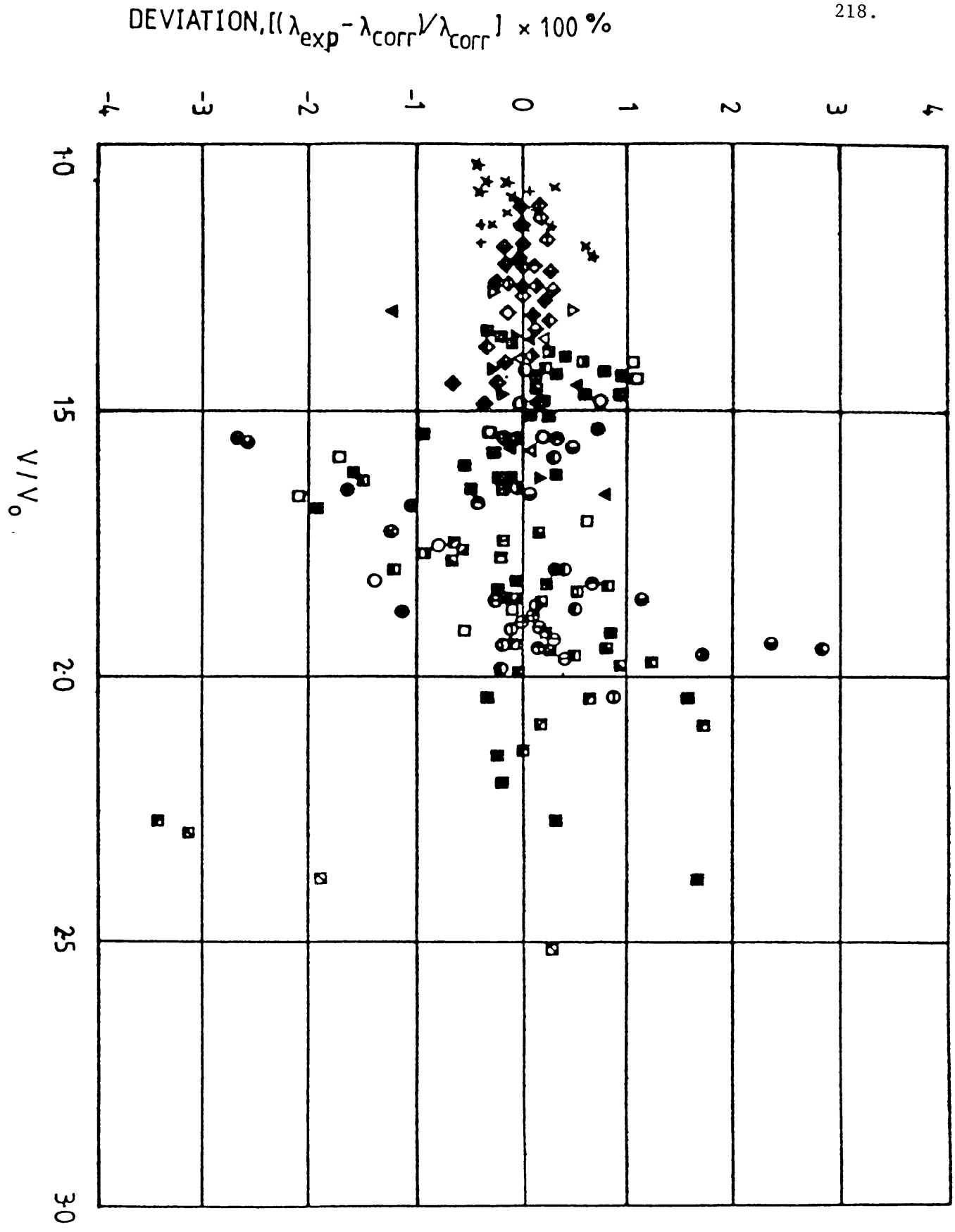
DEVIATION, $[(\lambda_{exp} - \lambda_{corr})/\lambda_{corr}] \times 100\ \%$
-4
-3
-2
-1
0
1
2
3
4
1·0
1·5
2·0
2·5
3·0
V/V_o

number of carbon atoms at one temperature (307 K).

Figure (6.27) displays the deviations of the experimental thermal conductivity from the correlation of Equation (6.7). The maximum deviation now amounts to as much as ± 4%, and the standard deviation is one of ± 0.68% for the entire set of experimental data, consisting of over 900 points.

The deviations therefore exceed the estimated uncertainty of the thermal conductivity and density and are slightly larger than the corresponding values when each liquid is treated independently. Nevertheless it is remarkable that a single equation should be capable of describing the thermal conductivity of liquids as diverse as propane and benzene with an accuracy of ± 4% over such a wide range of temperature and pressure. The near universality of the relationship of λ^* to (V/V_o) immediately suggests a reliable means of estimating the thermal conductivity of the liquids studied here, since all that is required is the characteristic volume V_o^u for the prescribed temperature. In the best case this could be deduced from a measurement of the thermal conductivity at one density at the temperature of interest. Failing this the value of V_o^u could be obtained by interpolation within or extrapolation outside of the range of the values given in Table 6.3. Figure (6.28) plots the values of V_o^u for each liquid as a function of temperature and reveals that such an interpolation is relatively straight forward. With some further loss of accuracy estimated values of V_o^u could also be obtained from the

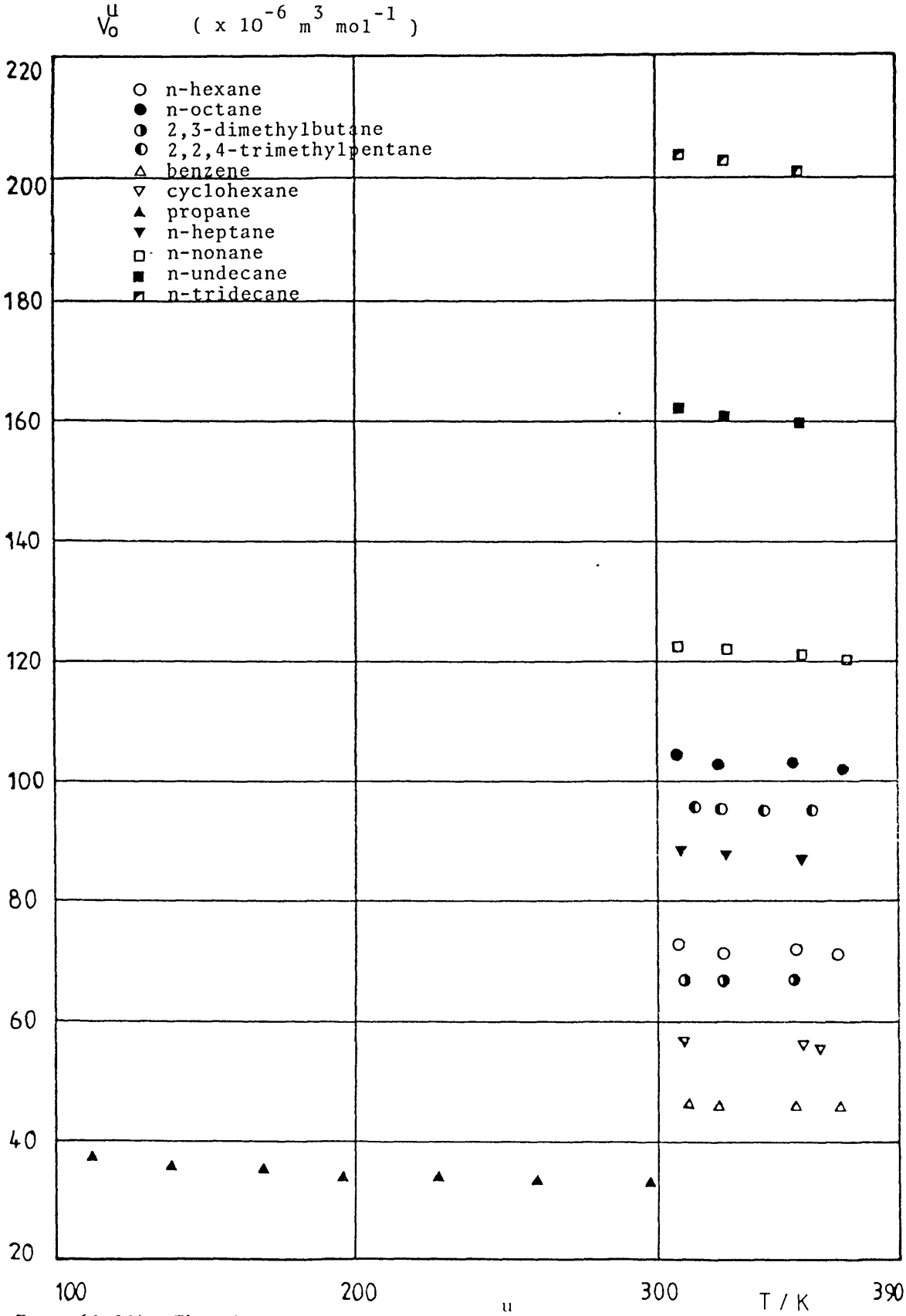

Fig. (6.28) The characteristic volume V_o^u for liquid hydrocarbons

viscosity for fluids whose thermal conductivity has not been measured in the same way as described in 6.2.1. The near universality of λ^* vs V/V_o for hydrocarbons therefore provides a powerful tool for the estimation of the thermal conductivity of such liquids. Obviously progressively more general and increasingly empirical schemes can be established on the basis of that employed here. An example would be to investigate the possibility of prediciting the thermal conductivity of members of a homologous series by making use of the regular dependence of the characteristic volume V_o on the number of carbon atoms. However, this investigation is considered beyond the scope of the present work.

From a more fundamental point of view the deviation plot in Fig (6.27) shows that the relationship of λ^* to (V/V_o) is not completely universal as indicated by the systematic trend of some of the deviations. Within the accuracy of the available data, particularly for the density these systematic deviations are only just significant. However, given more accurate density data, it would be interesting to examine these trends more closely in conjunction with a more advanced theory of transport in dense fluids.

Table 6.1

Coefficients of the Correlation of Equation (6.5) for Individual Isotherms and the Characteristic Volumes

Liquid	Temp (K)	a_o	a_1	V_o x10^6 m^3 mol^{-1}	Standard deviation
Hexane	307	4.9318	2.3312	72.64	0.34
	321	4.9427	2.3551	71.77	0.47
	345	4.8880	2.2394	71.24	0.47
	360	4.8619	2.1862	70.86	0.55
Octane	307	5.0665	2.2701	97.48	0.32
	321	5.0643	2.2651	96.51	0.19
	345	5.0764	2.2928	96.33	0.32
	362	5.0524	2.2382	95.59	0.58
2,3-dimethylbutane	309	4.8988	2.2684	67.15	0.21
	321	4.8687	2.2093	66.99	0.34
	345	4.7847	2.0474	66.62	0.39
2,2,4-trimethylepentane	313	5.1610	2.4696	89.06	0.22
	321	5.1265	2.3958	89.07	0.44
	337	5.1271	2.3998	89.07	0.52
	381	5.1097	2.3648	89.14	0.55
Benzene	310	4.3698	2.1753	57.67	0.17
	320.5	4.3502	2.1268	57.50	0.13
	344	4.3440	2.1111	57.11	0.23
	360.5	4.3699	2.1757	57.00	0.42
Cyclohexane	309	4.2622	2.2205	74.14	0.07
	324	4.2390	2.1579	73.84	0.23
	353	4.2599	2.2151	73.40	0.30

Table 6.2

Coefficients of the Correlation of Equation (6.5) for Individual Liquids

Liquid	a_o	a_1	Standard deviation
n-hexane	4.9120	2.2889	0.70
n-octane	5.0625	2.2607	0.41
2,3-dimethylbutane	4.8583	2.1899	0.79
2,2,4-trimethylpentane	5.1274	2.3995	0.50
Benzene	4.3586	2.1475	0.31
Cyclohexane	4.2556	2.2031	0.24

Table 6.3

The Characteristic Volumes, V_o^u, for the Correlation of Equation (6.7)

n-hexane

T(K)	307	321	345	360
$V_o^u \times 10^6$ m^3 mol^{-1}	72.64	71.74	71.18	70.79

n-octane

T(K)	307	321	345	362
$V_o^u \times 10^6$ m^3 mol^{-1}	104.76	103.69	103.49	102.70

2,3-dimethylbutane

T(K)	309	321	345
$V_o^u \times 10^6$ m^3 mol^{-1}	66.99	66.83	66.90

2,2,4-trimethylpentane

T(K)	313	321	337	351
$V_o^u \times 10^6$ m^3 mol^{-1}	95.67	95.75	95.61	95.62

benzene

T(K)	310	320.6	344	360.6
$V_o^u \times 10^6$ m^3 mol^{-1}	46.33	46.18	45.86	45.76

cyclohexane

T(K)	309	324	353
$V_o^u \times 10^6$ m^3 mol^{-1}	56.27	56.05	55.72

propane

T(K)	112	140	170	196	227	260	298
$V_o^u \times 10^6$ m^3 mol^{-1}	37.47	36.56	35.47	34.70	33.84	33.57	33.32

n-heptane

T(K)	308	323	348
$V_o^u \times 10^6$ m^3 mol^{-1}	87.88	87.52	86.84

n-nonane

T(K)	308	323	348	363
$V_o^u \times 10^6$ m^3 mol^{-1}	122.52	122.09	121.36	120.79

n-undecane

T(K)	308	323	348
$V_o^u \times 10^6$ m^3 mol^{-1}	161.57	160.96	159.71

n-tridecane

T(K)	308	321	348
$V_o^u \times 10^6$ m^3 mol^{-1}	204.18	202.83	200.97

CHAPTER 7

SUGGESTIONS FOR FUTURE WORK

A transient hot-wire instrument for the accurate measurement of the thermal conductivity of liquids has been further refined. In the present work a complete and analytic solution to the simultaneous radiation and conduction problem in this instrument has been developed. It is believed that the measurements obtained using the present instrument are the most accurate available at present. Thus it is recommended that further experimental studies of the thermal conductivity of liquids should be undertaken to enable the establishment of a comprehensive database for this property. In particular, the high accuracy of the present experimental results means that they should be useful in the establishment of a standard for the calibration of other thermal conductivity instruments.

Specific recommendations concerning the possibility of using this type of instrument to measure the thermal diffusivity and heat capacity of fluids have been made in appendix 1. It is envisaged that, with the improvements suggested here some useful results can be obtained relatively easily together with high quality thermal conductivity data.

The theroretical studies in Chapter Six (6.4.2) revealed that there is a need for experimental data for the thermal conductivity over a wider temperature range and for more accurate density data. The former can be implemented most easily in the present instrument by an improvement of the temperature control system. Specifically, a higher

quality oil and a better insulated oil bath can raise the upper temperature limit considerably. The determination of liquid phase densities at high pressures with an accuracy of better than 0.1% is however a more difficult problem.

With regard to the development of the theories of the liquid state, the present experimental data would provide a rigorous test for any models and theories of dense polyatomic fluids which are proposed in the future and which will supersede the rough hard sphere theory. On the one hand, it is certain that the increasing use of molecular dynamics simulations will play a major part in these developments. On the other hand it cannot be overemphasised that valuable information can be extracted from the use of appropriate models of the molecular transport processes. Thus it would be worthwhile to pursue further investigations in both of these respects along with the development of rigorous statistical mechanical theories.

Already it has been shown that a reliable correlation scheme can be established on the basis of a very simple rough hard sphere model. Undoubtedly more realistic models and rigorous theories will become available. An extension of these ideas into the treatment of a wider range of thermodynamic conditions and substances clearly seems possible. In other words we can foresee future techniques helping us to predict transport property data of dense polyatomic fluids for the design of chemical processes with the same degree of confidence which we now have when dealing with dilute monatomic fluids.

A P P E N D I X 1

THE EXPERIMENTAL DETERMINATION OF THE THERMAL DIFFUSIVITY OF LIQUIDS USING A TRANSIENT HOT-WIRE APPARATUS

Introduction

In the last decade, the transient hot-wire technique has become established as an accurate method for the determination of the thermal conductivity of liquids and gases (see Chapter 2).

Because the thermal diffusivity of the fluid also enters the working equation of the method, it is possible, at least in principle, to measure this quantity at the same time. The combination of the results of measurements of the two quantities with density data (ρ) then permits the heat capacity of the fluid at constant pressure (C_p) to be evaluated. Measurements of this quantity by the transient hot-wire method have indeed already been reported [157]. It is the purpose of this Appendix to examine the measurement more closely in order to establish its likely precision.

Applying an analysis similar to that described in Chapter 2, the working equation for the measurement of the thermal diffusivity can be written as:

$$\mathcal{K}_o = \frac{\lambda_o}{\rho_o C_{p_o}} = \frac{a^2 c}{4} \exp\left\{ \frac{\Delta T_w(t=1s) + \delta T_1(t=1s) + \delta T_2(t=1s)}{S} \right\} \quad \text{(A1.1)}$$

where the subscript o denotes equilibrium condition (i.e. before initiation of the heat flux). ΔT_w is the measured temperature rise of the wire, and δT_1 and δT_2 are small corrections which are discussed in Chapter 2. a is the radius of the wire and $c = \exp(\gamma) = 1.78107$.

S is the slope of the linear regression line between ΔT_{id} and $\ell n\ t$.

$$S = \frac{d(\Delta T_{id})}{d\ \ell n\ t} \tag{A1.2}$$

or from equation (2.9)

$$S = \frac{q}{4\pi\lambda(T_r,\ \rho_r)} \tag{A1.3}$$

In equation A1.1, a time t = 1 s has been chosen as the (arbitrary) point of evaluation of the temperature rise since at this time all but the corrections δT_1 and δT_2 are entirely negligible and even there the corrections do not amount to more than ±0.3% of the temperature rise.

Error Analysis

In a transient hot-wire instrument, the temperature rise of the wire is inferred from the resistance change of the wire by means of a suitable calibration of the resistance-temperature characteristics of the wire (see §3.4). The temperature rise is then calculated from the equation (see §3.4.1)

$$\Delta T_w = \frac{(R_\ell - R_s) - (R_{\ell(o)} - R_{s(o)})}{\alpha(T_o,\ P)\ [R_{\ell(o)} - R_{s(o)}]} \tag{A1.4}$$

in which R_ℓ is the resistance of the long wire in the system and R_s is the resistance of the short wire employed to compensate for unaccounted effects at the ends of the wire (see §3.4.1). The quantity $(T_o,\ P)$ is a pseudo-linear temperature coefficient of resistance (see §3.4.1).

For the automatic bridge employed in our measurements, shown schematically in Fig. 3.4, the resistance difference $R_\ell - R_s$ is determined directly from the value of the fixed resistors in the bridge according to the equation (see §3.4.1)

$$R_\ell - R_s = (C_1 \cdot R_2 - R_1)\left(\frac{Z-1}{Z-C_1}\right) \tag{A1.5}$$

where

$$Z = \frac{R_\ell}{R_s} \tag{A1.6}$$

and C_1 is given by equation (3.11) and can be written in the form

$$C_1 = 1 - \frac{R_1 - RS}{R + RS + R'(1 + \frac{RS}{R})} \tag{A1.7}$$

with R_1, R_2, RS, R and R' denoting bridge resistors in Fig. 3.4 and equation (3.14). Throughout all of our measurements the values of R_1, R and R' remain fixed. During the course of any one transient measurement the times at which a sequence of bridge balance occur for a series of preset values of C_1 or, equivalently, R_s, are determined. The bridge is designed so that C_1 is exactly unity when measurements are carried out under equilibrium conditions and when the transient heating has proceeded for about 1 second. Consequently, neither C_1 nor Z contribute to the evaluation of $R_\ell - R_s$ at either of these extremes. Furthermore, the value of C_1 departs very little from unity at any time [58, 59]. Thus if R_{2f} denotes the value of R_2 employed for a transient measurement of 1 s and R_{2i} denotes its value for the equilibrium measurement the equation for the evaluation of the temperature rise of the wire may, to a very good approximation, be written as

$$\Delta T_w = \frac{C_1 R_{2f} - R_{2i}}{\alpha(T_o, P)(R_{2i} - R_1)} \tag{A1.8}$$

which becomes exact when $C_1 = 1$ at the end of a measurement. Ignoring the small difference between ΔT_{id} and ΔT_w for the purpose of the present error analysis we find that

$$\mathcal{K}_o = \frac{a^2 c}{4} \exp\left\{(1 - \frac{R_{2i}}{R_{2f}})\left(\frac{d\, C_1}{d\, \ell n\, t}\right)^{-1}\right\} \tag{A1.9}$$

The error in the quantity $(dC_1/d\ \ell n\ t)^{-1}$ is made negligible in the design of the bridge [58], so that the only significant error in the determination of the thermal diffusivity arises from errors in the resistance R_2 and the radius of the wire a. In particular, errors in the remainder of the bridge resistors and in the temperature coefficient of resistance $\alpha(T_o)$ do not propagate to the thermal diffusivity.

However, the thermal diffusivity is very sensitive to the values of both a and R_2. Thus differentiating equation (A1.9) and inserting the values of the various parameters characteristic of our instrument we find

$$\frac{d\mathcal{K}_o}{\mathcal{K}_o} = 5\ d\ R_2 \qquad (A.10)$$

where 5 has unit of 1/resistance and

$$\frac{d\mathcal{K}_o}{\mathcal{K}_o} = 2\ \frac{da}{a} \qquad (A.11)$$

The first of these results (A1.10) shows that an uncertainty of just 0.02 ohm in the value of R_2, which is typically 400 ohm (tolerance 0.005%) produces a 10% error in the measured thermal diffusivity. Because this is strictly a random error, there is nothing that can be done to reduce the contribution to the error in $\mathcal{K}_o$ and hence C_p apart from improving the precision of R_2.

The error in the radius a is also significant because the hot-wire employed in our measurements has a radius of a $\hat{\sim}$ 3.5 μm and it is therefore difficult to achieve a high precision in its measurement and to ensure uniformity along the length of the wire. To some extent this latter difficulty could be overcome by means of a calibration with respect to a fluid of known thermal diffusivity since the effect is systematic.

Results

Using equation (A1.1) the thermal diffusivity has been calculated from experimental data on a number of liquids in the temperature range 35 - 90°C and pressure range 0.1 to 650 MPa obtained with the present instrument. Subsequently the heat capacity of these liquids are calculated as explained earlier.

Figure (A1) illustrates a plot of the heat capacity of n-hexane as a function of pressure. It can be seen that there is a large scatter in the experimental data for the heat capacity determined in this fashion, as has been found by other workers [157]. This observation confirms the result of the analysis of the previous section, that the random error in R_2 significantly affects the accuracy of the thermal diffusivity. It is clear that the present instrument is not suitable for the determination of the thermal diffusivity of liquids. Furthermore, resistors of a higher precision than are normally available would be necessary to design an instrument for this purpose. Evaluations of this type have been performed for all the liquids studied in this work and the results are similar to those shown for n-hexane. That is, the most that can be said is that the heat capacity of the liquids does not vary by more than ±20% over the range of pressure 0 - 650 MPa. The poor precision of the measurements makes any more definite statements impossible, so the data are not included in this thesis.

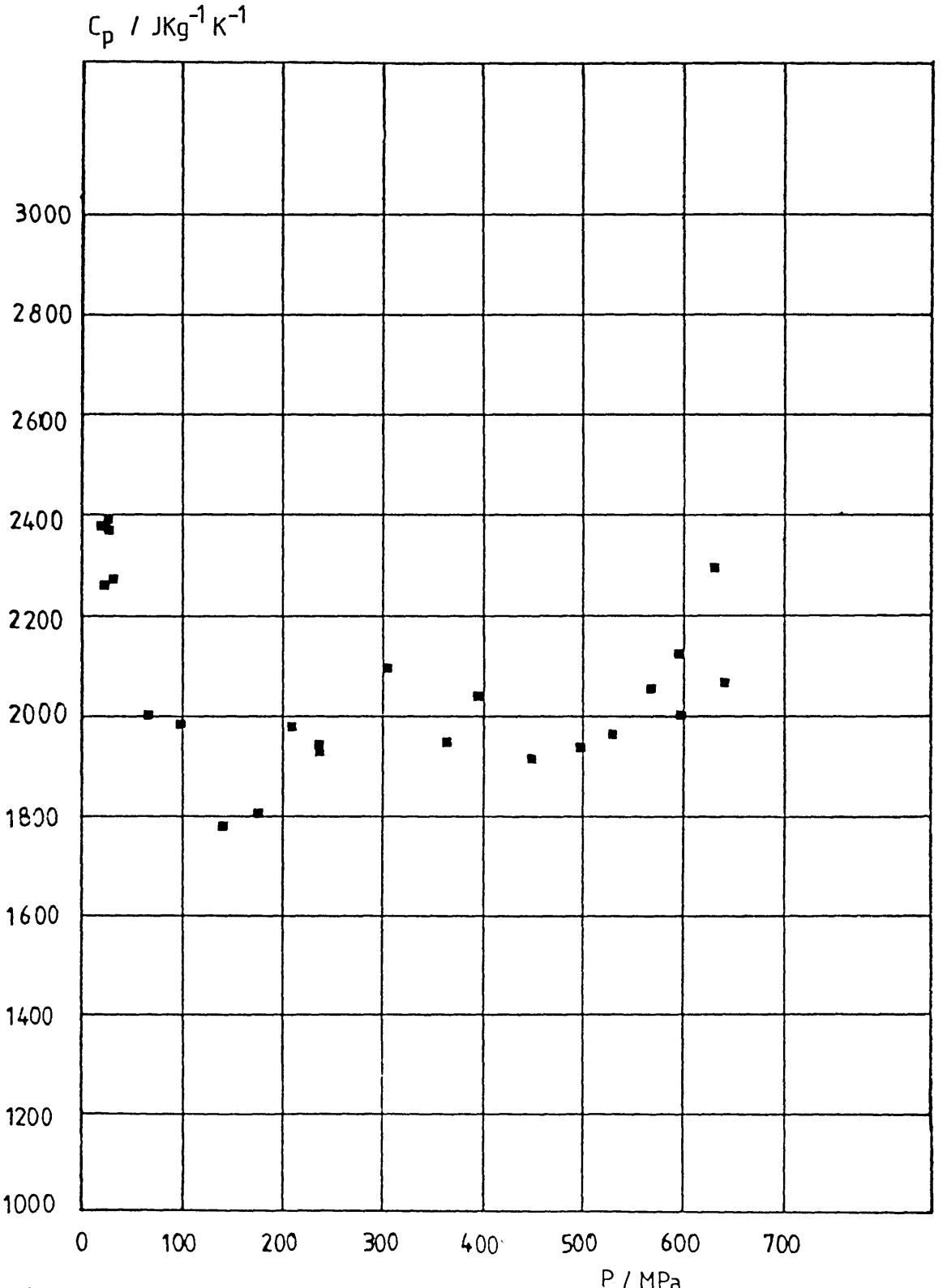

Fig. A1(a) Heat capacity of n-hexane as a function of pressure T=34°C

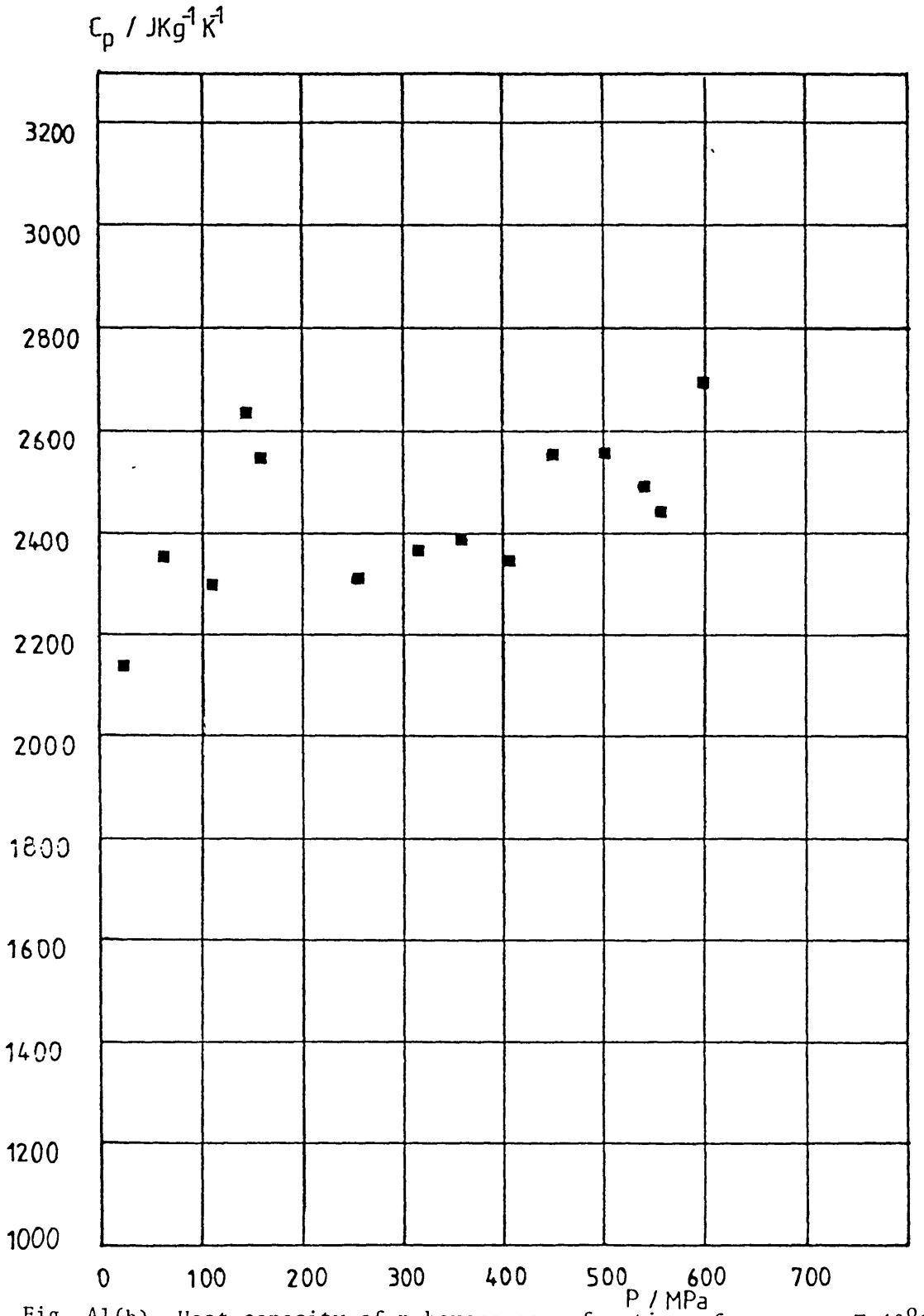

Fig. A1(b) Heat capacity of n-hexane as a function of pressure T=48°C

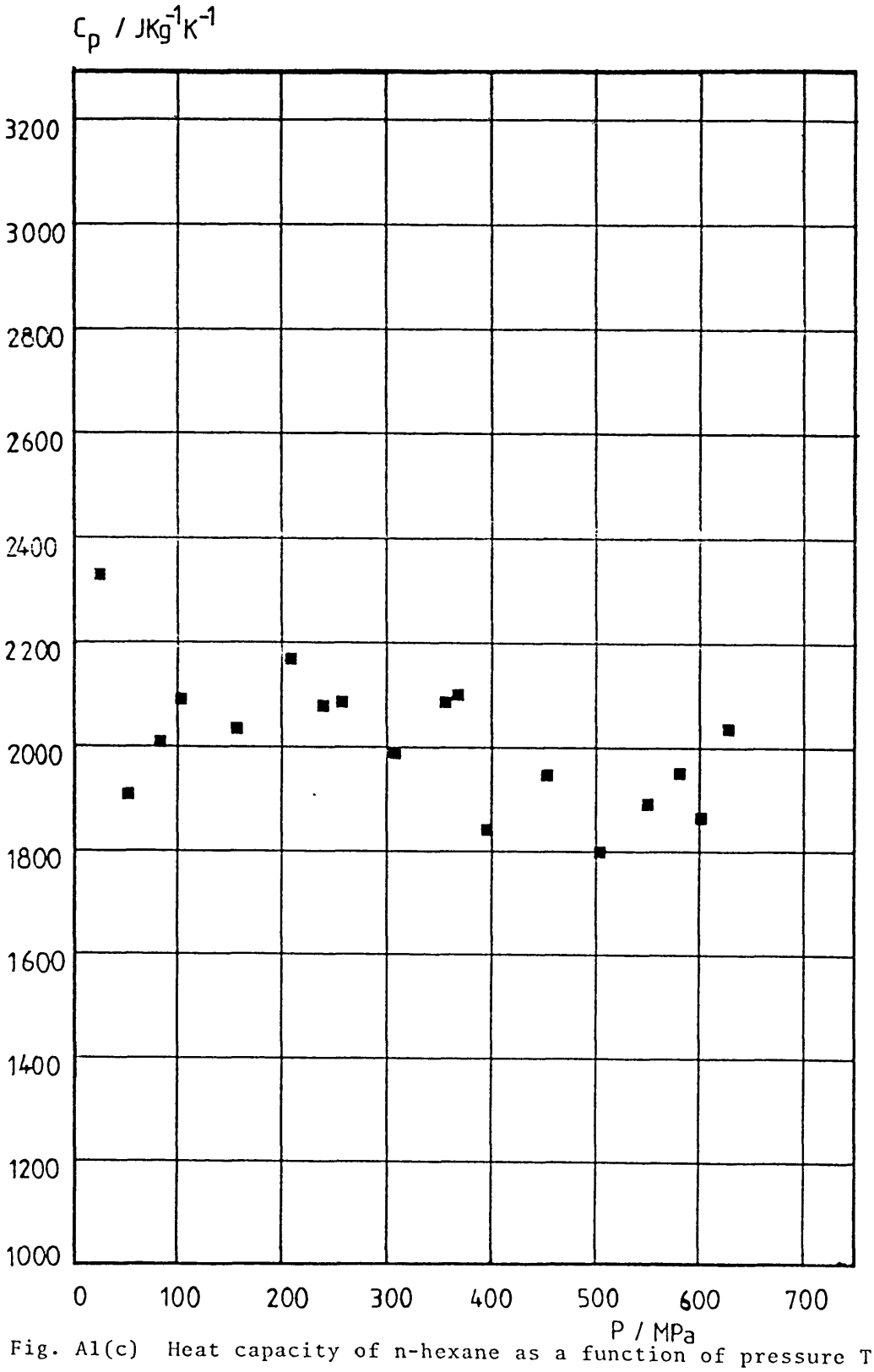

Fig. A1(c) Heat capacity of n-hexane as a function of pressure T=72°C

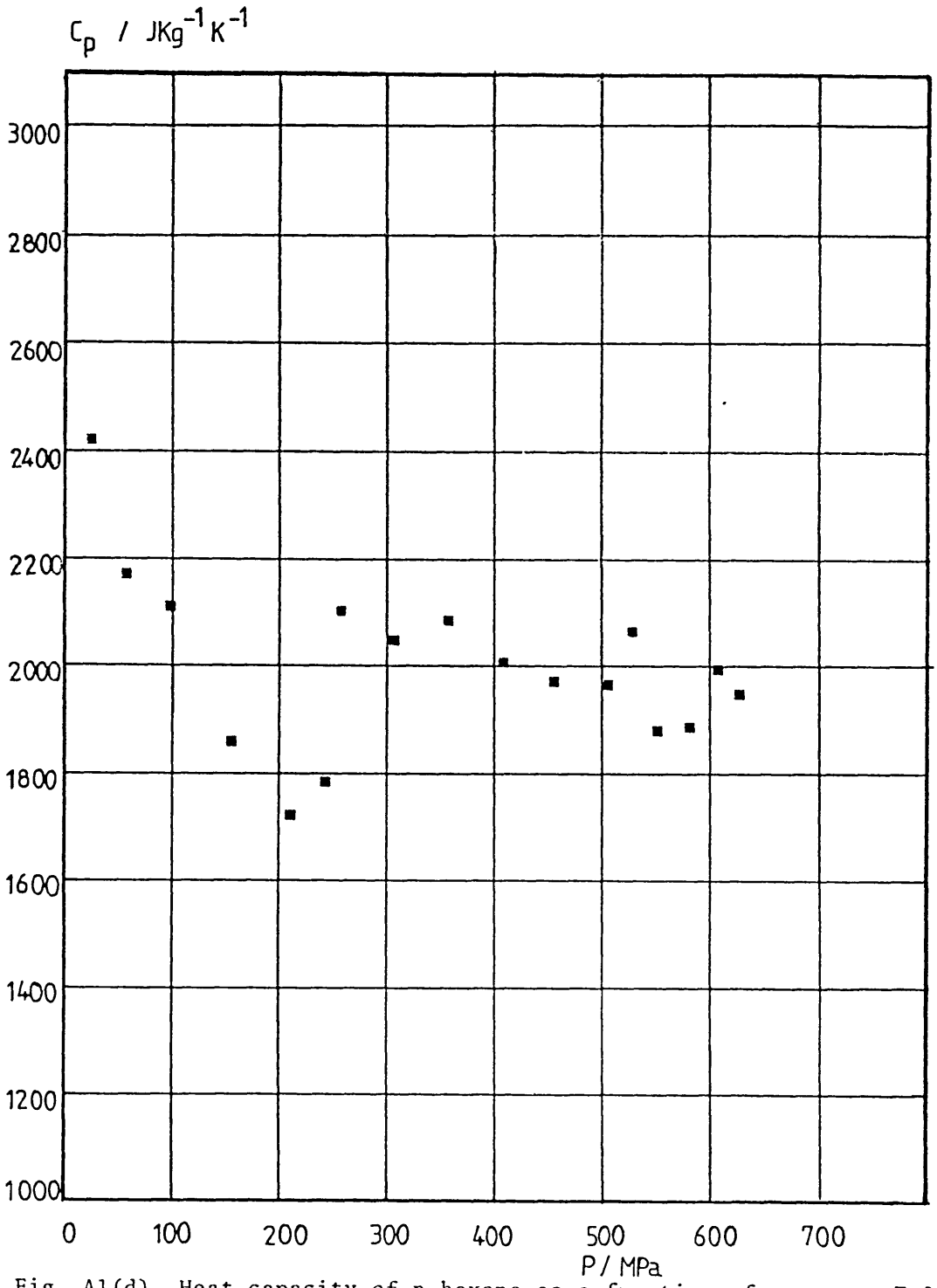

Fig. A1(d) Heat capacity of n-hexane as a function of pressure T=87°C

A P P E N D I X 2

A2.1 Gauge Calibration

The gauges used for measuring the pressure within the autoclave were calibrated against a dead weight tester. The dead weight tester has an accuracy of better than 1 MPa at 700 MPa [158], and has been calibrated by the National Physical Laboratory. This calibration can be found elsewhere [27].

Table A(2.1) - Gauge Calibration

Temperature (°C)	Gauge Reading (Bar)	Mass (kg)	Absolute Pressure (MPa)
23·3	670	22·31585	67·81088
23·3	960	31·97359	97·14940
23·3	1250	41·61469	126·43226
23·3	1536	51·28094	155·78669
23·3	1826	61·00004	185·29643
23·3	2112	70·61094	214·47269
23·3	2407	80·23314	243·67766
23·3	2701	89·89324	272·99267
23·3	2998	99·54039	302·26298
23·3	3280	109·16680	331·46666
23·3	3580	118·78980	360·65312
23·3	3896	128·45180	389·95101
23·3	4193	138·06325	419·09226
23·3	4468	147·70490	448·32294
23·3	4773	157·35160	477·55990
23·3	5070	167·08395	507·05277
23·3	5366	176·70065	536·19056
23·3	5635	186·36505	565·47059
23·3	5950	194·17085	589·09997

The calibration of the gauge used in the pressure system is given in Table A(2.1) and the pressure inside the autoclave is determined from the gauge reading by interpolating the calibration data.

A2.2 The Physical Properties of the Liquids Investigated

The density of n-hexane, n-octane, 2,2,4-trimethylpentane and benzene have been taken from the measurement of Dymond et al. [137, 159-161] and are calculated using the secant bulk modulus equation:

$$\overline{K} = K_o + K_1 P + K_2 P^2 \qquad (A2.1)$$

where the constants K_i are given in Table A2.2 and $\overline{K}$ is defined by

$$\overline{K} = P\rho/(\rho-\rho_o)$$

where ρ_o is the density at atmospheric pressure. The density at the required pressures has been calculated for all the isotherms for which the coefficients have been given. A quadratic interpolation between these isotherms yields the density at the required temperature.

It is estimated that the measurements in Table A2.2 are accurate to within ±0.2%, and the interpolation introduces errors of no more than ±0.1% in density. Thus the overall uncertainty is estimated to be ±0.3%.

For cyclohexane the combined results of two investigations by Isdale and his collaborators were employed [161, 162]. The accuracy in the reported densities is between ±0.1% and ±0.2%. Tables A2.3 and A2.4 list the densities obtained from those sources.

Table A2.2 - Values of coefficients in equation (A2.1) for secant bulk modulus for n-hexane, n-octane, 2,2,4-trimethylpentane and benzene

Liquid	Temperature (°C)	k_o (Pa) x 10^9	k_1	$-k_2$ (Pa^{-1}) x 10^{-9}
n-hexane	25	0·6682	4·156	1·580
	50	0·5312	4·016	1·442
	75	0·4548	3·636	1·156
	100	0·3324	3·731	1·636
n-octane	25	0·7847	4·846	2·448
	50	0·6495	4·776	2·548
	75	0·5277	4·647	2·587
2,2,4-trimethylpentane	25	0·68821	4·4989	1·7645
	50	0·57396	4·3028	1·7295
	75	0·45967	4·1713	1·7148
	100	0·36293	4·0580	1·8363
benzene	25	1·0351	5·876	9·450
	50	0·8578	5·313	5·290
	75	0·6993	4·785	3·046
	100	0·5325	5·022	3·674

Table A2.3 - Density of cyclohexane [161]

T (°C)	P (MPa)	ρ (kg m^{-3})
25	0·1	773·8
	10·0	781·8
	20·0	789·2
75	0·1	725·9
	10·0	737·6
	20·0	747·8
	50·0	772·0
	100·0	802·0

Table A2.4 - Density of cyclohexane [162]

T (°C)	Density (kg m^{-3})								
	P (MPa)								
	0·1	2.6	5·1	7·6	10·1	12·6	15·1	17·6	20·1
25	773·8	775·9	778·0	780·0	781·9	783·9	785·7	787·5	789·3
50	750·3	752·9	755·4	757·8	760·1	762·4	764·6	766·8	768·8
75	725·9	729·0	732·1	735·0	737·7	740·4	743·0	745·5	747·9
95	705·9	709·6	713·1	716·4	719·6	722·6	725·5	728·4	731·1

For 2,3-dimethylbutane, the measurements by Bridgman [163] were used. The density is estimated to have an uncertainty of ±0·3% over the pressure range of interest. Table A2.5 lists these data. The experimental data for cyclohexane and 2,3-dimethylbutane have been fitted to cubic polynomials in pressure for each isotherm. Quadratic interpolations between isotherms have been carried out to obtain densities at the required temperature. The total uncertainty in the data is estimated to be ±0·4%.

Table A2.5 - Density of 2,3-dimethylbutane

Pressure (bar)	Density (kg m^{-3})		
	0°C	50°C	95°C
0	680·8	635·0	592·2
1000	744·3	716·4	691·8
2000	783·0	759·8	740·2
3000	810·9	788·6	770·5
4000	832·3	812·1	795·1
5000	850·6	831·7	816·3
6000	866·7	848·0	834·1
7000	-	863·8	850·1

The density data for toluene at high pressure are so scarce that it is not possible to use them to examine the density dependence of the thermal conductivity. However, density data are still required for the application of small corrections in the reduction of the thermal conductivity data. For this purpose the density has been estimated using the limited data available along one isotherm at 60°C [164]

P (atm)	V(P, T)/V(1 atm, T)
1810	·885
2930	·853
4400	·824

and the tabulated density along the saturation line [165]. Assuming that the pressure dependence of the density is the same at all temperatures and that the value at the saturation vapour pressure is the same as that at atmospheric pressure, this is sufficient information for the estimation. The errors in the density incurred by this process may be as large as 5%, but this is not significant to the evaluation of small corrections.

The specific heat capacities of the liquids are also required for the small corrections of the experimental data (see §2.5). For n-hexane, n-octane, benzene, cyclohexane and toluene, these values have been taken from the compilation of Vargaftik [165]. For 2,3-dimethylbutane and 2,2,4-trimethylpentane, the tabulations of Shaw [166] have been used.

A2.3 The Physical, Electrical, and Mechanical Properties of Platinum

Table A2.6 contains the physical, electrical and mechanical properties of the 7 μm platinum wire which was used as a heat source in the transient hot-wire measurement cell.

λ	=	67·05 W/m/K
ρ	=	2137 kg m^{-3}
C_p	=	131·3 J kg^{-1} K^{-1}
ν	=	Poisson's ratio $\sim$ 0·35
ε_{2s}	=	$\frac{1}{R}\frac{\partial R}{\partial s}$ = 2·77 x 10^{-7} MPa^{-1}
ε_p	=	$\frac{1}{R}\frac{\partial R}{\partial p}$ = 1·6 x 10^{-6} MPa^{-1}
S_y	=	yield stress $\sim$ 150 MPa^{-1}

Table A2.6 - Physical, electrical and mechanical properties of platinum

A P P E N D I X 3

RESULTS OF DAHLER'S ROUGH HARD SPHERE THEORY FOR VISCOSITY AND THERMAL CONDUCTIVITY

An outline of the moment method

An n^{th} order moment tensor of the distribution function may be defined

$$S^{(n)}_{ijk} = \int c^{(n)}_{ijk} \ldots\ldots f(\underline{r},\underline{c},t)\, d\underline{c}$$

where $\underline{r}$ is the position vector, $\underline{c}$ the velocity vector and t the time. The quantity

$$c^{(n)}_{ijk} = c_i c_j c_k \ldots\ldots$$

is a tensor of order n formed from the components of the velocity $\underline{c}$. The zero moment is the number density. The first moment is the macroscopic flux nc_o. Higher moments are related to the temperature, pressure tensor and energy flux vector. If the Boltzmann equation(or other kinetic equations) is multiplied sucessively by each of the $c^{(n)}$ and integrated over the velocities, we obtained successive equation for the moments. To solve the moment equations, a trial function is set up in which a number (v) of arbitrary parameters are included. These parameters may be written in terms of the first v moments. The remaining moments may then be written in terms of lower moments. The first v equations of the set of moment equation are thenassumed to describe the time variation of the parameters and consequently the behaviour of the fluid. Thus from these equations the transport coefficients describing the behaviour of the fluid can be identified.

The application of this method to the derivation of kinetic theories can be found elsewhere [129,130]. In this appendix we concentrated on analyzing the results derived for the transprot properties of a dense rough hard sphere fluid [130]. The aim is to cast these results into a form which can be used directly for the interpretation and correlation of experimental data.

Viscosity Coefficient

From Eq. (5.50) and (5.51)

$$\eta_{RHS,D} = \eta^{(k)}\left\{1 + \frac{5\chi+2}{5(\chi+1)} b n g\right\}^2 + \frac{1}{10}\rho\sigma\left(\frac{kT}{\pi m}\right)^{1/2} b n g \frac{(7\chi+4)}{(\chi+1)} \qquad (A\ 3.1)$$

where Pidduck's approximation is given by

$$\eta^{(k)} = \frac{15}{8\sigma^2 g}\left(\frac{m k T}{\pi}\right)^{1/2} \frac{(\chi+1)^2}{(13\chi+6)} \qquad (A\ 3.2)$$

By defining

$$H^0 = \frac{5}{16\sigma^2}\left(\frac{m k T}{\pi}\right)^{1/2} \qquad (A\ 3.3)$$

we can rewrite equation A3.2 in the form

$$\eta^{(k)} = H^0 \frac{6(\chi+1)^2}{g(13\chi+6)} \qquad (A\ 3.4)$$

Also

$$\rho\sigma\left(\frac{kT}{\pi m}\right)^{1/2} = n\sigma^3 \frac{1}{\sigma^2}\left(\frac{m k T}{\pi}\right)^{1/2}$$

$$= \frac{3}{2\pi} \frac{b}{V} \frac{1}{\sigma^2} \left(\frac{m k T}{\pi} \right)^{1/2}$$

$$= \frac{32}{15\pi} \frac{b}{V} H^0 \qquad (A\ 3.5)$$

where b is given by Eq.(5.17). Hence the ratio of $\eta_{RHS,D}$ to H^0 is

$$\frac{\eta_{RHS,D}}{H^0} = \frac{6(\chi+1)^2}{g(13\chi+6)} \left[1 + \frac{5\chi+2}{5(\chi+1)} bng \right]^2 + \frac{12}{25\pi} \frac{b}{V} bng \frac{(7\chi+4)}{(\chi+1)} \qquad (A\ 3.6)$$

Also from Eq. (5.17)

$$bn = \frac{2}{3} \pi \sqrt{2} \frac{V_c}{V} \equiv \frac{b}{V} = f\left(\frac{V}{V_c}\right) \qquad (A\ 3.7)$$

and from Equations (5.21) and (5.23)

$$g = f\left(\frac{V}{V_c}\right) \qquad (A\ 3.8)$$

so that we can express Eq. A3.6 as

$$\frac{\eta_{RHS,D}}{H^0} = f_1\left(\frac{V}{V_c}, \chi\right) \qquad (A\ 3.9)$$

Simplifying Eq. A3.6 by grouping powers of (b/V)

$$\frac{\eta_{RHS,D}}{H^0} = \frac{6(\chi+1)^2}{g(13\chi+6)} + \frac{6(\chi+1)^2}{13\chi+6} \frac{2(5\chi+2)}{5(\chi+1)} \frac{b}{V} + \left\{ \frac{6(\chi+1)^2}{(13\chi+6)} \times \left[\frac{5\chi+2}{5(\chi+1)} \right]^2 + \frac{12}{25\pi} \frac{(7\chi+4)}{(\chi+1)} \right\} \times \left(\frac{b}{V}\right)^2 g \qquad (A\ 3.10)$$

When K = 0,

$$\frac{\eta_{RHS,D}}{H^0} = \frac{1}{g} + 0.8\,\frac{b}{V} + 0.771\left(\frac{b}{V}\right)^2 g \qquad (A\ 3.11)$$

Thermal Conductivity

The thermal conductivity for a rough hard sphere fluid is given by Eqn's (5.52) to (5.54). To determine the coefficients λ_k^t, λ_k^r and β, the determinants of the matrices given by Eqn's (5.56) to (5.59) have been obtained. The results are:

$$\lambda_k^t = \frac{\left\{-\left[\frac{kp}{m}d^2\right]\times\left[-\frac{64}{9}\left(5+\frac{5k+3}{k+1}bng\right)\frac{(2k^2+2k+1)}{(k+1)^2}+\frac{320}{9}\frac{k}{(k+1)^2}\left(1+\frac{2}{3}\frac{bng}{k+1}\right)+\frac{640}{27}\frac{k^2}{(k+1)^4}bng\right]+\left[\frac{kp}{m}\frac{kT}{I}\right]\times\left[\frac{1}{3}\left(5+\frac{5k+3}{k+1}bng\right)(bng)^2\left(\frac{k}{k+1}\right)^2\right]\right\}}{\left\{\left[d^3\right]\times\left[\frac{512(34k+8)}{135(k+1)^4}(2k^2+2k+1)-\frac{512}{81}\frac{k^2}{(k+1)^4}\right]+\left[d\frac{kT}{I}\right]\times\left[\frac{8}{45}\frac{(34k+8)k^2}{(k+1)^4}(bng)^2\right]\right\}}$$

(A 3.12)

$$\lambda_K^r = \frac{\left\{ -\left[\frac{kP}{m} d^2\right] \times \left[\frac{32(34K+8)}{15(K+1)^2}\left(1 + \frac{2}{3}\frac{bng}{K+1}\right) + \frac{64}{15}\frac{(34K+8)}{(K+1)^4} bng - \frac{64}{9}\left(5 + \frac{5K+3}{K+1} bng\right)\frac{K}{(K+1)^2} \right] \right\}}{\left\{ \left[d^3\right] \times \left[\frac{512}{135}\frac{34K+8}{(K+1)^4}(2K^2+2K+1) - \frac{512}{81}\frac{K^2}{(K+1)^4} \right] + \left[d\frac{k\Gamma}{I}\right] \times \left[\frac{8}{45}\frac{(34K+8)K^2}{(K+1)^4}(bng)^2 \right] \right\}}$$

(A 3.13)

$$\beta = \frac{\left\{ -\left[d^2\frac{Pd}{m\Gamma} I\right] \times \left[\frac{512(34K+8)(2K^2+2K+1)}{135 (K+1)^5} - \frac{5120}{81}\frac{K^2}{(K+1)^5} \right] - \left[d\frac{kP}{m}\right] \times \left[\frac{4(34K+8)K}{15(K+1)^3}\left(1 + \frac{2bng}{3K+1}\right) bng + \frac{8}{9}\left(5 + \frac{5K+3}{K+1} bng\right)\frac{K^2}{(K+1)^3} bng \right] \right\}}{\left\{ \left[d^3\right] \times \left[\frac{512(34K+8)}{135(K+1)^4}(2K^2+2K+1) - \frac{512}{81}\frac{K^2}{(K+1)^4} \right] + \left[d\frac{k\Gamma}{I}\right] \times \left[\frac{8(34K+8)K^2}{45(K+1)^4}(bng)^2 \right] \right\}}$$

(A 3.14)

In order to simplify these equations, we need to establish a number of algebraic relationship, which are

(i) From the definition of d given by Eq. (5.60), we obtain

$$d^2 = n^2 g^2 \sigma^4 \frac{\pi k T}{m}$$

$$= \frac{N_A^2 \sigma^4}{V^2} g^2 \frac{\pi k T}{m}$$

$$= \frac{N_A^2 \sigma^6}{V^2} \frac{1}{\sigma^2} g^2 \frac{\pi k T}{m}$$

$$= \frac{2}{\sigma^2}\left(\frac{V_c}{V}\right)^2 g^2 \frac{\pi k T}{m}$$

$$= 2\pi g^2 \left(\frac{V_c}{V}\right)^2 \frac{1}{\sigma^2}\left(\frac{kT}{m}\right) \qquad (A\ 3.15)$$

where

$$V_c = \frac{N_A \sigma^3}{\sqrt{2}}$$

being the close-packing volume of rigid spheres. N_A is the Avogadro's constant and V is the molar volume. The remaining symbols are as defined in 5.4.3.

(ii) From the definition of K in terms of I, we obtain

$$\frac{kT}{I} = \frac{4kT}{m\sigma^2 k} = \frac{4}{k}\frac{1}{\sigma^2}\left(\frac{kT}{m}\right) \qquad (A\ 3.16)$$

(iii) Again using the definition for d

$$\left(\frac{kp}{m}\right)/d = \left(\frac{kp}{m}\right)/ng\sigma^2\left(\frac{\pi kT}{m}\right)^{1/2} = \frac{1}{g\sigma^2}\left(\frac{k^3 T}{\pi m}\right)^{1/2}$$

We have defined a quantity Λ^0.

$$\Lambda^0 = \frac{75}{64\sigma^2}\left(\frac{k^3 T}{\pi m}\right)^{1/2}$$

It should be noted that Λ^c does not represent the low density result for the thermal conductivity of the rough hard sphere fluid. The advantage of using this quantity as a reducing parameter is that the functional dependence of the thermal conductivity can be represented in a convenient form, as it will become apparent later. For example, we can write

$$\left(\frac{k\rho}{m}\right)\Big/ d \;=\; \frac{64\,\Lambda^c}{75\,g} \qquad (A\ 3.17)$$

(iv) Considering the group

$$\frac{d^2\,\frac{\rho d}{mT}\,I\left(\frac{kT}{\pi I}\right)^{1/2}}{d\times\frac{1}{\sigma^2}\,\frac{kT}{m}} \;=\; \frac{2\pi g^2\left(\frac{V_c}{V}\right)^2\frac{1}{\sigma^2}\left(\frac{kT}{m}\right)\frac{\rho I}{mT}\left(\frac{kT}{\pi I}\right)^{1/2}}{\frac{1}{\sigma^2}\left(\frac{kT}{m}\right)}$$

$$= 2\pi g^2\left(\frac{V_c}{V}\right)^2\frac{\rho I}{mT}\left(\frac{kT}{\pi I}\right)^{1/2}$$

$$= 2\pi g^2\left(\frac{V_c}{V}\right)^2\frac{nkI}{m}\left(\frac{kT}{\pi I}\right)^{1/2}$$

$$= 2\pi g^2\left(\frac{V_c}{V}\right)^2\frac{n}{m}\left(\frac{k^3T}{\pi}\right)^{1/2}\left(\frac{m\sigma^2k}{4}\right)^{1/2}$$

$$= 2\pi g^2\left(\frac{V_c}{V}\right)^2\left(\frac{k^3T}{\pi m}\right)^{1/2}\frac{n\sigma\,k^{1/2}}{2}$$

$$= 2\pi g^2\left(\frac{V_c}{V}\right)^2\frac{1}{\sigma^2}\left(\frac{k^3T}{\pi m}\right)^{1/2}\sqrt{2}\,\frac{V_c}{V}\,\frac{k^{1/2}}{2}$$

$$= 2\pi g^2\left(\frac{V_c}{V}\right)^2\frac{64}{75}\,\Lambda^0\,\frac{\sqrt{2}}{2}\left(\frac{V_c}{V}\right)k^{1/2}$$

$$(A\ 3.18)$$

(v) Also the group

$$\frac{d\,\frac{kp}{m}\left(\frac{kT}{\pi I}\right)^{1/2}}{d\times\frac{1}{\sigma^2}\left(\frac{kT}{m}\right)} = n k \sigma^2\left(\frac{kT}{\pi I}\right)^{1/2}$$

$$= n k \sigma^2\left(\frac{kT}{\pi}\,\frac{4}{m\sigma^2 k}\right)^{1/2}$$

$$= \frac{2 n k \sigma}{k^{1/2}}\left(\frac{kT}{\pi m}\right)^{1/2}$$

$$= \frac{2 n \sigma^3}{k^{1/2}}\,\frac{1}{\sigma^2}\left(\frac{k^3 T}{\pi m}\right)^{1/2}$$

$$= \frac{2\sqrt{2}}{k^{1/2}}\,\frac{V_c}{V}\,\frac{64}{75}\,\Lambda^0 \qquad (A\ 3.19)$$

(vi) and finally,

$$\left(\frac{kT}{\pi m}\right)^{1/2}\frac{p\sigma}{T} = \left(\frac{k^3 T}{\pi m}\right)^{1/2} n\ \sigma$$

$$= \frac{1}{\sigma^2}\left(\frac{k^3 T}{\pi m}\right)^{1/2} n\ \sigma^3$$

$$= \frac{1}{\sigma^2}\left(\frac{k^3 T}{\pi m}\right)^{1/2}\sqrt{2}\,\frac{V_c}{V}$$

$$= \frac{64}{75}\,\Lambda^0\,\sqrt{2}\,\frac{V_c}{V}$$

(A 3.20)

A3.9

By examining Eqn's (5.53) and (5.54), together with (A3.12) to (A3.14) for the occurence of the groups on the left hand side of conditions (i) to (vi) and substituting with the appropriate right hand side of the relations, we have arrived at the following equations for λ^t and λ^r.

$$\frac{\lambda^t}{\frac{64}{75}\lambda^0} = \left[2\pi g^2\left(\frac{V_0}{V}\right)^2 \left\{ \frac{512\,(34k+8)}{135\,(k+1)^4}(2k^2+2k+1) - \frac{512}{81}\frac{k^2}{(k+1)^4} \right\} + \frac{32\,(34k+8)\,k}{45\,(k+1)^4}(bng)^2 \right]^{-1}$$

$$\times \left\{ \left[-\frac{1}{9}\times\left[-\frac{64}{9}\left(5+\frac{(5k+3)}{(k+1)}bng\right)\frac{(2k^2+2k+1)}{(k+1)^2} + \frac{320\,k}{9\,(k+1)^2}\left(1+\frac{2}{3}\frac{bng}{k+1}\right) + \frac{640\,k^2}{27\,(k+1)^4}bng \right] + \frac{4}{3k}\left(5+\frac{5k+3}{k+1}bng\right)(bng)^2\left(\frac{k}{k+1}\right)^2 \right] \times \left[1 + \frac{1}{5}\frac{(5k+3)}{(k+1)}bng \right] \right.$$

$$+ \left[-\frac{1}{9}\times 2\pi g\left(\frac{V_0}{V}\right)^2 \left\{ \frac{32}{15}\frac{(34k+8)}{(k+1)^2}\left(1+\frac{2}{3}\frac{bng}{k+1}\right) + \frac{64}{15}\frac{(34k+8)k}{(k+1)^4}bng - \frac{64}{9}\left(5+\frac{5k+3}{k+1}bng\right)\frac{k}{(k+1)^2} \right] \right.$$

$$\left. \times \left[\frac{1}{3}\frac{(3k+2)}{(k+1)}bng \right] \right\}$$

$$+\Bigg[-\pi g^2\left(\frac{V_c}{V}\right)^2\sqrt{2}\,K^{1/2}\left\{\frac{512}{135}\,\frac{(34K+8)(2K^2+2K+1)}{(K+1)^5}\right.$$

$$-\frac{5120\,K}{81\,(K+1)^5}-\frac{2\sqrt{2}}{K^{1/2}}\left(\frac{V_c}{V}\right)\times\left\{\frac{4}{15}\,\frac{(34K+8)K}{(K+1)^3}\left(1+\frac{2}{3}\frac{bng}{(K+1)}\right)bng\right.$$

$$\left.+\frac{8}{9}\left(5+\frac{5K+3}{K+1}\,bng\right)\frac{K^2}{(K+1)^3}\,bng\right\}\Bigg]$$

$$\left.\times\frac{K^{1/2}}{(K+1)}\,bng\right\}$$

$$+\sqrt{2}\,\frac{V_c}{V}\,\frac{(2K+1)}{(K+1)}\,bng \qquad (A\ 3.21)$$

Since

$$b_n=\frac{b}{V}=\frac{2}{3}\pi\sqrt{2}\,\frac{V_c}{V} \qquad (A\ 3.22)$$

and g is a function of (V/V_o) only, Eq. (A3.21) indicates that $\left(\frac{\lambda^t}{\lambda^o}\right)$ is a function of (V/V_o) and K only.

$$\frac{\lambda^r}{\frac{64}{15}\lambda^0} = \left[2\pi g^2\left(\frac{V_0}{V}\right)^2 \left\{ \frac{512\,(34k+8)}{135\,(k+1)^4}\,(2k^2+2k+1) \right.\right.$$

$$\left.\left. - \frac{512}{81}\frac{k^2}{(k+1)^4} \right\} + \frac{32}{45}\frac{(34k+8)}{(k+1)^4}(bng)^2 \right]^{-1}$$

$$\times \left\{ \left[-\frac{1}{g}\,2\pi g^2\left(\frac{V_0}{V}\right)^2 \left\{ \frac{32\,(34k+8)}{15\,(k+1)^2}\left(1+\frac{2}{3}\frac{bng}{(k+1)}\right) \right.\right.\right.$$

$$\left.\left.\left. + \frac{64}{15}\frac{(34k+8)\,k}{(k+1)^4}\,bng - \frac{64}{9}\left(5+\frac{5k+3}{k+1}bng\right)\frac{k}{(k+1)^2} \right]\right.$$

$$\times \left(1+\frac{2}{3}\frac{1}{(k+1)}\,bng\right)$$

$$+ \left[-\pi g^2\left(\frac{V_0}{V}\right)\sqrt{2}\,k^{1/2} \left\{ \frac{512}{135}\frac{(34k+8)(2k^2+2k+1)}{(k+1)^5} \right.\right.$$

$$\left.\left. - \frac{5120}{81}\frac{k}{(k+1)^5} \right\} - \frac{2\sqrt{2}}{k^{1/2}}\left(\frac{V_0}{V}\right)\times\left\{ \frac{4}{15}\frac{(34k+8)k}{(k+1)^3}\left(1+\frac{2}{3}\frac{bng}{k+1}\right)bng \right.\right.$$

$$\left.\left. + \frac{8}{9}\left(5+\frac{5k+3}{k+1}bng\right)\frac{k^2}{(k+1)^3}\,bng \right\} \right]$$

$$\times \frac{k^{1/2}}{(k+1)}\,bng \Bigg\}$$

$$+ \sqrt{2}\left(\frac{V_0}{V}\right)\frac{1}{(k+1)}\,bng$$

(A 3.23)

The right hand side of Eq. A3.23 contains terms involving only (V/V_o) or functions of (V/V_o) and K only, so that we can conclude that $\left(\frac{\lambda^r}{\lambda^0}\right)$ is a function of(V/V_o) and K only.

Combining Eqn's A3.21 and A3.23 gives the total thermal conductivity for the rough hard sphere fluid, which of course is a function of (V/V_o) and K only. Thus $\left(\frac{\lambda_{RHS,D}}{\lambda^0}\right) = f_2\left(\frac{V}{V_c}, k\right)$. By collecting terms in ascending powers of bn or (b/V), we have obtained an expression for $\lambda_{RHS,D}$ given by Eq. (5.64).

REFERENCES

1. J.B. Armstrong, S.F.Y. Li and W.A. Wakeham, Proc. of ASME Annual Meeting, Publication no. 82-WA/HT-84, (1982).
2. M.J. Assael, C.A. Nieto de Castro and W.A. Wakeham, Chempor 1978, Braga, Portugal, pp. 16.1-16.9 (1978).
3. D.T. Jamieson, J.B. Irving and J.S. Tudhope, Liquid thermal conductivity data survey to 1973 (Edinburgh, HMSO, 1973).
4. C.A. Nieto de Castro, S.F.Y. Li, G.C. Maitland and W.A. Wakeham, Int. J. Thermophys. 4, 311 (1983).
5. J. Menashe and W.A. Wakeham, Ber. Bunsenges. Phys. Chem. 85, 340 (1981).
6. S.F.Y. Li, G.C. Maitland and W.A. Wakeham, Ber. Bunsenges. Phys. Chem. 88, 32 (1984).
7. J.M.N.A. Fareleira, S.F.Y.Li, G.C. Maitland and W.A. Wakeham, High Temp.-High Press. (in press).
8. S.F.Y. Li, G.C. Maitladn and W.A. Wakeham, Int. J. Thermophys. (in press).
9. J.A.A. Snel,N.J. Trappeniers and A. Botzen, Proc. Kon. Ned. Akad. Wet. 82B, 303 (1979).
10. R. Tufeu, PhD Thesis, University of Paris IV, (1971).
11. H. Ziebland and J.T.A. Burton, Int. J. Heat and Mass Transfer 1, 242 (1960).
12. L. Riedel, Chemie Ing. Technik. 23, 321 (1951).
13. G.N. Richter and B.H. Sage, Ind. Eng. Chem. Eng. Data Series 2(1), 61 (1957).
14. B.C. Sakiadis and J. Coates, A.I.Ch.E. J. 1, 275 (1955).

15. H.M. Roder and D.E. Diller, J. Chem. Phys. 52, 5928 (1970).

16. A. Michels and A. Botzen, Physica 18, 605 (1952).

17. J. Kestin and W.A. Wakeham, Transport properties of fluids: thermal conductivity, viscosity and diffusion coefficients, McGraw-Hill (1984).

18. A. Michels, J.V. Sengers and P.S. Van der Gulik, Physica 28, 1202 (1962).

19. B. Stalhane and S. Pyk, Tecknish Tidskrift 61, 389 (1931).

20. E.E. Shpil'rain, A.S. Umanskii and Yu. A. Gorshkov, High Temp.-High Press. 7, 361 (1975).

21. J.W. Haarman, PhD Thesis, Technische Hogeschool, Delft, The Netherlands (1959).

22. J.J. de Groot, J. Kestin and H. Sookiazian, Physica 75, 454 (1974).

23. J.J. Healy, J.J. de Groot and J. Kestin, Physica 82C, 392 (1976).

24. J. Kestin and W.A. Wakeham, Physica 92A, 102 (1978).

25. C.A.Nieto de Castro, J.C.G. Calado, W.A. Wakeham and M. Dix, J. Phys. E: Scient. Instrum. 9, 1073 (1976).

26. J. Kestin, R. Paul, A.A. Clifford and W.A. Wakeham, Physica 100A, 349 (1980).

27. J. Menashe, PhD. Thesis, Imperial College, University of London (1980).

28. H.S. Carslaw and J.C. Jaeger, Conduction of heat in solids, 2nd Edition, Oxford Univ. Press, 261 (1959).

29. M. Smoluchowski, Ann. Phys. Chem. 35, 983 (1911).

30. M. Smoluchowski, Phil. Mag. 21, 11 (1911).

31. J. Fisher, Ann. Phys. 34, 669 (1939).

32. R. Siegel, Trans. ASME 80, 347 (1958).

33. J.A. Schetz and R.J. Eichhorn, J.Heat Transfer, Trans. ASME 84, Ser. C, 334 (1962).

34. R.J. Goldstein and D.G. Briggs, J. Heat Transfer, Trans. ASME 86, Ser. C, 490 (1964).

35. J. Pantaloni, E. Guyon, M.G.Velarde, R. Balleux adn S.G. Finiel, Revue de Physique appliquee 12, 1849 (1977).

36. H. Poltz, Int. J. Heat and Mass Trans. 8, 515 (1965).

37. Ibid., p. 609.

38. H. Poltz and R. Jugel, Int. J. Heat Mass Trans. 10, 1075 (1967).

39. W. Leidenfrost, paper to Thermal Conductivity Conference, Gatlingburg, Tennessee (1963).

40. I. Rhyming, Int. J. Heat Mass Trans. 9, 315 (1960).

41. R.G. Diessler, J. Heat Trans. ASME 86, 240 (1960).

42. R. Grief and G.P. Clapper, Appl. Sci. Res. (15)A

43. S. Rosseland. Astrophysik und Atom-Theoretische Grundlage, Springer Verlag, Berlin 41 (1931).

44. M. Perlmutter and J.R. Howell, J. Heat Trans., Trans. ASME 86, 69 (1964).

45. E.F.M. Van der Held, Appl. Sci. Res. 3A, 237 (1952).

46. E.F.M. Van der Held, Appl. Sci. Res. 4A, 77 (1952).

47. A. Saito, N. Mani and J.E.S. Venart, Proc. 16th National Heat Transf. Conf., 76-CSME/CSChE-6 (1976).

48. A. Saito adn J.E.S. Venart, Proc. 6th Int. Heat Transf. Conf. 3, 79 (1978).

49. A. Saito, Bulletin of the JSME 23, 1459 (1980).

50. J. Menashe and W.A. Wakeham, Int. J. Heat Mass Transf. 25, 661 (1982).

51. Lowan, Davids and Levenson, Bull. Amer. Math. Sco. 48, 739 (1942).

52. O.A.Liskovets, J. Diff. Eqs. 1, 1308 (1965).

53. C.W. Gear, Comm. of the ACM 14(3), 176 (1971).

54. Hindmarsh Lawrence Livermore Laboratory report, UCID-30001, Rev.2 (1972).

55. M. Abramowitz and I.A. Stegun (Eds.), Handbook of Mathematical Functions, NBS (1964).

56. M. Assael, PhD. Thesis, Imperial College, University of London, (1980).

57. International Practical Temperature Scale of 1976 (NPL), Revised ed. (HMSO, London, 1976).

58. Property of Fluids Internal Report No. 144 (NEL, East Kilbride, 1976).

59. Property of Fluids Internal Report No. 145, (NEL, East Kilbride, 1976).

60. I. Kh. Mukhamedzyanov. G. Kh. Mukhamedzyanov and A.G. Usmanov, Trudy Kazan. Khim. Tekhnol. In-ta 47, 22 (1971).

61. I.F.Golubev and Ya. M. Naziev, Trudy Energ. Inst. AN. Azerb. SSR. 15, 84 (1962).

62. Yu, L. Rastorguev and V.V. Pugach, Izv. Vyssh. ucheb. Zaved., Neft'i Gaz. 13, 69 (1970).

63. Y. Nagasaka and A. Nagashima, First Symp. on Thermophysical Properties, 67 (1980).

64. Y. Nagasaka and A. Nagashima, I & EC Fundamentals 20, 216 (1981).

65. C.A. Nieto de Castro, J.C.G. Calado and W.A. Wakeham, Proc. of 7th Symposium on Thermophysical Properties, A. Cezairliyan, Ed., 730 (ASME, New York, 1977).

66. L. Boltzmann, Akad. der Wissenschaften 66(2), 275 (1872).

67. L. Boltzmann, Akad. der Wissenschaften 72(2), 427 (1875).

68. D. Enskog, Physik. Zeitschr. 12, 533 (1911).

69. D. Enskog, PhD Thesis, Uppsala (1917).

70. S. Chapman, Trans. Roy. Soc. (LON) 216, 279 (1917).

71. S. Chapman, Trans. Roy. Soc. (LON) 217, 118 (1917).

72. S. Chapman and J.G. Cowling, Mathemaical Theory of Transport Processes in Gases, North Holland Publ. Co. (1972).

73. P. Resibois and M. de Leener, Classical Kinetic Theory of Fluids, John Wiley & Sons, Inc. (1977).

74. S.A. Rice and P. Gray, The Statistical Mechanics of Simple Liquids, (Interscience, New YOrk, 1965).

75, P. Gray in Physics of Simple Liquids, H.N.V. Temperley, J.S. Rowlinson and G.S. Rushbrooke, Eds., (North Holland, Amsterdam, 1968).

76. S.A. Rice, J.P.Boon and H.T. Davıs ın Sımple Dense Fluids, H.L. Frisch and Z.W. Salsburg, Eds., (Academic, New York, 1968).

77. R.J. Bearman and J.G.Kirkwood, J. Chem. Phys. 28, 136 (1958).

78. R.J. Bearman, J.G. Kırkwood and M. Fixman, Adv. Chem. Phys 1, 1 (1958).

79. R.J. Bearman, J. Chem. Phys. 29, 1278 (1958).

80. R.J. Bearman, J. Chem. Phys. 30, 835 (1959).

81. R.J.Bearman, J. Chem. Phys. 31, 751 (1959).

82. R.J. Bearman, J. Chem. Phys. 32, 1308 (1960).

83. S.A. Rıce and J.G. Kirkwood, J. Chem. Phys. 31, 901 (1959).

84. S.A. Rice and A.R. Allnatt, J. Chem. Phys. 34, 409 (1961).

85. F.C. Collins and M. Raffel, J. Chem. Phys. 29, 699 (1958).

86. S.R. de Groot and P. Mazur, Non-equilıbrium thermodynamics, (North Holland, Amsterdam, 1962).

87. W.A. Steel in Transport Phenomena ın Fluids, H.J.M. Hanley, Ed., (Marcel Dekker, New York, 1969).

88. R. Zwanzig, Ann. Rev. Phys. Chem. 16, 67 (1965).

89. B.J. Alder and T.E. Wainright in Transport Processes in Statistical Mechanics, I. Prigogine (Interscience, New York, 1958).

90. J.E.Erpenbeck and W.W. Wood in Statistical Mechanics B: Time Dependent Processes, B.J. Berne, Ed. (Plenum, New YOrk, 1977).

91. J. Kushick and B.J. Berne in Statistical Mechanics B: Time Dependent Processes, B.J. Berne, Ed. (Plenum, New YOrk, 1977).

92. B.J. Alder and W.G. Hoover in Physics of Simple Liquids, H.N.V. Temperley, J.S. Rowlinson and G.S. Rushbrooke, Eds. (North Holland, Amsterdam, 1968).

93. J.H. Dymond, J. Chem. Phys. 60, 969 (1974).

94. P. Gosting and N.J. Trappeniers, Physica 51, 418 (1971).

95. R. Dawson, F. Khoury and R. Kobayashi, AIChE J. 16, 725 (1970).

96. E.T.S. Huang, G.W. Swift and F. Kurata, AIChE J. 12, 932 (1966).

97. J.P.Boon, J.L. Legross and G. Thomaes, Physica 33, 547 (1967).

98. J. Hellemans, H. Zink and O. Van Paemel, Physica 46, 395 (1970).

99. J.H. Dymond, Proc. 6th Symp. Thermophys. Properties, ASME, 143 (New York, 1973).

100. S. Glasstone, K.J. Laidler and H. Eyring, The Theory of Rate Processes (McGraw-Hill, New York, 1941).

101. B.J. Alder and T. Einwohner, J. Chem. Phys. 43, 3399 (1965).

102. J.H. Dymond and B.J. Alder, J. Chem. Phys. 45, 2061 (1966).

103. J.H. Dymond, Physica 79, 65 (1975).

104. K.C. Mo, K.E. Gubbins and J.W. Duffy, Proc. 6th Symp. on Thermophys. Props. 158 (ASME, New York, 1973).

105. P. Resibois, J. Piasecki and Y.Pomeau, Phys. Rev. Letts. 28, 882 (1972).

106. D. Enskog, Kinetische Theorie der Wärmeleitung, Reibung und Selbstdiffusion in Gewissen Verdichteten Gasen und Flüssigkeiten, Kungl. Svenska. Vet.-Ak. Handl. 63(4), (1922).

107. B.J. Alder, D.M.Gass and T.E. Wainwright, J. Chem. Phys. 53, 3813 (1970).

108. B.J. Alder and T.E. Wainwright, Phys. Rev. A1, 18 (1970).

109. N.F.Carnahan and K.E. Starling, J. Chem. PHys. 51, 635 (1969).

110. J.H. Dymond, Physica 75, 100 (1974).

111. J.H. Dymond, Physica 85A, 175 (1976).

112. J.H. Dymond, J. Chem. Soc. Faraday Trans. II 68, 1789 (1972).

113. J.H. Dymond and T.A. Brawn, Proc. 7th Symp. on Thermophys. Props., 660 (ASME, New York, 1977).

114. J.H. Dymond and T.A. Brawn, Symposium on Transport Properties of Fluids and Fluid Mixtures: Their Measurement, Estimation and Correlation, National Engineering Laboratory, East Kilbride, Glasgow (1979).

115. J.J. Van Loef, Physica 75, 115 (1974).

116. J.J. Van Loef, Physica 87A, 258 (1977).

117. J.J. Van Loef, Proc. 8th Symp. on Thermophys. Props., p. 158 (ASME, New York, 1981).

118. J.Menashe, M.Mustafa, M. Sage and W.A. Wakeham, Proc. 8th Symp. on Thermophys. Props., p. 254 (ASME, New York, 1981).

119. G.H. Bryan, British Assoc. Reports, p. 64 (1894).

120. F.B. Pidduck, Proc. R. Soc. A101, 101 (1922).

121. Y. Kagan and A.M. Afanes'ev, Sov. Phys.-JETP 14, 1096 (1962).

122. L. Waldmann, Z. Naturforsch A18, 1033 (1963).

123. W. Condiff, W. Lu and J.S.Dahler, J. Chem. Phys. 42, 3445 (1965).

124. B.J.McCoy, S.I.Sandler and J.S. Dahler, J. Chem. Phys. 45, 3485 (1966).

125. W.M. Klein, D.K. Hoffman and J.S.Dahler, J. Chem. Phys. 49, 2321 (1968).

126. D. Chandler, J. Chem. Phys. 60, 3500 (1974).

127. D. Chandler, J. Chem. Phys. 60, 3508 (1974).

128. D. Chandler, J. Chem. Phys. 62, 1358 (1975).

129. M. Theodosopulu and J.S. Dahler, J. Chem. Phys. 60, 3567 (1974).

130. M. Theodosopulu and J.S. Dahler, J. Chem. Phys. 60, 4048 (1974).

131. K.R. Harris and N.J. Trappeniers, Physica A104(1-2), 262 (1980).

132. L.A. Woolf, J. Chem. Soc. Faraday I 78(2), 583 (1982).

133. R.L. Hurle and L.A. Woolf, Aust. J. Chem. 33, 1947 (1980).

134. J.H. Dymond, K.J.Young and J.D. Isdale, Int. J. Thermophys. 1, 345 (1980).

135. J.H. Dymond, J. Robertson and J.D. Isdale, Int. J. Thermophys. 2, 133 (1981).

136. J.D. Isdlae, J.H. Dymond and T.A. Brawn, High Temp.-High Press. 11, 571 (1979).

137. J.H. Dymond, J.Robertson and J.D. Isdale, Int. J. Thermophys. 2, 223 (1981).

138. H.M. Roder and C.A. Nieto de Castro, J. Chem. Eng. Data 27, 12 (1982).

139. J. Menashe and W.A. Wakeham, Ber. Bunsenges. Phys. Chem. 86, 541 (1982).

140. M.Mustafa, M. Sage and W.A. Wakeham, Int. J. Thermophys. 3, 217 (1982).

141. G.C. Maitland, M. Rigby, E.B. Smith and W.A. Wakeham, Intermolecular Forces - Their Origin and Determination, Oxford University Press (1980).

142. C.A. Nieto de Castro, J.C.G. Calado and W.A. Wakeham, High Temp.-High Press. 11, 551 (1979).

143. B.C. Sakiadis and J. Coates, J.Amer. Inst. Chem. Engrs. 3, 121 (1957).

144. A.M.Kerimov, F.G. El'Darov and V.S. El'Darov, Isv. vyssh. uched. Zaved., Nefti' i Gaz 13, 77 (1970).

145. Yu. L. Rastorguev, G.F. Bogatov and B.A. Grigor'ev, Teplo. Svoisva. Zhidk; Mater. Vses. Teplofiz. Konf. Svoistva. Vesch. Vys. Temp. 3rd, 88 (1970).

146. Yu. L. Rastorguev and A. Yu. Ganiev, Russian J. Phys. Chem. 41, 1557 (1967).

147. G. Kh. Mukhamedzyanov, A.G. Usmanov and A.A. Tarzimanov, Izv. vyssh. ucheb. Zaved. Neft'i Gaz. 7, 70 (1964).

148. V.P. Frontasev and M.Y. Gusakov. Zh. Tekhn. Fiz. 29, 1277 (1959).

149. L.P.Filippov, Vestnik Mosk. gos. Univ. Ser. Fiz-Mat.; Estestven. Nouk 9, 45 (1954).

150. L. Riedel, Mitt. Kaltetech. Inst. Karlsruhe (2), (1948).

151. J.C.G. Calado, J.M.N.A. Fareleira, C.A. Nieto de Castro and W.A. Wakeham, Int. J. Thermophys. 4, 193 (1983).

152. H. Kashiwagi, M. Oishi, Y. Tanaka and T. Makita, Int. J. Thermophys. 3, 101 (1982).

153. J.K. Horrocks, E. McLaughlin and A.R. Ubbelohde, Trans. Faraday Soc. 59, 1110 (1963).

154. E. Schmidt and W. Leidenfrost, Chem. Ingr. Tech. 26, 35 (1954).

155. W.J. Barnette, PhD Thesis, Louisiana State University (1967).

156. D.K.H. Briggs, Industr. Engng. Chem. 49, 418 (1957).

157. H. Forsman, P. Andersson and G. Bäckström, Physica 114B, 287 (1982).

158. A. Harlow, PhD Thesis, Imperial College, University of London (1967).

159. J.H. Dymond, K.J. Young and J.D.Isdale, J. Chem. Thermodyn. 11, 887 (1979).

160. J.H. Dymond, J. Robertson and J.D. Isdale, J. Chem. Thermodyn. 14, 51 (1982).

161. J.D. Isdale, J.H. Dymond and T.A. Brawn, High Temp.-High Press. 11, 571 (1979).

162. J.D. Isdale (private communication).

163. P.W. Bridgman, Proc. Am. Acad. Arts Sci. 66, 185 (1931).

164. A.C. Toohey, PhD Thesis, Imperial College, University of London, (1961).

165. N.B. Vargaftik, Tables of the Thermodynamic Properties of Liquids and Gases, 2nd Ed., (Wiley, New York, 1975).

166. R. Shaw, J. Chem. Eng. Data 14, 461 (1969).

P U B L I C A T I O N S

1. The effect of errors in the thermophysical properties of fluids upon plant design: Proc. of ASME Annual Meeting, Publication No. 82-WA/HT-84 (1982).

2. The thermal conductivity of n-hexane and n-octane at pressures up to 0.64 GPa in the temperature range 34-90°C: Ber. Bunsenges. Phys. Chem. 88, 32 (1984).

3. The thermal conductivity of toluene in the temperature range 35-90°C at pressures up to 600 MPa: Int. J. of Thermophys. 4, 311 (1983).

4. The thermal conductivity of two branched alkanes in the temperature range 36-90°C at pressures up to 0.6 GPa: High Temp.-High Press. (in press).

5. The thermal conductivity of benzene and cyclohexane in the temperature range 36-90°C at pressures up to 0.33 GPa: Int. J. of Thermophys. (in press).

6. The thermal conductivity of oct-1-ene (to be published).

7. The thermal conductivity of liquid hydrocarbons: Proc. of Ninth Symposium on Thermophysical Properties (1984).

8. Liquid thermal conductivity standard (to be published).